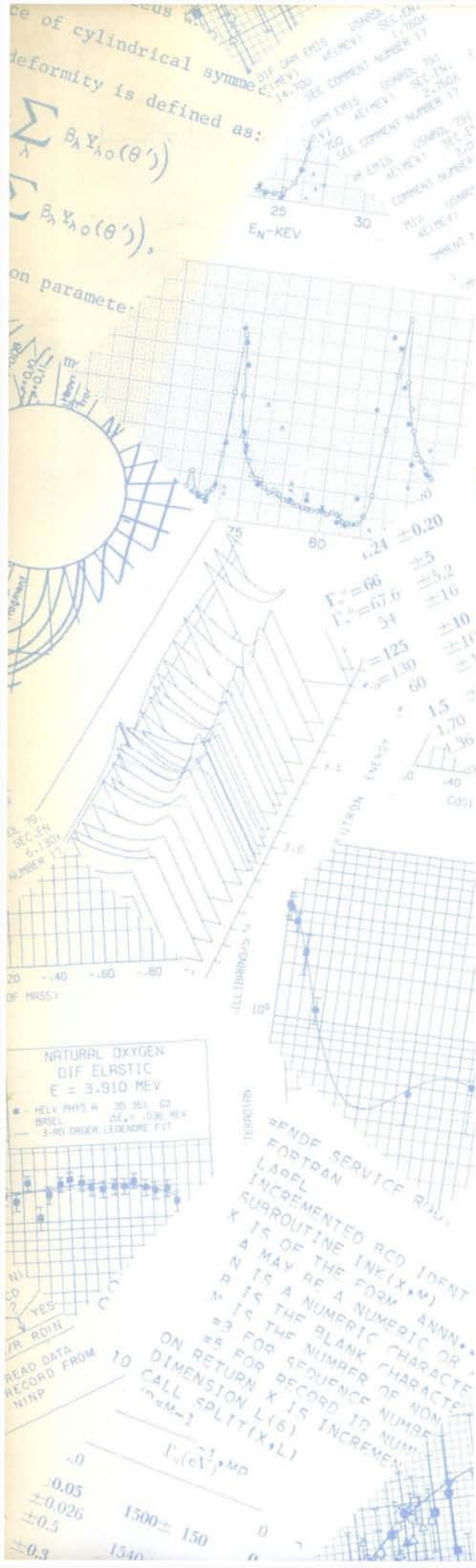

BNL-NCS-26133
DOE/NDC-15/U
NEANDC(US)-205/U
INDC(USA)-81/U
Informal Report
Limited Distribution

REPORTS TO THE DOE NUCLEAR DATA COMMITTEE

Edited by
NATIONAL NUCLEAR DATA CENTER
for the
U.S. Department of Energy
Nuclear Data Committee

April 1979

BROOKHAVEN NATIONAL LABORATORY
ASSOCIATED UNIVERSITIES, INC.
UPTON, NEW YORK 11973

national
nuclear
data
Center

BNL-NCS-26133
DOE/NDC-15/U

REPORTS TO THE DOE NUCLEAR DATA COMMITTEE

April 1979

Edited by
NATIONAL NUCLEAR DATA CENTER
for the
U.S. Department of Energy
Nuclear Data Committee

NATIONAL NUCLEAR DATA CENTER

BROOKHAVEN NATIONAL LABORATORY

ASSOCIATED UNIVERSITIES, INC.

UNDER CONTRACT NO. EY-76-C-02-0016 WITH THE

UNITED STATES DEPARTMENT OF ENERGY

PREFACE

The reports in this document were submitted to the Department of Energy, Nuclear Data Committee (DOE-NDC) in April, 1979. The reporting laboratories are those having a substantial effort in measuring neutron and nuclear cross sections of relevance to the U.S. applied nuclear energy program.

The authors of the Status Report contributions are responsible for collecting and editing individual contributions from their laboratory and are not necessarily the sole authors of the contributions. The scientists responsible for the work described in each individual contribution are listed at the beginning of the contribution.

The material contained in these reports is to be regarded as comprised of informal statements of recent developments and preliminary data. Persons wishing to make use of these data should contact the individual experimenter for further details. The data which appear in this document should be quoted only by permission of the contributor and should be referenced as private communication, and not by this document number. Appropriate subjects are listed as follows:

1. Microscopic neutron cross sections relevant to the nuclear energy program, including shielding. Inverse reactions where pertinent are included.

2. Charged-particle cross sections, where they are relevant to "1" above, and where relevant to developing and testing nuclear models.

3. Gamma-ray production, radioactive decay, and theoretical developments in nuclear structure which are applicable to nuclear energy programs.

4. Proton and alpha-particle cross sections, at energies of up to 1 GeV, which are of interest to the space program.

These reports cannot be regarded as a complete summary of the nuclear research efforts in the U.S. A number of laboratories, whose research is less programmatically oriented do not submit reports; neither do the submitted reports reflect all the work related to nuclear data in progress at the submitting laboratory.

This compilation has been produced almost completely from master copies prepared by the individual contributors listed in the Table of Contents.

The CINDA-type index and CPND-type index, which follow the Table of Contents, were prepared by Gail Waite and Thomas Burrows, respectively, of the National Nuclear Data Center, Brookhaven National Laboratory, Upton, New York.

TABLE OF CONTENTS

TABLE OF CONTENTS (CONT.)

ELEMENT S	A	QUANTITY	TYPE	ENERGY MIN	MAX	DOCUMENTATION REF	VOL	PAGE	DATE	LAB	COMMENTS
H	001	TOTAL XSECT	EXPT-PROG	NDG		DOE-NDC-15		23	479	ANL	POENITZ.TRNS.NDG.ANAL TBD.
H	001	TOTAL XSECT	EXPT-PROG	30+6	45+7	DOE-NDC-15		151	479	NBS	KELLIE+TOF.LINAC.NDG.CFD OTH.TBP.
H	001	TOTAL XSECT	EXPT-PROG	50+5	50+7	DOE-NDC-15		166	479	ORL	LARSON+TRNS.ORELA.CFD.NDG
H	001	SPECT N,GAMM	EXPT-PROG	MAXW		DOE-NDC-15		49	479	BNL	GREENWOOD+2223.247 KEV G RAY MEAS.
HE	003	N, PROTON	EXPT-PROG	MAXW	20+3	DOE-NDC-15		157	479	NBS	BOWMAN+2ES.HE-3(N,P)/B(F)3(N,A).NDG.
LI	006	TOTAL XSECT	EXPT-PROG	30+6	45+7	DOE-NDC-15		151	479	NBS	KELLIE+TOF.LINAC.NDG.ANAL TBC.TBP.
LI	006	ELASTIC SCAT	EXPT-PROG	70+6	14+7	DOE-NDC-15		209	479	TNL	BEYERLE+NDG.CFD.SEE NSE 69 P 22.
LI	006	DIFF ELASTIC	EXPT-PROG	40+6	75+6	DOE-NDC-15		184	479	OHO	KNOX+CS MEAS.NDG.TBP IN NSE.
LI	006	DIFF ELASTIC	EXPT-PROG	22+6	41+6	DOE-NDC-15		184	479	OHO	KNOX+5 ES.TOF.NDG.
LI	006	DIFF ELASTIC	EXPT-PROG	70+6	14+7	DOE-NDC-15		209	479	TNL	BEYERLE+NDG.CFD.SEE NSE 69 P 22.
LI	006	DIFF ELASTIC	EXPT-PROG	18+6	40+6	DOE-NDC-15		225	479	YAL	CHIU+CS MEAS.NDG.GLOBAL ANAL PAR GVN
LI	006	DIFF ELASTIC	EVAL-PROG	10-2	40+6	DOE-NDC-15		225	479	YAL	CHIU+PARS FROM GLOBAL ANAL.TEL.TEC.
LI	006	POLARIZATION	EXPT-PROG	18+6	40+6	DOE-NDC-15		225	479	YAL	CHIU+ASSYM.NDG.GLOBAL ANAL PARS GVN.
LI	006	POLARIZATION	EVAL-PROG	10-2	40+6	DOE-NDC-15		225	479	YAL	CHIU+PARS FROM GLOBAL ANAL.TBL.TBC.
LI	006	DIFF INELAST	EXPT-PROG	22+6	41+6	DOE-NDC-15		184	479	OHO	KNOX+5 ES.TOF.NDG.
LI	006	DIFF INELAST	EXPT-PROG	70+6	14+7	DOE-NDC-15		209	479	TNL	BEYERLE+NDG.CFD.SEE NSE 69 P 22.
LI	006	NEUT EMISSN	EXPT-PROG	60+6	10+7	DOE-NDC-15		122	479	LAS	DRAKE+3ES.10 ANGS.N EMIS SPEC.NDG.
LI	006	N, TRITON	EXPT-PROG	20+3	24+4	DOE-NDC-15		30	479	BNL	STELTS+2 RES.ANGDIST.GRPHS.CFD
LI	006	N, TRITON	EVAL-PROG	NDG		DOE-NDC-15		131	479	LAS	STEWART+REVISIONS FOR ENDF/B-V.NDG.
LI	006	N, TRITON	EXPT-PROG	23+4		DOE-NDC-15		147	479	MHG	ENGDAHL+ANGDIST.22.8 KEV CS GVN.
LI	006	N, TRITON	EXPT-PROG	70+4	30+6	DOE-NDC-15		167	479	ORL	MACKLIN+PEAK VALUE CFD ENDF/B-V.
LI	007	TOTAL XSECT	EXPT-PROG	30+6	45+7	DOE-NDC-15		151	479	NBS	KELLIE+TOF.LINAC.NDG.ANAL TEC.TBP.
LI	007	ELASTIC SCAT	EXPT-PROG	70+6	14+7	DOE-NDC-15		209	479	TNL	BEYERLE+NDG.CFD.SEE NSE 69 P 22.
LI	007	DIFF ELASTIC	EXPT-PROG	40+6	75+6	DOE-NDC-15		184	479	OHO	KNOX+CS MEAS.NDG.TBP IN NSE.
LI	007	DIFF ELASTIC	EXPT-PROG	22+6	41+6	DOE-NDC-15		184	479	OHO	KNOX+5 ES.TOF.NDG.
LI	007	DIFF ELASTIC	EXPT-PROG	70+6	14+7	DOE-NDC-15		209	479	TNL	BEYERLE+NDG.CFD.SEE NSE 69 P 22.
LI	007	DIFF INELAST	EXPT-PROG	22+6	41+6	DOE-NDC-15		184	479	OHO	KNOX+5 ES.478 MEV LVL.ANAL TBD.NDG.
LI	007	DIFF INELAST	EXPT-PROG	70+6	14+7	DOE-NDC-15		209	479	TNL	BEYERLE+NDG.CFD.SEE NSE 69 P 22.

ELEMENT S	A	QUANTITY	TYPE	ENERGY MIN	MAX	DOCUMENTATION REF	VOL	PAGE	DATE	LAB	COMMENTS
LI	007	INELST GAMMA	EXPT-PROG	48+5	50+6	DOE-NDC-15		165	479	ORL	OLSEN+125DEG.NDG.ABST ORNL-TM-6832.
LI	007	NEUT EMISSN	EXPT-PROG	60+6	10+7	DOE-NDC-15		122	479	LAS	DRAKE+3ES.10 ANGS.N EMIS SPEC.NDG.
BE	009	DIFF ELASTIC	EXPT-PROG	70+6	14+7	DOE-NDC-15		210	479	TNL	BEYERLE+NDG.SEE NSE 68 P 38.
BE	009	DIFF ELASTIC	EVAL-PROG	10-2	40+6	DOE-NDC-15		226	479	YAL	MCGUIRE+CS MEAS.ANAL OF OTH TBD.NDG
BE	009	DIFF ELASTIC	EXPT-PROG	20+6	40+6	DOE-NDC-15		226	479	YAL	MCGUIRE+CS MEAS.ANAL OF OTH TBD.NDG
BE	009	POLARIZATION	EVAL-PROG	10-2	40+6	DOE-NDC-15		226	479	YAL	MCGUIRE+ASSYM.NDG.ANAL OF OTH TBD
BE	009	POLARIZATION	EXPT-PROG	20+6	40+6	DOE-NDC-15		226	479	YAL	MCGUIRE+ASSYM.NDG.ANAL OF OTH TBD.
BE	009	DIFF INELAST	EXPT-PROG	70+6	14+7	DOE-NDC-15		210	479	TNL	BEYERLE+NDG. SEE NSE 68 P 38
B		N,ALPHA REAC	EXPT-PROG	10+0	10+4	DOE-NDC-15		155	479	NBS	BOWMAN+B VS BORON-TRIFLOURIDE.GRPH.
B	010	ELASTIC SCAT	EXPT-PROG	80+6	14+7	DOE-NDC-15		210	479	TNL	BEYERLE+8 ANGDISTS.TBP.GRPH.
B	010	DIFF ELASTIC	EXPT-PROG	80+6	14+7	DOE-NDC-15		210	479	TNL	BEYERLE+8 ANGDISTS.TBP.NDG.
B	010	DIFF INELAST	EXPT-PROG	80+6	14+7	DOE-NDC-15		210	479	TNL	BEYERLE+8 ANGDISTS.TBP.NDG.
B	010	NEUT EMISSN	EXPT-PROG	60+6	10+7	DOE-NDC-15		122	479	LAS	DRAKE+3ES.10 ANGS.N EMIS SPEC.NDG.
B	010	N,ALPHA REAC	EXPT-PROG	20+3	24+4	DOE-NDC-15		30	479	BNL	STELTS+2 RES.ANGDIST.GRPHS.CFD
B	010	N,ALPHA REAC	EVAL-PROG	NDG		DOE-NDC-15		131	479	LAS	STEWART+REVISIONS FOR ENDF/B-V.NDG.
B	011	ELASTIC SCAT	EXPT-PROG	80+6	14+7	DOE-NDC-15		210	479	TNL	BEYERLE+8 ANGDISTS.TBP.GRPH.
B	011	DIFF ELASTIC	EXPT-PROG	55+6	60+6	DOE-NDC-15		184	479	OHO	RESLER+ANGDISTR.3ES.NDG.ANAL TBD.
B	011	DIFF ELASTIC	EXPT-PROG	20+6	80+6	DOE-NDC-15		185	479	OHO	WHITE+ANAL TBD WITH ORMAP.NDG.
B	011	DIFF ELASTIC	EXPT-PROG	80+6	14+7	DOE-NDC-15		210	479	TNL	BEYERLE+8 ANGDISTS.TBP.NDG.
B	011	DIFF INELAST	EXPT-PROG	55+6	60+6	DOE-NDC-15		184	479	OHO	RESLER+ANGDISTR.3ES.NDG.ANAL TBD.
B	011	DIFF INELAST	EXPT-PROG	80+6	14+7	DOE-NDC-15		210	479	TNL	BEYERLE+8 ANGDISTS.TBP.NDG.
B	011	NEUT EMISSN	EXPT-PROG	60+6	10+7	DOE-NDC-15		122	479	LAS	DRAKE+3ES.10 ANGS.N EMIS SPEC.NDG.
B	CMP	N,ALPHA REAC	EXPT-PROG	MAXW	20+3	DOE-NDC-15		157	479	NBS	BOWMAN+2ES.HE-3(N,P)/B(F)3(N,A).NDG.
B	CMP	N,ALPHA REAC	EXPT-PROG	10+0	10+4	DOE-NDC-15		155	479	NBS	BOWMAN+B VS BORON-TRIFLOURIDE.GRPH.
C	012	EVALUATION	EVAL-PROG	NDG		DOE-NDC-15		176	479	ORL	FU+EVAL FOR ENDF/B-V.NDG.
C	012	TOTAL XSECT	EXPT-PROG	20+4	48+6	DOE-NDC-15		23	479	ANL	POENITZ.TRNS.CS GRPH.CFD ENDF/B-V.
C	012	TOTAL XSECT	EXPT-PROG	20+5	50+6	DOE-NDC-15		68	479	KTY	HARPER+NDG.CFD TO NBS RESULTS.
C	012	TOTAL XSECT	EXPT-PROG	30+6	45+7	DOE-NDC-15		151	479	NBS	KELLIE+TOF.LINAC.NDG.CFD ENDF.TBP.

ELEMENT S A	QUANTITY	TYPE	ENERGY MIN	ENERGY MAX	DOCUMENTATION REF	VOL	PAGE	DATE	LAB	COMMENTS
C 012	TOTAL XSECT	EXPT-PROG	50+5	50+7	DOE-NDC-15		166	479	ORL	LARSON+TRNS.ORELA.NDG.
C 012	DIFF ELASTIC	EXPT-PROG	90+6	15+7	DOE-NDC-15		210	479	TNL	BEYERLE+15 ES.28 ANG.SEE NSE 61 P521
C 012	DIFF INELAST	EXPT-PROG	90+6	15+7	DOE-NDC-15		210	479	TNL	BEYERLE+15 ES.28 ANG.SEE NSE 61 P521
C 012	NEUT EMISSN	EXPT-PROG	14+7		DOE-NDC-15		122	479	LAS	DRAKE+10 ANGS.N EMISSION SPEC.NDG.
C 012	N, PROTON	EXPT-PROG	14+7	15+7	DOE-NDC-15		99	479	LRL	HAIGHT+PRELIM MEAS.NDG.2ES
C 012	N, DEUTERON	EXPT-PROG	14+7	15+7	DOE-NDC-15		99	479	LRL	HAIGHT+PRELIM MEAS.NDG.2ES
C 012	N,ALPHA REAC	EXPT-PROG	14+7	15+7	DOE-NDC-15		99	479	LRL	HAIGHT+PRELIM MEAS.NDG.2ES
C 012	RESON PARAMS	EVAL-PROG	21+6		DOE-NDC-15		177	479	ORL	PEREY.EO FROM COVARIANCE MATRIX.NDG.
C 013	TOTAL XSECT	EXPT-PROG	20+4	48+6	DOE-NDC-15		23	479	ANL	POENITZ.TRNS.CS GRPH.CFD ENDF/B-V.
C 013	DIFF ELASTIC	EXPT-PROG	53+6	60+6	DOE-NDC-15		184	479	OHO	RESLER+ANGDISTR.2ES.NDG.ANAL TBD.
C 013	DIFF INELAST	EXPT-PROG	53+6	60+6	DOE-NDC-15		184	479	OHO	RESLER+ANGDISTR.2ES.NDG.ANAL TBD.
C 013	GAMMA,N	THEO-PROG	77+6	93+6	DOE-NDC-15		18	479	ANL	HOLT+R-MATRIX ANAL
N 014	SPECT N,GAMM	EXPT-PROG	NDG		DOE-NDC-15		50	479	BNL	GREENWOOD+TEL G ES.
N 014	N, PROTON	EXPT-PROG	50+5	70+6	DOE-NDC-15		168	479	ORL	MORGAN.CFD EVAL.NDG.SEE ORNL-TM-6528
N 014	N,ALPHA REAC	EXPT-PROG	10+6	15+7	DOE-NDC-15		168	479	ORL	MORGAN.GND,ISOM.NDG.ABST ORNL-TM6528
O 016	TOTAL XSECT	EXPT-PROG	24+6		DOE-NDC-15		167	479	ORL	FOWLER+TOF.TRNS.THICK SAMPLE.CS GVN.
O 016	TOTAL XSECT	EXPT-PROG	50+5	50+7	DOE-NDC-15		166	479	ORL	LARSON+TRNS.ORELA.NDG.
O 016	ELASTIC SCAT	EXPT-PROG	93+6	15+7	DOE-NDC-15		210	479	TNL	BEYERLE+12 ANGS.GRPH.CFD ENDF.PRELIM
O 016	DIFF ELASTIC	EXPT-PROG	93+6	15+7	DOE-NDC-15		210	479	TNL	BEYERLE+12 ANGS.SEL GRPH.CFD.PRELIM
O 016	DIFF INELAST	EXPT-PROG	93+6	15+7	DOE-NDC-15		210	479	TNL	BEYERLE+PARTIAL ANGDIST.NDG.ANAL TBD
O 016	NONEL GAMMAS	EXPT-PROG	65+6	20+7	DOE-NDC-15		164	479	ORL	MORGAN+125 DEG.NDG.TBP.SEE ORNL-5545
F 019	EVALUATION	EVAL-PROG	NDG		DOE-NDC-15		176	479	ORL	FU+EVAL FOR ENDF/B-V.NDG.
F 019	N, PROTON	EXPT-PROG	FAST		DOE-NDC-15		11	479	ANL	SMITH+ACT.HL GVN.CS GRPH.
F 019	N,ALPHA REAC	EXPT-PROG	FAST		DOE-NDC-15		11	479	ANL	SMITH+ACT.HL GVN.NDG.ANAL TBC.
NA 023	EVALUATION	EVAL-PROG	NDG		DOE-NDC-15		176	479	ORL	FU+EVAL FOR ENDF/B-V.NDG.
NA 023	NONEL GAMMAS	EXPT-PROG	20+5	20+7	DOE-NDC-15		164	479	ORL	LARSON+125 DEG.NDG.CFD CALC.TBP NSE
NA 023	NEUT EMISSN	EVAL-PROG	NDG		DOE-NDC-15		176	479	ORL	FU+ENDF/B-V CFD EXPT.SEE ORNL-TM6637
MG	EVALUATION	EVAL-PROG	NDG		DOE-NDC-15		176	479	ORL	FU+EVAL FOR ENDF/B-V.NDG.

ELEMENT S	A	QUANTITY	TYPE	ENERGY MIN	MAX	DOCUMENTATION REF	VOL	PAGE	DATE	LAB	COMMENTS
MG		TOTAL XSECT	EXPT-PROG	90+3	39+7	DOE-NDC-15		166	479	ORL	LARSON+TRNS.NDG.ABST ORNL-TM-6420
MG		NEUT EMISSN	EVAL-PROG	15+7		DOE-NDC-15		176	479	ORL	FU+ENDF/B-V CFD EXPT.SEE ORNL-TM6637
MG		N,ALPHA REAC	EXPT-PROG	14+7	15+7	DOE-NDC-15		119	479	LAS	REEDY.MASS SPEC.3 CS AT 2 ES GVN.
AL	027	INELST GAMMA	EXPT-PROG	11+6	25+6	DOE-NDC-15		5	479	ANL	SMITH.8 ES.ANGDIST.CFD EXPT,CALC.NDG
AL	027	NXN REACTION	THEO-PROG	14+7		DOE-NDC-15		175	479	ORL	FU+(N,XN) H-F CALC.CFD EXPT.NDG.TBP.
AL	027	NEUT EMISSN	EVAL-PROG	15+7		DOE-NDC-15		176	479	ORL	FU+ENDF/B-V CFD EXPT.SEE ORNL-TM6637
AL	027	N, PROTON	EVAL-PROG	NDG		DOE-NDC-15		131	479	LAS	STEWART+VERSION 4 CARRIED OVER ENDF5
AL	027	N, PROTON	THEO-PROG	14+7		DOE-NDC-15		175	479	ORL	FU+(N,XP) H-F CALC.CFD EXPT.NDG.TBP.
AL	027	N,ALPHA REAC	EVAL-PROG	NDG		DOE-NDC-15		131	479	LAS	STEWART+VERSION 4 CARRIED OVER ENDF5
AL	027	N,ALPHA REAC	THEO-PROG	14+7		DOE-NDC-15		175	479	ORL	FU+(N,XA) H-F CALC.CFD EXPT.NDG.TBP.
SI		EVALUATION	EVAL-PROG	NDG		DOE-NDC-15		176	479	ORL	FU+EVAL FOR ENDF/B-V.NDG.
SI		NEUT EMISSN	EVAL-PROG	15+7		DOE-NDC-15		176	479	ORL	FU+ENDF/B-V CFD EXPT.SEE ORNL-TM6637
SI	028	INELST GAMMA	EXPT-PROG	96+5	42+6	DOE-NDC-15		142	479	LTI	COUCHELL+125 DEG.ANGINTEG CALC.NDG.
CA		EVALUATION	EVAL-PROG	NDG		DOE-NDC-15		176	479	ORL	FU+EVAL FOR ENDF/B-V.NDG.
CA		NEUT EMISSN	EVAL-PROG	15+7		DOE-NDC-15		176	479	ORL	FU+ENDF/B-V CFD EXPT.SEE ORNL-TM6637
TI		NONEL GAMMAS	EXPT-PROG	10+6	20+7	DOE-NDC-15		168	479	ORL	MORGAN.130DEG.NDG.ABST ORNL-5544 TBP
TI		NXN REACTION	EXPT-PROG	10+6	20+7	DOE-NDC-15		168	479	ORL	MORGAN.130DEG.NDG.ABST ORNL-5544 TBP
TI		NEUT EMISSN	EVAL-PROG	15+7		DOE-NDC-15		176	479	ORL	FU+ENDF/B-V CFD EXPT.SEE ORNL-TM6637
TI	046	NXN REACTION	THEO-PROG	14+7		DOE-NDC-15		175	479	ORL	FU+(N,XN) H-F CALC.CFD EXPT.NDG TBP.
TI	046	NXN REACTION	THEO-PROG	14+7		DOE-NDC-15		175	479	ORL	FU+(N,XP) H-F CALC.CFD EXPT.NDG TBP.
TI	046	N,ALPHA REAC	THEO-PROG	14+7		DOE-NDC-15		175	479	ORL	FU+(N,XA) H-F CALC.CFD EXPT.NDG.TBP.
TI	048	NXN REACTION	THEO-PROG	14+7		DOE-NDC-15		175	479	ORL	FU+(N,XN) H-F CALC.CFD EXPT.NDG TBP.
TI	048	NXN REACTION	THEO-PROG	14+7		DOE-NDC-15		175	479	ORL	FU+(N,XP) H-F CALC.CFD EXPT.NDG TBP.
TI	048	N,ALPHA REAC	THEO-PROG	14+7		DOE-NDC-15		175	479	ORL	FU+(N,XA) H-F CALC.CFD EXPT.NDG.TBP.
V	051	NXN REACTION	THEO-PROG	14+7		DOE-NDC-15		175	479	ORL	FU+(N,XN) H-F CALC.CFD EXPT.NDG TBP.
V	051	NXN REACTION	THEO-PROG	14+7		DOE-NDC-15		175	479	ORL	FU+(N,XP) H-F CALC.CFD EXPT.NDG TBP.
V	051	NEUT EMISSN	EVAL-PROG	15+7		DOE-NDC-15		176	479	ORL	FU+ENDF/B-V CFD EXPT.SEE ORNL-TM6637
V	051	N,ALPHA REAC	THEO-PROG	14+7		DOE-NDC-15		175	479	ORL	FU+(N,XA) H-F CALC.CFD EXPT.NDG.TBP.

ELEMENT S A	QUANTITY	TYPE	ENERGY MIN	MAX	DOCUMENTATION REF	VOL	PAGE	DATE	LAB	COMMENTS
CR	TOTAL XSECT	EXPT-PROG	+5	50+6	DOE-NDC-15		3	479	ANL	SMITH+BROAD RESOL.NDG.ANAL TBD.
CR	DIFF ELASTIC	EXPT-PROG	+5	50+6	DOE-NDC-15		3	479	ANL	SMITH+50 KEV RESOL.NDG.ANAL TBD.
CR	DIFF INELAST	EXPT-PROG	+5	50+6	DOE-NDC-15		5	479	ANL	SMITH+50 KEV RESOL.NDG.ANAL TBD.
CR	INELST GAMMA	EXPT-PROG	84+5	40+6	DOE-NDC-15		142	479	LTI	COUCHELL+125 DEG.TOF.ANGINTEG.NDG.
CR	NEUT EMISSN	EVAL-PROG	15+7		DOE-NDC-15		176	479	ORL	FU+ENDF/B-V CFD EXPT.SEE ORNL-TM6637
CR	N, PROTON	EXPT-PROG	15+7		DOE-NDC-15		99	479	LRL	HAIGHT+TBP PR/C.CS=180+-25 MB.
CR	N, DEUTERON	EXPT-PROG	15+7		DOE-NDC-15		99	479	LRL	HAIGHT+TBP PR/C.CS=10+- 3MB.
CR	N,ALPHA REAC	EXPT-PROG	15+7		DOE-NDC-15		99	479	LRL	HAIGHT+TBP PR/C.CS=38+- 6 MB.
CR 050	DIFF INELAST	EXPT-PROG	84+5	40+6	DOE-NDC-15		142	479	LTI	COUCHELL+FROM CR DNG.NDG.ENDF NOT OK
CR 050	NXN REACTION	THEO-PROG	14+7		DOE-NDC-15		175	479	ORL	FU+(N,XP) H-F CALC.CFD EXPT.NDG TBP.
CR 050	NXN REACTION	THEO-PROG	14+7		DOE-NDC-15		175	479	ORL	FU+(N,XN) H-F CALC.CFD EXPT.NDG TBP.
CR 050	N, PROTON	EXPT-PROG	15+7		DOE-NDC-15		99	479	LRL	HAIGHT+TBP PR/C.CS=830+-100 MB.
CR 050	N, DEUTERON	EXPT-PROG	15+7		DOE-NDC-15		99	479	LRL	HAIGHT+TBP PR/C.CS=12+-4 MB.
CR 050	N,ALPHA REAC	EXPT-PROG	15+7		DOE-NDC-15		99	479	LRL	HAIGHT+TBP PR/C.CS=94+- 15 MB.
CR 050	N,ALPHA REAC	THEO-PROG	14+7		DOE-NDC-15		175	479	ORL	FU+(N,XA) H-F CALC.CFD EXPT.NDG.TBP.
CR 052	DIFF INELAST	EXPT-PROG	84+5	40+6	DOE-NDC-15		142	479	LTI	COUCHELL+FROM CR DNG.NDG.ENDF NOT OK
CR 052	NXN REACTION	THEO-PROG	14+7		DOE-NDC-15		175	479	ORL	FU+(N,XP) H-F CALC.CFD EXPT.NDG TBP.
CR 052	NXN REACTION	THEO-PROG	14+7		DOE-NDC-15		175	479	ORL	FU+(N,XN) H-F CALC.CFD EXPT.NDG TBP.
CR 052	N, PROTON	EXPT-PROG	FAST		DOE-NDC-15		11	479	ANL	SMITH+ACT.HL GVN CS GRPH.
CR 052	N, PROTON	EXPT-PROG	15+7		DOE-NDC-15		99	479	LRL	HAIGHT+TBP PR/C.CS=180+-25 MB.
CR 052	N, DEUTERON	EXPT-PROG	15+7		DOE-NDC-15		99	479	LRL	HAIGHT+TBP PR/C.CS=8+-3 MB
CR 052	N,ALPHA REAC	EXPT-PROG	15+7		DOE-NDC-15		99	479	LRL	HAIGHT+TBP PR/C.CS=36+- 6 MB.
CR 052	N,ALPHA REAC	THEO-PROG	14+7		DOE-NDC-15		175	479	ORL	FU+(N,XA) H-F CALC.CFD EXPT.NDG.TBP.
CR 053	DIFF INELAST	EXPT-PROG	84+5	40+6	DOE-NDC-15		142	479	LTI	COUCHELL+FROM CR DNG.NDG.ENDF NOT OK
CR 054	DIFF INELAST	EXPT-PROG	84+5	40+6	DOE-NDC-15		142	479	LTI	COUCHELL+FROM CR DNG.NDG.ENDF NOT OK
FE	EVALUATION	EVAL-PROG	NDG		DOE-NDC-15		176	479	ORL	FU+EVAL FOR ENDF/B-V.NDG.
FE	TOTAL XSECT	EXPT-PROG	50+5	50+7	DOE-NDC-15		166	479	ORL	LARSON+TRNS.ORELA.NDG.
FE	DIFF ELASTIC	EXPT-PROG	15+6	40+6	DOE-NDC-15		5	479	ANL	SMITH+50 KEV RESOL.ANGDIST.GRPHS.

ELEMENT S A	QUANTITY	TYPE	ENERGY MIN	MAX	DOCUMENTATION REF	VOL	PAGE	DATE	LAB	COMMENTS
FE	DIFF INELAST	EXPT-PROG	15+6	40+6	DOE-NDC-15		5	479	ANL	SMITH+50 KEV RESOL.ANGDIST.GRPHS.
FE	DIFF INELAST	EXPT-PROG	12+7	14+7	DOE-NDC-15		217	479	TNL	BEYERLE+2ES.CONTINUIM MEAS.NDG.TBC.
FE	INELST GAMMA	EXPT-PROG	90+5	39+6	DOE-NDC-15		139	479	LTI	COUCHELL+125 DEG.GRPH.TBP.
FE	NEUT EMISSN	EVAL-PROG	15+7		DOE-NDC-15		176	479	ORL	FU+ENDF/B-V CFD EXPT.SEE ORNL-TM6637
FE 054	DIFF ELASTIC	EXPT-PROG	10+7	12+7	DOE-NDC-15		210	479	TNL	BEYERLE+ANGDISTS.NDG.EXPT TBC.
FE 054	DIFF INELAST	EXPT-PROG	90+5	39+6	DOE-NDC-15		139	479	LTI	COUCHELL+TBP.4 LVLS FROM DNG.GRPH
FE 054	DIFF INELAST	EXPT-PROG	10+7	12+7	DOE-NDC-15		210	479	TNL	BEYERLE+ANGDISTS.NDG.EXPT TBC.
FE 054	DIFF INELAST	EXPT-PROG	59+6	10+7	DOE-NDC-15		217	479	TNL	BEYERLE+3ES.CONTINUIM MEAS.NDG
FE 054	NXN REACTION	THEO-PROG	14+7		DOE-NDC-15		175	479	ORL	FU+(N,XN) H-F CALC.CFD EXPT.NDG TBP.
FE 054	N, PROTON	THEO-PROG	14+7		DOE-NDC-15		175	479	ORL	FU+(N,XP) H-F CALC.CFD EXPT.NDG.TBP.
FE 054	N,ALPHA REAC	THEO-PROG	14+7		DOE-NDC-15		75	479	ORL	FU+(N,XA) H-F CALC.CFD EXPT.NDG.TBP.
FE 054	RESON PARAMS	EVAL-PROG	NDG		DOE-NDC-15		177	479	ORL	PEREY+ENDF/B-V.NDG.SEE ORNL-TM-6405
FE 056	TOTAL XSECT	EXPT-PROG	22+4	25+4	DOE-NDC-15		30	479	BNL	LIOU+TRNS.GRPH.24.37KEV CS GVN.GRPH
FE 056	DIFF ELASTIC	EXPT-PROG	10+7	12+7	DOE-NDC-15		210	479	TNL	BEYERLE+ANGDISTS.NDG.EXPT TBC.
FE 056	DIFF INELAST	EXPT-PROG	90+5	39+6	DOE-NDC-15		139	479	LTI	COUCHELL+TBP.12 LVLS FROM DNG.GRPH
FE 056	DIFF INELAST	EXPT-PROG	10+7	12+7	DOE-NDC-15		210	479	TNL	BEYERLE+ANGDISTS.NDG.EXPT TBC.
FE 056	DIFF INELAST	EXPT-PROG	59+6	10+7	DOE-NDC-15		217	479	TNL	BEYERLE+3ES.CONTINUIM MEAS.TOF SPEC.
FE 056	SCATTERING	EXPT-PROG	NDG		DOE-NDC-15		167	479	ORL	PEREY+HIGH RESOL SCT MEAS.RES.NDG.
FE 056	NXN REACTION	THEO-PROG	14+7		DOE-NDC-15		175	479	ORL	FU+(N,XN) H-F CALC.CFD EXPT.NDG TBP.
FE 056	N, PROTON	THEO-PROG	14+7		DOE-NDC-15		175	479	ORL	FU+(N,XP) H-F CALC.CFD EXPT.NDG.TBP.
FE 056	N,ALPHA REAC	THEO-PROG	14+7		DOE-NDC-15		75	479	ORL	FU+(N,XA) H-F CALC.CFD EXPT.NDG.TBP.
FE 056	RESON PARAMS	EXPT-PROG	24+4		DOE-NDC-15		30	479	BNL	LIOU+TRNS.27.85 EV RES.WN,RADIUS GVN
FE 056	RESON PARAMS	EVAL-PROG	NDG		DOE-NDC-15		177	479	ORL	PEREY+ENDF/B-V.NDG.SEE ORNL-TM-6405
FE 056	RESON PARAMS	EXPT-PROG		40+5	DOE-NDC-15		167	479	ORL	PEREY+HIGH RESOL SCT MEAS.NDG.
CO 059	DIFF INELAST	EXPT-PROG	11+6	33+6	DOE-NDC-15		143	479	LTI	COUCHELL+FROM DNG.19 LVLS.NDG.
CO 059	INELST GAMMA	EXPT-PROG	11+6	33+6	DOE-NDC-15		143	479	LTI	COUCHELL+TOF.GE-LI.NDG.DIN CALC.
NI	DIFF INELAST	EXPT-PROG	59+6	14+7	DOE-NDC-15		217	479	TNL	BEYERLE+2ES.CONTINUIM MEAS.NDG.TBC.
NI	NEUT EMISSN	EVAL-PROG	15+7		DOE-NDC-15		176	479	ORL	FU+ENDF/B-V CFD EXPT.SEE ORNL-TM6637

ELEMENT S A	QUANTITY	TYPE	ENERGY MIN	ENERGY MAX	DOCUMENTATION REF	VOL	PAGE	DATE	LAB	COMMENTS
NI 058	TOTAL XSECT	EXPT-PROG		12+5	DOE-NDC-15		167	479	ORL	PEREY+TRNS,CAPT.NDG.
NI 058	TOTAL XSECT	EXPT-PROG	20+3	14+4	DOE-NDC-15		166	479	ORL	HARVEY+THICK SAMPLE.3ES.NDG
NI 058	DIFF INELAST	EXPT-PROG	14+6	40+6	DOE-NDC-15		143	479	LTI	COUCHELL+FROM DNG.NDG.ENDF NOT OK.
NI 058	N, GAMMA	EXPT-PROG		12+5	DOE-NDC-15		167	479	ORL	PEREY+TRNS,CAPT.NDG.
NI 058	INELST GAMMA	EXPT-PROG	14+6	40+6	DOE-NDC-15		143	479	LTI	COUCHELL+125 DEG EXCIT FNS.NDG.TBP.
NI 058	NXN REACTION	THEO-PROG	14+7		DOE-NDC-15		175	479	ORL	FU+(N,XN) H-F CALC.CFD EXPT.NDG TBP.
NI 058	NXN REACTION	THEO-PROG	14+7		DOE-NDC-15		175	479	ORL	FU+(N,XP) H-F CALC.CFD EXPT.NDG TBP.
NI 058	N,ALPHA REAC	THEO-PROG	14+7		DOE-NDC-15		175	479	ORL	FU+(N,XA) H-F CALC.CFD EXPT.NDG.TBP.
NI 058	RESON PARAMS	EXPT-PROG		12+5	DOE-NDC-15		167	479	ORL	PEREY+TRNS,CAPT.NDG.
NI 060	TOTAL XSECT	EXPT-PROG	50+5	50+6	DOE-NDC-15		5	479	ANL	SMITH+50 KEV RESOL.NDG
NI 060	TOTAL XSECT	EXPT-PROG	20+3	14+4	DOE-NDC-15		166	479	ORL	HARVEY+THICK SAMPLE.3ES.NDG
NI 060	DIFF ELASTIC	EXPT-PROG	15+6	40+6	DOE-NDC-15		5	479	ANL	SMITH+50 KEV RESOL.ANGDIST.GRPHS.
NI 060	DIFF INELAST	EXPT-PROG	15+6	40+6	DOE-NDC-15		5	479	ANL	SMITH+6 Q VALS. ANGDIST.GRPHS.
NI 060	DIFF INELAST	EXPT-PROG	14+6	40+6	DOE-NDC-15		143	479	LTI	COUCHELL+FROM DNG.NDG.ENDF NOT OK.
NI 060	INELST GAMMA	EXPT-PROG	14+6	40+6	DOE-NDC-15		143	479	LTI	COUCHELL+125 DEG EXCIT FN.NDG.TBP
NI 060	NXN REACTION	THEO-PROG	14+7		DOE-NDC-15		175	479	ORL	FU+(N,XN) H-F CALC.CFD EXPT.NDG TBP.
NI 060	NXN REACTION	THEO-PROG	14+7		DOE-NDC-15		175	479	ORL	FU+(N,XP) H-F CALC.CFD EXPT.NDG TBP.
NI 060	N,ALPHA REAC	THEO-PROG	14+7		DOE-NDC-15		175	479	ORL	FU+(N,XA) H-F CALC.CFD EXPT.NDG.TBP.
NI 062	DIFF INELAST	EXPT-PROG	14+6	40+6	DOE-NDC-15		143	479	LTI	COUCHELL+FROM DNG.NDG.ENDF NOT OK.
NI 062	INELST GAMMA	EXPT-PROG	14+6	40+6	DOE-NDC-15		143	479	LTI	COUCHELL+125 DEG EXCIT FN.NDG.TBP
NI 064	DIFF INELAST	EXPT-PROG	14+6	40+6	DOE-NDC-15		143	479	LTI	COUCHELL+FROM DNG.NDG.ENDF NOT OK.
NI 064	INELST GAMMA	EXPT-PROG	14+6	40+6	DOE-NDC-15		143	479	LTI	COUCHELL+125 DEG EXCIT FN.NDG.TBP
CU	EVALUATION	EVAL-PROG	NDG		DOE-NDC-15		176	479	ORL	FU+EVAL FOR ENDF/B-V.NDG.
CU	TOTAL XSECT	EXPT-PROG	75+3		DOE-NDC-15		166	479	ORL	HARVEY+THICK SAMPLE.NDG
CU	DIFF INELAST	EXPT-PROG	12+7	14+7	DOE-NDC-15		217	479	TNL	BEYERLE+2ES.CONTINUIM MEAS.NDG.TBC.
CU	NONEL GAMMAS	EXPT-PROG	10+6	20+7	DOE-NDC-15		168	479	ORL	MORGAN+TOF.NDG.CFD.ABST ORNL-TM-5499
CU	NXN REACTION	EXPT-PROG	10+6	20+7	DOE-NDC-15		168	479	ORL	MORGAN+TOF.NDG.CFD.ABST ORNL-TM-5499
CU	NEUT EMISSN	EVAL-PROG	15+7		DOE-NDC-15		176	479	ORL	FU+ENDF/B-V CFD EXPT.SEE ORNL-TM6637

ELEMENT S A	QUANTITY	TYPE	ENERGY MIN	MAX	DOCUMENTATION REF	VOL	PAGE	DATE	LAB	COMMENTS
CU 063	SPECT N,GAMM	EXPT-PROG	NDG		DOE-NDC-15		40	479	BNL	CHRIEN+SPEC FOR TESTING NUCL MDL.NDG
CU 063	NXN REACTION	THEO-PROG	14+7		DOE-NDC-15		175	479	ORL	FU+(N,XP) H-F CALC.CFD EXPT.NDG TBP.
CU 063	NXN REACTION	THEO-PROG	14+7		DOE-NDC-15		175	479	ORL	FU+(N,XN) H-F CALC.CFD EXPT.NDG TBP.
CU 063	N,ALPHA REAC	EXPT-PROG	TR	10+7	DOE-NDC-15		10	479	ANL	WINKLER+REL U-238.ACT.NDG.TBC.
CU 063	N,ALPHA REAC	THEO-PROG	14+7		DOE-NDC-15		75	479	ORL	FU+(N,XA) H-F CALC.CFD EXPT.NDG.TBP.
CU 065	SPECT N,GAMM	EXPT-PROG	NDG		DOE-NDC-15		40	479	BNL	CHRIEN+SPEC FOR TESTING NUCL MDL.NDG
CU 065	NXN REACTION	THEO-PROG	14+7		DOE-NDC-15		175	479	ORL	FU+(N,XP) H-F CALC.CFD EXPT.NDG TBP.
CU 065	NXN REACTION	THEO-PROG	14+7		DOE-NDC-15		175	479	ORL	FU+(N,XN) H-F CALC.CFD EXPT.NDG TBP.
CU 065	N,ALPHA REAC	THEO-PROG	14+7		DOE-NDC-15		75	479	ORL	FU+(N,XA) H-F CALC.CFD EXPT.NDG.TBP.
ZN 064	TOTAL XSECT	EXPT-PROG	20+3	14+4	DOE-NDC-15		166	479	ORL	HARVEY+THICK SAMPLE.3ES.NDG
KR	TOTAL XSECT	EXPT-PROG		90+3	DOE-NDC-15		191	479	RPI	MAGUIRE+TRNS,TOF.RES PAR ANAL.CURV.
KR	N, GAMMA	EXPT-PROG		90+3	DOE-NDC-15		191	479	RPI	MAGUIRE+CAPT YLDS.GRPH.RES PAR ANAL
KR	RESON PARAMS	EXPT-PROG	28+1	84+3	DOE-NDC-15		191	479	RPI	MAGUIRE+TRNS,CAPT.TBL EO,WN,WG.
KR 078	TOTAL XSECT	EXPT-PROG		90+3	DOE-NDC-15		191	479	RPI	MAGUIRE+TRNS.TOF.RES PAR ANAL
KR 078	RES INT ABS	EXPT-PROG	20+1	12+3	DOE-NDC-15		191	479	RPI	MAGUIRE+RIA=20+-1B.CFD BNL 325.
KR 078	N, GAMMA	EXPT-PROG		90+3	DOE-NDC-15		191	479	RPI	MAGUIRE+CAPT YLDS.RES PAR ANAL
KR 078	RESON PARAMS	EXPT-PROG	11+2	84+3	DOE-NDC-15		191	479	RPI	MAGUIRE+TRNS,CAPT.TBL EO,WN,WG.
KR 080	TOTAL XSECT	EXPT-PROG		90+3	DOE-NDC-15		191	479	RPI	MAGUIRE+TRNS.TOF.RES PAR ANAL
KR 080	RES INT ABS	EXPT-PROG	20+1	12+3	DOE-NDC-15		191	479	RPI	MAGUIRE+RIA=56+-7B.CFD BNL 325.
KR 080	N, GAMMA	EXPT-PROG		90+3	DOE-NDC-15		191	479	RPI	MAGUIRE+CAPT YLDS.RES PAR ANAL
KR 080	RESON PARAMS	EXPT-PROG	89+1	84+3	DOE-NDC-15		191	479	RPI	MAGUIRE+TRNS,CAPT.TBL EO,WN,WG.
KR 082	RESON PARAMS	EXPT-PROG	40+1	81+3	DOE-NDC-15		191	479	RPI	MAGUIRE+TRNS,CAPT.TBL EO,WN,WG.
KR 083	RESON PARAMS	EXPT-PROG	28+1	64+3	DOE-NDC-15		191	479	RPI	MAGUIRE+TRNS,CAPT.TBL EO,WN,WG.
KR 084	RESON PARAMS	EXPT-PROG	12+2	64+2	DOE-NDC-15		191	479	RPI	MAGUIRE+TRNS,CAPT.TBL EO,WN,WG.
KR 086	RESON PARAMS	EXPT-PROG	12+2	64+2	DOE-NDC-15		191	479	RPI	MAGUIRE+TRNS,CAPT.TBL EO,WN,WG.
Y 088	N2N REACTION	EXPT-PROG	15+7		DOE-NDC-15		119	479	LAS	PRESTWOOD+14.8 MEV CS MEAS.NDG.
ZR 088	N2N REACTION	EXPT-PROG	15+7		DOE-NDC-15		119	479	LAS	PRESTWOOD+14.8 MEV CS MEAS.NDG.
ZR 088	N,N PROTON	EXPT-PROG	15+7		DOE-NDC-15		119	479	LAS	PRESTWOOD+14.8 MEV CS MEAS.NDG.

ELEMENT S A	QUANTITY	TYPE	ENERGY MIN	ENERGY MAX	DOCUMENTATION REF	VOL	PAGE	DATE	LAB	COMMENTS
ZR 090	N, PROTON	EXPT-PROG	15+7		DOE-NDC-15		99	479	LRL	HAIGHT+PRELIM MEAS.NDG.
ZR 090	N, DEUTERON	EXPT-PROG	15+7		DOE-NDC-15		99	479	LRL	HAIGHT+PRELIM MEAS.NDG.
ZR 090	N,ALPHA REAC	EXPT-PROG	15+7		DOE-NDC-15		99	479	LRL	HAIGHT+PRELIM MEAS.NDG.
NB 093	N, GAMMA	THEO-PROG	10+3	40+6	DOE-NDC-15		110	479	LRL	GARDNER+STATMDL CALC.NDG.TBC.
NB 093	SPECT N,GAMM	THEO-PROG	10+3	40+6	DOE-NDC-15		110	479	LRL	GARDNER+STATMDL CALC.NDG.TBC.
NB 093	NXN REACTION	THEO-PROG	14+7		DOE-NDC-15		175	479	ORL	FU+(N,XN) H-F CALC.CFD EXPT.NDG.TBP.
NB 093	NEUT EMISSN	EVAL-PROG	15+7		DOE-NDC-15		176	479	ORL	FU+ENDF/B-V CFD EXPT.SEE ORNL-TM6637
NB 093	N, PROTON	THEO-PROG	14+7		DOE-NDC-15		175	479	ORL	FU+(N,XP) H-F CALC.CFD EXPT.NDG.TBP.
NB 093	N,ALPHA REAC	THEO-PROG	14+7		DOE-NDC-15		175	479	ORL	FU+(N,XA) H-F CALC.CFD EXPT.NDG.TBP.
NB 094	N, GAMMA	THEO-PROG	10+3	40+6	DOE-NDC-15		110	479	LRL	GARDNER+STATMDL CALC.NDG.TBC.
NB 094	SPECT N,GAMM	THEO-PROG	10+3	40+6	DOE-NDC-15		110	479	LRL	GARDNER+STATMDL CALC.NDG.TBC.
NB 095	N, GAMMA	THEO-PROG	10+3	40+6	DOE-NDC-15		110	479	LRL	GARDNER+STATMDL CALC.NDG.TBC.
NB 095	SPECT N,GAMM	THEO-PROG	10+3	40+6	DOE-NDC-15		110	479	LRL	GARDNER+STATMDL CALC.NDG.TBC.
NB 095	RESON PARAMS	THEO-PROG	10+3	40+6	DOE-NDC-15		110	479	LRL	GARDNER+AVG WG/D CALC FROM G STF.NDG
NB 095	RESON PARAMS	THEO-PROG	10+3	40+6	DOE-NDC-15		110	479	LRL	GARDNER+AVG WG/D CALC FROM G STF.NDG
NB 095	RESON PARAMS	THEO-PROG	10+3	40+6	DOE-NDC-15		110	479	LRL	GARDNER+AVG WG/D CALC FROM G STF.NDG
MO	N, PROTON	EXPT-PROG	15+7		DOE-NDC-15		99	479	LRL	HAIGHT+PRELIM MEAS.NDG.
MO	N, DEUTERON	EXPT-PROG	15+7		DOE-NDC-15		99	479	LRL	HAIGHT+PRELIM MEAS.NDG.
MO	N,ALPHA REAC	EXPT-PROG	15+7		DOE-NDC-15		99	479	LRL	HAIGHT+PRELIM MEAS.NDG.
MO 092	N, PROTON	EXPT-PROG	15+7		DOE-NDC-15		99	479	LRL	HAIGHT+PRELIM MEAS.NDG.
MO 092	N, PROTON	EXPT-PROG	14+7	15+7	DOE-NDC-15		103	479	LRL	NAGLE.2ES,2ANGS.PRELIM CS GVN.REL AL
MO 092	N, DEUTERON	EXPT-PROG	15+7		DOE-NDC-15		99	479	LRL	HAIGHT+PRELIM MEAS.NDG.
MO 092	N,ALPHA REAC	EXPT-PROG	15+7		DOE-NDC-15		99	479	LRL	HAIGHT+PRELIM MEAS.NDG.
MO 092	N,ALPHA REAC	EXPT-PROG	14+7	15+7	DOE-NDC-15		103	479	LRL	NAGLE.2ES,2ANGS.PRELIM CS GVN.REL AL
MO 098	N,ALPHA REAC	EXPT-PROG	14+7	15+7	DOE-NDC-15		103	479	LRL	NAGLE.2ES,2ANGS.PRELIM CS GVN.REL AL
RU 100	N, GAMMA	EXPT-PROG		10+5	DOE-NDC-15		165	479	ORL	MACKLIN+CS MEAS.NDG.RES PAR ANAL TBD
RU 100	RESON PARAMS	EXPT-PROG		10+4	DOE-NDC-15		165	479	ORL	MACKLIN+CAPT.NDG.RESPAR ANAL TBD.
RU 100	STRNGTH FUNC	EXPT-PROG		10+4	DOE-NDC-15		165	479	ORL	MACKLIN+CAPT MEAS.STF TO BE CALC.NDG

ELEMENT S	A	QUANTITY	TYPE	ENERGY MIN	MAX	DOCUMENTATION REF	VOL	PAGE	DATE	LAB	COMMENTS
RU	101	N, GAMMA	EXPT-PROG		10+5	DOE-NDC-15		165	479	ORL	MACKLIN+CS MEAS.NDG.RES PAR ANAL TBD
RU	101	RESON PARAMS	EXPT-PROG		10+4	DOE-NDC-15		165	479	ORL	MACKLIN+CAPT.NDG.RESPAR ANAL TBD.
RU	101	STRNGTH FUNC	EXPT-PROG		10+4	DOE-NDC-15		165	479	ORL	MACKLIN+CAPT MEAS.STF TO BE CALC.NDG
RU	102	N, GAMMA	EXPT-PROG		10+5	DOE-NDC-15		165	479	ORL	MACKLIN+CS MEAS.NDG.RES PAR ANAL TBD
RU	102	RESON PARAMS	EXPT-PROG		10+4	DOE-NDC-15		165	479	ORL	MACKLIN+CAPT.NDG.RESPAR ANAL TBD.
RU	102	STRNGTH FUNC	EXPT-PROG		10+4	DOE-NDC-15		165	479	ORL	MACKLIN+CAPT MEAS.STF TO BE CALC.NDG
RU	104	N, GAMMA	EXPT-PROG		10+5	DOE-NDC-15		165	479	ORL	MACKLIN+CS MEAS.NDG.RES PAR ANAL TBD
RU	104	RESON PARAMS	EXPT-PROG		10+4	DOE-NDC-15		165	479	ORL	MACKLIN+CAPT.NDG.RESPAR ANAL TBD.
RU	104	STRNGTH FUNC	EXPT-PROG		10+4	DOE-NDC-15		165	479	ORL	MACKLIN+CAPT MEAS.STF TO BE CALC.NDG
PD	104	N, GAMMA	EXPT-PROG		10+5	DOE-NDC-15		165	479	ORL	MACKLIN+CS MEAS.NDG.RES PAR ANAL.
PD	104	RESON PARAMS	EXPT-PROG		10+4	DOE-NDC-15		165	479	ORL	MACKLIN+CAPT.RES PAR ANAL.NDG.
PD	104	STRNGTH FUNC	EXPT-PROG		10+4	DOE-NDC-15		165	479	ORL	MACKLIN+CAPT MEAS.STF OBTAINED.NDG
PD	105	N, GAMMA	EXPT-PROG		10+5	DOE-NDC-15		165	479	ORL	MACKLIN+CS MEAS.NDG.RES PAR ANAL.
PD	105	RESON PARAMS	EXPT-PROG		10+4	DOE-NDC-15		165	479	ORL	MACKLIN+CAPT.RES PAR ANAL.NDG.
PD	105	STRNGTH FUNC	EXPT-PROG		10+4	DOE-NDC-15		165	479	ORL	MACKLIN+CAPT MEAS.STF OBTAINED.NDG
PD	106	N, GAMMA	EXPT-PROG		10+5	DOE-NDC-15		165	479	ORL	MACKLIN+CS MEAS.NDG.RES PAR ANAL.
PD	106	RESON PARAMS	EXPT-PROG		10+4	DOE-NDC-15		165	479	ORL	MACKLIN+CAPT.RES PAR ANAL.NDG.
PD	106	STRNGTH FUNC	EXPT-PROG		10+4	DOE-NDC-15		165	479	ORL	MACKLIN+CAPT MEAS.STF OBTAINED.NDG
PD	108	N, GAMMA	EXPT-PROG		10+5	DOE-NDC-15		165	479	ORL	MACKLIN+CS MEAS.NDG.RES PAR ANAL.
PD	108	RESON PARAMS	EXPT-PROG		10+4	DOE-NDC-15		165	479	ORL	MACKLIN+CAPT.RES PAR ANAL.NDG.
PD	108	STRNGTH FUNC	EXPT-PROG		10+4	DOE-NDC-15		165	479	ORL	MACKLIN+CAPT MEAS.STF OBTAINED.NDG
PD	110	N, GAMMA	EXPT-PROG		10+5	DOE-NDC-15		165	479	ORL	MACKLIN+CS MEAS.NDG.RES PAR ANAL.
PD	110	RESON PARAMS	EXPT-PROG		10+4	DOE-NDC-15		165	479	ORL	MACKLIN+CAPT.RES PAR ANAL.NDG.
PD	110	STRNGTH FUNC	EXPT-PROG		10+4	DOE-NDC-15		165	479	ORL	MACKLIN+CAPT MEAS.STF OBTAINED.NDG
AG	107	TOTAL XSECT	EXPT-PROG	25+6	45+6	DOE-NDC-15		3	479	ANL	SMITH+10KEV INTERVALS.CFD CALC.NDG
AG	107	DIFF ELASTIC	EXPT-PROG	15+6	40+6	DOE-NDC-15		8	479	ANL	SMITH+GRPHS.CFD OPT-STAT MDL CALCS.
AG	107	DIFF INELAST	EXPT-PROG	15+6	40+6	DOE-NDC-15		8	479	ANL	SMITH+GRPHS.CFD OPT-STAT MDL CALCS.
AG	107	N, GAMMA	EXPT-PROG	16+1		DOE-NDC-15		32	479	BNL	LIOU+CAPT YLD 3 TEMPS.WG GVN

ELEMENT S	A	QUANTITY	TYPE	ENERGY MIN	MAX	DOCUMENTATION REF	VOL	PAGE	DATE	LAB	COMMENTS
AG	107	SPECT N,GAMM	EXPT-PROG	NDG		DOE-NDC-15		40	479	BNL	CHRIEN+SPEC FOR TESTING NUCL MDL.NDG
AG	107	RESON PARAMS	EXPT-PROG	16+1		DOE-NDC-15		32	479	BNL	LIOU+CAPT YLD 3 TEMPS.WG GVN
IN	115	N, GAMMA	EXPT-PROG	23+4	96+5	DOE-NDC-15		149	479	MHG	ENGDAHL+PRELIM MEAS.NDG.TBC.
SN	116	TOTAL XSECT	EXPT-PROG	20+5	50+6	DOE-NDC-15		68	479	KTY	HARPER+NDG.ANAL VIA.OPTMDL.
SN	116	DIFF ELASTIC	EXPT-PROG	10+6	40+6	DOE-NDC-15		68	479	KTY	HARPER+3ES.TOF.NDG.ANAL TBD.TBC 9MEV
SN	116	DIFF INELAST	EXPT-PROG	10+6	40+6	DOE-NDC-15		68	479	KTY	HARPER+3ES.TOF.NDG.ANAL TBD.TBC 9MEV
SN	118	TOTAL XSECT	EXPT-PROG	20+5	50+6	DOE-NDC-15		68	479	KTY	HARPER+NDG.ANAL VIA.OPTMDL.
SN	118	DIFF ELASTIC	EXPT-PROG	10+6	40+6	DOE-NDC-15		68	479	KTY	HARPER+3ES.TOF.NDG.ANAL TBD.TBC 9MEV
SN	118	DIFF INELAST	EXPT-PROG	10+6	40+6	DOE-NDC-15		68	479	KTY	HARPER+3ES.TOF.NDG.ANAL TBD.TBC 9MEV
SN	120	TOTAL XSECT	EXPT-PROG	20+5	50+6	DOE-NDC-15		68	479	KTY	HARPER+NDG.ANAL VIA.OPTMDL.
SN	120	DIFF ELASTIC	EXPT-PROG	10+6	40+6	DOE-NDC-15		68	479	KTY	HARPER+3ES.TOF.NDG.ANAL TBD.TBC 9MEV
SN	120	DIFF INELAST	EXPT-PROG	10+6	40+6	DOE-NDC-15		68	479	KTY	HARPER+3ES.TOF.NDG.ANAL TBD.TBC 9MEV
SN	122	TOTAL XSECT	EXPT-PROG	20+5	50+6	DOE-NDC-15		68	479	KTY	HARPER+NDG.ANAL VIA.OPTMDL.
SN	122	DIFF ELASTIC	EXPT-PROG	10+6	40+6	DOE-NDC-15		68	479	KTY	HARPER+3ES.TOF.NDG.ANAL TBD.TBC 9MEV
SN	122	DIFF INELAST	EXPT-PROG	10+6	40+6	DOE-NDC-15		68	479	KTY	HARPER+3ES.TOF.NDG.ANAL TBD.TBC 9MEV
SN	124	TOTAL XSECT	EXPT-PROG	20+5	50+6	DOE-NDC-15		68	479	KTY	HARPER+NDG.ANAL VIA.OPTMDL.
SN	124	DIFF ELASTIC	EXPT-PROG	10+6	40+6	DOE-NDC-15		68	479	KTY	HARPER+3ES.TOF.NDG.ANAL TBD.TBC 9MEV
SN	124	DIFF INELAST	EXPT-PROG	10+6	40+6	DOE-NDC-15		68	479	KTY	HARPER+3ES.TOF.NDG.ANAL TBD.TBC 9MEV
ND	150	DIFF INELAST	EXPT-PROG	NDG		DOE-NDC-15		69	479	KTY	TRIPATHI+DIN FROM DNG.TBL.CFD PRED.
ND	150	INELST GAMMA	EXPT-PROG	NDG		DOE-NDC-15		69	479	KTY	TRIPATHI+G SPEC.LVLS,DECAY SCH.
SM	147	SPECT N,GAMM	EXPT-PROG	NDG		DOE-NDC-15		40	479	BNL	CHRIEN+SPEC FOR TESTING NUCL MDL.NDG
SM	149	SPECT N,GAMM	EXPT-PROG	NDG		DOE-NDC-15		40	479	BNL	CHRIEN+SPEC FOR TESTING NUCL MDL.NDG
SM	152	DIFF INELAST	EXPT-PROG	NDG		DOE-NDC-15		69	479	KTY	TRIPATHI+DIN FROM DNG.TBL.CFD PRED.
SM	152	INELST GAMMA	EXPT-PROG	NDG		DOE-NDC-15		69	479	KTY	TRIPATHI+G SPEC.LVLS,DECAY SCH.
EU	151	SPECT N,GAMM	EXPT-PROG	NDG		DOE-NDC-15		40	479	BNL	CHRIEN+SPEC FOR TESTING NUCL MDL.NDG
HO	165	SPECT N,GAMM	EXPT-PROG	NDG		DOE-NDC-15		40	479	BNL	CHRIEN+SPEC FOR TESTING NUCL MDL.NDG
YB	171	SPECT N,GAMM	EXPT-PROG	NDG		DOE-NDC-15		40	479	BNL	CHRIEN+SPEC FOR TESTING NUCL MDL.NDG
YB	173	SPECT N,GAMM	EXPT-PROG	NDG		DOE-NDC-15		40	479	BNL	CHRIEN+SPEC FOR TESTING NUCL MDL.NDG

ELEMENT S	A	QUANTITY	TYPE	ENERGY MIN	MAX	DOCUMENTATION REF	VOL	PAGE	DATE	LAB	COMMENTS
TA	181	TOTAL XSECT	EXPT-PROG	40+4	48+6	DOE-NDC-15		1	479	ANL	POENITZ+TOF.PRELIM GRPH.TO BE ANAL.
W		NEUT EMISSN	EVAL-PROG	15+7		DOE-NDC-15		176	479	ORL	FU+ENDF/B-V CFD EXPT.SEE ORNL-TM6637
W	182	SPECT N,GAMM	EXPT-PROG	NDG		DOE-NDC-15		40	479	BNL	CHRIEN+SPEC FOR TESTING NUCL MDL.NDG
W	184	TOTAL XSECT	EXPT-PROG	16+2		DOE-NDC-15		166	479	ORL	HARVEY+THICK SAMPLE.NDG
OS	186	TOTAL XSECT	EXPT-PROG	20+2	30+5	DOE-NDC-15		165	479	ORL	WINTERS+NDG.FOR NUCLEOSYNTHESIS
OS	186	N, GAMMA	EXPT-PROG	+3		DOE-NDC-15		165	479	ORL	WINTERS+NDG.FOR NUCLEOSYNTHESIS
OS	187	TOTAL XSECT	EXPT-PROG	20+2	30+5	DOE-NDC-15		165	479	ORL	WINTERS+NDG.FOR NUCLEOSYNTHESIS
OS	187	DIFF INELAST	EXPT-PROG	24+4		DOE-NDC-15		165	479	ORL	WINTERS+TOF.NDG.TBD.NUCLEOSYNTHESIS
OS	187	N, GAMMA	EXPT-PROG	+3		DOE-NDC-15		165	479	ORL	WINTERS+NDG.FOR NUCLEOSYNTHESIS
OS	188	TOTAL XSECT	EXPT-PROG	20+2	30+5	DOE-NDC-15		165	479	ORL	WINTERS+NDG.FOR NUCLEOSYNTHESIS
OS	188	N, GAMMA	EXPT-PROG	+3		DOE-NDC-15		165	479	ORL	WINTERS+NDG.FOR NUCLEOSYNTHESIS
PT	195	SPECT N,GAMM	EXPT-PROG	NDG		DOE-NDC-15		40	479	BNL	CHRIEN+SPEC FOR TESTING NUCL MDL.NDG
AU	197	TOTAL XSECT	EXPT-PROG	40+4	48+6	DOE-NDC-15		1	479	ANL	POENITZ+TOF.PRELIM GRPH.TO BE ANAL.
PB		EVALUATION	EVAL-PROG	NDG		DOE-NDC-15		176	479	ORL	FU+EVAL FOR ENDF/B-V.NDG.
PB		NEUT EMISSN	EVAL-PROG	15+7		DOE-NDC-15		176	479	ORL	FU+ENDF/B-V CFD EXPT.SEE ORNL-TM6637
PB	206	TOTAL XSECT	EXPT-PROG	NDG		DOE-NDC-15		169	479	ORL	HOREN+TRNS,SCT.J,L,WN,EO,NDG
PB	206	SCATTERING	EXPT-PROG	NDG		DOE-NDC-15		169	479	ORL	HOREN+TRNS,SCT.J,L,WN,EO,NDG
PB	206	RESON PARAMS	EXPT-PROG		60+5	DOE-NDC-15		169	479	ORL	HOREN+HIGH RESOL TRNS,SCT.J,L,WN.NDG
PB	207	INELST GAMMA	EXPT-PROG	TR	50+6	DOE-NDC-15		10	479	ANL	WINKLER+.8SEC ISOM STATE CS.CFD.NDG
PB	208	N, GAMMA	THEO-PROG	60+6	16+7	DOE-NDC-15		108	479	LRL	DIETRICH+DSD,PRM MDL CALC CFD EXPT.
BI	209	TOTAL XSECT	EXPT-PROG	10+6	45+6	DOE-NDC-15		8	479	ANL	SMITH+CS MEAS.ANAL TBD.NDG.EVAL TBD
BI	209	DIFF ELASTIC	EXPT-PROG	10+6	45+6	DOE-NDC-15		8	479	ANL	SMITH+CS MEAS.ANAL TBD.NDG.EVAL TBD
BI	209	POLARIZATION	EXPT-PROG	20+6	45+6	DOE-NDC-15		226	479	YAL	AHMED+ASSYM MEAS.NDG.
BI	209	DIFF INELAST	EXPT-PROG	10+6	45+6	DOE-NDC-15		8	479	ANL	SMITH+CS MEAS.ANAL TBD.NDG.EVAL TBD
TH	232	TOTAL XSECT	EXPT-PROG	40+4	48+6	DOE-NDC-15		1	479	ANL	POENITZ+TOF.PRELIM GRPH.TO BE ANAL.
TH	232	TOTAL XSECT	EXPT-PROG	70+0	10+2	DOE-NDC-15		28	479	BNL	CHRIEN+TOT,CAPT.R-MATRIX.NDG
TH	232	TOTAL XSECT	THEO-PROG	10+4	10+7	DOE-NDC-15		130	479	LAS	MADLAND+CC OPTMDL CALC.CFD.NDG
TH	232	TOTAL XSECT	EXPT-PROG	60-3	18+1	DOE-NDC-15		195	479	RPI	LITTLE+TRNS,TOF.GRPH.NOT OK ENDF/B4.

25-Apr-79

ELEMENT S	A	QUANTITY	TYPE	ENERGY MIN	MAX	DOCUMENTATION REF VOL	PAGE	DATE	LAB	COMMENTS
TH	232	DIFF ELASTIC	EXPT-PROG	15+6	25+6	DOE-NDC-15	3	479	ANL	SMITH+TOF.20-160 DEG.ANAL TBD.TBC.
TH	232	DIFF INELAST	EXPT-PROG	15+6	25+6	DOE-NDC-15	3	479	ANL	SMITH+TOF.20-160 DEG.ANAL TBD.TBC.
TH	232	DIFF INELAST	EXPT-PROG	NDG		DOE-NDC-15	139	479	LTI	KEGEL+NDG.TBD.TO BE CFD DNG DATA.
TH	232	SCATTERING	EXPT-PROG	25-2		DOE-NDC-15	195	479	RPI	LITTLE+DRVD FROM TOT CS.CFD ENDF
TH	232	N, GAMMA	EXPT-PROG	30-2	15+1	DOE-NDC-15	28	479	BNL	CHRIEN+EPITHERMAL,THERMAL.GRPH.CS.
Th	232	N, GAMMA	EXPT-PROG	20+3	24+4	DOE-NDC-15	28	479	BNL	CHRIEN+ACT.4FBR.CS GVN FOR 2 ES.
TH	232	N, GAMMA	EXPT-PROG	NDG		DOE-NDC-15	149	479	MHG	ENGDAHL+ACT.NDG.EXPT.TBD.
TH	232	N, GAMMA	EXPT-PROG	26+3	80+5	DOE-NDC-15	169	479	ORL	DABBS+REVISED+UPDATED CS.NDG
TH	232	N, GAMMA	EXPT-PROG	25-2		DOE-NDC-15	195	479	RPI	LITTLE+DRVD FROM TOT CS.CFD ENDF
TH	232	INELST GAMMA	EXPT-PROG	85+5	21+6	DOE-NDC-15	139	479	LTI	KEGEL+125 DEG G PROD CS.NDG.ANAL TBD
TH	232	NONEL GAMMAS	EXPT-PROG	30+5	20+7	DOE-NDC-15	164	479	ORL	MORGAN+125 DEG.NDG.TBP ORNL-TM-6758
TH	232	FISSION	EXPT-PROG	+5	98+6	DOE-NDC-15	1	479	ANL	MEADOWS.TH 232/U235.NDG.ANAL TBD.
TH	232	FISSION	EXPT-PROG	60+5	10+6	DOE-NDC-15	170	479	ORL	PLATTARD+232-TH-NF/235-U-NF.NDG.CFD
TH	232	NUBAR,(NU)	EXPT-PROG	60+6	18+7	DOE-NDC-15	114	479	LRL	BERMAN+LINAC.NDG.TBP.TBL NU,GRPH NU.
TH	232	NUBAR,(NU)	EXPT-PROG	TR	30+7	DOE-NDC-15	104	479	LRL	HOWE.REL U235.NDG.
TH	232	FISS YIELD	EXPT-PROG	20+6	80+6	DOE-NDC-15	11	479	ANL	GLENDENIN+MASS YLD CURVS 6ES.CFD.
TH	232	FISS YIELD	EXPT-PROG	60+5	10+6	DOE-NDC-15	170	479	ORL	PLATTARD+FRAG ANISOTROPY MEAS.NDG.
TH	232	RESON PARAMS	EXPT-PROG	21+1	10+2	DOE-NDC-15	28	479	BNL	CHRIEN+TOT,CAPT.R-MATRIX.NDG
TH	232	PHOTO-FISSN	EXPT-PROG	60+6	18+7	DOE-NDC-15	114	479	LRL	BERMAN+LINAC.NDG.TBP.TBL NU,GRPH NU.
PA	229	FISSION	THEO-PROG	50+5	60+6	DOE-NDC-15	120	479	LAS	BRITT+CALC FROM HE3 FISS.NDG.TBP NSE
PA	230	FISSION	THEO-PROG	50+5	60+6	DOE-NDC-15	120	479	LAS	BRITT+CALC FROM HE3 FISS.NDG.TBP NSE
PA	231	FISSION	THEO-PROG	50+5	60+6	DOE-NDC-15	120	479	LAS	BRITT+CALC FROM HE3 FISS.NDG.TBP NSE
PA	232	FISSION	THEO-PROG	50+5	60+6	DOE-NDC-15	120	479	LAS	BRITT+CALC FROM HE3 FISS.NDG.TBP NSE
U	230	FISSION	THEO-PROG	50+5	60+6	DOE-NDC-15	120	479	LAS	BRITT+CALC FROM HE3 FISS.NDG.TBP NSE
U	231	FISSION	THEO-PROG	50+5	60+6	DOE-NDC-15	120	479	LAS	BRITT+CALC FROM HE3 FISS.NDG.TBP NSE
U	233	EVALUATION	EVAL-PROG	10-2	20+7	DOE-NDC-15	131	479	LAS	STEWART+ENDF/B-V CS FILES.NDG
U	233	TOTAL XSECT	EXPT-PROG	40+4	48+6	DOE-NDC-15	1	479	ANL	POENITZ+TOF.PRELIM GRPH.TO BE ANAL.
U	233	TOTAL XSECT	THEO-PROG	10+4	10+7	DOE-NDC-15	130	479	LAS	MADLAND+CC OPTMDL CALC.CFD.NDG

ELEMENT S	A	QUANTITY	TYPE	ENERGY MIN	MAX	DOCUMENTATION REF VOL	PAGE	DATE	LAB	COMMENTS
U	233	DIFF ELASTIC	EXPT-PROG	15+6	25+6	DOE-NDC-15	3	479	ANL	SMITH+TOF.20-160 DEG.ANAL TBD.TBC.
U	233	DIFF INELAST	EXPT-PROG	15+6	25+6	DOE-NDC-15	3	479	ANL	SMITH+TOF.20-160 DEG.ANAL TBD.TBC.
U	233	FISSION	EXPT-PROG	23+4	96+5	DOE-NDC-15	145	479	MHG	ENGDAHL+2E.ABSOL FISS CS.ANAL TBD.
U	233	FISSION	EXPT-PROG		14+7	DOE-NDC-15	149	479	MHG	ENGDAHL+NDG.EXPT TBD.
U	233	FISS PROD GS	EXPT-PROG	MAXW		DOE-NDC-15	126	479	LAS	JURNEY+SPEC.CFD.NDG.SEE LA-7620-MS
U	234	FISSION	EXPT-PROG	NDG		DOE-NDC-15	169	479	ORL	DABBS+ORELA.NDG.SEE PUBLISHED PAPER.
U	235	TOTAL XSECT	EXPT-PROG	40+4	48+6	DOE-NDC-15	1	479	ANL	POENITZ+TOF.PRELIM GRPH.TO BE ANAL.
U	235	TOTAL XSECT	THEO-PROG	10+4	10+7	DOE-NDC-15	130	479	LAS	MADLAND+CC OPTMDL CALC.CFD.NDG
U	235	N2N REACTION	THEO-PROG	60+6	22+7	DOE-NDC-15	129	479	LAS	ARTHUR.GNASH CODE CALC OF SPEC.NDG.
U	235	NXN REACTION	THEO-PROG	60+6	22+7	DOE-NDC-15	129	479	LAS	ARTHUR.GNASH CALC.CS.N3N SPEC.NDG
U	235	FISSION	EVAL-PROG	10+5	20+7	DOE-NDC-15	24	479	ANL	POENITZ.CS GRPH.SEE ANL-NDM-15.
U	235	FISSION	EXPT-PROG	10+5	98+6	DOE-NDC-15	1	479	ANL	MEADOWS.PU239,242,TH 232 RATIOS.GRPH
U	235	FISSION	THEO-PROG	60+6	22+7	DOE-NDC-15	129	479	LAS	ARTHUR.GNASH CALC.GRPH.CFD.DATA.
U	235	FISSION	EXPT-PROG		14+7	DOE-NDC-15	149	479	MHG	ENGDAHL+NDG.EXPT TBD.
U	235	FISSION	EXPT-PROG	10+6	20+7	DOE-NDC-15	153	479	NBS	CARLSON+TOF.TBP.GRPH PRELIM RESULTS.
U	235	FISSION	EXPT-PROG	20+5	12+6	DOE-NDC-15	151	479	NBS	WASSON+VDG.ABSL CS.GRPH.CFD ENDF,OTH
U	235	FISSION	EXPT-PROG	FISS		DOE-NDC-15	158	479	NBS	GILLIAM+PRELIM.ISNF.NP237/U235=.510
U	235	FISSION	EXPT-PROG	NDG		DOE-NDC-15	169	479	ORL	DABBS+ORELA.NDG.SEE PR/C 18 P1328.
U	235	FISSION	EXPT-PROG	10+5	25+7	DOE-NDC-15	171	479	ORL	DIFILIPPO+U238/235.NDG.SEE NSE68 P43
U	235	FISSION	EXPT-PROG	60+5	10+6	DOE-NDC-15	170	479	ORL	PLATTARD+232-TH-NF/235-U-NF.NDG.CFD
U	235	FISSION	EXPT-PROG	10+0	10+5	DOE-NDC-15	197	479	RPI	BICKNELL+HEMISPH FISCH.GRPH.CFD ENDF
U	235	FISSION	EXPT-PROG	NDG		DOE-NDC-15	219	479	TNL	CUSSON+CALC CFD EXPT.NDG.TBP
U	235	NUBAR,(NU)	THEO-PROG	53+6		DOE-NDC-15	130	479	LAS	MADLAND+PROMPT SPEC CALC.GRPH.CFD.
U	235	NUBAR,(NU)	EXPT-PROG	60+6	18+7	DOE-NDC-15	114	479	LRL	BERMAN+LINAC.NDG.TBP.TBL NU,GRPH NU.
U	235	FISS PROD GS	EXPT-PROG	MAXW		DOE-NDC-15	126	479	LAS	JURNEY+SPEC.CFD.NDG.SEE LA-7620-MS
U	235	FISS PROD GS	EXPT-PROG	MAXW		DOE-NDC-15	171	479	ORL	DICKENS+SPEC.NDG.ABST ORNL-NUREG-39
U	235	FISS PROD BS	EXPT-PROG	MAXW		DOE-NDC-15	171	479	ORL	DICKENS+SPEC.NDG.ABST ORNL-NUREG-39
U	235	FISS YIELD	EXPT-PROG	NDG		DOE-NDC-15	40	479	BNL	CHRIEN+NFY FROM MASS SPEC.NDG.TBD.

ELEMENT S	A	QUANTITY	TYPE	ENERGY MIN	MAX	DOCUMENTATION REF VOL	PAGE	DATE	LAB	COMMENTS
U	235	FISS YIELD	EXPT-PROG	MAXW		DOE-NDC-15	185	479	BNW	REEDER+INDEP ISOM YLD RATIOS.NDG.TBD
U	235	RESON PARAMS	EXPT-PROG	NDG		DOE-NDC-15	169	479	ORL	DABBS+ORELA.NDG.SEE PR/C 18 P1328.
U	235	PHOTO-FISSN	EXPT-PROG	60+6	18+7	DOE-NDC-15	114	479	LRL	BERMAN+LINAC.NDG.TBP.TBL NU,GRPH NU.
U	236	SPECT N,GAMM	EXPT-PROG	NDG		DOE-NDC-15	40	479	BNL	CHRIEN+SPEC FOR TESTING NUCL MDL.NDG
U	236	SPECT N,GAMM	EXPT-PROG	20+3	24+4	DOE-NDC-15	36	479	BNL	CHRIEN+2 ES.STF FROM RES AVG SPEC.
U	236	FISSION	EXPT-PROG	NDG		DOE-NDC-15	219	479	TNL	CUSSON+CALC CFD EXPT.NDG.TBP
U	236	NUBAR,(NU)	EXPT-PROG	60+6	18+7	DOE-NDC-15	114	479	LRL	BERMAN+LINAC.NDG.TBP.TBL NU,GRPH NU.
U	236	STRNGTH FUNC	EXPT-PROG	20+3	24+4	DOE-NDC-15	36	479	BNL	CHRIEN+2 ES.SO,S1 FROM G RES SPEC.
U	236	PHOTO-FISSN	EXPT-PROG	60+6	18+7	DOE-NDC-15	114	479	LRL	BERMAN+LINAC.GRPH.TBP.TBL NU.GRPH NU
U	237	FISSION	EXPT-PROG	NDG		DOE-NDC-15	219	479	TNL	CUSSON+CALC CFD EXPT.NDG.TBP
U	238	TOTAL XSECT	EXPT-PROG	40+4	48+6	DOE-NDC-15	1	479	ANL	POENITZ+TOF.PRELIM GRPH.TO BE ANAL.
U	238	TOTAL XSECT	THEO-PROG	10+4	10+7	DOE-NDC-15	130	479	LAS	MADLAND+CC OPTMDL CALC.CFD.NDG
U	238	DIFF ELASTIC	EXPT-PROG	90+5	31+6	DOE-NDC-15	144	479	LTI	COUCHELL+TOF.ANGDISTS.NDG.CFD ENDF.
U	238	DIFF INELAST	EXPT-PROG	90+5	31+6	DOE-NDC-15	144	479	LTI	COUCHELL+TOF.ANGDIST.NDG.NOT OK ENDF
U	238	DIFF INELAST	EXPT-PROG	NDG		DOE-NDC-15	139	479	LTI	KEGEL+NDG.TBD.TO BE CFD DNG DATA.
U	238	DIFF INELAST	EXPT-PROG	NDG		DOE-NDC-15	165	479	ORL	OLSEN+FROM DNG.NDG.ABST ORNL-TM-6832
U	238	N, GAMMA	EXPT-PROG	50+3	10+5	DOE-NDC-15	172	479	ORL	PEREZ+STAT TESTS ON MEAS CS.NDG.TBP.
U	238	N, GAMMA	EXPT-PROG	67+0	81+1	DOE-NDC-15	197	479	RPI	BLOCK+NDG.SELF-INDIC.SEE NP-996 2/79
U	238	INELST GAMMA	EXPT-PROG	48+5	50+6	DOE-NDC-15	165	479	ORL	OLSEN+125DEG.NDG.ABST ORNL-TM-6832.
U	238	N2N REACTION	THEO-PROG	60+6	22+7	DOE-NDC-15	129	479	LAS	ARTHUR.GNASH CODE CALC OF SPEC.NDG.
U	238	NXN REACTION	THEO-PROG	60+6	22+7	DOE-NDC-15	129	479	LAS	ARTHUR.GNASH CALC.CS.N3N SPEC.NDG
U	238	FISSION	THEO-PROG	60+6	22+7	DOE-NDC-15	129	479	LAS	ARTHUR.GNASH CALC.GRPH.CFD.DATA.
U	238	FISSION	EXPT-PROG	10+5	25+7	DOE-NDC-15	171	479	ORL	DIFILIPPO+U238/235.NDG.SEE NSE68 P43
U	238	FISSION	EXPT-PROG	50+0	35+6	DOE-NDC-15	172	479	ORL	PEREZ+ORELA.NDG.ABST ORNL-TM-6788.
U	238	FISSION	EXPT-PROG	NDG		DOE-NDC-15	219	479	TNL	CUSSON+CALC CFD EXPT.NDG.TBP
U	238	NUBAR,(NU)	EXPT-PROG	60+6	18+7	DOE-NDC-15	114	479	LRL	BERMAN+LINAC.NDG.TBP.TBL NU,GRPH NU.
U	238	RESON PARAMS	EVAL-PROG	15+2	25+3	DOE-NDC-15	177	479	ORL	PEREY.5EO FROM COVARIANT MATRIX.NDG
U	238	RESON PARAMS	EXPT-PROG	50+0	20+5	DOE-NDC-15	172	479	ORL	PEREZ+ORELA.NDG.ABST ORNL-TM-6788.

25-Apr-79

.LEMENT S	A	QUANTITY	TYPE	ENERGY MIN	MAX	DOCUMENTATION REF VOL	PAGE	DATE	LAB	COMMENTS
	235	FISS YIELD	EXPT-PROG	MAXW		DOE-NDC-15	185	479	BNW	REEDER+INDEP ISOM YLD RATIOS.NDG.TBD
	235	RESON PARAMS	EXPT-PROG	NDG		DOE-NDC-15	169	479	ORL	DABBS+ORELA.NDG.SEE PR/C 18 P1328.
	235	PHOTO-FISSN	EXPT-PROG	60+6	18+7	DOE-NDC-15	114	479	LRL	BERMAN+LINAC.NDG.TBP.TBL NU,GRPH NU.
	236	SPECT N,GAMM	EXPT-PROG	NDG		DOE-NDC-15	40	479	BNL	CHRIEN+SPEC FOR TESTING NUCL MDL.NDG
	236	SPECT N,GAMM	EXPT-PROG	20+3	24+4	DOE-NDC-15	36	479	BNL	CHRIEN+2 ES.STF FROM RES AVG SPEC.
	236	FISSION	EXPT-PROG	NDG		DOE-NDC-15	219	479	TNL	CUSSON+CALC CFD EXPT.NDG.TBP
	236	NUBAR,(NU)	EXPT-PROG	60+6	18+7	DOE-NDC-15	114	479	LRL	BERMAN+LINAC.NDG.TBP.TBL NU,GRPH NU.
	236	STRNGTH FUNC	EXPT-PROG	20+3	24+4	DOE-NDC-15	36	479	BNL	CHRIEN+2 ES.S0,S1 FROM G RES SPEC.
	236	PHOTO-FISSN	EXPT-PROG	60+6	18+7	DOE-NDC-15	114	479	LRL	BERMAN+LINAC.GRPH.TBP.TBL NU.GRPH NU
	237	FISSION	EXPT-PROG	NDG		DOE-NDC-15	219	479	TNL	CUSSON+CALC CFD EXPT.NDG.TBP
	238	TOTAL XSECT	EXPT-PROG	40+4	48+6	DOE-NDC-15	1	479	ANL	POENITZ+TOF.PRELIM GRPH.TO BE ANAL.
	238	TOTAL XSECT	THEO-PROG	10+4	10+7	DOE-NDC-15	130	479	LAS	MADLAND+CC OPTMDL CALC.CFD.NDG
	238	DIFF ELASTIC	EXPT-PROG	90+5	31+6	DOE-NDC-15	144	479	LTI	COUCHELL+TOF.ANGDISTS.NDG.CFD ENDF.
	238	DIFF INELAST	EXPT-PROG	90+5	31+6	DOE-NDC-15	144	479	LTI	COUCHELL+TOF.ANGDIST.NDG.NOT OK ENDF
	238	DIFF INELAST	EXPT-PROG	NDG		DOE-NDC-15	139	479	LTI	KEGEL+NDG.TBD.TO BE CFD DNG DATA.
	238	DIFF INELAST	EXPT-PROG	NDG		DOE-NDC-15	165	479	ORL	OLSEN+FROM DNG.NDG.ABST ORNL-TM-6832
	238	N, GAMMA	EXPT-PROG	50+3	10+5	DOE-NDC-15	172	479	ORL	PEREZ+STAT TESTS ON MEAS CS.NDG.TBP.
	238	N, GAMMA	EXPT-PROG	67+0	81+1	DOE-NDC-15	197	479	RPI	BLOCK+NDG.SELF-INDIC.SEE NP-996 2/79
	238	INELST GAMMA	EXPT-PROG	48+5	50+6	DOE-NDC-15	165	479	ORL	OLSEN+125DEG.NDG.ABST ORNL-TM-6832.
	238	N2N REACTION	THEO-PROG	60+6	22+7	DOE-NDC-15	129	479	LAS	ARTHUR.GNASH CODE CALC OF SPEC.NDG.
	238	NXN REACTION	THEO-PROG	60+6	22+7	DOE-NDC-15	129	479	LAS	ARTHUR.GNASH CALC.CS.N3N SPEC.NDG
	238	FISSION	THEO-PROG	60+6	22+7	DOE-NDC-15	129	479	LAS	ARTHUR.GNASH CALC.GRPH.CFD.DATA.
	238	FISSION	EXPT-PROG	10+5	25+7	DOE-NDC-15	171	479	ORL	DIFILIPPO+U238/235.NDG.SEE NSE68 P43
	238	FISSION	EXPT-PROG	50+0	35+6	DOE-NDC-15	172	479	ORL	PEREZ+ORELA.NDG.ABST ORNL-TM-6788.
	238	FISSION	EXPT-PROG	NDG		DOE-NDC-15	219	479	TNL	CUSSON+CALC CFD EXPT.NDG.TBP
	238	NUBAR,(NU)	EXPT-PROG	60+6	18+7	DOE-NDC-15	114	479	LRL	BERMAN+LINAC.NDG.TBP.TBL NU,GRPH NU.
	238	RESON PARAMS	EVAL-PROG	15+2	25+3	DOE-NDC-15	177	479	ORL	PEREY.5EO FROM COVARIANT MATRIX.NDG
	238	RESON PARAMS	EXPT-PROG	50+0	20+5	DOE-NDC-15	172	479	ORL	PEREZ+ORELA.NDG.ABST ORNL-TM-6788.

:LEMENT S	A	QUANTITY	TYPE	ENERGY MIN	MAX	DOCUMENTATION REF	VOL	PAGE	DATE	LAE	COMMENTS
I	238	RESON PARAMS	EXPT-PROG	10+0	34+1	DOE-NDC-	15	197	479	RPI	BLOCK+NDG.SELF-INDIC.SEE NP-996 2/79
I	238	PHOTO-FISSN	EXPT-PROG	60+6	18+7	DOE-NDC-	15	114	479	LRL	BERMAN+LINAC.NDG.TBP.TEL NU.GRPH NU.
I	239	FISSION	EXPT-PROG	NDG		DOE-NDC-	15	219	479	TNL	CUSSON+CALC CFD EXPT.NDG.TBP
IP	232	FISSION	THEO-PROG	50+5	60+6	DOE-NDC-	15	120	479	LAS	BRITT+CALC FROM HE3 FISS.NDG.TBP NSE
IP	233	FISSION	THEO-PROG	50+5	60+6	DOE-NDC-	15	120	479	LAS	BRITT+CALC FROM HE3 FISS.NDG.TBP NSE
IP	234	FISSION	THEO-PROG	50+5	60+6	DOE-NDC-	15	120	479	LAS	BRITT+CALC FROM HE3 FISS.NDG.TBP NSE
IP	235	FISSION	THEO-PROG	50+5	60+6	DOE-NDC-	15	120	479	LAS	BRITT+CALC FROM HE3 FISS.NDG.TBP NSE
IP	236	FISSION	THEO-PROG	50+5	60+6	DOE-NDC-	15	120	479	LAS	BRITT+CALC FROM HE3 FISS.NDG.TBP NSE
IP	237	N, GAMMA	EXPT-PROG	10-2	40+5	DOE-NDC-	15	169	479	ORL	DABBS+NDG.DATA REDUCTION,ANAL TBD.
IP	237	FISSION	THEO-PROG	50+5	60+6	DOE-NDC-	15	120	479	LAS	BRITT+CALC FROM HE3 FISS.NDG.TBP NSE
IP	237	FISSION	EXPT-PROG	77+5	96+5	DOE-NDC-	15	145	479	MHG	ENGDAHL+5E.ABSOL FISS CS.NDG.TBD
IP	237	FISSION	EXPT-PROG		14+7	DOE-NDC-	15	145	479	MHG	ENGDAHL+NDG.EXPT TBD.
IP	237	FISSION	EXPT-PROG	10+6	20+7	DOE-NDC-	15	153	479	NBS	CARLSON+TOF.ANAL TBD.PRELIM CS GRPH.
IP	237	FISSION	EXPT-PROG	FISS		DOE-NDC-	15	158	479	NBS	GILLIAM+PRELIM.ISNF.NP237/U235=.510
IP	237	RESON PARAMS	EXPT-PROG	10-2	40+5	DOE-NDC-	15	169	479	ORL	DABBS+NDG.DATA REDUCTION,ANAL TBD.
IP	238	FISSION	THEO-PROG	50+5	60+6	DOE-NDC-	15	120	479	LAS	BRITT+CALC FROM HE3 FISS.NDG.TBP NSE
U	236	FISSION	THEO-PROG	50+5	60+6	DOE-NDC-	15	120	479	LAS	BRITT+CALC FROM HE3 FISS.NDG.TBP NSE
U	239	TOTAL XSECT	EXPT-PROG	40+4	48+6	DOE-NDC-	15	1	479	ANL	POENITZ+TOF.PRELIM GRPH.TO BE ANAL.
U	239	TOTAL XSECT	THEO-PROG	10+4	10+7	DOE-NDC-	15	130	479	LAS	MADLAND+CC OPTMDL CALC.CFD.NDG
U	239	FISSION	EXPT-PROG	10+5	98+6	DOE-NDC-	15	1	479	ANL	MEADOWS.PU 239/U235.GRPH.CFD OTH.
U	239	FISSION	EXPT-PROG		14+7	DOE-NDC-	15	149	479	MHG	ENGDAHL+NDG.EXPT TBD.
U	239	FISS PROD GS	EXPT-PROG	MAXW		DOE-NDC-	15	126	479	LAS	JURNEY+SPEC.CFD.NDG.SEE LA-7620-MS
U	239	FISS YIELD	EXPT-PROG	MAXW		DOE-NDC-	15	172	479	ORL	DICKENS+49 FISS PROD YLDS.NDG
U	239	FRAG SPECTRA	EXPT-PROG	27+5	96+5	DOE-NDC-	15	145	479	MHG	ENGDAHL+3E.ANGDISTR.TBL ANISOTROPY.
U	240	EVALUATION	EVAL-PROG	NDG		DOE-NDC-	15	176	479	ORL	FU+EVAL FOR ENDF/B-V.NDG.
U	240	TOTAL XSECT	EXPT-PROG	40+4	48+6	DOE-NDC-	15	1	479	ANL	POENITZ+TOF.PRELIM GRPH.TO BE ANAL.
U	240	DIFF ELASTIC	EXPT-PROG	15+6	25+6	DOE-NDC-	15	3	479	ANL	SMITH+TOF.20-160 DEG.ANAL TBD.TBC.
U	240	DIFF INELAST	EXPT-PROG	15+6	25+6	DOE-NDC-	15	3	479	ANL	SMITH+TOF.20-160 DEG.ANAL TBD.TBC.

LEMENT S	A	QUANTITY	TYPE	ENERGY MIN	MAX	DOCUMENTATION REF VOL	PAGE	DATE	LAB	COMMENTS
U	240	N, GAMMA	EXPT-PROG	NDG		DOE-NDC-15	169	479	ORL	DABBS+ORELA.NDG.SEE NSE 68 P125.
U	240	N, GAMMA	REVW-PROG	NDG		DOE-NDC-15	178	479	ORL	WESTON.RVW OF RESONANCE REGION.NDG
U	240	FISSION	REVW-PROG	NDG		DOE-NDC-15	178	479	ORL	WESTON.RVW OF RESONANCE REGION.NDG
U	240	F NEUT DELAY	EXPT-PROG	FAST		DOE-NDC-15	224	479	WAU	GRANT+SPEC MEAS.CFD PREV EXPT.NDG.
U	240	RESON PARAMS	REVW-PROG	NDG		DOE-NDC-15	178	479	ORL	WESTON.RVW OF RESONANCE REGION.NDG
U	241	EVALUATION	EVAL-PROG	NDG		DOE-NDC-15	176	479	ORL	FU+EVAL FOR ENDF/B-V.NDG.
U	241	N, GAMMA	EXPT-PROG	NDG		DOE-NDC-15	169	479	ORL	DABBS+ORELA.NDG.SEE NSE 68 P125.
U	241	N, GAMMA	REVW-PROG	NDG		DOE-NDC-15	178	479	ORL	WESTON.RVW OF RESONANCE REGION.NDG
U	241	FISSION	EXPT-PROG	NDG		DOE-NDC-15	169	479	ORL	DABBS+ORELA.NDG.SEE NSE 68 P125.
U	241	FISSION	REVW-PROG	NDG		DOE-NDC-15	178	479	ORL	WESTON.RVW OF RESONANCE REGION.NDG
U	241	FISS PROD GS	EXPT-PROG	MAXW		DOE-NDC-15	173	479	ORL	DICKENS+SPEC.NDG.SEE ORNL-NUREG-47.
U	241	FISS PROD BS	EXPT-PROG	MAXW		DOE-NDC-15	173	479	ORL	DICKENS+SPEC.NDG.SEE ORNL-NUREG-47.
U	241	FISS YIELD	EXPT-PROG	MAXW		DOE-NDC-15	174	479	ORL	DICKENS.17 FISS PROD YLDS.NDG.TBP.
U	241	RESON PARAMS	EXPT-PROG	NDG		DOE-NDC-15	169	479	ORL	DABBS+ORELA.NDG.SEE NSE 68 P125.
U	241	RESON PARAMS	REVW-PROG	NDG		DOE-NDC-15	178	479	ORL	WESTON.RVW OF RESONANCE REGION.NDG
U	242	EVALUATION	EVAL-PROG	10-5	20+7	DOE-NDC-15	132	479	LAS	MADLAND+ENDF/B-V EVAL.NDG.
U	242	DIFF ELASTIC	EXPT-PROG	57+5	15+6	DOE-NDC-15	120	479	LAS	DRAKE+10 ANGS.3ES.GRPH ANGDIST.
U	242	DIFF INELAST	EXPT-PROG	57+5	15+6	DOE-NDC-15	120	479	LAS	DRAKE+10 ANGS.3ES.GRPH ANGDIST.
U	242	N, GAMMA	EXPT-PROG	25-2		DOE-NDC-15	119	479	LAS	BENDT+G SPEC.2200 M/S SIG=18.5+-1B.
U	242	N, GAMMA	REVW-PROG	NDG		DOE-NDC-15	178	479	ORL	WESTON.RVW OF RESONANCE REGION.NDG
U	242	SPECT N,GAMM	EXPT-PROG	MAXW		DOE-NDC-15	119	479	LAS	BENDT+NA-I DET.SPEC GRPH.THR CS GVN.
U	242	FISSION	EXPT-PROG	40+5	98+6	DOE-NDC-15	1	479	ANL	MEADOWS.PU 242/U235.GRPH.CFD OTH.
U	242	FISSION	REVW-PROG	NDG		DOE-NDC-15	178	479	ORL	WESTON.RVW OF RESONANCE REGION.NDG
U	242	RESON PARAMS	REVW-PROG	NDG		DOE-NDC-15	178	479	ORL	WESTON.RVW OF RESONANCE REGION.NDG
U	244	SPECT N,GAMM	EXPT-PROG	NDG		DOE-NDC-15	40	479	BNL	CHRIEN+SPEC FOR TESTING NUCL MDL.NDG
M	238	FISSION	THEO-PROG	50+5	60+6	DOE-NDC-15	120	479	LAS	BRITT+CALC FROM HE3 FISS.NDG.TBP NSE
M	239	FISSION	THEO-PROG	50+5	60+6	DOE-NDC-15	120	479	LAS	BRITT+CALC FROM HE3 FISS.NDG.TBP NSE
M	240	FISSION	THEO-PROG	50+5	60+6	DOE-NDC-15	120	479	LAS	BRITT+CALC FROM HE3 FISS.NDG.TBP NSE

LEMENT S A	QUANTITY	TYPE	ENERGY MIN	ENERGY MAX	DOCUMENTATION REF VOL	PAGE	DATE	LAB	COMMENTS
M 241	FISSION	THEO-PROG	50+5	60+6	DOE-NDC-15	120	479	LAS	BRITT+CALC FROM HE3 FISS.NDG.TBP NSE
M 241	FISSION	EXPT-PROG	20-2	20+7	DOE-NDC-15	169	479	ORL	DABBS+ORELA.CFD EARLIER MEAS.NDG.
M 242	FISSION	THEO-PROG	50+5	60+6	DOE-NDC-15	120	479	LAS	BRITT+CALC FROM HE3 FISS.NDG.TBP NSE
M 242	FISSION	EXPT-PROG	10-2	20+7	DOE-NDC-15	104	479	LRL	BROWNE+RES PARS.SEE 78HARWEL.NDG.TBP
M 242	RESON PARAMS	EXPT-PROG	10-2	20+1	DOE-NDC-15	104	479	LRL	BROWNE+RES PARS.SEE 78HARWEL.NDG.TBP
M 243	FISSION	THEO-PROG	50+5	60+6	DOE-NDC-15	120	479	LAS	BRITT+CALC FROM HE3 FISS.NDG.TBP NSE
M 244	FISSION	THEO-PROG	50+5	60+6	DOE-NDC-15	120	479	LAS	BRITT+CALC FROM HE3 FISS.NDG.TBP NSE
M 240	FISSION	THEO-PROG	50+5	60+6	DOE-NDC-15	120	479	LAS	BRITT+CALC FROM HE3 FISS.NDG.TBP NSE
M 241	FISSION	THEO-PROG	50+5	60+6	DOE-NDC-15	120	479	LAS	BRITT+CALC FROM HE3 FISS.NDG.TBP NSE
M 242	FISSION	THEO-PROG	50+5	60+6	DOE-NDC-15	120	479	LAS	BRITT+CALC FROM HE3 FISS.NDG.TBP NSE
M 243	FISSION	THEO-PROG	50+5	60+6	DOE-NDC-15	120	479	LAS	BRITT+CALC FROM HE3 FISS.NDG.TBP NSE
M 245	FISSION	EXPT-PROG	10+0	10+5	DOE-NDC-15	200	479	RPI	BLOCK+GRPH.CFD OTH.IN JAPANESE.
M 245	FISSION	EXPT-PROG	10+0	10+5	DOE-NDC-15	200	479	RPI	NAKAGOME+FISCH.GRPH.CFD OTH EXPTS.
M 248	SPECT N,GAMM	EXPT-PROG	NDG		DOE-NDC-15	104	479	ILL	HOFF+G RAY,CONVERSION ELEC.SPEC.NDG
K 244	FISSION	THEO-PROG	50+5	60+6	DOE-NDC-15	120	479	LAS	BRITT+CALC FROM HE3 FISS.NDG.TBP NSE
K 245	FISSION	THEO-PROG	50+5	60+6	DOE-NDC-15	120	479	LAS	BRITT+CALC FROM HE3 FISS.NDG.TBP NSE
K 246	FISSION	THEO-PROG	50+5	60+6	DOE-NDC-15	120	479	LAS	BRITT+CALC FROM HE3 FISS.NDG.TBP NSE
K 247	FISSION	THEO-PROG	50+5	60+6	DOE-NDC-15	120	479	LAS	BRITT+CALC FROM HE3 FISS.NDG.TBP NSE
K 249	TOTAL XSECT	EXPT-PROG	NDG		DOE-NDC-15	169	479	ORL	DABBS+TRNS.NDG.
F 249	TOTAL XSECT	EXPT-PROG	NDG		DOE-NDC-15	169	479	ORL	DABBS+TRNS.NDG.
F 249	RESON PARAMS	EXPT-PROG	NDG		DOE-NDC-15	169	479	ORL	DABBS+TRNS.RES ANAL TBD.NDG.
F 252	FISSION	EXPT-PROG	10+0	10+5	DOE-NDC-15	197	479	RPI	BICKNELL+HEMISPH FISCH.NDG.
F 252	NUBAR,(NU)	EXPT-PROG	SPON		DOE-NDC-15	57	479	INL	SMITH+MN BATH TECHNIQUE.NDG.ANAL TBC
F 252	NUBAR,(NU)	EXPT-PROG	SPON		DOE-NDC-15	174	479	ORL	SPENCER+VAL GVN.SEE ORNL-TM-6805.
F 252	FISS YIELD	EXPT-PROG	SPON		DOE-NDC-15	53	479	INL	GEHRKE+SHORT HL FISS PROD.NDG.
S 248	FISSION	THEO-PROG	50+5	60+6	DOE-NDC-15	120	479	LAS	BRITT+CALC FROM HE3 FISS.NDG.TBP NSE
S 249	FISSION	THEO-PROG	50+5	60+6	DOE-NDC-15	120	479	LAS	BRITT+CALC FROM HE3 FISS.NDG.TBP NSE
S 250	FISSION	THEO-PROG	50+5	60+6	DOE-NDC-15	120	479	LAS	BRITT+CALC FROM HE3 FISS.NDG.TBP NSE

ELEMENT S	A	QUANTITY	TYPE	ENERGY MIN	MAX	DOCUMENTATION REF	VOL	PAGE	DATE	LAB	COMMENTS
MD	259	FISS YIELD	EXPT-PROG	SPON		DOE-NDC-15		117	479	LRL	WILD+MASS AND TOT KE DISTRIB.GRPH.
MD	259	FRAG SPECTRA	EXPT-PROG	SPON		DOE-NDC-15		117	479	LRL	WILD+MASS AND TOT KE DISTRIB.GRPH.
MANY		FISSION	THEO-PROG	50+5	60+6	DOE-NDC-15		120	479	LAS	BRITT+CALC FROM HE3 FISS.NDG.TBP NSE

REFERENCES

No.	Lab	Work Type	Reference	Emin (MeV)	Emax (MeV)	Author, Comments
			^{3}H(p,total scattering)t product yield			
1	LAS	Eval P	DOE-NDC-15 127 479	NDG		Hale+ NDG. NEW DATA INCLUDED IN ANALYS
			^{3}H(p,n)^{3}He product yield			
2	LAS	Eval P	DOE-NDC-15 127 479	NDG		Hale+ NDG. NEW DATA INCLUDED IN ANALYS.
			^{6}Li(p,e)^{3}He σ(E)			
3	LAS	Eval P	DOE-NDC-15 128 479	TR	2.5+0	Hale+ NDG. SEE HARWELL CONF.
			^{6}Li(p,^{3}He)a σ(E)			
4	ANL	Expt P	DOE-NDC-15 16 479	1.0-1	3.0+0	Elwyn+ CURV. PAPER IN PREPARATION.
			^{6}Li(p,^{3}He)a σ(E;θ)			
5	ANL	Expt P	DOE-NDC-15 16 479	1.0-1	3.0+0	Elwyn+ NDG. PAPER IN PREPARATION.
			^{88}Sr(p,x)γ σ(E)			
6	LRL	Expt P	DOE-NDC-15 105 479	3.0+0	+1	Dietrich+ NDG. GE(LI),NAI. CFD STAT MOD
			^{88}Sr(p,x)γ σ(E;E')			
7	LRL	Expt P	DOE-NDC-15 105 479	3.0+0	+1	Dietrich+ NDG. GE(LI),NAI. CFD STAT MOD
			^{89}Y(p,x)γ σ(E)			
8	LRL	Expt P	DOE-NDC-15 105 479	3.0+0	+1	Dietrich+ NDG. GE(LI),NAI. CFD STAT MOD
			^{89}Y(p,x)γ σ(E;E')			
9	LRL	Expt P	DOE-NDC-15 105 479	3.0+0	+1	Dietrich+ NDG. GE(LI),NAI. CFD STAT MOD
			^{88}Zr(p,x)γ σ(E)			
10	LRL	Expt P	DOE-NDC-15 105 479	3.0+0	+1	Dietrich+ NDG. GE(LI),NAI. CFD STAT MOD
			^{90}Zr(p,x)γ σ(E;E')			
11	LRL	Expt P	DOE-NDC-15 105 479	3.0+0	+1	Dietrich+ NDG. GE(LI),NAI. CFD STAT MOD
			^{151}Eu(p,inelastic)^{151}Eu partial σ(E;θ)			
12	LRL	Expt P	DOE-NDC-15 105 479	1.2+1		Lanier+ NDG. 30-140DEG. DED. DEFORM.
			^{152}Eu(p,inelastic)^{152}Eu partial σ(E;θ)			
13	LRL	Expt P	DOE-NDC-15 105 479	1.2+1		Lanier+ NDG. 30-140DEG. DED. DEFORM.
			^{153}Eu(p,inelastic)^{153}Eu partial σ(E;θ)			
14	LRL	Expt P	DOE-NDC-15 105 479	1.2+1		Lanier+ NDG. 30-140DEG. DED. DEFORM.
			^{154}Eu(p,inelastic)^{154}Eu partial σ(E;θ)			
15	LRL	Expt P	DOE-NDC-15 105 479	1.2+1		Lanier+ NDG. 30-140DEG. DED. DEFORM.
			^{234}U(p,fission)mass distribution σ(E)			
16	TNL	Expt P	DOE-NDC-15 219 479	6.5+0	1.4+1	Cusson+ NDG. FROM ENERGY CORRELATIONS.
			^{235}U(p,fission)mass distribution σ(E)			
17	TNL	Expt P	DOE-NDC-15 219 479	6.2+0	3.0+1	Cusson+ NDG. FROM ENERGY CORRELATIONS.
			^{236}U(p,fission)mass distribution σ(E)			
18	TNL	Expt P	DOE-NDC 15 219 479	6.2+0	3.0+1	Cusson+ NDG. FROM ENERGY CORRELATIONS.
			^{1}H(d,n+p)p polarization(E;θ)			
19	LAS	Expt P	DOE-NDC-15 125 479	1.6+1		Ohlsen+ NDG. KINET. INCOMP. DATA MEAS.
		Expt P	DOE-NDC-15 125 479	1.6+1		Ohlsen+ NDG. KINET. COMPLETE IN PROGRES
			^{2}H(d,^{3}He)n σ(E)			
20	LAS	Expt P	DOE-NDC-15 121 479	5.0-2	1.2-1	Jarmie+ NDG. UNDER CONSTRUCTION.
			^{2}H(d,p)t product yield			
21	LAS	Eval P	DOE-NDC-15 127 479	NDG		Hale+ NDG. NEW DATA INCLUDED IN ANALYS.

No.	Lab	Work Type	Reference	Emin (MeV)	Emax (MeV)	Author, Comments
^{2}H(d,p)t σ(E)						
22	LAS	Expt	P DOE-NDC-15 121 479	5.0-2	1.2-1	Jarmie+ NDG. UNDER CONSTRUCTION.
^{2}H(d,n)^{3}He product yield						
23	LAS	Eval	P DOE-NDC-15 127 479	NDG		Hale+ NDG. NEW DATA INCLUDED IN ANALYS.
^{4}He(d,total scattering)e σ(E;θ)						
24	LAS	Expt	P DOE-NDC-15 125 479	1.2+1	1.7+1	Brown+ NDG. SEE LA-7378-MS.
^{4}He(d,total scattering)e polarization(E;θ)						
25	LAS	Expt	P DOE-NDC-15 125 479	1.2+1	1.7+1	Brown+ NDG. VECTOR TENSOR. LA-7378-MS.
^{6}Li(d,α)α σ(E)						
26	ANL	Theo	P DOE-NDC-15 15 470	1.0-1	1.0+0	Elwyn+ NDG. WIGNER-EISENBUD FORMALISM.
^{6}Li(d,α)α σ(E;θ)						
27	ANL	Theo	P DOE-NDC-15 15 470	1.0-1	1.0+0	Elwyn+ NDG. WIGNER-EISENBUD FORMALISM.
^{6}Li(d,n+^{3}He)α σ(E)						
28	ANL	Expt	P DOE-NDC-15 16 479	1.0-1	8.0-1	Holland+ NDG. 10 TO 17 PRCT ACCURACY.
^{6}Li(d,n+^{3}He)α σ(E;θ)						
29	ANL	Expt	P DOE-NDC-15 16 479	1.0-1	8.0-1	Holland+ NDG. 10 TO 17 PRCT ACCURACY.
^{6}Li(d,n+^{3}He)α σ(E;E')						
30	ANL	Expt	P DOE-NDC-15 16 479	1.0-1	8.0-1	Holland+ NDG. COMPARED TO SIMPLE MODELS
^{6}Li(d,p)^{7}Li σ(E)						
31	ANL	Theo	P DOE-NDC-15 15 470	1.0-1	1.0+0	Elwyn+ NDG. WIGNER-EISENBUD FORMALISM.
^{6}Li(d,p)^{7}Li σ(E;θ)						
32	ANL	Theo	P DOE-NDC-15 15 470	1.0-1	1.0+0	Elwyn+ NDG. WIGNER-EISENBUD FORMALISM.
^{6}Li(d,n)^{7}Be σ(E)						
33	ANL	Theo	P DOE-NDC-15 15 470	1.0-1	1.0+0	Elwyn+ NDG. WIGNER-EISENBUD FORMALISM.
^{6}Li(d,n)^{7}Be σ(E;θ)						
34	ANL	Theo	P DOE-NDC-15 15 470	1.0-1	1.0+0	Elwyn+ NDG. WIGNER-EISENBUD FORMALISM.
^{2}H(t,α)n σ(E)						
35	LAS	Expt	P DOE-NDC-15 121 479	5.0-2	1.2-1	Jarmie+ NDG UNDER CONSTRUCTION.
^{3}H(t,α+n)n σ(E)						
36	LAS	Expt	P DOE-NDC-15 121 479	5.0-2	1.2-1	Jarmie+ NDG. UNDER CONSTRUCTION.
^{3}H(t,elastic)t σ(E)						
37	LAS	Eval	P DOE-NDC-15 127 479	2.0-2	2.0+0	Hale+ NDG. R-MATRIX ANALYSIS.
^{3}H(t,2n)α σ(E)						
38	LAS	Eval	P DOE-NDC-15 127 479	2.0-2	2.0+0	Hale+ CURV. R-MATRIX. CFD TO EXPTS.
^{4}He(t,p)^{6}He partial σ(E;θ)						
39	LAS	Expt	P DOE-NDC-15 190 479	2.3+1		Ajzenberg-Selove+ NDG. SEE PR/C 17,1283
^{6}Li(t,p)^{8}Li partial σ(E;θ)						
40	LAS	Expt	P DOE-NDC-15 190 479	2.3+1		Ajzenberg-Selove+ NDG. SEE PR/C 17,1283
^{7}Li(t,p)^{9}Li partial σ(E;θ)						
41	LAS	Expt	P DOE-NDC-15 190 479	2.3+1		Ajzenberg-Selove+ NDG. SEE PR/C 17,1283
^{9}Be(t,p)^{11}Be partial σ(E;θ)						
42	LAS	Expt	P DOE-NDC-15 190 479	2.3+1		Ajzenberg-Selove+ NDG. SEE PR/C 17,1283
^{10}B(t,p)^{12}B partial σ(E;θ)						
43	LAS	Expt	P DOE-NDC-15 190 479	2.3+1		Ajzenberg-Selove+ NDG. SEE PR/C 17,1283
^{11}B(t,p)^{13}B partial σ(E;θ)						
44	LAS	Expt	P DOE-NDC-15 190 479	2.3+1		Ajzenberg-Selove+ NDG. SEE PR/C 17,1283

No.	Lab	Work Type	Reference	Emin (MeV)	Emax (MeV)	Author, Comments
$^{12}C(t,p)^{14}C$ partial σ(E;θ)						
45	LAS	Expt P	DOE-NDC-15 190 479	2.3+1		Ajzenberg-Selove+ NDG. SEE PR/C 17,1283
$^{78}Se(t,^{3}He)^{78}As$ partial σ(E;θ)						
46	LAS	Expt P	DOE-NDC-15 190 479	2.3+1		Ajzenberg-Selove+ TBP. IN PHYS. REV. C
$^{80}Se(t,^{3}He)^{80}As$ partial σ(E;θ)						
47	LAS	Expt P	DOE-NDC-15 190 479	2.3+1		Ajzenberg-Selove+ TBP. IN PHYS. REV. C
$^{82}Se(t,^{3}He)^{82}As$ partial σ(E;θ)						
48	LAS	Expt P	DOE-NDC-15 190 479	2.3+1		Ajzenberg-Selove+ TBP. IN PHYS. REV. C
$^{122}Sn(t,^{3}He)^{122}In$ partial σ(E;θ)						
49	LAS	Expt P	DOE-NDC-15 190 479	2.3+1		Ajzenberg-Selove+ NDG. SEE PR C 17, 960
$^{124}Sn(t,^{3}He)^{124}In$ partial σ(E;θ)						
50	LAS	Expt P	DOE-NDC-15 190 479	2.3+1		Ajzenberg-Selove+ NDG. SEE PR C 17, 960
$^{3}He(^{3}He,total)$ σ(E)						
51	LAS	Expt P	DOE-NDC-15 125 479	1.8+1	2.4+1	Brown+ NDG. FROM CP YIELDS.
$^{3}He(^{3}He,x)p$ σ(E)						
52	LAS	Expt P	DOE-NDC-15 125 479	1.8+1	2.4+1	Brown+ NDG. MEASURED MOST CP YIELDS.
$^{3}He(^{3}He,x)d$ σ(E)						
53	LAS	Expt P	DOE-NDC-15 125 479	1.8+1	2.4+1	Brown+ NDG. MEASURED MOST CP YIELDS.
$^{3}He(^{3}He,x)t$ σ(E)						
54	LAS	Expt P	DOE-NDC-15 125 479	1.8+1	2.4+1	Brown+ NDG. MEASURED MOST CP YIELDS.
$^{3}He(^{3}He,x)^{3}He$ σ(E)						
55	LAS	Expt P	DOE-NDC-15 125 479	1.8+1	2.4+1	Brown+ NDG. MEASURED MOST CP YIELDS.
$^{3}He(^{3}He,2p)α$ σ(E)						
56	LAS	Expt P	DOE-NDC-15 125 479	1.8+1	2.4+1	Brown+ NDG. FROM CP YIELDS.
$^{3}He(^{3}He,x)α$ σ(E)						
57	LAS	Expt P	DOE-NDC-15 125 479	1.8+1	2.4+1	Brown+ NDG. MEASURED MOST CP YIELDS.
$^{6}Li(^{3}He,p+α)α$ σ(E)						
58	ANL	Expt P	DOE-NDC-15 16 479	4.0-1	2.0+0	Holland+ NDG. TBD. NORM. TO P0 PARTIAL
$^{6}Li(^{3}He,p+α)α$ σ(E;θ ,E')						
59	ANL	Expt P	DOE-NDC-15 16 479	4.0-1	2.0+0	Holland+ NDG. TOF. IN PROGRESS.
$^{6}Li(^{3}He,p)^{8}Be$ partial σ(E)						
60	ANL	Expt P	DOE-NDC-15 16 479	4.0-1	2.0+0	Holland+ NDG. P0. LAST YEARS WORK.
$^{229}Th(^{3}He,d+fission)$ σ(E)×factor						
61	LAS	Expt P	DOE-NDC-15 120 479	TR	+1	Britt+ NDG. SIMULATED (N,F)
$^{229}Th(^{3}He,t+fission)$ σ(E)×factor						
62	LAS	Expt P	DOE-NDC-15 120 479	TR	+1	Britt+ NDG. SIMULATED (N,F)
$^{231}Th(^{3}He,d+fission)$ σ(E)×factor						
63	LAS	Expt P	DOE-NDC-15 120 479	TR	+1	Britt+ NDG. SIMULATED (N,F)
$^{231}Th(^{3}He,t+fission)$ σ(E)×factor						
64	LAS	Expt P	DOE-NDC-15 120 479	TR	+1	Britt+ NDG. SIMULATED (N,F)
$^{230}Pa(^{3}He,d+fission)$ σ(E)×factor						
65	LAS	Expt P	DOE-NDC-15 120 479	TR	+1	Britt+ NDG. SIMULATED (N,F)
$^{230}Pa(^{3}He,t+fission)$ σ(E)×factor						
66	LAS	Expt P	DOE-NDC-15 120 479	TR	+1	Britt+ NDG. SIMULATED (N,F)
$^{232}U(^{3}He,d+fission)$ σ(E)×factor						
67	LAS	Expt P	DOE-NDC-15 120 479	TR	+1	Britt+ NDG. SIMULATED (N,F)

No.	Lab	Work Type	Reference	Emin (MeV)	Emax (MeV)	Author, Comments
	$^{232}U(^{3}He,t+fission)$ σ(E)×factor					
68	LAS	Expt P	DOE-NDC-15	120	479 TR	+1 Britt+ NDG. SIMULATED (N,F)
	$^{233}U(^{3}He,d+fission)$ σ(E)×factor					
69	LAS	Expt P	DOE-NDC-15	120	479 TR	+1 Britt+ NDG. SIMULATED (N,F)
	$^{234}U(^{3}He,d+fission)$ σ(E)×factor					
70	LAS	Expt P	DOE-NDC-15	120	479 TR	+1 Britt+ NDG. SIMULATED (N,F)
	$^{235}U(^{3}He,d+fission)$ σ(E)×factor					
71	LAS	Expt P	DOE-NDC-15	120	479 TR	+1 Britt+ NDG. SIMULATED (N,F)
	$^{236}U(^{3}He,d+fission)$ σ(E)×factor					
72	LAS	Expt P	DOE-NDC-15	120	479 TR	+1 Britt+ NDG. SIMULATED (N,F)
	$^{237}U(^{3}He,d+fission)$ σ(E)×factor					
73	LAS	Expt P	DOE-NDC-15	120	479 TR	+1 Britt+ NDG. SIMULATED (N,F)
	$^{236}Np(^{3}He,t+fission)$ σ(E)×factor					
74	LAS	Expt P	DOE-NDC-15	120	479 TR	+1 Britt+ NDG. SIMULATED (N,F)
	$^{238}Pu(^{3}He,d+fission)$ σ(E)×factor					
75	LAS	Expt P	DOE-NDC-15	120	479 TR	+1 Britt+ NDG. SIMULATED (N,F)
	$^{238}Pu(^{3}He,t+fission)$ σ(E)×factor					
76	LAS	Expt F	DOE-NDC-15	120	479 TR	+1 Britt+ NDG. SIMULATED (N,F)
	$^{239}Pu(^{3}He,d+fission)$ σ(E)×factor					
77	LAS	Expt P	DOE-NDC-15	120	479 TR	+1 Britt+ NDG. SIMULATED (N,F)
	$^{241}Pu(^{3}He,d+fission)$ σ(E)×factor					
78	LAS	Expt P	DOE-NDC-15	120	479 TR	+1 Britt+ NDG. SIMULATED (N,F)
	$^{241}Pu(^{3}He,t+fission)$ σ(E)×factor					
79	LAS	Expt P	DOE-NDC-15	120	479 TR	+1 Britt+ NDG. SIMULATED (N,F)
	$^{243}Pu(^{3}He,d+fission)$ σ(E)×factor					
80	LAS	Expt P	DOE-NDC-15	120	479 TR	+1 Britt+ NDG. SIMULATED (N,F)
	$^{243}Pu(^{3}He,t+fission)$ σ(E)×factor					
81	LAS	Expt P	DOE-NDC-15	120	479 TR	+1 Britt+ NDG. SIMULATED (N,F)
	$^{248}Cm(^{3}He,d+fission)$ σ(E)×factor					
82	LAS	Expt P	DOE-NDC-15	120	479 TR	+1 Britt+ NDG. SIMULATED (N,F)
	$^{248}Cm(^{3}He,t+fission)$ σ(E)×factor					
83	LAS	Expt P	DOE-NDC-15	120	479 TR	+1 Britt+ NDG. SIMULATED (N,F)
	$^{242}Cm(^{3}He,d+fission)$ σ(E)×factor					
84	LAS	Expt P	DOE-NDC-15	120	479 TR	+1 Britt+ NDG. SIMULATED (N,F)
	$^{242}Cm(^{3}He,t+fission)$ σ(E)×factor					
85	LAS	Expt P	DOE-NDC-15	120	479 TR	+1 Britt+ NDG. SIMULATED (N,F)
	$^{244}Bk(^{3}He,d+fission)$ σ(E)×factor					
86	LAS	Expt P	DOE-NDC-15	120	479 TR	+1 Britt+ NDG. SIMULATED (N,F)
	$^{244}Bk(^{3}He,t+fission)$ σ(E)×factor					
87	LAS	Expt P	DOE-NDC-15	120	479 TR	+1 Britt+ NDG. SIMULATED (N,F)
	$^{245}Bk(^{3}He,d+fission)$ σ(E)×factor					
88	LAS	Expt P	DOE-NDC-15	120	479 TR	+1 Britt+ NDG. SIMULATED (N,F)
	$^{246}Bk(^{3}He,d+fission)$ σ(E)×factor					
89	LAS	Expt P	DOE-NDC-15	120	479 TR	+1 Britt+ NDG. SIMULATED (N,F)

No.	Lab	Work Type	Reference	Emin (MeV)	Emax (MeV)	Author, Comments
$^{249}Cf(^{3}He,d+fission)$ σ(E)×factor						
90	LAS	Expt P	DOE-NDC-15 120 479	TR	+1	Britt+ NDG. SIMULATED (N,F)
$^{249}Cf(^{3}He,t+fission)$ σ(E)×factor						
91	LAS	Expt P	DOE-NDC-15 120 479	TR	+1	Britt+ NDG. SIMULATED (N,F)
$^{249}Cf(^{3}He,d+fission)$ σ(E)×factor						
92	LAS	Expt P	DOE-NDC-15 120 479	TR	+1	Britt+ NDG. SIMULATED (N,F)
$^{56}Fe(\alpha,n)^{59}Ni$ σ(E)						
93	KTY	Expt P	DOE-NDC-15 72 479	TR	6.5+0	Flynn+ CURV. 4PI DET. ALSO REACT. RATES
systematics(α,x)n σ(E)						
94	WAU	Expt P	DOE-NDC-15 224 479	TR	9.0+0	Grant+ LOW Z TRGTS. UNDER CONSTRUCTION.
$^{208}Pb(^{40}Ar,x)^{212m2}Bi$ product yield						
95	BRK	Expt P	DOE-NDC-15 88 479	NDG		Balsden+ NDG. POSSIBLE 9-MIN ISOMER.
$^{238}U(^{40}Ar,x)^{212m2}Bi$ product yield						
96	BRK	Expt P	DOE-NDC-15 88 479	NDG		Baisden+ NDG. POSSIBLE 9-MIN ISOMER.
$^{238}U(^{48}Ca,x)^{212m2}Bi$ product yield						
97	BRK	Expt P	DOE-NDC-15 88 479	NDG		Baisden+ NDG. POSSIBLE 9-MIN ISOMER.
$^{248}Cm(^{48}Ca,x)^{212m2}Bi$ product yield						
98	BRK	Expt P	DOE-NDC-15 88 479	NDG		Baisden+ NDG. POSSIBLE 9-MIN ISOMER.
$^{238}U(^{136}Xe,x)$ σ(E)						
99	BRK	Exth P	DOE-NDC-15 93 479	NDG		Otto+ SUPER-HEAVY .LE. 4.E-36 CM2
$^{238}U(^{136}Xe,x)^{212m2}Bi$ product yield						
100	BRK	Expt P	DOE-NDC-15 88 479	NDG		Baisden+ NDG. POSSIBLE 9-MIN ISOMER.

Target	Inc	Emin (MeV)	Emax (MeV)	Lab	W	Author	No.
			γ σ(E)				
^{88}Sr	p	3.0+0	+1	LRL	E	Dietrich+	6
^{89}Y	p	3.0+0	+1	LRL	E	Dietrich+	8
^{90}Zr	p	3.0+0	+1	LRL	E	Dietrich+	10
			γ σ(E;E')				
^{88}Sr	p	3.0+0	+1	LRL	E	Dietrich+	7
^{89}Y	p	3.0+0	+1	LRL	E	Dietrich+	9
^{90}Zr	p	3.0+0	+1	LRL	E	Dietrich+	11
			n σ(E)				
^{2}H	d	5.0-2	1.2-1	LAS	E	Jarmie+	20
^{2}H	t	5.0-2	1.2-1	LAS	E	Jarmie+	35
^{3}H	t	5.0-2	1.2-1	LAS	E	Jarmie+	36
Many	α	TR	9.0+0	HAU	E	Grant+	94
			p σ(E)				
^{3}He	^{3}He	1.8+1	2.4+1	LAS	E	Brown+	52
			p polarization(E;θ)				
^{1}H	d	1.6+1		LAS	E	Ohlsen+	19
			d σ(E)				
^{3}He	^{3}He	1.8+1	2.4+1	LAS	E	Brown+	53
			t product yield				
^{2}H	d	NDG		LAS	D	Hale+	21
^{3}H	p	NDG		LAS	D	Hale+	1
			t σ(E)				
^{2}H	d	5.0-2	1.2-1	LAS	E	Jarmie+	22
^{3}H	t	2.0-2	2.0+0	LAS	D	Hale+	37
^{3}He	^{3}He	1.8+1	2.4+1	LAS	E	Brown+	54
			^{3}He product yield				
^{2}H	d	NDG		LAS	D	Hale+	23
^{3}H	p	NDG		LAS	D	Hale+	2
			^{3}He σ(E)				
^{3}He	^{3}He	1.8+1	2.4+1	LAS	E	Brown+	55
^{6}Li	p	TR	2.5+0	LAS	D	Hale+	3
			α σ(E)				
^{3}H	t	2.0-2	2.0+0	LAS	D	Hale+	38
^{3}He	^{3}He	1.8+1	2.4+1	LAS	E	Brown+	56

Target	Inc	Emin (MeV)	Emax (MeV)	Lab	W	Author	No.
			α σ(E)				
^{3}He	^{3}He	1.8+1	2.4+1	LAS	E	Brown+	57
^{6}Li	p	1.0-1	3.0+0	ANL	E	Elwyn+	4
^{6}Li	d	1.0-1	1.0+0	ANL	T	Elwyn+	26
^{6}Li	d	1.0-1	8.0-1	ANL	E	Holland+	28
^{6}Li	^{3}He	4.0-1	2.0+0	ANL	E	Holland+	58
			α σ(E;θ)				
^{4}He	d	1.2+1	1.7+1	LAS	E	Brown+	24
^{6}Li	p	1.0-1	3.0+0	ANL	E	Elwyn+	5
^{6}Li	d	1.0-1	1.0+0	ANL	T	Elwyn+	27
^{6}Li	d	1.0-1	8.0-1	ANL	E	Holland+	29
			α σ(E;θ,E')				
^{6}Li	^{3}He	4.0-1	2.0+0	ANL	E	Holland+	59
			α σ(E;E')				
^{6}Li	d	1.0-1	8.0-1	ANL	E	Holland+	30
			α polarization(E;θ)				
^{4}He	d	1.2+1	1.7+1	LAS	E	Brown+	25
			^{6}He partial σ(E;θ)				
^{4}He	t	2.3+1		LAS	E	Ajzenberg-Selove+	39
			^{7}Li σ(E)				
^{6}Li	d	1.0-1	1.0+0	ANL	T	Elwyn+	31
			^{7}Li σ(E;θ)				
^{6}Li	d	1.0-1	1.0+0	ANL	T	Elwyn+	32
			^{8}Li partial σ(E;θ)				
^{6}Li	t	2.3+1		LAS	E	Ajzenberg-Selove+	40
			^{9}Li partial σ(E;θ)				
^{7}Li	t	2.3+1		LAS	E	Ajzenberg-Selove+	41
			^{7}Be σ(E)				
^{6}Li	d	1.0-1	1.0+0	ANL	T	Elwyn+	33
			^{7}Be σ(E;θ)				
^{6}Li	d	1.0-1	1.0+0	ANL	T	Elwyn+	34
			^{8}Be partial σ(E)				
^{6}Li	^{3}He	4.0-1	2.0+0	ANL	E	Holland+	60

Target	Inc	Emin (MeV)	Emax (MeV)	Lab W	Author	No.
			^{11}Be partial e(E;e)			
^{9}Be	t	2.3+1		LAS E	Ajzenberg-Selove+	42
			^{12}B partial e(E;e)			
^{10}B	t	2.3+1		LAS E	Ajzenberg-Selove+	43
			^{13}B partial e(E;e)			
^{11}B	t	2.3+1		LAS E	Ajzenberg-Selove+	44
			^{14}C partial e(E;e)			
^{12}C	t	2.3+1		LAS E	Ajzenberg-Selove+	45
			^{59}Ni e(E)			
^{56}Fe	a	TR	6.5+0	KTY E	Flynn+	93
			^{78}As partial e(E;e)			
^{78}Se	t	2.3+1		LAS E	Ajzenberg-Selove+	46
			^{80}As partial e(E;e)			
^{80}Se	t	2.3+1		LAS E	Ajzenberg-Selove+	47
			^{82}As partial e(E;e)			
^{82}Se	t	2.3+1		LAS E	Ajzenberg-Selove+	48
			^{122}In partial e(E;e)			
^{122}Sn	t	2.3+1		LAS E	Ajzenberg-Selove+	49
			^{124}In partial e(E;e)			
^{124}Sn	t	2.3+1		LAS E	Ajzenberg-Selove+	50
			^{151}Eu partial e(E;e)			
^{151}Eu	p	1.2+1		LRL E	Lanier+	12
			^{152}Eu partial e(E;e)			
^{152}Eu	p	1.2+1		LRL E	Lanier+	13
			^{153}Eu partial e(E;e)			
^{153}Eu	p	1.2+1		LRL E	Lanier+	14
			^{154}Eu partial e(E;e)			
^{154}Eu	p	1.2+1		LRL E	Lanier+	15
			^{212m}Bi product yield			
^{208}Pb	^{40}Ar	NDG		BRK E	Baisden+	95
^{238}U	^{40}Ar	NDG		BRK E	Baisden+	96

Target	Inc	Emin (MeV)	Emax (MeV)	Lab W	Author	No.
			^{212m}Bi product yield			
^{238}U	^{48}Ca	NDG		BRK E	Baisden+	97
^{238}U	^{136}Xe	NDG		BRK E	Baisden+	100
^{248}Cm	^{48}Ca	NDG		BRK E	Baisden+	98

ARGONNE NATIONAL LABORATORY

A. NEUTRON PHYSICS

1. Systematics of Neutron Total Cross Sections of Heavy and Actinide Nuclei (W. Poenitz, J. Whalen and A. Smith)

Measurements of the total neutron cross sections of ^{181}Ta, ^{197}Au, ^{232}Th, ^{233}U, ^{235}U, ^{238}U, ^{239}Pu, and ^{240}Pu were made between 40 keV and 4.8 MeV. The experiment provided consistent data with usually $\lesssim 1\%$ statistical uncertainty. Numerous checks were applied to assure proper experimental procedures and to limit the systematic uncertainties at most energies to less than 0.5%. Therefore the remaining systematic uncertainty is mainly due to that associated with the sample mass and impurity. An exception is the low energy region where additional uncertainties are due to backgrounds associated with the white-spectra time-of-flight technique and the resonance self-shielding effect of the samples (corrections yet to be made). Preliminary results from the present measurements are shown in Fig. A-1. These data will be analyzed in terms of the optical model using coupled-channels calculations.

2. Fast-neutron Fission Cross Sections Relative to that of ^{235}U (J. W. Meadows)

a. Pu-239

The measurement of the $^{239}Pu/^{235}U$ fission-cross-section ratio has been completed over the energy range 0.1 to 9.8 MeV. The ratio of the sample masses was determined by; (1) low geometry alpha counting and (2) measurements of the relative thermal fission rates. Thus the sample assays depend on the ^{234}U and ^{239}Pu alpha half-lives and the ^{235}U and ^{239}Pu thermal-fission cross sections, respectively. The results are outlined in Fig. A-2.

b. Pu-242

The $^{242}Pu/^{235}U$ fission-cross-section ratio has been measured from near threshold to about 9.8 MeV. The sample masses were determined by low-geometry alpha counting. The ^{235}U sample was referenced to other ^{235}U samples that were spiked with small amounts of ^{234}U or ^{233}U

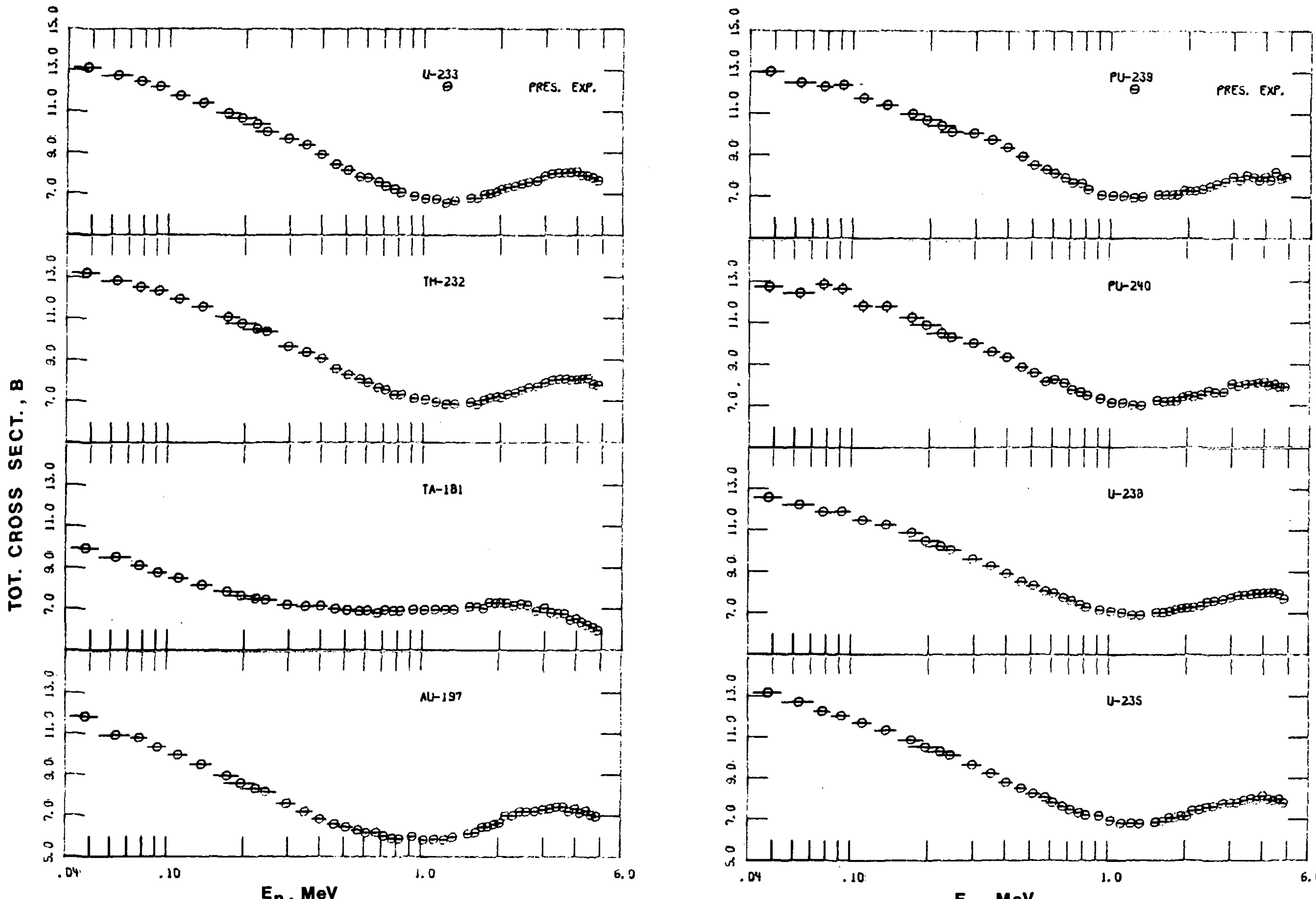

Fig. A-1. Measured Neutron Total Cross Sections. Data points indicate the present results.

and the mass is dependent on the half-lives of these isotopes. The ^{242}Pu sample was referenced to the ^{239}Pu half-life. The alpha-decay rate of ^{242}Pu was compared to ^{239}Pu using samples that were spiked with about 9% ^{239}Pu.[1] The results are outlined in Fig. 2A-2B.[1]

c. ^{232}Th

The $^{232}Th/^{235}U$ fission-cross section ratio has been measured from threshold to about 9.8 MeV using thorium samples spiked with about 0.5% ^{230}Th. The final results await the completion of the determination of the specific activity of the thorium-sample mixture.

3. Fast-neutron Scattering from the Actinides ^{232}Th, ^{233}U and ^{240}Pu (A. Smith, P. Guenther and G. Winkler)

Neutron elastic and inelastic scattering cross sections of ^{232}Th, ^{233}U and ^{240}Pu have been measured over the incident-energy region 1.5-2.5 MeV and the angular range 20-160 deg. Scattered-neutron flight paths of 5.4 and 20.0 m were employed to resolve the low-lying inelastic components from the elastically-scattered neutron groups. A number of inelastic neutron groups were observed in each case. The ^{232}Th results were processed in a routine manner. The ^{233}U and ^{240}Pu results involved the analysis of measurements made with very active canned samples. As a consequence, detailed attention was given to background effects and to the influence of the necessary containers. This included an extensive Monte-Carlo simulation of the experimental measurements. The measurements are continuing over a wider energy region with particular attention to the data requirements of the Th/U cycle.

4. Neutron Cross Sections of Structural Materials (A. Smith, P. Guenther, D. Smith and J. Whalen)

a. Elemental Chromium

Neutron total and scattering cross sections of elemental chromium have been measured from a few hundred keV to 5.0 MeV. Total cross sections were determined with broad resolution portraying intermediate resonance structure and with a variety of sample thicknesses

[1] J. W. Meadows, "The Alpha and Spontaneous Fission Half-Lives of ^{242}Pu," ANL/NDM-38, Argonne National Laboratory (1977).

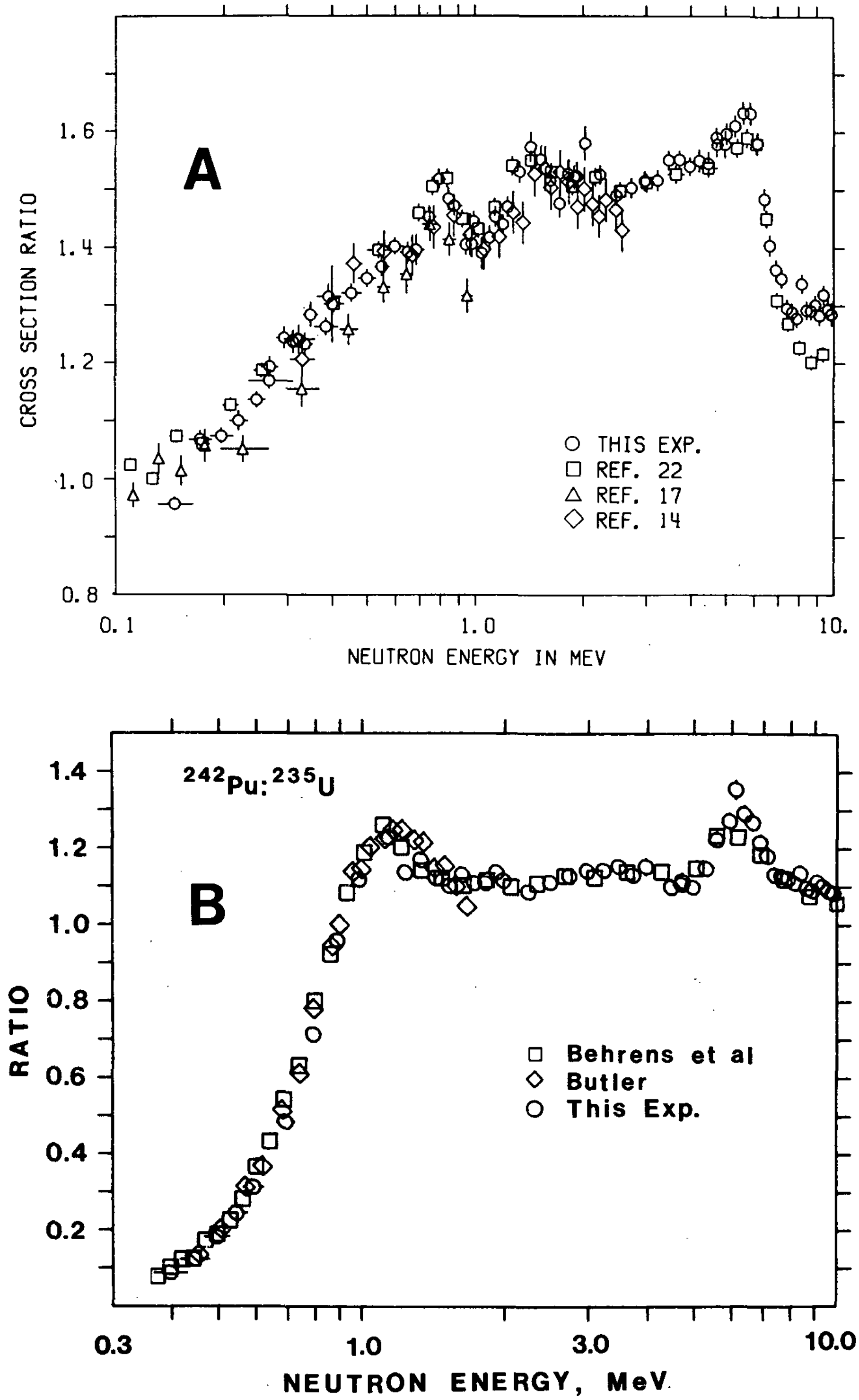

Fig. A-2. (A) The Pu-239/U-235 Fission Cross Section Ratio. Ref. 14 - Smirenkin, Nesterov and Bondarinko, 17 - Pfletschinger and Kaeppeler, and 22 - Carlson and Behrens.
(B) The Pu-242/U-235 Fission Cross Section Ratio.

permitting extrapolation to the thin sample limit. Scattering cross sections were measured at 50-keV incident-neutron-intervals in sufficient detail to follow the intermediate resonance fluctuations. The experimental results are now being analyzed in terms of optical and coupled-channels models.

b. Elemental Iron

Neutron elastic- and inelastic-scattering cross sections of elemental iron were measured from 1.5 to 4.0 MeV with incident-neutron resolutions of $\lesssim$50 keV and at incident-neutron energy intervals of $\lesssim$50 keV. Cross sections for the excitation of observed levels at 0.853, 1.389, 2.097, 2.579, 2.677, 2.974 and 3.152 MeV were determined. The observed elastic- and inelastic-scattering angular distributions strongly fluctuated with incident energy. The experimental results were averaged over broad energy intervals and interpreted in terms of spherical optical-statistical and coupled-channels models including consideration of direct-vibrational excitations. The importance of a comprehensive data base in such energy-averaged interpretations and of the direct-vibrational excitations is stressed. The present measured and calculated results, combined with those reported in literature, were used to formulate an evaluated scattered-neutron data file in the ENDF format extending from 1.0 to 4.0 MeV. Some illustrative results are shown in Fig. A-3.

c. The Interaction of Fast-neutrons with ^{60}Ni

Neutron total cross sections of ^{60}Ni were measured with broad resultion from $\sim$0.5 to 5.0 MeV at intervals of $\sim$50 keV. Differential elastic-neutron-scattering cross sections were measured from 1.5 to 4.0 MeV at intervals of $\lesssim$50 keV over the scattered-neutron angular range of $\sim$20-160 deg. Differential cross sections for the inelastic-neutron excitation states of 1.342 ± 0.013, 2.168 ± 0.010, 2.304 ± 0.026, 2.509 ± 0.072, 2.636 ± 0.019 and 3.164 ± 0.041 MeV were measured. The experimental results were interpreted in terms of optical-statistical and coupled-channels models including considerations of compound-nucleus fluctuations and direct-vibrational processes. Illustrative results are shown in Fig. A-4.

d. Measurement of Cross Sections for the ^{27}Al(n;n',γ)^{27}Al Reaction Near Threshold (D. L. Smith)

Cross-section ratios for production of 0.843-, 1.013- and 2.209-MeV gamma rays at 55 deg. by the ^{27}Al(n,n'γ)^{27}Al reaction relative

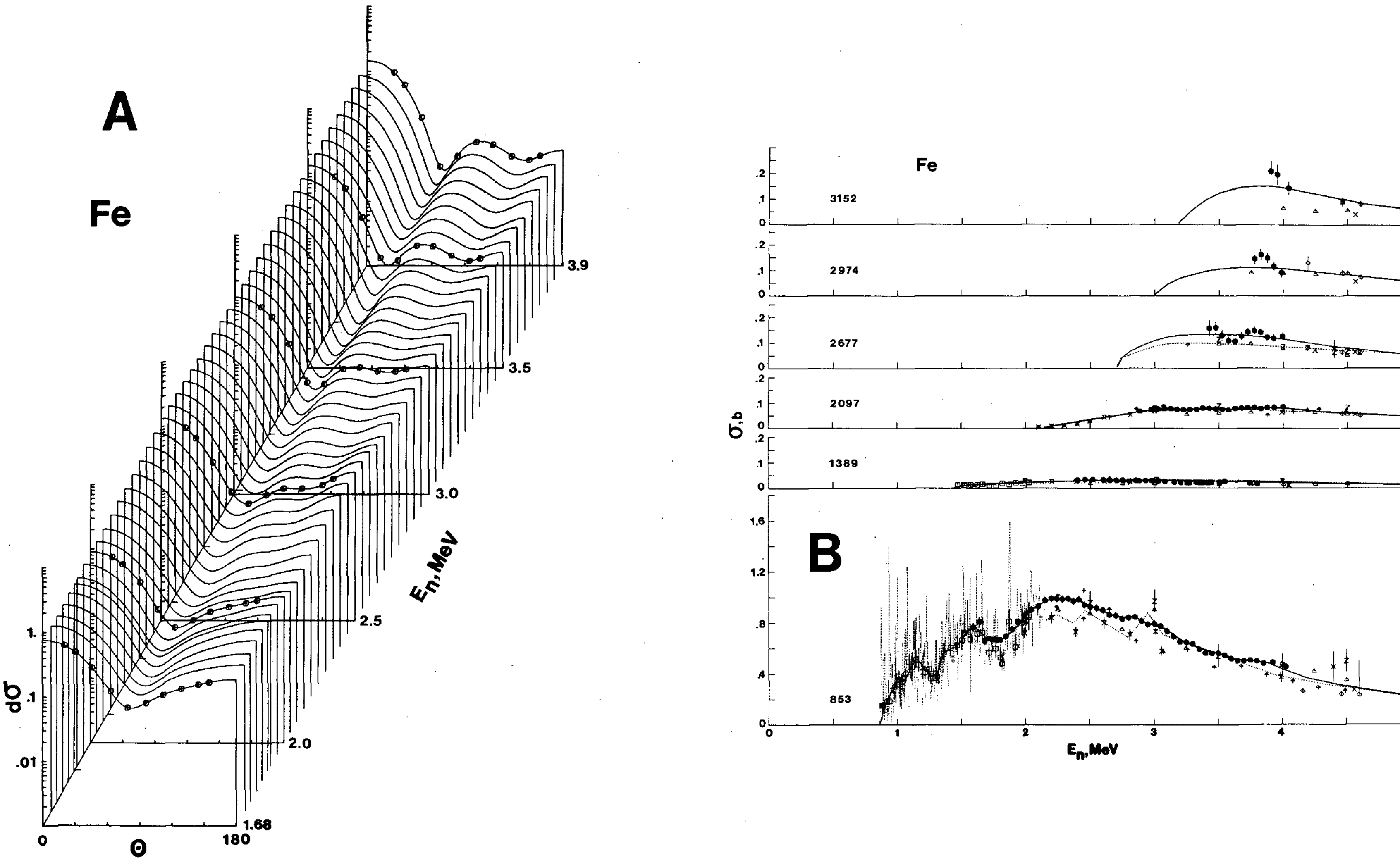

Fig. A-3. Measured Neutron Scattering Cross Sections of Elemental Iron. (A) - Elastic Scattering. (B) - Inelastic Scattering. Present results are indicated by solid data points and, for elastic-scattering, by curves.

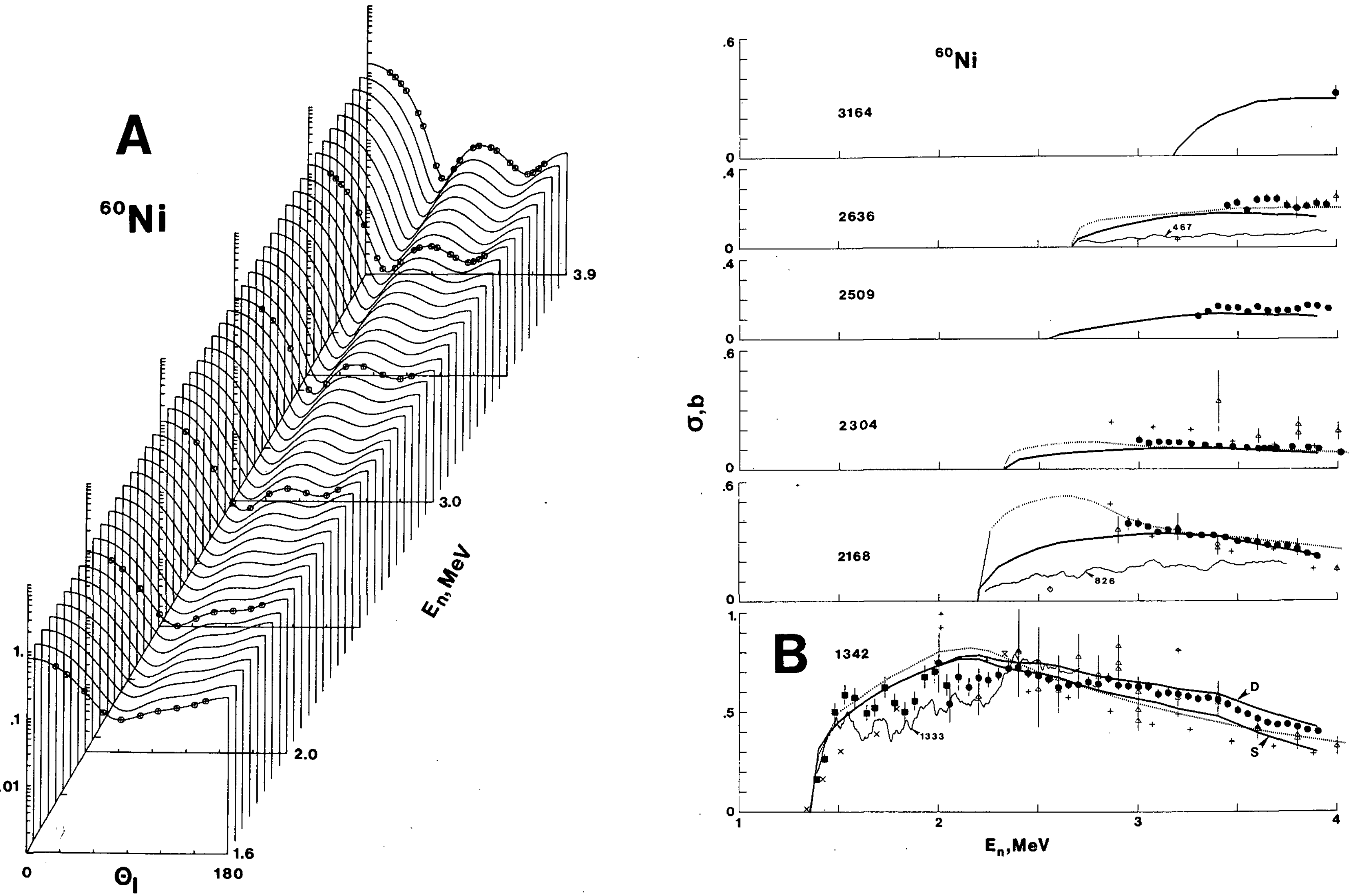

Fig. A-4. Neutron Scattering Cross Sections of Ni-60. (A) - Elastic Scattering. (B) - Inelastic Scattering. Present results are noted by solid data points and (for elastic scattering) by curves.

to fast neutron fission of ^{235}U have been measured at intervals of ∿0.05 MeV from threshold up to ∿2.5 MeV with an average neutron energy resolution of ∿0.08 MeV. These ratios and the ENDF/B-IV fission cross sections were used to compute gamma-ray production cross sections. Gamma-ray angular distributions were measured at E_n = 1.112, 1.310, 1.512, 1.714, 1.914, 2.118, 2.310, and 2.512 MeV. These distributions were found to be isotropic within the experimental errors. The experimental results were compared with data from the literature and with results from optical/statistical model calculations of neutron inelastic scattering from aluminum. Agreement with the energy-averaged data of Voss[1] is quite good with the exception of the 0.843-MeV gamma ray.

5. Neutron Cross Sections of Fission Products

a. Fast-neutron Total and Scattering Cross Section of ^{107}Ag in the MeV Region (A. Smith, P. Guenther, G. Winkler and J. Whalen)

Neutron total cross sections were measured from 0.25 to 4.5 MeV at intervals of $\lesssim$10 keV. Neutron differential elastic- and inelastic-scattering cross sections were measured from 1.5 to 4.0 MeV at intervals of ≤0.2 MeV. Cross sections for scattering into more than 20 energy groups were determined. Cross sections calculated from an optical-statistical model were in quantitative agreement with measured neutron total and elastic-scattering cross sections and in qualitative agreement with measured neutron inelastic-scattering cross sections. The interpretation of the observed neutron inelastic-scattering results was consistent with previously reported J^{π} assignments and systematics of nuclear-level densities. A significant dependence of the inelastic-scattering process on parity and/or deformation was not observed. Illustrative experimental results are given in Fig. A-5.

6. Neutron Cross Sections for Fusion Applications

a. Measured and Evaluated Neutron Cross Sections of Elemental Bismuth (A. Smith, P. Guenther, D. Smith and J. Whalen (ANL) and R. Howerton (LLL)).

Measurements of neutron total and scattering cross sections of elemental bismuth have been completed over the energy range $\lesssim$1.0 to

[1]W. Voss, Proc. 3rd Conf. Neutron Cross Sections and Technology, Knoxville, Tennessee, CONF-710301, Vol. 1, p. 218, U.S. Atomic Energy Commission (1971).

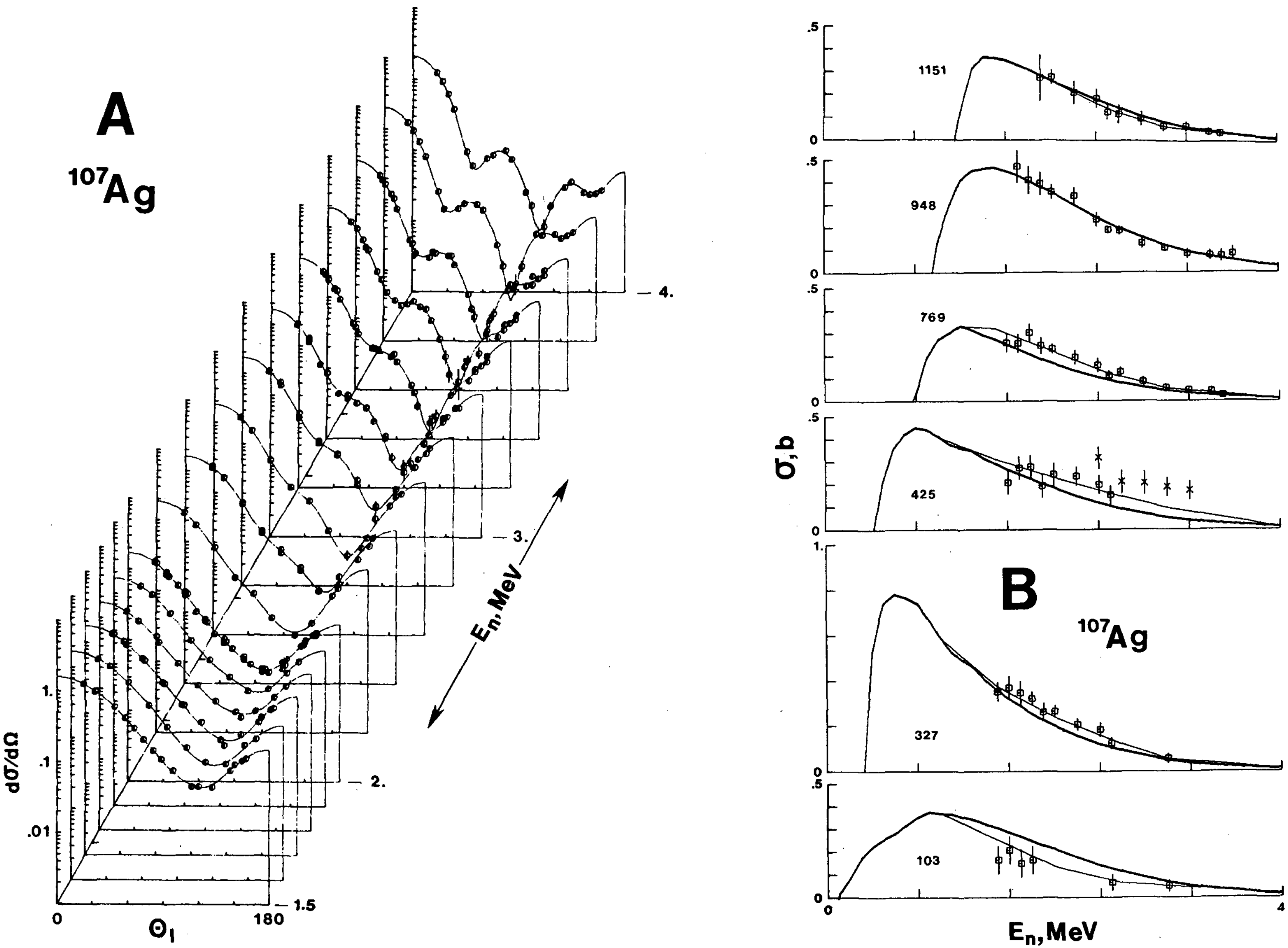

Fig. A-5. Measured Neutron Elastic-Scattering (A) and Inelastic-Scattering Cross Sections of the Fission Product Ag-107. Measured values are noted by data points.

4.5 MeV. The physical analysis of the measured values is now in progress. Concurrently, the measured and calculated results, together with those previously reported in the liturature, are being used to construct a comprehensive evaluated nuclear data file in the ENDF format. Particular attention is being given to the high-energy processes of importance in the conceptual design of fusion-fission hybrid and electro-nuclear breeding systems.

7. Neutron Cross Sections for Damage, Dosimetry and Other Applications

a. Measurement of the Excitation Function for the Reaction $^{207}Pb(n;n',\gamma)^{207m}Pb$ (G. Winkler, ANL and the Institute fur Radiumforschung und Kernphysik, Vienna)

Cross sections for the excitation of the 0.8 sec. isomeric state at 1.633 MeV in ^{207}Pb have been measured from near threshold to $\sim$5 MeV. The gamma-ray activity induced in natural lead samples was measured by means of a Ge(Li)-detector; the neutron fluence was determined with a fission chamber containing a ^{238}U-deposit. Measurements were carried out using a slow-pulsed accelerator technique,[1] due to the short half-life of the reaction product. The excitation function shows distinctive structure indicating that additional levels of ^{207}Pb contribute to the feeding of the isomeric level at increasing neutron energy. The results are compared with optical-statistical model calculations.

b. Measurements of the Cross Sections of the $^{63}Cu(n;\alpha)^{60}Co$ Reaction from Threshold to 10 MeV (G. Winkler, D. Smith and J. Meadows)

Measurements of cross sections for the $^{63}Cu(n,\alpha)^{60}Co$ reaction relative to fast-neutron fission of ^{238}U are in progress at intervals of $\leq$0.4 MeV from threshold to about 10 MeV with an average neutron energy resolution of about 0.1 MeV. Activation techniques are used, with counting of the ^{60}Co-activity induced in copper samples conducted with a high-efficiency sandwich arrangement between two 3" x 3" NaI(Tℓ) detectors in a low-level counting facility.

---

[1] D. L. Smith, J. W. Meadows and J. F. Whalen, Bull. Am. Phys. Soc. 23, 936 (1978).

The reaction $^{63}Cu(n,\alpha)$ is of special importance as a threshold detector in reactor dosimetry and as a long-term flux monitor. In the past a discrepancy of about 40% has been found between spectrum-averaged cross sections as obtained from integral measurements and values calculated from microscopic experimental data. The measurement results may give an explanation for this discrepancy. The results should also be useful for calculating helium-production rates, particularly in fusion systems.

c. Cycle-activation Measurements for Some Short-half-life Reactions (D. Smith, J. Meadows and J. Whalen)

A procedure for measuring cross sections of fast-neutron activation reactions with product half lives in the range from a few hundred milli-seconds to several minutes has been implimented at the ANL-FNG facility. The method involves post-acceleration pulsing of an accelerator so as to provide alternating time intervals of a few tens of milliseconds during which the charged-particle beam is allowed either to imping upon a target to produce neutrons or is blocked from reaching the target. Neutron fluence is measured with a fission chamber while the beam is on target, and the fast-neutron-induced gamma-ray activity is measured with a shielded Ge(Li) detector during beam-off intervals. This method has been used to measure cross sections for the $^{19}F(n;p)^{19}O$ ($t_{1/2}$ = 26.8 sec), $^{19}F(n;\alpha)^{16}N$ ($t_{1/2}$ = 7.10 sec), and $^{52}Cr(n;p)^{52}V$ ($t_{1/2}$ = 3.76 min) reactions. Results from the $^{19}F(n;p)^{19}O$ and $^{52}Cr(n;p)^{52}V$ measurements appear in Fig. A-6. Work on the $^{19}F(n;\alpha)^{16}N$ is in progress.

This technique appears to have potential applications in other technologies - e.g. in process-stream-composition analysis of coal. This particular application is being explored. Preliminary studies indicate that analysis for Na, P and Si is readily done using this method. Development of higher-sensitivity equipment for this investigation is in progress.

B. FISSION PHYSICS AND NUCLEAR PROPERTIES

1. Fission-product Yields for Monoenergetic-Neutron-Induced Fission of ^{232}Th (L. E. Glendenin, J. E. Gindler, I Ahmad and J. W. Meadows)

Yields of 37 masses were determined for fission of ^{232}Th with monoenergetic neutrons at 2.0, 3.0, 4.0, 5.9, 6.4, 6.9, 7.6, and 8.0 MeV.

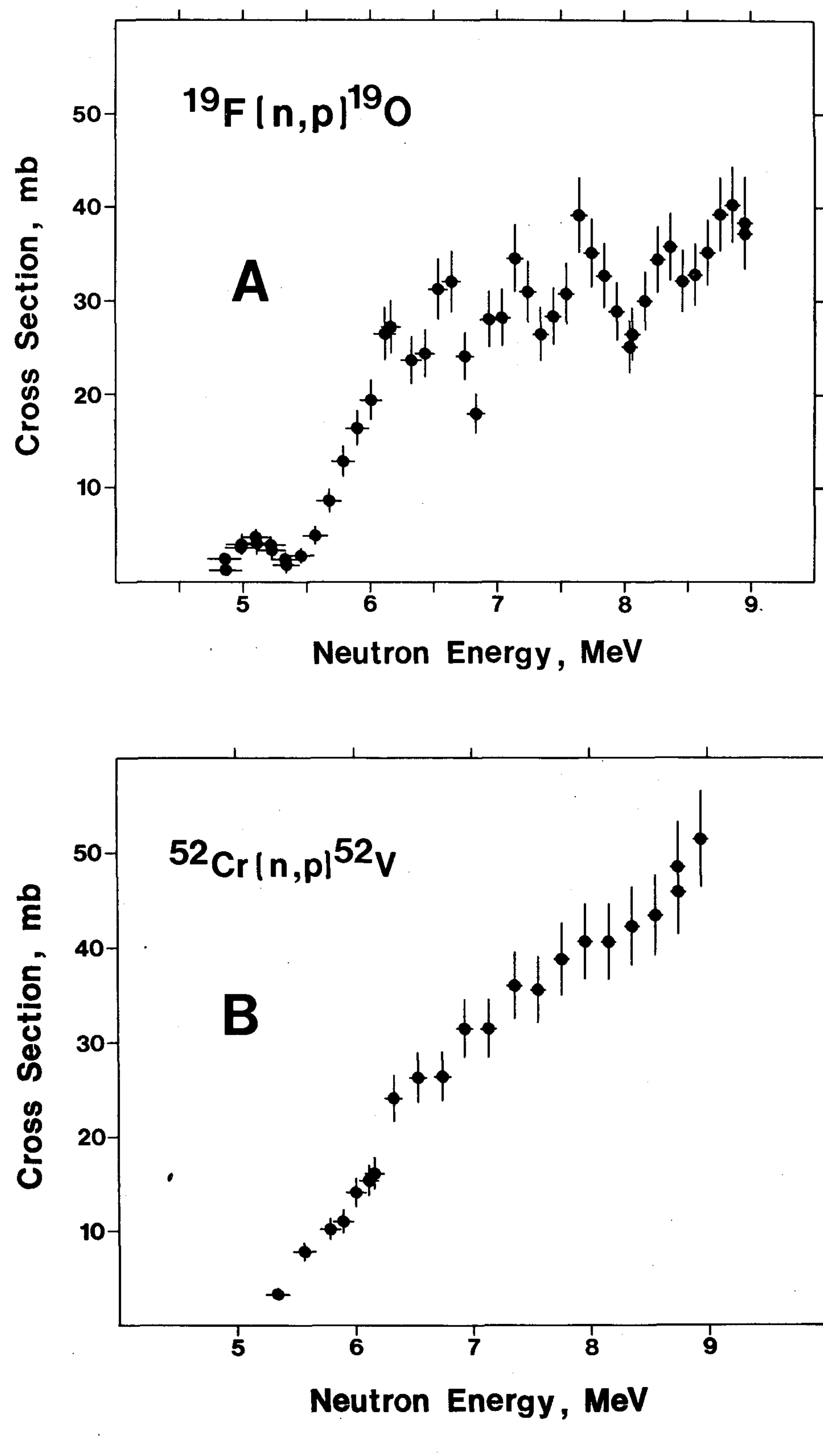

Fig. A-6. Measured Cross Sections for the Reactions $^{19}F(n;p)^{19}O$ (A) and $^{52}Cr(n;p)^{52}V$ (B).

The fission product activities were measured by γ-ray spectrometry of irradiated ^{232}Th foils and by chemical separation for some of the fission product elements followed by beta counting and/or γ-ray spectrometry. The fission-yield values, and their errors determined from these measurements, are available. The mass distributions based on these data are shown in Fig. B-1 with the mass distribution for 14.7-MeV neutron fission of ^{232}Th also shown for comparison. In contrast with our previously reported[1] data for ^{238}U (n,f), the ^{232}Th valley mass region is considerably more sensitive to increasing incident neutron energy, and there is a very pronounced dip in valley yields at the onset of second-chance fission just above the neutron binding energy (∿6 MeV) where excitation energy is lowered by competition with neutron emission.

2. <u>Precise Measurement of Intensities of Alpha-groups in the Decay of Actinide Nuclides</u> (I. Ahmad)

Our precision measurements of α-transition intensities of actinide nuclides is part of the IAEA Coordinated Research Program on Transactinium Decay Data. The measurement of intensities of α groups in the decay of ^{238}Pu, ^{239}Pu, ^{240}Pu and ^{242}Pu is currently in progress. The isotopically enriched sources of these nuclides were prepared using the Argonne electro-magnetic isotope separator and their spectra are being measured with a high-resolution (FWHM$\leq$12 keV) solid-state detector. We anticipate that the measurement of α intensities of Pu isotopes will be completed by the end of calendar year 1979.

3. <u>Decay Properties of ^{237}Pu, ^{247}Cf and ^{257}Fm</u> (I. Ahmad and R. K. Sjoblom)

The decay scheme schemes of ^{237}Pu, ^{247}Cf and ^{257}Fm have been investigated by measuring the γ rays and conversion electrons associated with their decay. Intensities of γ rays in percent per decay have been obtained for these nuclei. Alpha-particle energies of ^{247}Cf and ^{257}Fm α groups were measured and the α branching ratio for ^{247}Cf was also derived.

---

[1]Nagy et al., Phys. Rev. C <u>17</u>, 163 (1978).

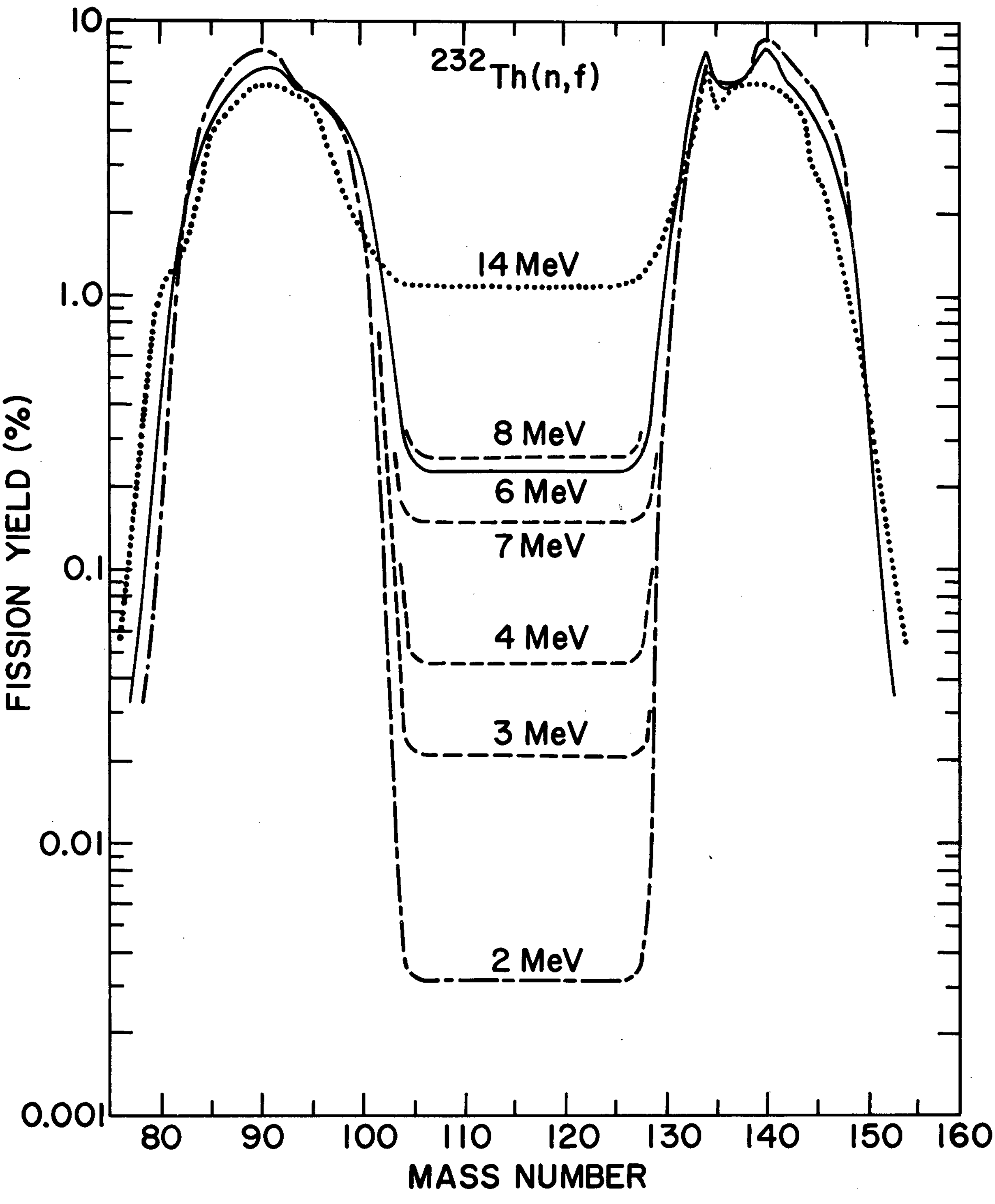

Fig. B-1. Mass-yield Curves for Monoenergetic-Neutron-Induced Fission of ^{232}Th.

4. Nuclear Structure of the Actinide Elements (R. Chasman)

A detailed understanding of the low-lying excited states of the actinides is being developed. The ingredients of the ANL program necessary to achieve this goal are the acquitition of extensive experimental data on single-particle states and transition probabilities in actinide nuclides and development of accurate theoretical treatment of the nuclear single-particle potential and two-body interactions. A long-term study of actinide nuclear structures, the single-particle potential and the effects of pairing forces on the nuclear structure of the actinides has recently been completed. This work is summarized in the paper "Survey of Single-Particle-States in the Mass Region A>228," Rev. Mod. Phys. 49, 833-891 (1977).

Currently, the emphasis of this program is on the accurate treatment of particle-hole interactions in the actinides. The most important of the particle-hole interactions appears to be the $K^{\pi}=0^{-}$ octupole interaction, as indicated by the ubiquitous low-lying 0^{-} band in the mass 230 region. Calculations have been carried out for ^{232}U, ^{234}U and ^{236}U in which the effects of 0^{-} correlations were investigated. These calculations indicate a generic relation between $K^{\pi}=0^{-}$ and $K^{\pi}=0^{+}$ in excited state bands in these nuclides.

C. CHARGED-PARTICLE REACTIONS

1. On d + ^{6}Li Reactions at Low Energy: (A. J. Elwyn and J. E. Monahan)

Recent differential and total cross-section data relating to the $^{6}Li(d,\alpha)\alpha$, $^{6}Li(d,p)^{7}Li$ and $^{6}Li(d,n)^{7}Be$ reactions at neutron energies between 0.1 and 1.0 MeV are analyzed in terms of the Wigner-Eisenbud formalism with the R-matrix elements assumed constant, i.e., independent of the energy of the incident deuteron. For the (d,p) and (d,n) reactions the possibility of an additional coherent direct-reaction contribution is also considered. The data are reasonably well reproduced by these calculations. The results thus give an indication of the magnitude of the direct contributions to these reactions. The results also show that the observation of a resonance-like structure in, e.g., the $^{6}Li(d,\alpha)\alpha$ reaction, does not necessarily imply a corresponding state in ^{8}Be.

2. Absolute Cross Sections for Three-Body Breakup Reactions $^6Li(d,n\,^3He)^4He$ and $^6Li(d,p\,^3H)^4He$ (R. E. Holland, A. J. Elwyn, J. E. Monahan, C. N. Davids, L. Meyer-Schützmeister, and F. P. Mooring)

Absolute cross sections have been obtained for the reactions $^6Li(d,n\,^3He)^4He$ and $^6Li(d,p\,^3H)^4He$ for deuteron energies from 100 keV to 800 keV. The energy spectra of particles from these reactions are continua because of the three-body final state. Total cross sections as well as angular distributions have been obtained with accuracies of 10 to 17 percent. Comparisons of energy spectra are made to predictions of simple models.

3. The $^6Li(p,\,^3He)^4He$ Reaction at Low Energies: (A. J. Elwyn, R. E. Holland, C. N. Davids, L. Meyer-Schützmeister, and F. P. Mooring)

Over the past few years interest has been expressed in ^6Li-H as an advanced fuel for the future generation of fusion-power devices. Previous measurements of the cross sections for the $^6Li(p,\,^3He)^4He$ reaction, which provide part of the data base necessary to evaluate the feasibility of this fuel, are in considerable disagreement. Last year we reported measurements at incident proton energies between 0.1 and 1.0 MeV. During the past year we have extended the differential cross section studies up to 3.0 MeV. Analyses of these and the earlier data have led to the determination of total reaction cross sections accurate to better than 10% over the energy region of interest to the thermonuclear studies. Figure C-1. shows the final reaction cross sections from about 0.1 to 4.0 MeV. A paper describing our results is being prepared for publication.

4. Cross Sections for the $^6Li(^3He,p)$ Reactions at Low Energies: (R. E. Holland, A. J. Elwyn, J. E. Monahan, C. N. Davids, L. Meyer-Schützmeister, and F. P. Mooring)

Thermonuclear reaction rates arising from d + ^6Li and p + ^6Li reactions are expected to be influenced by contributions from reactions of ^3He + ^6Li, since ^3He is produced in these primary processes. We are not aware of any earlier measurements of total reaction cross sections for ^3He + ^6Li reactions in the energy region below about 2 MeV. Last year, data for $^6Li(^3He,p)^8Be$ (ground state) was obtained at energies down to 0.4 MeV. Currently, we are using time-of-flight techniques (to separate protons and alpha particles) in order to measure the differential cross sections for the three-body process (i.e. $^6Li + {}^3He \rightarrow p + 2\alpha$) in the same energy region. We expect that normalization of these data to the partial cross section for decay through the ^8Be ground state will allow the determination of absolute total reaction cross sections that will, therefore, include the important continuum contributions.

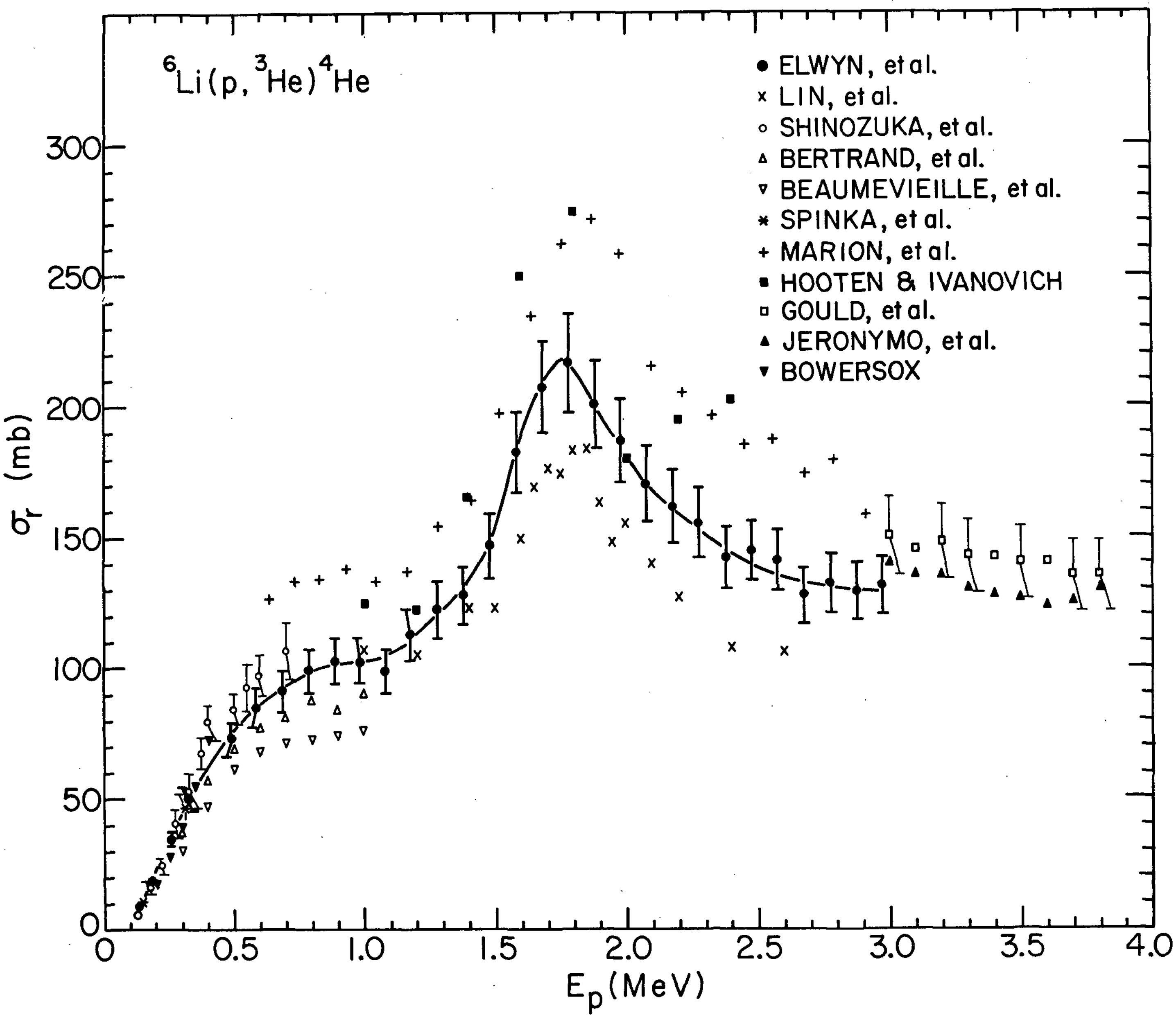

Fig. C-1. Total Reaction Cross Sections for the $^{6}Li(p,^{3}He)^{4}He$ Reaction. The present results are represented by the solid circles and the smooth curve, drawn to guide the eye.

D. PHOTO-NUCLEAR PHYSICS

1. Photodisintgration of the Deuteron (H. E. Jackson, R. J. Holt, G. Mavrogenes and J. R. Specht)

Measurements have focused on a determination of the angular distribution in the threshold region where the amplitude is particularly sensitive to mesonic effects. A precision of about 10% has been achieved, which is adequate to test the simple effective range theory. To date, measurements have been limited to observations at 90°, 135°, and 155°. It was evident from the data that a substantial improvement in precision would be possible only with measurements over the full angular range of photoneutron angles and with a direct means of calibrating the relative detection efficiency at each angle. To that end, a multidirectional photoneutron transport system was constructed in 1978. This system provides bremsstrahlung beams on demand, vertically for efficiency calibrations, and horizontally in modes corresponding to angles of observation along our photoneutron flight lines in either the forward or backward hemisphere. More precise determination of photoneutron angular distributions over the full range of angles possible with this system will facilitate our search for interference effects which are a signature of possible final-state interactions or momentum-dependent components in the nucleon potential.

2. R-Matrix Analysis of the $^{13}C(\gamma,n_0)^{12}C$ Reaction Below an Excitation of 9.3 MeV (R. J. Holt, H. E. Jackson, R. M. Laszewski, J. E. Monahan and J. R. Specht)

Electromagnetic transition rates in nuclei provide a particularly good test of nuclear-structure theories. The configurations of the 3/2+ resonances at 7.7 and 8.2 MeV in ^{13}C have been the subject of numerous theoretical calculations. These studies include the weak-coupling model, the Feshbach unified model, and full p-wave shell-model calculations. Unfortunately, the E1 ground-state radiative widths for these resonances have not been previously measured. This is due to the large resonant and nonresonant interference effects in this energy region. In order to extract accurate ground-state transition rates for these resonances, it it necessary to interpret the observed high-resolution photoneutron cross section, reported last year, in terms of a multilevel R-matrix analysis. In the analysis we have fully considered the well-known neutron scattering channel.

3. Doorway Resonances in ^{29}Si (R. J. Holt, H. E. Jackson, J. R. Specht)

In a recent study of the $^{29}Si(\gamma,n_0)^{28}Si$ reaction near threshold, we found evidence for a doorway state with $J^\pi = 3/2^-$ near $E_n = 750$ keV. Subsequent theoretical calculations supported the interpretation of this resonance as a doorway state. These calculations predict the existence of additional doorway resonances at higher energies. We have extended our measurements to higher excitation energies using the newly installed 25-m flight paths. Preliminary results suggest the existence of a localization of strength near 1.7 MeV. A doorway resonance at this energy is not consistent with the most recent theoretical models. Further experimental work will be necessary in order to extract accurate ground-state radiative widths.

4. The Giant M1 Resonance in ^{119}Sn (R. J. Holt, H. E. Jackson, R. M. Laszewski,* and J. R. specht)

The observation of a broad resonance structure at 7.8 MeV has spurred the speculation that this resonance is due to collective proton spin-flip oscillations ($g9/2 \rightarrow g7/2$ proton transitions). Furthermore, the observed amount of transition strength almost exactly exhausts the M1 sum rule. One would expect that a resonance of this multipolarity would produce a polarization in the emitted photoneutron beam at a reaction angle of 90°. With the ANL threshold photoneutron polarimeter we observed the photoneutron polarization from the $^{119}Sn(\gamma,n_0)^{118}Sn$ reaction at 90° to be zero within the statistical error limits. In order to establish an upper limit for the magnitude of the M1-ground-state radiative width in this resonance structure, we also observed the differential cross section throughout the resonance region. From these results we estimated that the ground-state radiation width of the resonance structure is predominately (>75%) E1 in nature.

5. Absence of Large M1 Excitations in ^{208}Pb Below 8.4 MeV (R. J. Holt, H. E. Jackson, R. M. Laszewski,* and J. R. Specht)

It has long been belived that the ^{208}Pb nucleus should provide an ideal example of a collective M1 resonance in nuclei. Early (γ,n)

*University of Illinois, Urbana, Illinois.

angular distribution experiments at Livermore suggested that seven strong resonances, centered at approximately 7.9 MeV, exhausted more than half of the M1 sum rule. Our threshold-photoneutron polarization studies showed that only one of these strong resonances at E_{exc} = 7.99 MeV could be assigned as an M1 excitation. Many of these resonances were found to have a large s-d-wave admixture which would explain the incorrect parity assignments in the Livermore work.

In order to study this energy region, 7.5-8.4 MeV, in ^{208}Pb in more detail we performed a very high-resolution measurement of the ^{208}Pb$(\gamma,n_0)^{207}$Pb reaction using the picopulse and the newly-installed neutron flight paths at the electron linac facility. The results are shown in Fig. D-1. We discovered that the 7.99 MeV (E_n = 610 keV) resonance exhibited a level-level interference pattern with the 7.98-MeV E1 resonance in ^{208}Pb. See the inset in Fig. D-1. Thus, the last candidate for a strong M1 excitation was ruled out. This is somewhat disconcerting since all published theories predict that the giant M1 resonance should occur below 8.4 MeV. This work has led G. Brown to speculate that our thinking about the unperturbed energies used in the particle-hole model must change. Having used an effective nucleon mass to calculate the single-particle, Brown predicts that the giant M1 resonance should occur at a much higher energy ($\sim$10 MeV) than previously believed.

Oak Ridge has recently observed many weak M1 excitations between 7.4 and 7.7 MeV using the (n,n) and (n,γ) techniques. However, the reported transition strengths for ^{208}Pb from the (n,γ) method seem to be consistently larger than those from the (γ,n) method. Fortunately, with the extended flight paths, we have been able to calibrate the radiative widths in ^{208}Pb relative to the well-known cross section for photodisintegration of the deuteron. This represents the first threshold (γ,n) measurement in ^{208}Pb which is independent of some allegedly known radiative width from (n,γ) studies. We found that the (n,γ) method consistently overestimates the transition strengths by a factor of approximately 1.5 in ^{208}Pb. Thus, the total known amount of M1 strength in ^{208}Pb accounts for less than 10% of the M1 sum rule.

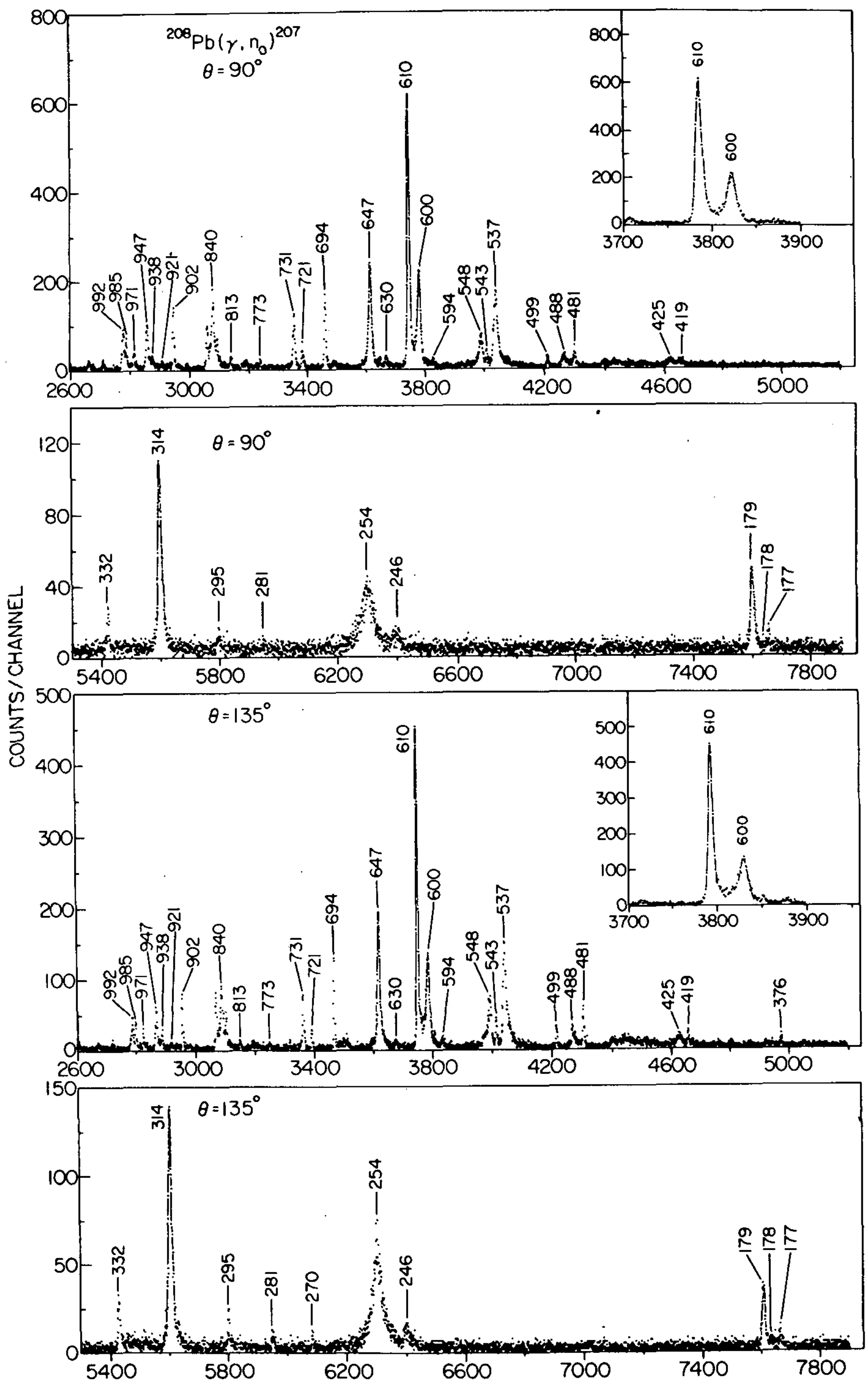

Fig. D-1. Photoneutron Time-of-Flight Spectra for the $^{208}Pb(\gamma,n_0)^{207}Pb$ Reaction at 90° and 135°. Photoneutron energies are given in keV. The constructive level-level interference for the 600- and 610-keV resonance is shown in detail in the inset figures.

6. <u>Polarization in Nuclear Reactions Involving Photons</u> (J. E. Monahan, R. J. Holt and R. M. Laszewski*)

Published formulae for polarization phenomena in photonuclear reactions are beset with phase and normalization errors. Expressions for the polarization tensors in reactions involving photons have been rederived. We found that our rederived coefficients for the differential photonucleon polarization are in agreement with those from the Stanford photonuclear group but differ in phase from those of Baldin et al.

7. <u>Background Photoneutrons from W(γ,n) at Radiation Therapy Centers</u> (R. J. Holt, H. E. Jackson and J. R. Specht)

Numerous facilities for radiation therapy use 10-MeV electron sources. We have measured the yield of photoneutrons from natural W when irradiated with 10-MeV electrons. At many medical electron accelerator centers the therapeutic radiation is derived from the bremsstrahlung process. Natural W is routinely used as a photon beam collimator or "hardener" at these facilities and represents a source of photoneutrons. The neutron yield per electron was measured as a function of the neutron energy. The results of this measurement are now under consideration by the Stanford Group.

8. <u>Photon Scattering by the Giant Dipole Resonance</u> (T. J. Bowles, R. J. Holt, H. E. Jackson, R. M. Laszewski,* A. M. Nathan,* J. R. Specht and R. Starr*)

Elastic and inelastic scattering is one of the simplest and most rigorous probes of the properties of the giant dipole resonance (GDR) in nuclei. Elastic scattering is constrained by its connection to the photoabsorption cross section through optical theorem and dispersion relations. Inelastic scattering provides a direct measure of the coupling between the giant-dipole excitation mode and other degrees of freedom such as collective surface and rotational excitations. In the past year, we observed elastic and inelastic scattering directly for the first time, in an experiment in which the incident photon energy is measured and the elastic and inelastic scattering is resolved. The experiment was performed at the University of Illinois MUSL-II microtron using the 100%-duty-factor electron beam to generate a

*University of Illinois, Urbanna, Illinois.

"tagged" photon beam whose energy is known with a resolution of 150-200 keV. The 120° differential cross sections for photons scattering to the ground and first excited states of ^{60}Ni were measured for excitations between 15 and 22 MeV. In addition, the cross sections were also measured for ^{40}Ar, ^{52}Cr, ^{56}Fe, ^{92}Mo and ^{96}Mo. The decay to the first excited state was observed to be most pronounced for ^{56}Fe. This is consistent with the notion that ^{56}Fe is a statically deformed nucleus. These results should provide a good test of the dynamic collective model.

E. NUCLEAR CONSTANTS AND STANDARDS

1. Standard-reference Neutron Cross Sections

a. The Neutron Total Cross Sections of Carbon and ^{13}C (W. P. Poenitz)

The carbon cross section is often used as a standard in scattering experiments, specifically below 2 MeV were it displays a smooth energy dependance. ^{13}C occurs with ∿1.1% abundance in natural carbon and may have some disturbing influence on the use of carbon as a standard, particularly where resonances occur in ^{13}C. The status of ENDF/B-V is unclear as to the inclusion of ^{13}C and there are few ^{13}C data available.

The present measurements of carbon total cross sections extend over the energy range from 20 keV to 4.8 MeV. Detailed measurements of the resonances above 2 MeV were not carried out. Major emphasis was on the range below 2 MeV. The data are compared with ENDF/B-V in Fig. F-1A. The present data support ENDF/B-V, usually within <0.5%. The peak cross section obtained for the 150 keV resonance in ^{13}C was 15% higher than the previous results reported from ORNL.

Measurements of the H(n;n) cross section, similar to those of carbon above), have been completed. The final results are awaiting the outcome of an analysis of the measurement sample.

2. Comparison and Standardization of ^{235}U Fission-foil Masses and Counting Procedures (W. Poenitz, J. Meadows and R. Armani)

Experimental data for the important fast-neutron-fission standard cross section of ^{235}U measured over the last 15 years generally fall in a ±3-4% wide band. This degree of uncertainty is still unsatisfactory relative to the ∿1% requested for reactor calculations. Therefore, a meeting was organized in 1978 at the NBS in order to discuss the planning of future work to improve the knowledge of this cross section. It was recognized than an increasingly important part of such future measurements is the standardization of the masses of ^{235}U samples.

The present work was an attempt to establish the present realistic level of uncertainty for ^{235}U sample masses. The work consisted of three parts:

1. A compilation was made of more recent sample intercomparisons which usually were carried out between two laboratories and most often involving the NBS sample set. The compilation revealed that the NBS mass scale is an average of ∿0.7% higher than those it has been compared with. Several mass scales (LASL, ANL-East and ANL-West, U. Michigan) appeared to agree rather well (±0.1 - 0.2%).

2. The masses of the eight samples used in the present intercomparison were determined for absolute alpha-counting.

3. The eight samples were intercompared in a fast neutron flux (∿600 keV).

The measurements imply a unified mass scale which is ∿0.8% lower than the NBS mass scale and has about half the uncertainty (∿0.6%). The mass scale is well supported by the LASL, ANL-East, ANL-West and the U. Michigan mass scales (all are within ±0.3%). However, there appears to exists a conflict with one ANL mass scale which casts some doubt on the half-life of ^{234}U.

F. EVALUATION

1. Evaluation of the Neutron-fission Cross Section of ^{235}U Between 0.1 and 20 MeV (W. P. Poenitz)

An evaluation of experimental fast-neutron-fission cross section data of ^{235}U, presented at the Symposium on Neutron Standards and Applications[1] in 1977, was updated to include data up to the 1978 Harwell Conference on Neutron Physics. The work consists of an

[1]W. Poenitz, NBS Spec. Pub. 493, 261 (1977).

analysis of evaluation procedures, the establishment and updating of a ^{235}U (n,f) file used for the evaluations, the evaluation of the cross-section shape, and the evaluation of the normalization to obtain the final evaluated ^{235}U cross section. Other cross sections will be evaluated at a later time and included in a consistent file.[1] A major attempt was made to keep the evaluation process free from any subjective elements. Inclusion of newer data from NBS (Wasson and Meier, Carlson and Patrick) and from KFK (Kari) resulted in few changes from the result presented at the 1977 NBS meeting, except at higher energies (>6.0 MeV). The normalization of the present result for ^{235}U (n,f) was based on a selection of some of the normalization factors established on predetermined criteria. The result is shown in Fig. F-1. The CESWG Subcommittee on Normalization and Standards utilized the present evaluation of the shape of the cross section but made a different selection of normalization factors in order to derive the ENDF/B-V file, which is also shown in Fig. F-1B.

Documentation of the evalution procedure and the results will be published as report ANL/NDM-45.

G. FACILITIES AND TECHNIQUES

1. Status of The Superconducting Linac Project (L. Bollinger)

This project is now in a phase in which two sections of the planned four-section linac are being operated regularly with the dual objectives of (1) developing the linac as a whole, and (2) providing a useful beam for nuclear-physics experiments. The fourth (month-long) set of runs, now in progress, is being carried out with seven high-β resonators. Under present operating conditions, this provides 7.5 MV of acceleration and, for example, allows a 85-MeV beam of ^{32}S from the tandem to be boosted to 178 MeV. This performance is approximately equivalent to that of an MP tandem with two strippers.

The fabrication of the resonators required for the third accelerator section is nearing completion, and assembly of the cryostat has started. This section will be put on line during the summer, and a run involving at least 12 resonators is scheduled for September. This should provide for 12 to 14 MV of acceleration, making an accelerator system whose performance is approximately equivalent to that of an 18 MV tandem for for A $\leq$ 40.

---

[1]W. Poenitz, AEC Sym. Series 23 331 (1970).

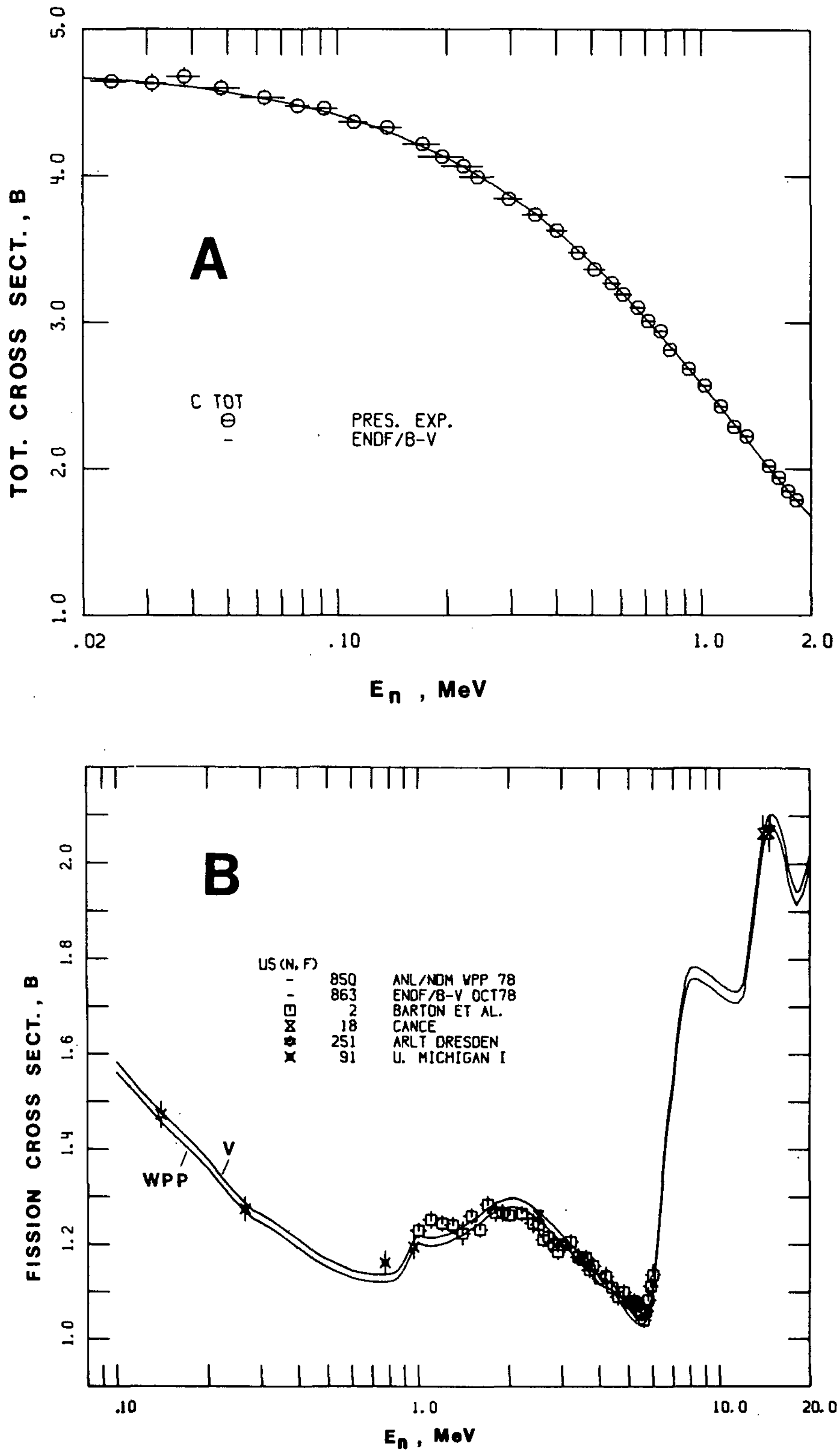

Fig. F-1. (A) Measured and Evaluated Neutron Total Cross Sections of Carbon.
(B) Comparison of U-235 Fission Evaluations with Recent Measured Values.

The present linac is effective only for ions with $A \leq 40$ because only the high-β resonators are in use. This limitation will begin to be removed during the summer, when one or perhaps two low-β resonators will be put into operation. The main batch of low-β resonators is planned for FY 1980.

BROOKHAVEN NATIONAL LABORATORY

A. NEUTRON NUCLEAR PHYSICS

1. Neutron Cross Sections in ^{232}Th (#62034,74204,76079,76080)

(R. E. Chrien, H. I. Liou, M. L. Stelts and M. J. Kenny (Guest Scientist from AAEC, Lucas Heights)

The potential energy supply contained in the large amount of thorium available in the earth's crust makes the consideration of the ^{232}Th-^{233}U fuel cycle attractive. Recently, there has been further increased interest in this fuel cycle for both thermal and fast reactors due to the problems of nuclear weapon proliferation commonly associated with the ^{238}U-^{239}Pu fuel cycle. Because of this interest there have been several reevaluations of the important nuclear cross sections for both ^{232}Th and ^{233}U. In particular the known accuracy of the currently known thermal and epithermal capture cross sections for ^{232}Th have been deemed inadequate for the design of thorium converters and breeders.

We have completed measurements of the total cross sections and resonance parameters of ^{232}Th below 100 eV, and capture cross sections at 2 and 24 keV. In addition the epithermal capture has been measured from thermal neutron energy to 15 eV by a method using the know low energy radiation transitions observed from ^{232}Th$(n,\gamma)^{233}$Th. The resonance parameters were reported in BNL-NCS-24273/DOE/NDC-12/U. The thermal, 2- and 24 keV capture cross sections were measured by an activation technique using the tailored-beam facility at HFBR.

The measured thermal cross section is 7.38 $\pm$ 0.08 barns, at 2 keV the cross section is 1.95 $\pm$ .10 barns, and at 24.3 keV it is 0.538 $\pm$ 0.014 barns.

These results are slightly different from those previously reported in the last DOE-NDC progress report and reflect the most recent measurements of the branching ratio of the 311 keV transition in the ^{233}Pu decay.

Figure A-1 shows the results obtained in the low energy region of the present experiment. These capture measurements use high resolution γ-ray spectroscopy to isolate the ^{232}Th capture lines from the background. The technique is identical to one recently employed for ^{238}U, and consists of using known capture lines to deduce the capture cross section between resonances where the capture cross sections are low compared to scattering. In the present case, the cross section is measured in the region above thermal to the first resonance, a region of crucial importance to thermal reactors operating as converters or breeders of the

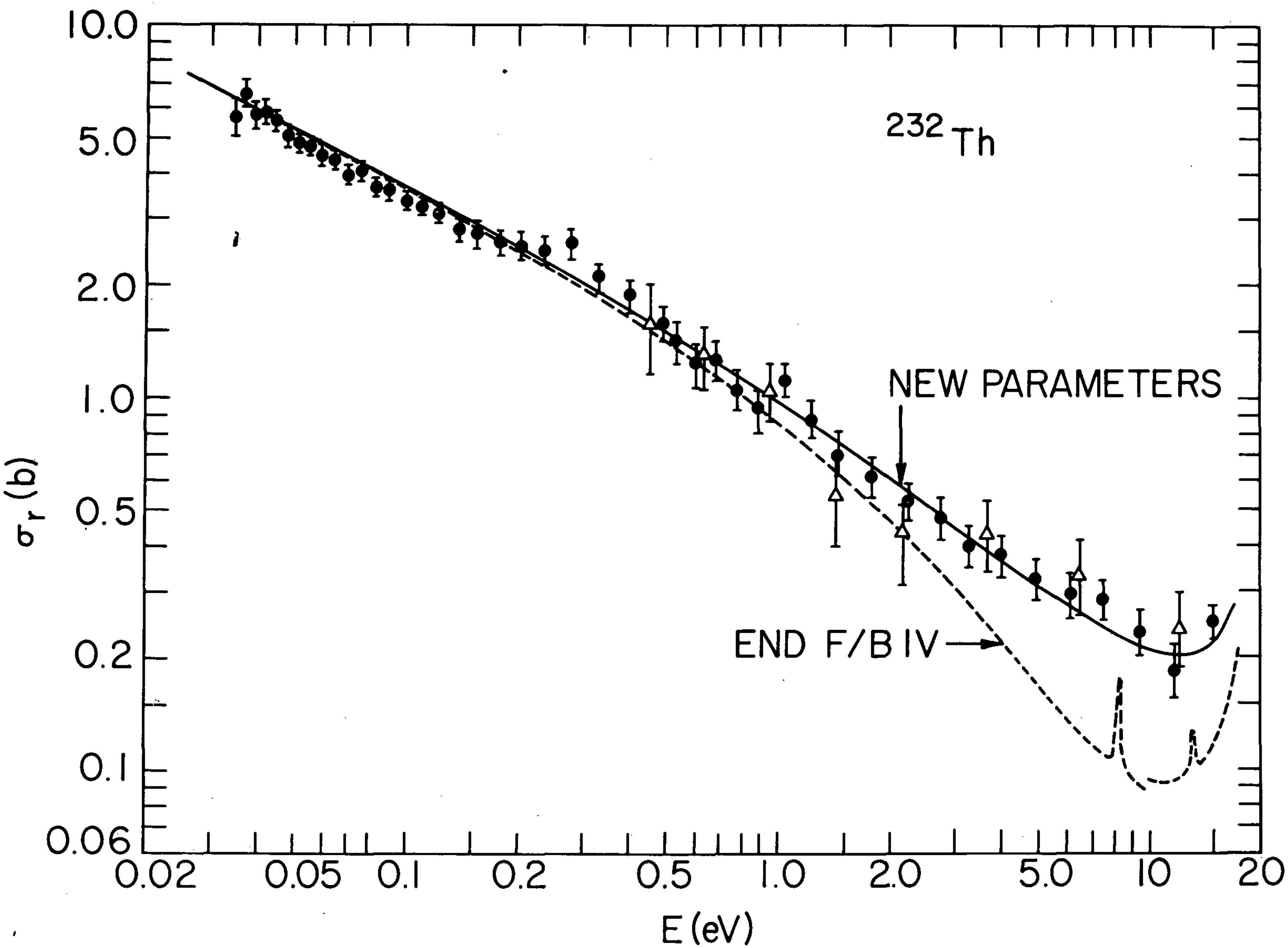

232 Th
NEW PARAMETERS
END F/B IV
σr (b)
E (eV)
10.0
5.0
2.0
1.0
0.5
0.2
0.1
0.06
0.02
0.05
0.1
0.2
0.5
1.0
2.0
5.0
10
20

FIG. A-1

fertile ^{232}Th. The measured cross sections shown in fig. 1 are compared to the ENDF/B-IV evaluation and also to a curve derived from an R-matrix fit to our total cross section results. A significant difference is observed in the region near 10 eV, with the new measurements indicating higher capture cross sections. The new results will serve to improve the agreement with integral experiments, since the ENDF/B-IV evaluation was found to underpredict the ratio of epithermal to thermal capture.

2. Transmission through the ^{56}Fe Window and the Parameters of the 28 keV Resonance (#74046)
(H. I. Liou, R. E. Chrien, R. C. Block (RPI), and U. Singh (RPI)

We have completed the analysis of the transmission of neutrons in the region of the iron window near 24.3 keV. Because of the extreme length of the sample, 68.58 cm of ^{56}Fe, we have had to reevaluate our data in the light of the presence of small amounts of impurities, the most important of which are copper, oxygen and hydrogen. The effect of a small p-wave resonance in ^{65}Cu at 24.133 keV has been explicitly taken into account. The new result is as follows:

$$\sigma_{min}(24.37 \text{ keV}) = 7.5 \pm 4.2 \text{ mb}.$$

Using a R-matrix analysis based on a shape fit near the minimum, (see fig. A-2) we have deduced parameters for the neighboring S-wave resonance. These are as follows:

$$E_o = 27.85 \pm 0.06 \text{ keV}$$

$$\Gamma_n = 1.43 \pm 0.06 \text{ keV}$$

$$R^1 = 5.67 \pm 0.16 \text{ fm}$$

By making a small correction (1.28 mb) for the expected $\ell=1$ scattering at the minimum, we can deduce a radiation width for this resonance. The result, 2 ± 1 eV, while not of high accuracy, is consistent with recent measurements using Moxon-Rae and scintillation tank detectors.

3. Angular Distribution of the ^{6}Li(n,t)α and ^{10}B(n,α)^{7}Li Reactions at 2 and 24 keV
(M. L. Stelts, R. E. Chrien, M. Goldhaber, M. J. Kenny and C. M. McCullagh)

Work on the α-particle angular distribution for ^{6}Li and ^{10}B initiated last year has now been completed.

The ^{6}Li(n,t)α and the ^{10}B(n,α)^{7}Li reactions have been used in

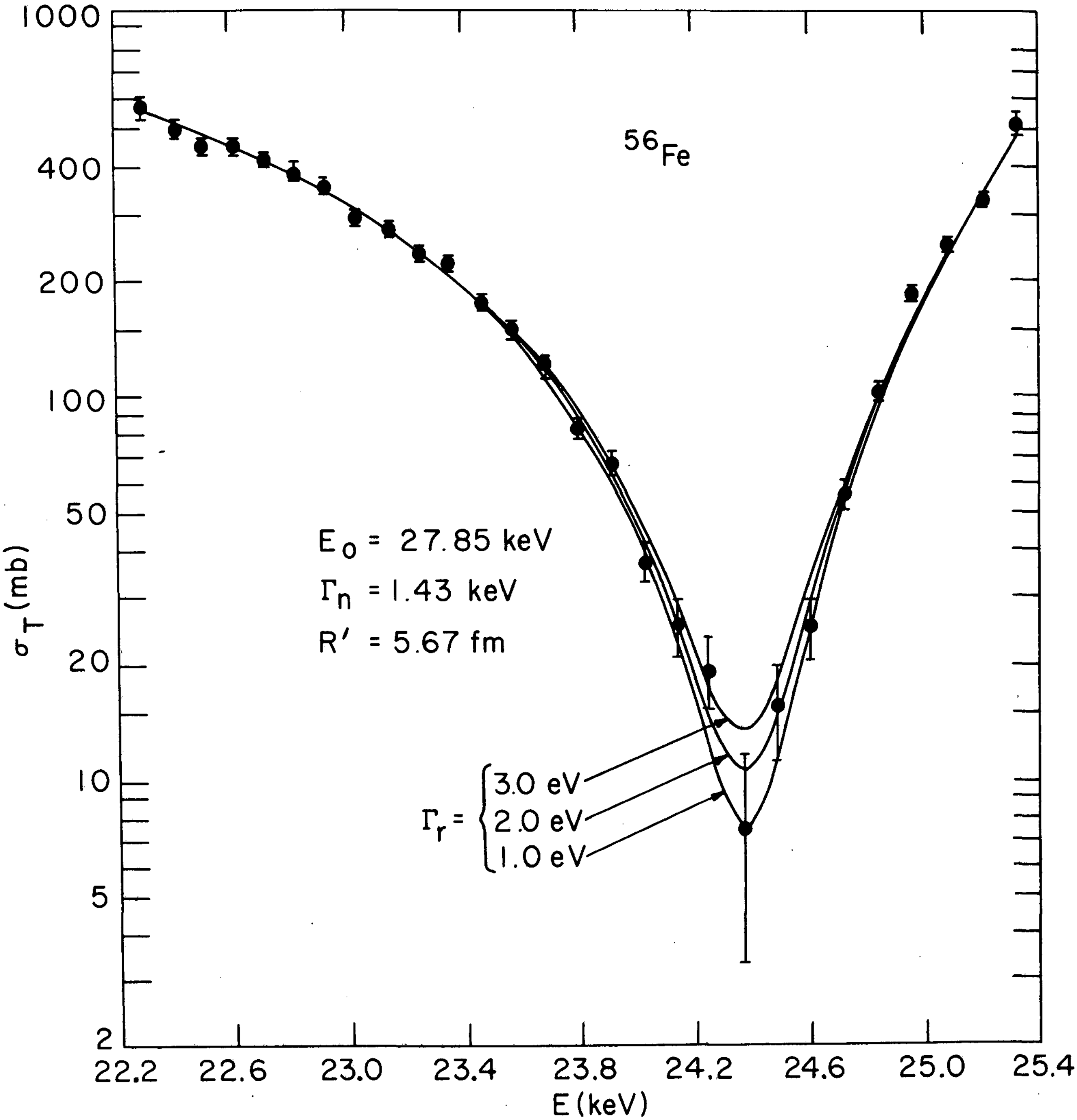

1000
400
200
100
50
20
10
5
2
σ_T (mb)
^{56}Fe
E_0 = 27.85 keV
Γ_n = 1.43 keV
R′ = 5.67 fm
Γ_r =
3.0 eV
2.0 eV
1.0 eV
22.2
22.6
23.0
23.4
23.8
24.2
24.6
25.0
25.4
E (keV)

FIG. A-2

the measurement of neutron fluxes for many years. The relatively high Q values, ease of detection of the reaction products, and the rather high cross sections with relatively smooth dependence on incident neutron energy make these reactions very convenient for monitoring neutron fluxes for neutron energies less than a few hundred keV. Consequently, considerable effort has been devoted to measuring these cross sections to an accuracy of a few percent.

Measurements of various reaction cross sections leading to the same compound nuclear states in ^{7}Li and ^{11}B have been made at various laboratories. It is therefore useful to develop a self-consistent R-matrix calculation which can generate a global fit to all these data. Measurements of the angular distributions can help to reduce the ambiguity of these fits. Anisotropies of the angular distribution can also affect the response of detectors of finite size through varying wall effects and detection efficiency as the distribution changes with energy. Therefore it is valuable to know the angular distributions for these reactions.

The angular distributions produced by very low energy neutrons are expected to be isotropic because of the dominance of s-wave neutrons in the entrance channels. Recently experiments below 100 keV with the $^{6}Li(n,t)\alpha$ reactions have measured sizable anisotropies for incident neutron energies of 24 keV or less. The experiments below 50 keV had rather poor angular definition, (solid angle $\gtrsim \pi sr$). The anisotropy is ascribed to s-p wave interference. There are no reported measurements of the $^{10}B(n,\alpha)^{7}Li$ angular distribution. Because of the intense quasi-mono-energetic beams at 2 and 24 keV available from the tailored beam facilities at HFBR, it was possible for us to make such measurements with good angular resolution.

The present results are summarized in figures A-3, A-4 and A-5. Shown in A-3 and A-4 are the observed angular distributions of ^{6}Li and ^{10}B respectively, where in ^{10}B we have resolved both α-particle groups. The solid lines shown are fits to the R-matrix calculations of Gerry Hale. These calculations were not adjusted to fit these new data and thus provide an independent check from other experiments. We find this agreement quite satisfying. Fig. A-5 shows our results from the branching ratio α_0/α_1 at thermal, 2, and 24 keV, compared to the ENDF/B-V evaluation. The agreement is reasonable.

4. Doppler Broadening of Neutron Resonances
(H. I. Liou, R. Moreh and R. E. Chrien)

The phonon absorption and emission for a nucleus bound in a lattice may influence the nuclear cross section, which in principle can be studied via the Doppler broadening of a neutron resonance. We have

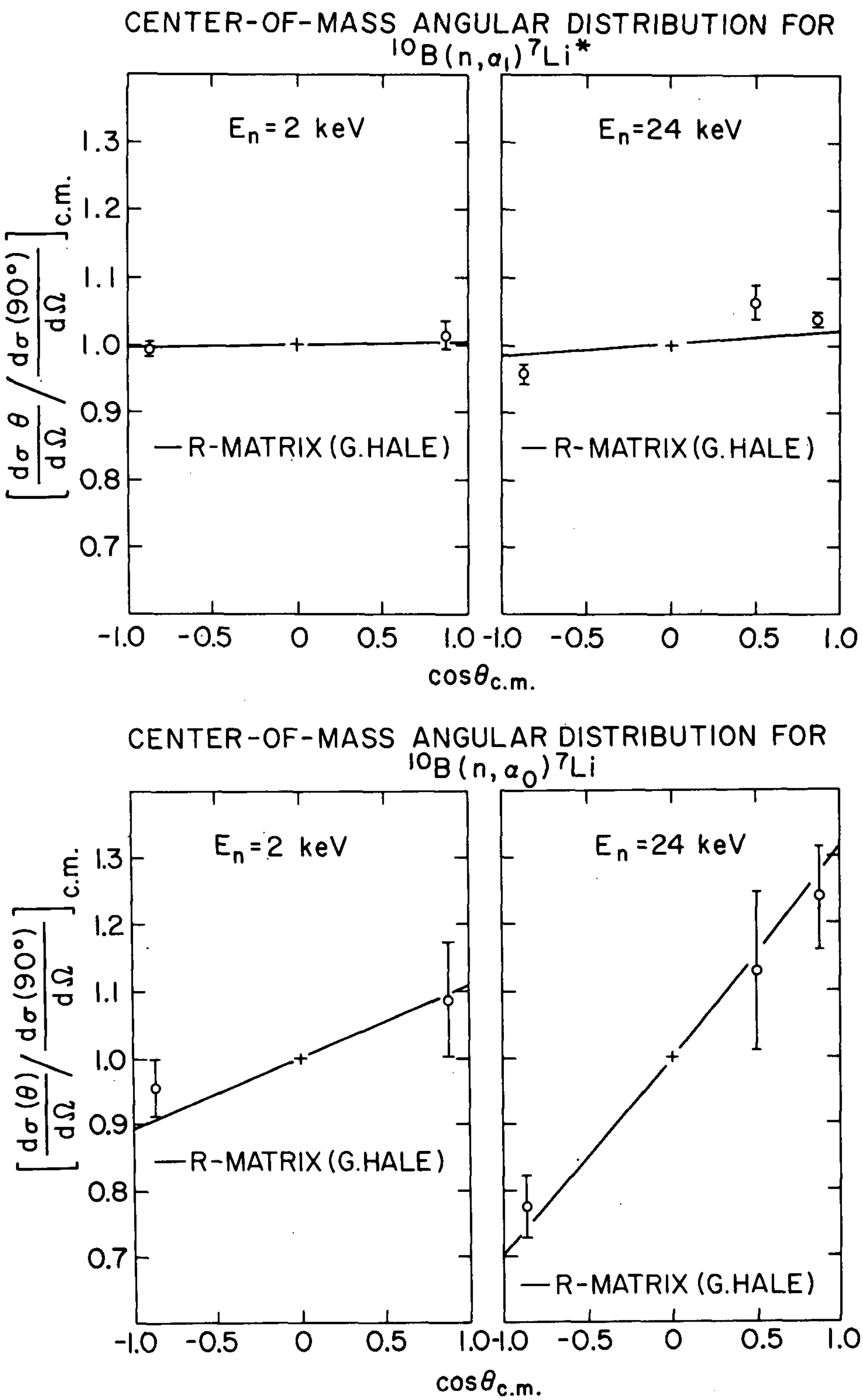
CENTER-OF-MASS ANGULAR DISTRIBUTION FOR
$^{10}B(n,\alpha_1)^7Li^*$
E_n=2 keV
E_n=24 keV
— R-MATRIX (G.HALE)
— R-MATRIX (G.HALE)
$\left[\frac{d\sigma\,\theta}{d\Omega} \Big/ \frac{d\sigma(90°)}{d\Omega}\right]_{c.m.}$
1.3
1.2
1.1
1.0
0.9
0.8
0.7
-1.0 -0.5 0 0.5 1.0 -1.0 -0.5 0 0.5 1.0
$\cos\theta_{c.m.}$
CENTER-OF-MASS ANGULAR DISTRIBUTION FOR
$^{10}B(n,\alpha_0)^7Li$
E_n=2 keV
E_n=24 keV
— R-MATRIX (G.HALE)
— R-MATRIX (G.HALE)
$\left[\frac{d\sigma(\theta)}{d\Omega} \Big/ \frac{d\sigma(90°)}{d\Omega}\right]_{c.m.}$
1.3
1.2
1.1
1.0
0.9
0.8
0.7
-1.0 -0.5 0 0.5 1.0 -1.0 -0.5 0 0.5 1.0
$\cos\theta_{c.m.}$

FIG. A-3

CENTER-OF-MASS ANGULAR DISTRIBUTION FOR $^{6}Li(n,t)\alpha$

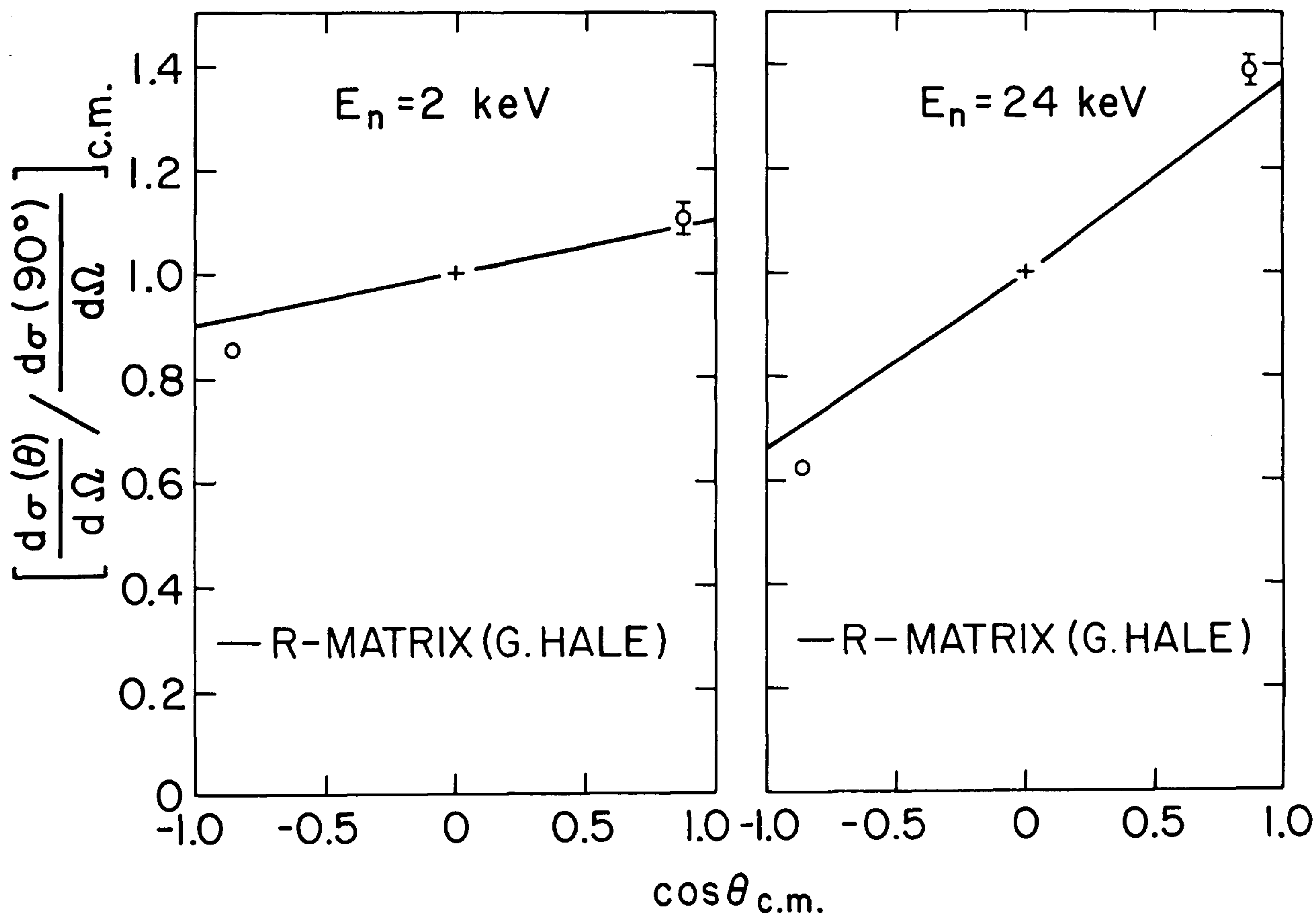

FIG. A-4

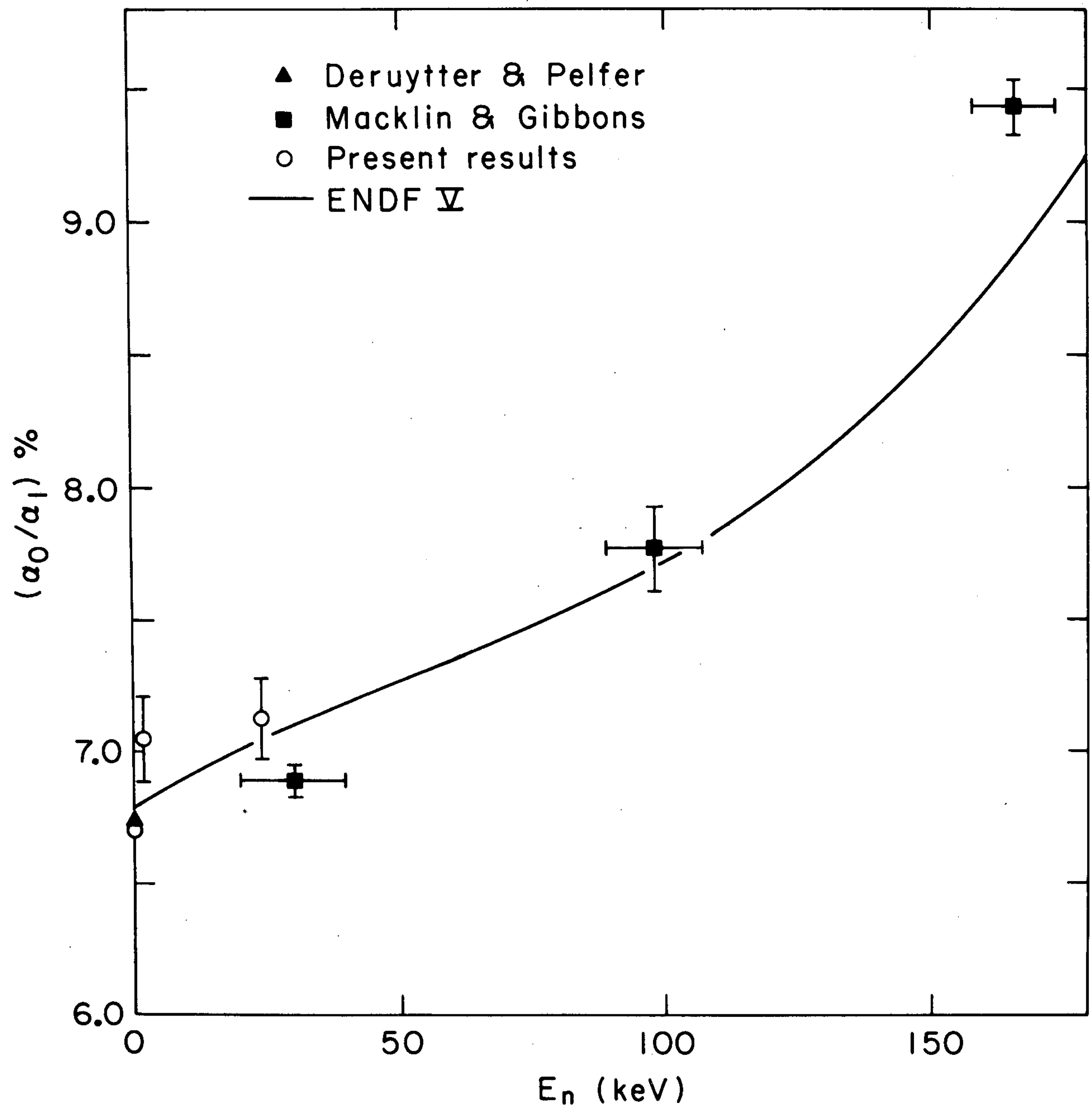

Deruytter & Pelfer
Macklin & Gibbons
Present results
ENDF V
9.0
8.0
7.0
6.0
(a_0/a_1) %
0
50
100
150
E_n (keV)

FIG. A-5

measured the capture yield of the 16.3 eV level in ^{107}Ag at room, liquid N_2 and He temperatures. Several targets of Ag metal, Ag_2O and AgCℓ were used. For each case the Doppler width and also the effective temperature T' was extracted by a least square shape fit. Assuming Lamb's theory holds for Ag at room temperature, $\Gamma_\gamma = 134 \pm 3$ meV is obtained for this level. We find that the measured T' values 108 ± 6 and 82 ± 7 for Ag at 77° and 4° agree with Lamb's theory. We find a T' of 66° and 64° at liquid He temperature for Ag_2O and AgCℓ, respectively. At low temperatures these values may be directly related to the zero-point energy of Ag in the two molecules. Further anlaysis of the data is underway.

5. Neutron Strength Functions Derived from Resonance-Averaged Gamma Ray Spectroscopy
(R. E. Chrien, M. L. Stelts and C. McCullagh)

We have developed a method for the extraction of neutron strength functions from the intensities of primary γ-ray transitions following neutron capture over many resonances. The method may be applied at the 2- and 24 keV neutron beam facilities at HFBR and is particularly useful in determining p-wave strength functions in mass region where the s-wave effects predominate.

The method may be briefly described as follows:

The intensities of the primary γ-ray lines at 2 and 24 keV are proportional to the average partial cross sections. It has been shown that, subject to the assumption of spin independent neutron strength functions, these partial cross sections may be expressed as follows:

$$\sigma_{n\gamma} = 2\pi^2\lambda^2 \; S_0\sqrt{E_n}\sum_s g \; F \; \frac{\langle\Gamma_{\gamma f}\rangle}{\langle\gamma\rangle} + \frac{S_1}{S_0}\,(ka)^2\sum_s g \; F_1 \; \frac{\langle\Gamma_\gamma\rangle}{\langle\Gamma\rangle}$$

where S_0, S_1 are the s- and p-wave neutron strength functions

S is channel spin

$\langle\Gamma\rangle = \langle\Gamma_n\rangle + \langle\Gamma_\gamma\rangle$, the total level width

g = statistical weight factor = $(2J + 1)/2(2I + 1)$

E_n = neutron energy

F_0, F_1 are fluctuations factors, defined by Lynn

$$F = (1 + r)\;\left[1-\left(\frac{\pi r}{2}\right)^{1/2} e^{r/2}\;\left(1-\mathrm{erf}\left(\frac{r}{2}\right)^{1/2}\right)\right]$$

where $r = \Gamma_\gamma/\langle\Gamma_n\rangle$

The values for the average partial photon widths, $\Gamma_{\gamma f}$, may be obtained from separate experiments in the discrete resonance regions, and we take these as known parameters. Likewise we use previously measured values for the total widths, Γ.

It is clear that the above expression can give us information on the relative magnitudes of s- and p-wave capture at 2 and 24 keV. For example, positive parity final states are fed by M-1 transitions from the $\ell=0$ states, and by E-1 transitions from the $\ell=1$ capture states. Thus the ratio of intensities for positive and negative parity final states gives us rather directly the neutron strength function ratio.

The method has recently been tested for the target nucleus ^{236}U, which has a level spacing D of 15.4 eV. The well known E-1 transitions at 4586 and 4572 keV, and the M-1 transitions at 5126, 5115, and 4462 keV (for s-wave capture) were used to form estimates for the average photon widths. These transitions were measured in discrete resonances at low neutron energies.

Applying the above equation, we find, for $S_0 = 1.3 \times 10^{-4}$, $S_1 = 3.5 \times 10^{-4}$, $E_n = 2$ keV, I(-parity final states)/I(+ parity final states) = 3.2, compared to the observed value of Fig. A-6, 3.4. The ratio of I(+ 1/2, 3/2)/I(5/2) is calculated as 1.6, compared to the observed ratio of 2.2

This value for S_1 we obtain, $S_1 = 3.5 \times 10^{-4}$, can be compared to a reported S_1 for ^{236}U of 2.3 + 0.6 from BNL-325, 2nd edition. At 24 keV, the calculated ratio I(-)/I(+) = 0.40, compared to the observed 0.49. We conclude that the p-wave neutron strength function is $(3.5 \pm 1.6) \times 10^{-4}$, or about 50% greater than that reported in BNL-325.

It is to be emphasized that information on the p-wave strength function is relatively scanty in many mass regions, and depends mainly on the identification and measurement of many small $\ell=1$ resonances distributed among the major s-wave resonances. Thus the present method should be exceedingly valuable for gauging the p-wave strengths.

One final remark that can be made about this method is that the result is sensitive only to the ratio $\langle\Gamma_\gamma(M1)\rangle/\langle\Gamma_\gamma(E1)\rangle$, and not to the absolute values. This ratio is easily derived from the data, and is free from the sizable systematic errors present in the absolute values for Γ_γ.

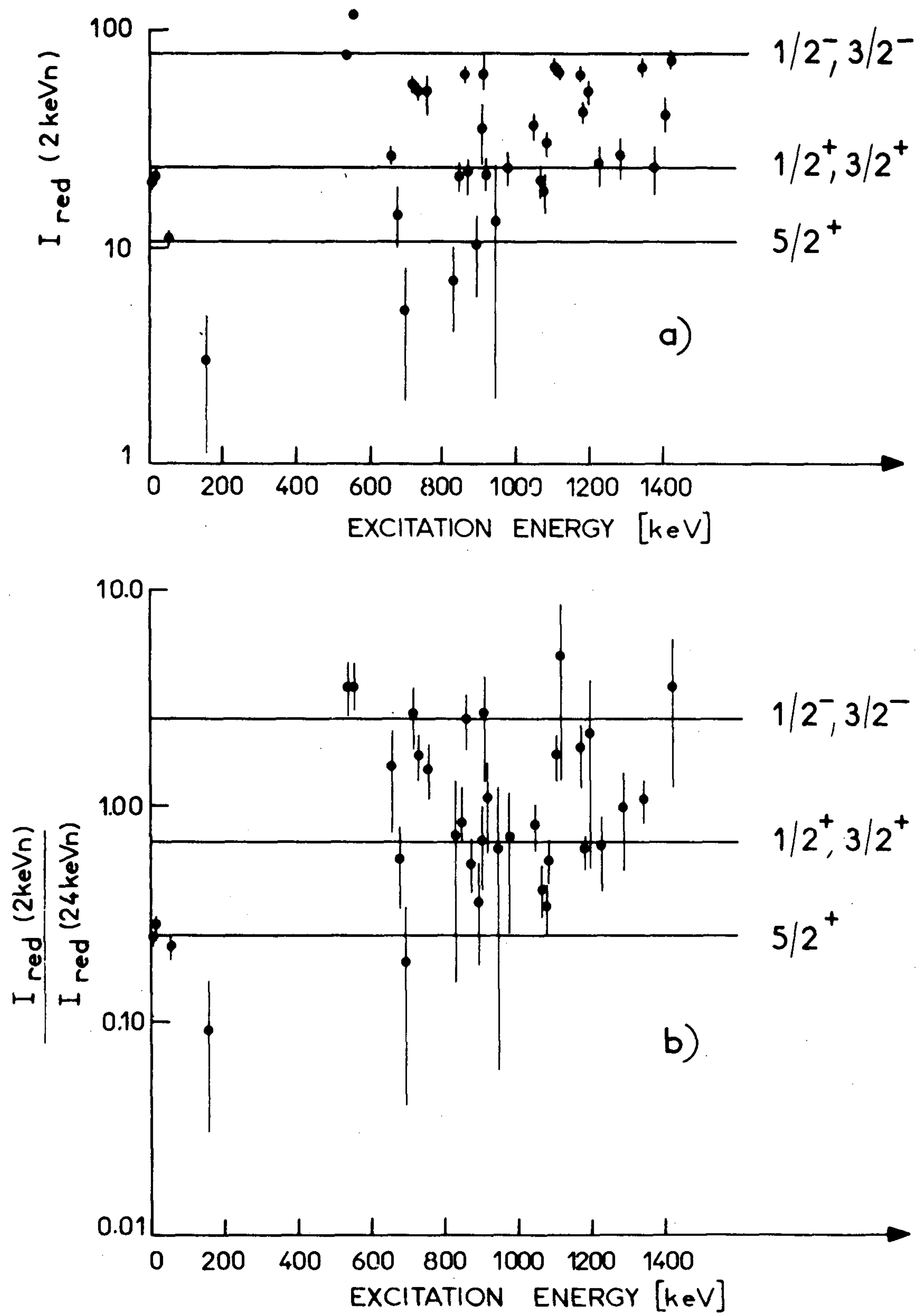
100
10
1
I red (2 keV n)
1/2⁻, 3/2⁻
1/2⁺, 3/2⁺
5/2⁺
a)
0 200 400 600 800 1000 1200 1400
EXCITATION ENERGY [keV]
10.0
1.00
0.10
0.01
I red (2keVn) / I red (24keVn)
1/2⁻, 3/2⁻
1/2⁺, 3/2⁺
5/2⁺
b)
0 200 400 600 800 1000 1200 1400
EXCITATION ENERGY [keV]

FIG. A-6

6. Capture of Neutrons by Hydrogen and the Neutron-Proton Mass Difference
(R. G. Greenwood, INEL, and R. E. Chrien)

The availability of high resolution γ-ray detectors has resulted in measurements of γ-ray transition energies of high precision than heretofore available. One of the more interesting of such measurements is that of the hydrogen capture γ ray,

$$^{1}H + n \rightarrow D + \gamma.$$

The measurement of this γ ray directly relates the mass of the neutron to that of the proton, once the mass difference between deuterium and the hydrogen molecule is known:

$$[N-{}^{1}H] = SN({}^{2}D) - [{}^{1}H_2-{}^{2}D].$$

The latter quantity is known from available mass spectroscopic data. We can infer $SN({}^{2}D)$ from a measurement of the hydrogen capture γ-ray and a small recoil correction. The γ-ray energy is related, through a series of accurately known intermediaries, to the very accurately known 411 keV γ ray from ^{198}Au.

The results are as follows:

$$E = 2223.247 \pm 0.017 \text{ keV}$$

and $$SN({}^{2}D) = 2224.564 \pm 0.017 \text{ keV}$$

and from $$[{}^{1}H_2-{}^{2}D] = 1442.232 \pm 0.007 \text{ keV}$$

we get $$[N-{}^{1}H] = 782.332 \pm 0.018 \text{ keV}$$

for the neutron-proton mass difference. The precision for this difference is only 18 eV and is indicative of the high precision obtainable in nuclear masses for (n,γ) techniques.

7. Photon Strength Functions
(C. McCullagh, R. E. Chrien and M. L. Stelts)

In the range from ∿ 5 to 10 MeV, discrete resonance neutron capture can provide the most reliable estimates for radiative strength function, which are of considerable importance in the calculation of photon production by neutrons. Previous compilations of E-1 and M-1 strengths have shown a wide spread of data. This spread is due to two factors: 1) difficulties in obtaining a sufficient number of transitions in overcoming Porter-Thomas statistics and 2) normalization of the values to obtain absolute widths. A comprehensive survey of M-1 and E-1 strengths obtained from partial width measurements has been made for about 50 data sets, with about 20 from BNL chopper data. These data were generally normalized to the absolute values of the widths for 5 eV resonance in 197 Au.

The behavior of the widths is shown in figs. A-7, where the E-1 strengths are shown compared to the prediction of the Axel-Brink Hypothesis. The (n,γ) data are in reasonable agreement with the Lorentzian tail of the giant dipole resonances, except that the values are typically about 30% lower than obtained for the photoneutron data and the principle of detailed balance.

8. Resonance (n,γ) Spectroscopy
(R. E. Chrien, H. I. Liou, M. L. Stelts, C. McCullagh, W. R. Kane, R. F. Casten, G. L. Smith and J. Cizewski)

The measurement of (n,γ) spectra for the purposes of testing models of the nucleus, for example the IBA model of Arima and Iachello, constitutes a major activity of the BNL neutron-nuclear physics group. In the past year the following target nuclides have been examined: ^{151}Eu, ^{107}Ag, ^{195}Pt, ^{244}Pu, ^{171,173}Yb, ^{165}Ho, ^{182}W, ^{63,65}Cu, ^{236}U, ^{147}Sm, and ^{149}Sm.

9. Evaluation of Shielding for Ge:Li Detectors
(E. Fleming (Alcorn State), M. L. Stelts and R. E. Chrien)

A method was devised to study the effectiveness of neutron shielding for a Ge(Li) spectrometer using an anti-coincidence NaI arrmulus. Since interactions of slow and fast neutrons produce different responses in a GeLi detector, the spectral characteristics of the incident neutrons can be inferred, and therefore the characteristics of the shielding from neutrons of different energies can be deduced. Thermal neutron interact primarily through (n,γ) on ^{73}Gev while fast neutrons produce a signal via the (n,n'γ) process in ^{74}Ge and ^{72}Ge.

The attenuation of a commercially available lithium-loaded polyethylene shield for fast and slow neutrons, and for γ-rays, has been evaluated with this technique.

10. TRISTAN Assembly and Construction

The basic components of TRISTAN, a mass separator formerly operational at the Ames Research Reactor, were shipped to BNL in April 1978. TRISTAN is now being reassembled and will be used for nuclear spectroscopic studies of neutron rich fission fragments from the neutron-induced fission of ^{235}U.

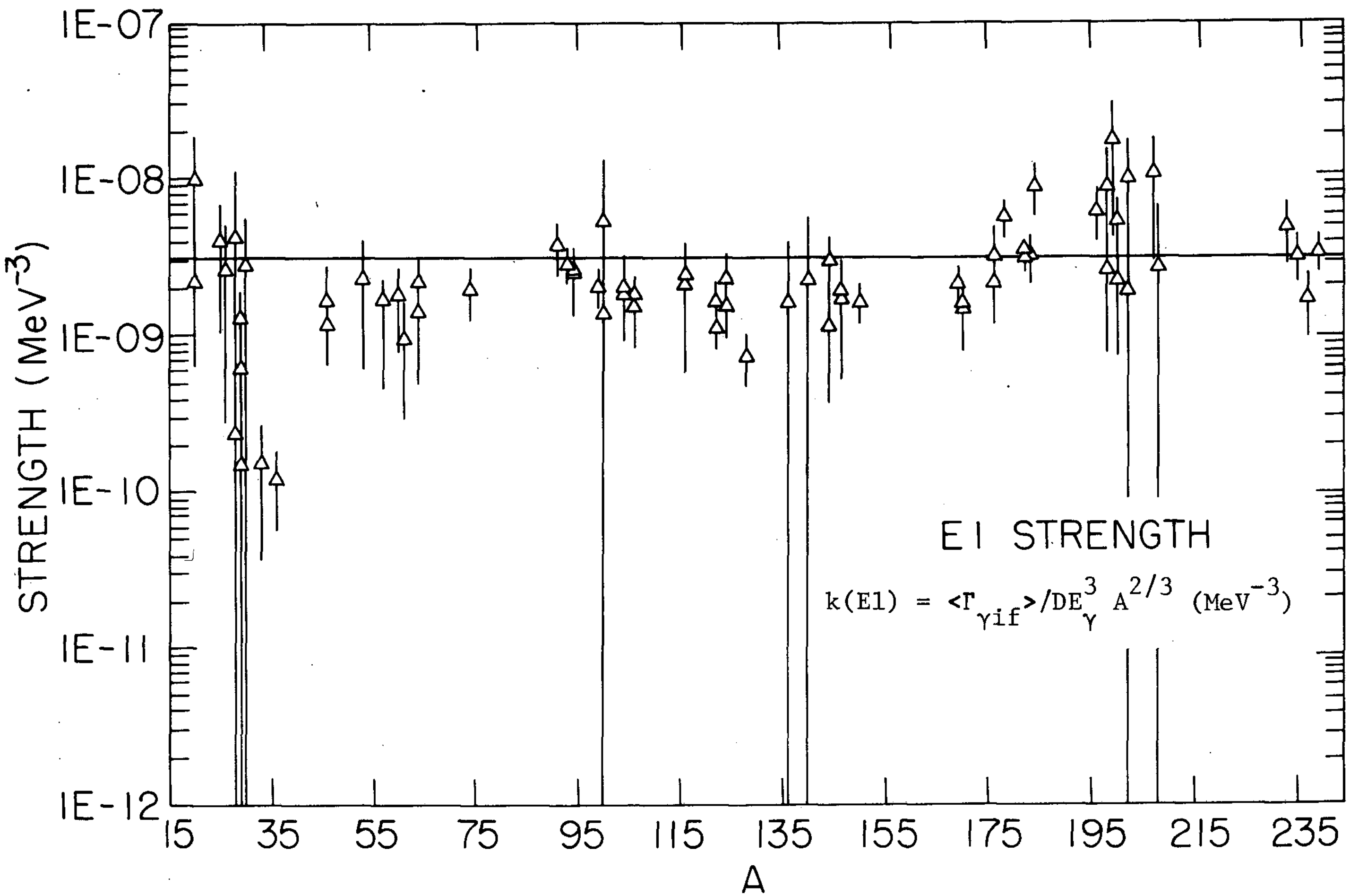

STRENGTH (MeV^{-3})
IE-07
IE-08
IE-09
IE-10
IE-11
IE-12
15
35
55
75
95
115
135
155
175
195
215
235
A
E1 STRENGTH
$k(E1) = \langle \Gamma_{\gamma if} \rangle / DE_{\gamma}^{3} A^{2/3}$ (MeV^{-3})

FIG. A-7

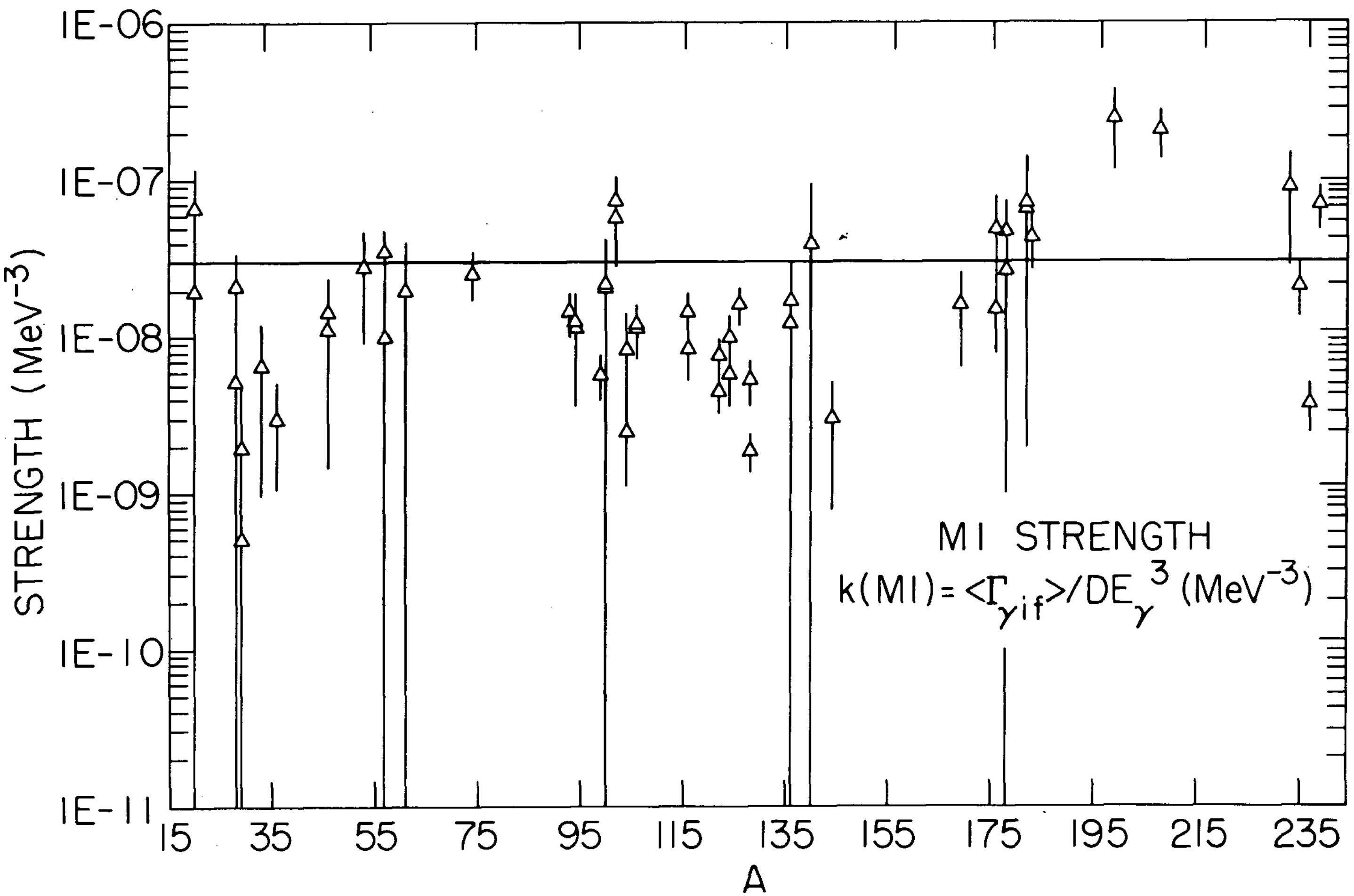

STRENGTH (MeV^{-3})
1E-06
1E-07
1E-08
1E-09
1E-10
1E-11
15
35
55
75
95
115
135
155
175
195
215
235
A
M1 STRENGTH
$k(M1) = \langle \Gamma_{\gamma if} \rangle / D E_{\gamma}^{3}$ (MeV^{-3})

FIG. A-7

The components have been assembled, except for the ion-source and moving tape collector system. The system is expected to be ready for beam testing in the summer of 1979. A data acquisition system incorporating a PDP-11/20, a CAMAC interface and a microprogrammed branch driver has been assembled and is being tested. The system will eventually accommodate up to four separate experimental inputs and allow a flexible handling of mutliparameter experiments. A PDP 11/34 will be available for off line processing of data tapes.

A users group for TRISTAN, TUG, has been established. TUG will coordinate the use of TRISTAN among the various university groups who will participate as TRISTAN Users. Approximately 10 letters of intent have been filed with TUG outlining a broad and varied program of nuclear research.

B. NATIONAL NUCLEAR DATA CENTER

The Center's computing facility was upgraded during the month of February. A DEC System-10, KL-10 central processing unit was installed to replace our present KA-10 purchased nine years ago. In addition the magnetic tape system was replaced and the on-line disk storage has been augmented.

1. Data Libraries

The review and correction activity for the U.S. and Canadian entries in the neutron bibliographic file, CINDA, has been completed. The 1979 archival edition of CINDA covering all publications before January 1, 1977 is now in press. Current literature continues to be entered in the CINDA file. The entries will appear in the regular CINDA 1979 edition now in press.

Data from 113 neutron experiments were compiled in the past year. In addition 132 entries were modified. The total contribution of four data centers of the international neutron data network to the neutron experimental data file in the past year has been 2000 data sets with 180,000 data points.

The release of ENDF/B-V data files within the U.S. has begun. Release of materials was delayed about six months after a decision was made to revise the $^{235}U(n,f)$ standard cross section. At present about 50% of the General Purpose File has been released; the remainder to be released by summer. The special purpose Actinide File has been released with a Dosimetry File due before summer and Fission Product, Gas Production, and Activation Files due before 1980.

The compilation of "integral" charged-particle nuclear data has continued. The second edition of a CINDA-like bibliography has been published covering the literature from January 1, 1976, through January 31, 1978. The next edition of the bibliography in cumulative form will go to press in March, 1979. Experimental data compiled at Karlsruhe and Kurchatov have been incorporated into the CSISRS data library, and evaluated data compiled at Vienna have been received by the Center. Work has begun at the Center of compiling charged-particle-induced neutron source reaction data.

Nuclear structure information at the Center has been updated by revisions of the RECENT REFERENCES and ENSDF data files prepared by the Oak Ridge Nuclear Data Project. File handling systems for each of these data files are nearly complete. The Center will offer retrieval services from these files by July, 1978.

Statistics for the services provided by NNDC to the nuclear community are attached.

2. Data Evaluation

The evaluations of the neutron cross sections of the nine stable isotopes of xenon and the six stable isotopes of krypton are completed. In addition, the resolved and unresolved resonance regions of $^{234,236}U$ were evaluated. Neutron cross section data of sulfur isotopes is being evaluated.

Work on the fourth edition of BNL-325 Vol. I--Resonance Parameters has started. It will be brought out in two sections: the first dealing with nuclei $Z \leq 60$ and the second containing the remaining nuclei. The expected date of completion of section one is the end of July, 1979, and section two December, 1979.

NNDC and NEANDC jointly hosted a two-day Specialists' Meeting on Nuclear Data of Higher Plutonium and Americium Isotopes for Reactor Applications on November 20-21, 1978. This meeting was in the form of a workshop to review and assess neutron cross section data and evaluations of $^{240,241,242}Pu$ and $^{241,243}Am$. NNDC collected experimental and evaluated data on these and provided data plots and other support for the meeting. Twelve foreign scientists were included among the thirty participants.

In the area of nuclear structure and decay data (NSDD), progress has been made on mass-chain evaluation in the region A=136-145 and A=112. A=136, 140, 144 have been completed and A=139, 145, 112 are in progress. NNDC continues to coordinate the U.S. Nuclear Data Network efforts in this area with the goal of having all mass chain evaluations completed on a four-year cycle.

A review of the status of charged-particle-induced neutron source reactions was begun with the T+D system being studied first.

3. DOE-NDC Secretariat

NNDC continues to perform secretariat functions for DOE-NDC. Document distribution lists for the committee have been maintained and corrections supplied to NEANDC and INDC were required. The following documents have been issued by NNDC on behalf of the committee:

ERDA/NDC-11/L	Symposium on Neutron Cross Sections from 10 to 40 MeV.
DOE/NDC-12/U	Reports to the DOE Nuclear Data Committee, April, 1978.

Request Statistics for NNDC
January 1, 1978 to December 31, 1978

1. Requests

a)	Number of requests	937

2. Origin of Requests

a)	Government Agencies	46
b)	Educational Institutions	118
c)	Industry	289
d)	Foreign	231
e)	National Laboratories	253

3. Mode of Response (may be more than one mode per request)

a)	Magnetic Tapes/Disk Files	416
	Total Number of Files on Magnetic Tape/Disk	1218
b)	Computer Listing	371
c)	Cards	2
d)	Plots	166
e)	Documentation	1055
f)	Telephone	27
g)	Microfiche	93
h)	Letters	90

IDAHO NATIONAL ENGINEERING LABORATORY

A. NUCLEAR-STRUCTURE AND DECAY-DATA EVALUATION ACTIVITIES

1. Mass-chain evaluations for the Nuclear Data Sheets (R. L. Bunting, M. A. Lee, C. W. Reich)

As our involvement in the International Nuclear-Structure and Decay-Data Evaluation Network, which has as its objective the establishment and maintenance of a four-year cycle time for the Nuclear Data Sheets, we have the responsibility for the ten mass chains in the region $153 \leq A \leq 162$. The first two A-chains undertaken have been A=157 and 159. The evaluation for A=159 has been completed, reviewed and submitted for publication. The A=157 evaluation is nearing completion. In keeping with our philosophy of evaluating the A-chains in approximate order of decreasing age, the next two chains to be evaluated will be those with A=153 and 158. Work on the A=158 mass chain is underway.

2. Decay-data evaluation for ENDF/B: The Version-V Fission-Product File (C. W. Reich, R. L. Bunting, M. A. Lee)

The compilation of evaluated fission-product decay data for the ENDF/B-V Fission-Product File has been completed. Decay-data sets for 317 fission-product nuclides (and isomeric states) have been prepared at INEL for inclusion in this version of the file. This represents a considerable expansion over the 180 such sets which were included in the first version of this file (which appeared in ENDF/B-IV.). Through our use of β-strength-function data, we have provided "experimentally based" average β- and γ-decay energy values for 38 short-lived nuclides for which previously only theoretically estimated values were available. Attention has been given to the problem of providing reliable estimates for the uncertainties in the average β- and γ-decay energies, particularly for those nuclides "important" for fission-product decay heat, in order to provide a more solid basis for the estimation of uncertainties in the calculated decay-heat source term. The delayed-neutron branchings (P_n values) have been completely re-done, incorporating the results of recent measurements and evaluations in this area.

3. Decay-data evaluation for ENDF/B: the Version-V Activation File (C. W. Reich, R. L. Bunting)

The decay-data evaluation effort for the ENDF/B-V Activation File is essentially complete. The following radioactive nuclides (and isomeric states) have been identified by the appropriate subcommittees of CSEWG as being required for inclusion in this File:

H-3	Cr-49,51	Sn-121,121m,123,125
C-14	Mn-54,56	I-126,128
F-18	Fe-55,59	La-140
Ne-23	Co-57,58,60	Dy-165
Na-22,24	Ni-57,59,63	Lu-177
Mg-27	Cu-64	Ta-182
Al-28	Zr-89,93,95	Au-195,196,198
Si-31	Nb-92,92m,93m,94	Th-231,233
P-32	Mo-93,99,101	Pa-232,233
Ar-41	Rh-103m	U-232,239
Ca-45,47	Ag-110m	Am-242
Sc-44,44m,47,48	In-115m,116	Cm-242

B. APPLICATIONS OF NUCLEAR-DECAY AND γ-SPECTROSCOPIC DATA

1. Absolute γ-ray intensities for ^{233}Pa decay (R. J. Gehrke R. G. Helmer, C. W. Reich)

Our measurement, using 4π β-γ coincidence techniques, of the absolute intensity of the prominent 311.9-keV γ ray from the decay of 27.0-d ^{233}Pa has been completed. Our result for this quantity is

$$I\gamma(311.9 \text{ keV}) = 38.6 \pm 0.5 \text{ photons/100 decays.}$$

This quantity is of considerable importance in the analysis of ^{232}Th capture cross-section measurements using activation techniques. Recent decay-data evaluations give widely differing values for it, viz. 33.7[1], 36. ± 2.[2] and 37. ± 2.[3] photons/100 decays. A 4π β-γ coincidence measurement some years ago gave the value 38. ± 4. photons/100 decays. Consequently, with the state of affairs prior to our measurement, the uncertainty in this absolute-intensity value represented a significant

---

[1] D. C. Kocher, ORNL/NUREG/TM-102 (August, 1977).

[2] Y. A. Ellis, Nuclear Data Sheets 24, No. 2, 289(1978).

[3] "Table of Isotopes, Seventh Edition", edited by C. M. Lederer and V. S. Shirley (John Wiley and Sons, New York, 1979).

[4] V. V. Berdikov and A. N. Silantev, Bull. Acad. Sci. USSR, phys. ser., 28, 310 (1965).

part of the overall uncertainty in the ^{232}Th capture cross sections measured using activation techniques. Our measured value is sufficiently precise that the absolute γ-ray intensity data for ^{233}Pa decay should no longer make a major contribution to the overall uncertainty in these activation-based measurements.

A paper describing these results has been prepared and has been accepted for publication in the journal Nuclear Science and Engineering.

2. The ^{1}H(n,γ)^{2}D reaction γ-ray energy: revised neutron mass and neutron binding energies for ^{3}T, ^{13}C, ^{14}C and ^{15}N (R. C. Greenwood, R. E. Chrien (BNL)).

With the recent availability of precise sets of γ-ray energies up to ∿3.5 MeV from radionuclide decay[1,2], based in a traceable manner on the ^{198}Au γ-ray energy value of 411.80441 keV reported by Kessler *et al.*[3], a remeasurement of the γ-ray energy from the ^{1}H(n,γ) reaction appeared appropriate, since this energy is directly relatable to the value computed for the neutron mass and to neutron separation energies computed from precisely measured mass differences.

Following the experimental procedures utilized in Refs. 1 and 2, we measured the energy difference between the 2223- ^{1}H(n,γ) and the 2185- ^{144}Ce γ rays and thus obtained a value of 2223.247 keV (σ_m=16 eV and σ_t=17 ev) for the energy of the ^{1}H(n,γ) reaction γ ray. Correcting for nuclear recoil (1.317 keV), we obtain the following value for the binding energy of the deuteron:

$$B_n(^{2}D) = 2224.564 \text{ keV } (\sigma_m = 16 \text{ eV and } \sigma_t = 17 \text{ eV}).$$

Combining the present value for $B_n(^{2}D)$ with existing mass differences[4,5], we obtain the revised neutron binding energies shown in Table B-1 together with the following revised values for the neutron-hydrogen atom mass difference and the neutron mass:

$$n - {}^{1}H = 782.332 \text{ keV} \quad (\sigma_m = 17 \text{ eV}, \sigma_t = 19 \text{ eV}) \text{ and}$$

$$n - 1 = 8071.366 \text{ eV}.$$

(This latter quantity represents the difference between the neutron mass and the atomic mass unit.)

TABLE B-1. Neutron binding energies obtained from mass-difference[4,5] and the present $B_n(^2D)$ data, together with resultant capture state-to-ground state γ-ray emission energies.

Product nucleus	B_n (keV)	Recoil energy (keV)	γ-ray energy (keV)	Error (ev)	
				σ_m	σ_t[a]
^3T	6257.268	6.953	6250.316	17	24
^{13}C	4946.329	1.010	4945.319	20	24
^{14}C	8176.477	2.561	8173.916	39	47
^{15}N	10833.297	4.196	10829.101	24	39

[a]Preliminary estimate: the σ_t contain contributions from both the voltage-wavelength and the mass(amu)-energy conversion factors and these have been assumed to be correlated. A correct accounting of the associated covariance terms may thus lead to smaller σ_t.

---

[1] R. G. Helmer, R. C. Greenwood and R. J. Gehrke, Nucl. Instr. and Methods 155, 189(1978).

[2] R. C. Greenwood, R. G. Helmer and R. J. Gehrke, Nucl. Instr. and Methods 159, 465(1979).

[3] E. G. Kessler, R. D. Deslattes, A. Henins and W. C. Sauder, Phys. Rev. Lett. 40, 171(1978).

[4] L. G. Smith and A. H. Wapstra, Phys. Rev. C 11, 1392(1975).

[5] A. H. Wapstra and K. Bos, At. Data and Nucl. Data Tables 20, 1(1977).

3. Gamma-ray energies from the $^{14}N(n,\gamma)$ reaction (R. C. Greenwood, R. E. Chrien (BNL)).

The $^{14}N(n,\gamma)$ reaction has long proven to be a valuable calibration source in neutron capture γ-ray spectroscopy. The improved accuracy of the present $B_n(^{15}N)$ value, obtained by combining mass-difference data with our recent $B_n(^2D)$ value, permits us to obtain improved accuracy for the $^{14}N(n,\gamma)$ reaction γ-ray energies. We have accomplished this utilizing the prominent cascade-crossover relationship

$$E_t(5534) + E_t(5292) = E_t(5563) + E_t(5270) = B_n(^{15}N)$$

and by measuring energy differences between these 5.2- and 5.5-MeV γ rays. Based on these difference measurements, together with additional cascade-sum relationships, we obtain the γ-ray energy set shown in Table B-2.

TABLE B-2. Summary of adopted $^{14}N(n,\gamma)$ reaction γ-ray energies

γ-ray energy (keV)	Error (eV)	
	σ_m	σ_t
1678.292	61	61
1681.44	220	220
1884.836	49	49
1999.647	79	79
3677.698	64	65
5269.154	47	49
5297.807	48	50
5533.385	48	50
5562.038	46	48
9148.76	220	220
10829.101	24	39

4. γ-ray energies for ^{228}Ra- ^{228}Ac decay and the ^{228}Th decay chain (R. G. Helmer)

The energies of over 100 γ rays from the decay of ^{228}Ra- ^{228}Ac have been determined in order to provide calibration energies for Ge(Li) and Ge semiconductor spectrometers. These energies were based on measurements of energy differences between a line in the ^{228}Ac decay and a calibration line or between two ^{228}Ac γ rays. The resulting γ-ray energies and the latter differences were used in a least-squares fit to the levels in ^{228}Th to obtain the best level energies. The best γ-ray energies were then computed from these level energies. These energies are on the scale based on a ^{198}Au γ-ray energy of 411.80441(108) keV[1]. Nominal precisions of the order of 5 eV at 200 keV and 15 eV at 1500 keV have been obtained for the more prominent γ-ray lines.

The energies of six γ rays from the daughters of ^{228}Th have also been determined from measured differences and a cascade-crossover relationship.

A paper presenting these results has been submitted for publication in Nuclear Instruments and Methods.

[1] E. G. Kessler, R. D. Deslattes, A. Henins and W. C. Sauder, Phys. Rev. Lett. 40, 171(1978).

5. γ-ray intensities from ^{197}Hg (64 h) decay (R. G. Helmer, R. J. Gehrke)

The relative γ-ray intensities for the decay of 64-h ^{197}Hg have been measured. For some experiments it is desired to assay the amount of ^{197}Hg (64 h) present. Since the strongest γ ray, at 77 keV, is mixed with the Au K_β x rays, it is desirable to be able to use the weaker 191-keV γ ray for such assays. An improved intensity was needed for this line. From careful measurements of the γ-ray spectrum, the relative intensities were determined to be 100.0(20), 3.38(11) and 0.21(1) for the 77-, 191- and 268-keV γ rays, respectively. From the known decay scheme, a $\approx$ 5% beta branch to the ground state, and the internal-conversion coefficients, the γ-ray emission probabilities were computed to be 18.1% and 0.64% for the 77- and 191-keV γ rays, respectively.

A paper describing this work has appeared in the literature[1].

---

[1] R. G. Helmer and R. J. Gehrke, Int. J. Appl. Rad. Isotopes 30, 15(1979).

6. γ-ray energies for ^{88}Rb decay (R. G. Helmer, J. W. Starner (LASL), M. E. Bunker (LASL))

The energies of the γ rays from the decay of ^{88}Rb(17.7 min) have been determined in order to provide new calibration energies, especially in the region above 3.5 MeV. The energies were determined primarily by the following methods: measurement of energy differences relative to known lines; and computation of crossover energies from the known cascade energies. Of the two energies above 3.5 MeV, the 4852-keV value was obtained from the 898 + 1836 + 2118 sum and then an energy difference measurement was used to obtain the value at 4742 keV. On the new energy scale based on a ^{198}Au energy of 411.80441 (108) keV[1], the γ-ray energies for the decay of ^{88}Rb are 898.042(4), 1382.449(46), 1779.870(22), 1836.064(13), 2111.498(36), 2118.867(21), 2577.791(29), 2677.892(22), 2734.086(15), 3009.517(36), 3218.483(49), 3486.473(56), 4742.424(84) and 4852.882(27) keV.

This work has recently been published[2].

---

[1] E. G. Kessler, R. D. Deslattes, A. Henins and W. C. Sauder, Phys. Rev. Lett. 40, 171(1978).

[2] R. G. Helmer, J. W. Starner and M. E. Bunker, Nucl. Instr. and Methods 158, 489(1979).

C. NUCLEAR LEVEL-SCHEMES STUDIES

1. Decay of ^{250}Bk (C. W. Reich, R. G. Helmer, R. J. Gehrke)

The study of the β^- decay of ^{250}Bk has been completed. A paper describing the results of this investigation has recently been published in Physical Review C. Since ^{250}Bk is one of the nuclides included in the ENDF/B-V Actinide File, the relevant decay data have also been incorporated into this File.

The following is the abstract of the paper which appeared in Phys. Rev. C 19, 188 (1979):

> The level scheme of doubly even $^{250}_{98}Cf_{152}$ has been studied from the β^- decay of ^{250}Bk. γ-ray energy and intensity measurements were made using Ge(Li) and Si(Li) detectors. Analysis of γ-singles and γ-γ coincidence data has revealed the existence of ~46 γ-ray transitions. Approximately 40 of these, accounting for $\gtrsim$ 99.97% of the observed γ-ray intensity, have been incorporated into a level scheme for ^{250}Cf consisting of 17 excited states with excitation energies up to 1695 keV. The following states, whose I^π values and energies (in keV) are well known from other experiments, are observed: the 0^+(0), 2^+(42.73), and 4^+(141.89) members of the ground-state band; the 2^-(871.56), 3^-(905.85), and 4^-(952.0) members of the $K^\pi = 2^-$ octupole band; and the 2^+(1031.85) and 3^+(1071.38) members of the γ-vibrational band. In addition, evidence is presented which permits the following I, K^π assignments to be made with reasonable confidence (the corresponding level energies - in keV - are given in parentheses): 1,1^-(1175.5); 2,2^+(1244.50); 2,0^+(1296.64); 2,2^+(1657.99); and 3,2^+(1695.2). The half-life of ^{250}Bk has been remeasured and a value of 192.7±0.3 m obtained. The absolute intensities (in photons/100 ^{250}Bk β^- decays) of the prominent 989- and (1028+1031)-keV γ rays have been measured using a 4π β-γ coincidence system and values of 45.0±0.8 and 40.6±0.7, respectively, have been obtained.

D. AUTOMATED FAST RADIOCHEMISTRY FACILITY FOR THE STUDY OF FISSION-PRODUCT RADIONUCLIDES (R. J. Gehrke, R. C. Greenwood, J. D. Baker, D. H. Meikrantz)

We have developed a facility at the INEL for the study of short (>10 sec) half-life fission products using open ^{252}Cf sources, a gas jet transport system and a microprocessor-controlled radiochemical purification system based on automated on-line solvent extraction and high-performance liquid chromatography. Two 100-μg sources of ^{252}Cf provide the source of fission products. Collected fission products are introduced as a solution into an on-line mixer/centrifuge to perform solvent extractions or onto an ion-exchange precolumn coupled in series with a high-pressure liquid chromatograph (HPLC). The microprocessor is used to control valves, pumps and motors on a time basis. With our solvent-extraction purification techniques, it is possible to study fission radionuclides with half-lives as short as ~10 sec. With the ion exchange columns we have identified rare-earth fission products with half-lives of 5 min. Initial studies of rare-earth fission products have been directed towards the Sm isotopes. Preliminary experiments have isolated the ^{157}Sm activity and measured its half-life to be 8 min, in agreement with the value reported by Kaffrell.[1]

---

[1] N. Kaffrell, Phys. Rev. C 8, 414 (1973).

E. INTEGRAL CROSS-SECTION AND REACTION-RATE MEASUREMENTS

1. Capture cross sections for "fission-product" and dosimetry materials (R. A. Anderl, Y. D. Harker)

Our program to provide integral cross sections of interest to the development of fast reactor systems has included measurements in the Coupled Fast Reactivity Measurements Facility (CFRMF) and in the EBR-II. A compilation of most of the fission-product studies in the CFRMF has been reported[1]. Included in the report are integral results for 52 (n,γ) reactions (including isomer production) for 39 enriched "fission-product" isotopes and results for 21 reactions in materials of interest to reactor dosimetry. The report also includes a specification description of the CFRMF pertinent to the integral studies. Recently the CFRMF fast neutron zone has been accepted by CSEWG as a benchmark neutron field for cross-section data testing and evaluation for "fission-product" and dosimetry materials.

More recent integral cross-section results have been obtained from an irradiation experiment in EBR-II. Neutron capture results for ^{143}Nd, ^{144}Nd, ^{145}Nd, ^{147}Sm and ^{149}Sm were given in the last USNDC report

---

[1] Y. D. Harker, J W Rogers and D. A. Millsap, "Fission Product and Reactor Dosimetry Studies at the Coupled Fast Reactivity Measurements Facility," DOE Report TREE-1259 (ENDF-266), March 1978.

and at the June, 1978 ANS meeting[2]. Subsequently, preliminary results have been obtained for the enriched samples of ^{151}Eu, ^{152g}Eu, ^{153}Eu and ^{154}Eu in the same irradiation. Integral cross sections relative to ^{235}U(n,f) were obtained from "capture-product-to-parent-nuclide" mass ratios for the irradiated samples. The measurement of the "capture-product-to-parent-nuclide" mass ratios for the ^{151}Eu, ^{152}Eu and ^{153}Eu samples required extensive chemistry prior to mass-spectrometric analysis. Mass ratios for the ^{154}Eu samples were obtained from measurements of the relative gamma-emission rates for the 105.3-keV and 123.1-keV gammas following the β decays of ^{155}Eu and ^{154}Eu, respectively. Appropriate decay corrections were applied and end-of-irradiation reaction rates were computed for each capture reaction. The results, divided by the fission rates for the corresponding ^{235}U dosimeters, are summarized in Table E-1. Included in the table are calculated estimates of the spectral-averaged cross sections relative to ^{235}U fission. These calculated cross sections were obtained from a numerical integration of the multigroup ENDF/B-IV differential cross sections for each isotope with the applicable neutron spectrum obtained from the unfolding analysis for the dosimeter reaction rates. The results indicate a reasonable agreement between calculation and measurement for the ^{151}Eu, ^{153}Eu and ^{154}Eu reactions in the "hard" neutron spectrum at midplane (axial position = 0). For all reactions in the "soft" neutron spectrum in the reflector (axial position = +35) the calculated spectral-averaged cross sections are significantly higher than the measured cross sections.

TABLE E-1. Spectral-averaged cross sections of europium isotopes relative to ^{235}U fission.

Isotope	Axial Position	Measured	Calculated	C/M
^{151}Eu	0	2.40	2.40	1.00
	+35	5.04	5.49	1.09
^{152g}Eu	0	2.43	2.73	1.12
	+35	3.18	5.05	1.59
^{153}Eu	0	1.41	1.45	1.03
	+35	2.87	3.48	1.21
^{154}Eu	0	1.68	1.75	1.04
	+35	2.64	3.51	1.33

---

2 R. A. Anderl, Y. D. Harker, R. L. Tromp, J. E. Delmore, "EBR-II Irradiation of Enriched Isotopes of Neodymium, Samarium and Europium," Trans. Am. Nucl. Soc. 28 (1978).

2. Capture and fission cross sections for actinides (R. A. Anderl, Y. D. Harker).

In progress are the measurements of the integral cross sections important to the production of ^{233}U and to the production and depletion of plutonium, americium and curium in advanced reactor systems[1]. To date integral capture and fission cross sections have been measured for ^{232}Th in the fast neutron zone of the CFRMF. The results, based on the measurement of the absolute gamma emission rates of the 311.9-keV gamma ray from the ^{233}Pa decay and of the 537- and 1596-keV gammas from the ^{140}Ba-^{140}La decay, are 295 mb/atom for capture and 20.2 mb/atom for fission. Corresponding integral values computed from ENDF/B-IV cross sections and the accepted CFRMF neutron spectrum are 291 mb/atom and 17.2 mb/atom.

A major effort will be made in FY 79 to measure the cross sections for production of ^{242}Cm and ^{244}Cm from ^{241}Am capture and ^{243}Am capture, respectively. These measurements will entail extensive quantitative chemistry and absolute alpha counting.

[1] Y. D. Harker, R. A. Anderl, E. H. Turk, "Review of Integral Data on Higher Transactinides", [review paper presented at Meeting on Nuclear Data of Higher Pu and Am Isotopes for Reactor Applications, BNL, Nov. 20-21, 1978].

3. Reaction-rate and fission-yield measurements in ^{252}Cf (R. C. Greenwood, R. G. Helmer)

Infinitely dilute reaction rates have been obtained from foil irradiations in the ^{252}Cf neutron facility at NBS for the $^{58}Ni(n,p)$ ^{58}Co reaction and for the production of ^{95}Zr, ^{103}Ru, ^{132}Te and ^{140}Ba-^{140}La following fission in ^{235}U using γ-ray spectrometry. Combining these reaction rates with the NBS-certified free-field neutron fluences and free-field fission rate for ^{235}U, we obtain a value of 119.4 ± 2.7 mb for the integral cross section of the $^{58}Ni(n,p)^{58}Co$ reaction together with the fission-yield values summarized in Table E-2.

TABLE E-2

Fission yields obtained for ^{235}U in a ^{252}Cf spontaneous-fission neutron field.

Fission Isotope	^{235}U Cumulative Fission Yield (%)
^{95}Zr	6.43 ± 0.16
^{103}Ru	3.38 ± 0.09
^{132}Te	6.4 ± 0.7
^{140}Ba-La	5.97 ± 0.14

4. Measurement of relative reaction rates in the ^{235}U cavity fission neutron facility at NBS (R. C. Greenwood, R. G. Helmer)

The relative rates for the $^{54}Fe(n,p)^{54}Mn$ and $^{58}Ni(n,p)^{58}Co$ reactions in a ^{235}U thermal-fission neutron field have been obtained by measuring the induced γ-ray activities in a foil of SRM-1158 high-nickel steel irradiated in the ^{235}U cavity fission neutron facility at NBS. From these data a value of 1.346 ± 0.007 was obtained for the $^{58}Ni(n,p)/^{54}Fe(n,p)$ reaction-rate ratio in this neutron field. This value is identical to that reported earlier by Fleming and Spiegel[1], but has an improved accuracy. With the present uncertainty it is now clear that there is a significant discrepancy between the measured value of this ratio and that predicted by ENDF/B-IV (i.e., 1.308).

---

[1] R. Fleming and V. Spiegel, Proc. 2nd ASTM-EURATOM Sym. on Reactor Dosimetry: Dosimetry Methods for Fuels, Cladding and Structural Materials, NUREG/CP-0004 (1977) Vol. 2, p. 953.

F. ^{252}Cf $\bar{\nu}$ MEASUREMENT PROGRAM

1. Measurement of $\bar{\nu}$ for ^{252}Cf (J. R. Smith, S. D. Reeder (ACC-Idaho), R. J. Gehrke)

The number of neutrons produced per fission ($\bar{\nu}$) is being determined for ^{252}Cf using the manganese bath technique. The manganese bath is used to determine the neutron yield of ^{252}Cf foils whose fission rate is determined by methods described in a separate section of this report. The bath itself consists of analytical Reagent Grade $MnSO_4$ dissolved in demineralized water; and extensive chemistry is performed to measure and monitor the concentration and impurity content. A key factor in determining the neutron yield from the observed ^{56}Mn activity induced in the bath is the calibration of the overall efficiency of the counters for detecting the ^{56}Mn disintegrations. The efficiency is determined by observing the counting rate due to an aliquot of a solution of activated ^{56}Mn, whose disintegration rate per gram is established by 4π β-γ coincidence counting. A separate section of this report describes the 4π β-γ system and its application to the absolute counting of ^{56}Mn.

Measurements of the neutron yields of the four ^{252}Cf fission foils at a fixed manganese-bath concentration are nearly complete. Measurements at several other concentrations will be made to establish an effective value of the hydrogen-to-manganese absorption ratio for the bath and to test the consistency of the applied corrections to the measurements.

2. Determination of Fission Rates for ^{252}Cf (J. R. Smith)

As part of the effort to measure $\bar{\nu}$ for ^{252}Cf, the absolute fission rates of four ^{252}Cf foils have been accurately determined, using a variety of techniques. The foils are mounted in NBS double fission chambers[1]. All four foils have been calibrated by both 2π counting and neutron-fission coincidence counting. The 2π values are of marginal utility, particularly for the first two foils obtained, because of the time-dependent effects of self-transfer of the ^{252}Cf from the foils. Two of the foils were mounted on ~200 μg/cm^2 Ni, making possible calibration by a fission-fission coincidence-counting technique. However, for all four chambers the greatest reliance has been on the neutron-fission coincidence technique, which has been used in several modes.

Two NE 213 neutron detectors were used, which, with two discriminators in the fission channel, formed two separate neutron-fission coincidence channels. It was thus possible to make simultaneous measurements using different fission-channel dead times, different neutron-channel geometries, and neutron energy biases. The fission chamber was mounted in a goniometer, which with the neutron detectors was mounted on an optical bench. This arrangement made it possible to vary the neutron detector geometry easily and reproducibly. Measurements were made both by varying the detector angle with fission-discriminator bias fixed and by varying the discriminator bias with the detector angle fixed. The former measurement yields the angular correlation function, which is appropriately averaged to find the fission rate. The latter measurement yields a family of curves, linear over the plateau region of the fission pulse-height distribution, which intersect at the point representing the true fission rate. The two types of measurements are in excellent agreement. In another variant of the n-f coincidence method, pulses from the two neutron detectors were placed in coincidence with the fission-chamber pulses. The resultant angular correlation functions have greater amplitude and sharper cusps in the plane of the fission foil than those obtained from single neutron-fission coincidence measurements.

It is expected that the combination of the various fission measurements will establish the fission rates to an accuracy between 0.1% and 0.2%.

---

[1] J. A. Grundl et al., "Measurement of Absolute Fission Rates," Nucl. Tech. 25, 237 (1975).

3. Efficiency Calibrations of the Manganese Bath Counters (R. J. Gehrke, J. R. Smith)

As part of the program to measure $\bar{\nu}$ we have been providing efficiency calibrations for the manganese bath counters by the use of

4π β-γ coincidence counting. Precisely determined mass aliquots for 4π β-γ and manganese-bath sources are prepared from a master solution of ^{56}Mn in 0.5 N HCl. Two 4π β-γ coincidence counting systems are used in these measurements. One system is a "classical" nonextendable dead-time system, and the other is based on a measured extendable dead time with an overlap coincidence circuit.

In order to provide calibrations of the manganese-bath counters to the accuracy required (<0.25%), a systematic search was made to estimate the magnitudes of the various sources of error: source purity (<0.05%); mass aliquots (<0.04%); dead-time measurement ($\lesssim$0.10%); coincidence timing ($\lesssim$0.15%); correction equations ($\lesssim$0.02%); and ^{56}Mn half-life ($\lesssim$0.1%). Uncertainties due to statistics contribute $\lesssim$0.1%.

As a result of our investigations into the sources of error in making accurate disintegration-rate measurements, we believe that in any one calibration, it is possible to determine the activity of the master solution to $\leq$ 0.25%. Further, by varying each of the above 4π β-γ parameters for several calibrations to average out the various error components the efficiency of the manganese-bath counters can be determined to an accuracy of $\leq$ 0.2%.

A. DECAY STUDIES OF GASEOUS FISSION PRODUCTS AND THEIR DAUGHTERS

Prior to 1976 studies of the decay of fission products at the TRISTAN on-line mass separator facility were confined mostly to the rare gases Kr and Xe and their daughters. Most of this work has been published and presented in past contributions to the Nuclear Data Committee.

1. The Decay of ^{90}Kr (C. L. Duke, W. L. Talbert, Jr., F. K. Wohn, J. K. Halbig, and K. Bonde Nielsen)

The study of the decay of ^{90}Kr to levels in ^{90}Rb is complete and has been accepted for publication in Phys. Rev. C. Of 103 γ transitions observed, 96 were placed in a level scheme consisting of 31 excited states. Levels up to 3881 keV were observed. The γ singles information is summarized in Table A-1. Internal conversion coefficients were determined for 4 transitions and that information is summarized in Table A-2.

Table A-1. γ-ray transitions observed in the decay of ^{90}Kr

Energy (keV)	Relative Intensity[a]	Energy (keV)	Relative Intensity[a]
106.05 ± 0.03	11.5 ± 0.7	465.28 ± 0.19	1.8 ± 0.3
106.92 ± 0.15	1.1 ± 0.3	470.34 ± 0.08	6.1 ± 0.4
120.92 ± 0.3	90 ± 6.	476.10 ± 0.11	3.4 ± 0.3
121.82 ± 0.03	910 ± 30.	492.63 ± 0.05	31.0 ± 0.8
180.66 ± 0.15	1.0 ± 0.5	498.59 ± 0.12	3.9 ± 0.3
220.82 ± 0.14	1.0 ± 0.5	508.0 ± 0.3	1.6 ± 0.5
227.76 ± 0.08	3.2 ± 0.3	539.49 ± 0.04	790 ± 18
234.44 ± 0.03	68 ± 3.	554.37 ± 0.05	130 ± 3
242.19 ± 0.03	255 ± 8.	565.19 ± 0.08	5.3 ± 0.4
249.32 ± 0.03	35 ± 3.	569.20 ± 0.05	15.5 ± 0.5
305.10 ± 0.18	1.4 ± 0.3	577.1 ± 0.3	1.4 ± 0.4
309.07 ± 0.09	3.5 ± 0.3	585.76 ± 0.20	1.3 ± 0.2
356.00 ± 0.20	2.7 ± 1.0	614.38 ± 0.09	5.4 ± 0.4
386.48 ± 0.09	3.3 ± 0.3	619.08 ± 0.05	27.8 ± 0.8
392.6 ± 0.4	0.6 ± 0.3	621.3 ± 0.9	1.0 ± 0.7
396.54 ± 0.21	1.3 ± 0.3	626.49 ± 0.8	7.3 ± 0.5
419.12 ± 0.05	8.2 ± 0.3	658.1 ± 0.5	0.8 ± 0.3
429.93 ± 0.14	3.8 ± 0.8	661.23 ± 0.5	8.5 ± 0.3
433.47 ± 0.05	33.5 ± 1.0	677.69 ± 0.7	9.8 ± 0.5
433.9 ± 0.3	2.6 ± 0.8	690.72 ± 0.7	10.2 ± 0.4

Table A-1 continued.

Energy (keV)	Relative Intensity[a]	Energy (keV)	Relative Intensity[a]
705.47 ± 0.12	3.2 ± 0.3	1819.1 ± 0.3	1.9 ± 0.3
731.33 ± 0.04	38.1 ± 1.0	1885.42 ± 0.15	5.8 ± 0.4
739.0 ± 1.0	0.6 ± 0.2	1899.61 ± 0.16	4.9 ± 0.4
745.8 ± 0.4	1.6 ± 0.5	1980.99 ± 0.15	4.4 ± 0.3
925.49 ± 0.09	5.7 ± 0.4	2006.00 ± 0.14	3.0 ± 0.5
941.86 ± 0.5	34.3 ± 0.9	2127.52 ± 0.07	35.3 ± 1.2
947.6 ± 0.4	1.5 ± 0.5	2149.51 ± 0.10	7.1 ± 0.3
967.33 ± 0.11	5.5 ± 0.5	2160.9 ± 0.6	0.81± 0.24
980.29 ± 0.11	4.8 ± 0.4	2191.46 ± 0.25	2.9 ± 0.3
1031.2 ± 0.3	1.6 ± 0.4	2205.6 ± 0..6	1.0 ± 0.3
1039.11 ± 0.8	10.7 ± 0.5	2352.7 ± 0.4	2.3 ± 0.4
1103.92 ± 0.07	8.8 ± 0.5	2417.33 ± 0.23	4.9 ± 0.4
1118.69 ± 0.05	1000 ± 22	2421.5 ± 0.8	1.3 ± 0.4
1165.56 ± 0.06	21.2 ± 0.8	2432.78 ± 0.21	3.9 ± 0.4
1240.34 ± 0.11	9.0 ± 0.6	2468.56 ± 0.11	12.0 ± 1.0
1293.7 ± 0.4	1.5 ± 0.4	2479.4 ± 0.7	1.0 ± 0.5
1303.36 ± 0.24	2.4 ± 0.4	2497.6 ± 1.5	0.4 ± 0.2
1309.68 ± 0.10	7.1 ± 0.4	2726.68 ± 0.11	22.4 ± 0.9
1341.31 ± 0.22	4.0 ± 0.5	2770.9 ± 0.4	1.5 ± 0.3
1386.62 ± 0.15	5.0 ± 0.5	2855.4 ± 0.3	8.3 ± 1.6
1423.77 ± 0.06	75.3 ± 1.7	2865.73 ± 0.21	4.8 ± 0.4
1460.6 ± 0.5	1.7 ± 0.5	2948.8 ± 0.5	1.0 ± 0.5
1466.26 ± 0.15	6.3 ± 0.5	3010.3 ± 0.8	0.79± 0.25
1530.50 ± 0.20	1.0 ± 0.5	3205.1 ± 0.6	0.89± 0.22
1537.85 ± 0.05	248 ± 5	3217.1 ± 2.1	0.28± 0.22
1552.18 ± 0.06	56.3 ± 1.4	3256.2 ± 1.2	0.53± 0.22
1620.22 ± 0.22	3.9 ± 0.4	3269.0 ± 0.4	1.7 ± 0.3
1658.18 ± 0.06	34.0 ± 0.9	3344.3 ± 0.3	2.9 ± 0.4
1692.6 ± 0.5	2.0 ± 0.5	3465.1 ± 0.9	0.9 ± 0.3
1695.2 ± 1.9	0.33± 0.19	3855.3 ± 0.4	3.1 ± 0.3
1751.0 ± 0.3	1.5 ± 0.3	4166.5 ± 1.0	0.8 ± 0.3
1780.04 ± 0.6	172 ± 4		

[a]The relative intensity can be converted to transitions per 100 β decays using the factor 0.0362, as calculated with a ground-state β granching of 29%.

Table A-2. Internal conversion coefficient results

E (keV)	Relative Intensity			Conv. Coeff.[a]	
	I_γ	I_K	I_L	α_K	α_L
106.0	11.5±0.7	2.54±0.08		0.22±0.06	
106.9	1.1±0.3	9.72±0.15	1.6[b]±0.3	8.84	1.4±0.5
120.9	90±6	13.1[b]±0.9		0.15±0.04	
121.8	910±30	128[b]±7		0.14±0.04	

[a]Obtained with 106.9-keV isomeric transition as pure M3.

[b]Intensities obtained using relation $(I_{120.9K}+I_{121.8K})/I_{106.9K}$ =14.6±0.5.[12]

2. Decay Energies of Gaseous Fission Products and their daughters for A=88 to 93 and A=138 to 142 (F. K. Wohn and W. L. Talbert, Jr.)

Decay energies for several mass-separated activities of Kr, Xe, and their daughters have been reported previously.[1] Using recently available decay energies for Rb and Cs fission products, the calibration curve for β energies above 5 MeV has been redetermined. The new Q_β values are reported for 23 fission products. This material has been published[2] and the new Q_β values reported in Table I of Ref. 2.

3. Identification of ^{147}Cs and Half-Life Determinations for Cs and Ba Isotopes with A=144-147 and Rb and Sr Isotopes with with A=96-98 (F. K. Wohn, K. D. Wünsch, H. Wollnik, R. Decker, G. Jung, E. Koglin, and G. Siegert)

Half-lives were obtained for a number of Rb and Cs fission products using the OSTIS separator facility. The resulting half-lives (in sec.) are ^{96}Rb (0.203±0.004), ^{96}Sr (1.015±0.019), ^{97}Rb (0.170±0.002), ^{97}Sr (0.441±0.015), ^{98}Rb (0.108±0.005), ^{98}Sr (0.66±0.07), ^{144}Cs (1.02 ±0.04), ^{144}Ba (12.3±0.4), ^{145}Cs (0.590±0.020), ^{145}Ba (4.31±0.16), ^{146}Cs (0.305±0.010), ^{146}Ba (2.18±0.11), ^{147}Cs (0.218±0.009), and ^{147}Ba (0.70±0.06). The work also provided an unambiguous identification

[1] Clifford, Talbett, Wohn, Adams, and McConnell, Phys. Rev. C 7, 2535 (1973). Adams, Carson, Lee, Talbert, Wohn, Clifford, and McConnell, Phys. Rev. C 8, 767 (1973).

[2] Wohn and Talbert, Phys. Rev. C 18, 2328 (1978).

of the new neutron-rich isotope ^{147}Cs. This material has been published[3] in Phys. Rev. C.

B. DECAY STUDIES OF NON-GASEOUS FISSION PRODUCTS WITH AN IN-BEAM ION SOURCE

In late 1976 a new target ion-source combination was installed and successfully operated at the TRISTAN facility at the Ames Laboratory. The new system was christened TRISTAN II and used to separate and study fission generated isotopes of Zn, Ga, Ag, Cd, and In. Measurements on the decay of ^{78}Zn, ^{78}Ga, ^{118}Ag, ^{120}Ag, ^{122}Ag, ^{126}Cd, ^{126}In, and ^{128}In were carried out. At the end of December 1977, the Ames Laboratory Research Reactor was permanently shut down and the TRISTAN II facility was moved to the High Flux Beam Reactor at Brookhaven National Laboratory. An extensive program on the measurement of the decay properties of mass-separated fission products is scheduled to begin in the Fall of 1979. Analysis is still continuing on decay data accumulated with TRISTAN II at Ames. Decay studies of ^{122}Ag[4] and ^{126}Cd[5] have been published and a study of the decay of the two isomers of ^{126}In has been submitted to Phys. Rev. C. A study of the decay of ^{78}Zn is almost complete.

1. Decay of ^{126}In and ^{126}In^{m} (M. L. Gartner and John C. Hill)

A study of ^{126}In (1.84±0.09s) and ^{126}In^{m} (1.96±0.1s) has been made. It is unclear which isomer is the ^{126}In ground state. All 48 γ rays observed were placed in a level scheme for ^{126}Sn. ^{126}In populates 16 levels up to 4304 keV while ^{126}In^{m} populates 11 levels up to 3856 keV. The γ singles information is summarized in Table B-1.

2. Decay of ^{78}Zn (D. A. Lewis, F. K. Wohn, John C. Hill, and M. L. Gartner)

A study of the decay of ^{78}Zn to levels in ^{78}Ga was made. A preliminary value of 1.4 sec was obtained for the ^{78}Zn half-life. A total of 36 γ transitions were ascribed to the decay of ^{78}Zn and a level scheme for ^{78}Ga is being constructed. A very preliminary list of γ-ray energies and intensities associated with ^{78}Zn decay is given in Table B-2.

---

[3] F. K. Wohn, K. D. Wünsch, H. Wollnik, R. Decker, G. Jung, E. Koglin, and G. Siegert, Phys. Rev. C 17, 2185 (1978).

[4] L. L. Shih, John C. Hill, and S. A. Williams, Phys. Rev. C 17, 1163 (1978).

[5] M. L. Gartner and John C. Hill, Phys. Rev. C 18, 1463 (1978).

Table B-1. γ-ray transitions observed in the decay of ^{126}In and ^{126}In^{m}

Energy (keV)	Relative Intensity A[a]	Relative Intensity B[b]	Relative Intensity C[c]
57.36 ± 0.16	11 ± 2		45 ± 8
111.79 ± 0.17	220 ± 20		905 ± 82
258.5 ± 0.2[d]	25 ± 8[d]		103 ± 33
269.26 ± 0.13	16 ± 2		66 ± 8
316.03 ± 0.16	28 ± 5		115 ± 21
363.3 ± 0.4	9 ± 3		37 ± 12
418.6 ± 0.5[e]	2 ± 1	3 ± 1	
444.2 ± 0.5[f]	4 ± 2[f]		16 ± 8
463.3 ± 0.7[g]	≤ 3[g]		≤ 12
501.5 ± 0.4[h]	11 ± 4[h]		45 ± 16
517.2 ± 0.5[e]	4 ± 2[e]	5 ± 3	
548.6 ± 0.5[h]	1.0 ± 0.5[i]	1.2 ± 0.6	
631.94 ± 0.09	27 ± 3	36 ± 4	
716.9 ± 0.5[j]	4 ± 1[j]	5 ± 1	
788.4 ± 0.51[h]	12 ± 5[k]		49 ± 20
905.8 ± 0.5[ℓ]	2 ± 1		8 ± 4
908.71 ± 0.08	243 ± 13		
969.74 ± 0.08	207 ± 11	273 ± 13	
1053.39 ± 0.17	29 ± 4	35 ± 7	
		3 ± 1	
1068.3 ± 0.4	14 ± 6	18 ± 8	
1135.88 ± 0.19	37 ± 7	32 ± 10	
		17 ± 4	
1141.36 ± 0.07	1000 ± 50	1000 ± 66	1000 ± 53
1192.80 ± 0.14	10 ± 2		41 ± 8
1229.61 ± 0.14	19 ± 4	25 ± 5	
1252.1 ± 0.2	29 ± 5	38 ± 7	
1327.7 ± 0.4[h]	9 ± 3[i]	12 ± 4	
1367.6 ± 0.5[g]	≤ 13[g]		≤ 53
1378.35 ± 0.13	56 ± 6		230 ± 25
1495.4 ± 0.3	16 ± 3	21 ± 4	
1571.24 ± 0.13	33 ± 4	44 ± 5	
1594.0 ± 0.3	17 ± 4	22 ± 5	
1601.8 ± 0.3	24 ± 4	32 ± 5	
1636.89 ± 0.11	57 ± 5		235 ± 21
1687.27 ± 0.17	30 ± 4	40 ± 5	
1755.0 ± 0.5[i]	4 ± 2[i]	5 ± 3	
2105.9 ± 0.3	30 ± 5	40 ± 7	
2111.4 ± 0.2	47 ± 5	62 ± 7	
2203.95 ± 0.16	36 ± 6	48 ± 8	
2371.1 ± 0.3	25 ± 5	33 ± 7	

Table B-1 continued.

Energy (keV)	Relative Intensity		
	A[a]	B[b]	C[c]
2637.2 ± 0.4	9 ± 3	12 ± 4	
2745.9 ± 0.4	11 ± 4	15 ± 5	
2822.7 ± 0.4	10 ± 4	13 ± 5	
3247.3 ± 0.3	28 ± 5	37 ± 7	
3345.5 ± 0.5	300 ± 16	396 ± 21	
3887.6 ± 0.5	64 ± 6	85 ± 8	
3964.7 ± 0.5	38 ± 6	50 ± 8	
4240.3 ± 0.7	21 ± 4	28 ± 5	
4304.2 ± 0.6	31 ± 4	41 ± 5	

[a]Intensities normalized to 1000 for the 1141-keV γ ray.

[b]Intensities normalized to 273 for the 970-keV γ ray.

[c]Intensities normalized to 1000 for the 909-keV γ ray.

[d]Energy and intensity determined from daughter singles spectrum.

[e]Energy and intensity determined from the spectrum in coincidence with the 1687-keV γ ray.

[f]Energy and intensity determined from the spectrum in coincidence with the 1193-keV γ ray.

[g]Energy and intensity determined from the spectrum in coincidence with the 269-keV γ ray.

[h]Energy determined from the coincidence profile.

[i]Intensity determined from the spectrum in coincidence with the 1141-keV γ ray.

[j]Energy and intensity determined from the spectrum in coincidence with the 970-keV γ ray.

[k]Intensity determined from the spectrum in coincidence with the 112-keV γ ray.

[ℓ]Energy and intensity determined from the spectrum in coincidence with the 789-keV γ ray.

Table B-2. γ-ray transitions observed in the decay of ^{78}Zn

Energy (keV)	Relative Intensity[a]	Energy (keV)	Relative Intensity[a]	Energy (keV)	Relative Intensity[a]
60.2	62	303.4	72	909.1	48
92.1	14	321.9	90	957.8	27
112.3	74	343.9	128	979.8	142
119.4	120	354.2	172	1006.2	185
132.7	15	386.2	43	1305.1	33
170.7	36	395.5	18	1345.2	107
172.5	53	453.9	463	2026.8	23
181.7	630	635.6	487	2060.6	33
187.8	49	749.7	86	2205.7	94
224.7	1000	808.0	73	2571.5	50
262.3	94	818.4	40	2693.6	20
281.3	440	860.3	531	2771.2	37

[a]Intensity normalized to 1000 for the 225-keV γ ray.

C. DECAY STUDIES OF LOW-MASS NEUTRON-RICH NUCLIDES AT LAMPF

A program is underway to characterize the decays of new or poorly studied neutron-rich nuclides in the mass region $30 < A < 70$. These nuclides are produced by irradiation of appropriate targets with intermediate energy neutrons generated at the area A beam stop of the LAMPF high current 800-MeV proton accelerator. No mass separator is available but the element of interest was separated from contamination by fast gas phase radiochemical procedures. We observed for the first time the decay of short-lived neutron-rich ^{39}S and ^{46}Ar.

1. Decays of ^{45}Ar and ^{46}Ar (R. F. Petry, D. G. Shirk, John C. Hill, and K. H. Wang)

The study of the decays of the neutron-rich isotopes ^{45}Ar ($T_{1/2}$=20.8±0.5 sec) and ^{46}Ar ($T_{1/2}$=8.9±0.7 sec) has been completed and published[6] in Phys. Rev. C. In ^{46}Ar only one γ ray was observed at 1944.32±0.19 keV. A total of 15 γ rays were ascribed to the decay of ^{45}Ar. This information is summarized in Table I of Ref. 6. All of the ^{45}Ar γ rays except one were placed in a level scheme for ^{45}K.

---

[6]R. F. Petry, D. G. Shirk, John C. Hill, and K. H. Wang, Phys. Rev. C 17, 2197 (1979).

2. Decay of ^{39}S (R. F. Petry, John C. Hill, and K. H. Wang)

Measurements on the decay of ^{39}S ($T_{1/2}$=11.5±0.5 sec) and analysis of the γ-ray singles and coincidence data has been completed. We attributed 6 γ rays to the decay of ^{39}S and were able to place all of them in a level scheme for ^{39}Cl with levels up to 257 keV. A summary of the γ-ray energy and intensity measurements is given in Table C-1. This material is being prepared for submission to Phys. Rev. C.

Table C-1. γ rays from ^{39}S decay

Energy (keV)	Relative Intensity[a]
396.50 ± 0.20	911 ± 80
484.85 ± 0.24	243 ± 30
874.31 ± 0.18	290 ± 33
903.8 ± 0.6	80 ± 25
1300.52 ± 0.16	1180 ±110
1696.62 ± 0.17	1000 ± 80

[a]Intensities normalized to 1000 for the 1697-keV γ ray.

UNIVERSITY OF KENTUCKY

A. NEUTRON SCATTERING

1. Total and Differential Elastic Scattering Measurements with Isotopically Enriched Sn Samples. (Harper, Weil, and McEllistrem)

A series of neutron scattering experiments have been completed for the even-A Sn isotopes with A = 116, 118, 120, 122, and 124. Total cross sections have been measured for incident energies (E_n) between 0.2 and 5.0 MeV with an energy spread which varied from ~90keV at low energies to ~30 keV at 5.0 MeV. Differential scattering cross sections have been measured as a function of angle between 20° and 150° at E_ns of 1.0, 1.63, and very recently 4.0 MeV. Both elastic and inelastic scattering cross sections have been measured. Measurements are planned in the near future for E_n ~9 MeV.

The differential cross section measurements used time-of-flight techniques and were normalized to previously published C scattering cross sections, with the aid of measured yields from a small C scattering sample. The total cross section measurements also included a C sample, and comparisons of our C measurements to recent NBS total cross sections indicate an accuracy of ±(1.5-2.0)% below E_n=2.0 MeV with the accuracy decreasing to ±4% at higher energies.

The scattering data at E_n = 1.0 and 1.63 MeV and the total cross section data have been reduced, corrected for sample-size effects, and analyzed in a conventional optical model. Good fits to these data are obtained, but require unusually strong neutron excess dependence of the surface absorptive potential. If the absorptive potential is written $W = W_o + W_1(N-Z/A)$, W_1 is found to be -49 ± 9 MeV at E_n = 1.0 MeV, and -58 ± 10 at 1.63 MeV. Combining the potential with the Wolfenstein-Hauser-Feshbach model, with fluctuation corrections, a good fit is obtained for inelastic scattering to the first 2^+ level. These inelastic scattering cross sections decrease 20% as A is changed from 116 to 124, and are isotropic to within 10% at E_n = 1.63 MeV. Data reduction and analyses are in progress for E_n = 4.0 MeV.

2. Excitations of Collective Modes in ^{150}Nd and ^{152}Sm in Neutron Scattering (Tripathi, Coope, Schell, McEllistrem)

The energy levels and decay schemes of ^{150}Nd and ^{152}Sm have been studied using the (n,n'γ) reaction. In ^{150}Nd several new levels are established and some new spin assignments are made. A remarkable feature of the γ-ray spectra for both ^{150}Nd and ^{152}Sm is the strong excitations of the 2_g^+, 4_g^+, and 6_g^+ members of the ground state band (gsb), and of the bandheads of the β,γ and octupole bands at 2.5 MeV incident neutron energy. The corresponding neutron inelastic scattering cross sections are factors of 2-4 larger than statistical model predictions. Unusually large inelastic scattering cross sections for scattering to members of the ground-state rotational band had been reported from this laboratory for deformed rare earths. Now these especially large cross sections are also observed for other bands: the γ-, β-, and octupole-bands excited with low energy (2.5 MeV) neutrons. Because the cross sections are unusually large, they are listed below for members of these bands, and then shown summed for an entire level.

3. E1 and Other Excitations in ^{208}Pb Induced by 7.0 MeV Neutrons (Coope, Hanly, Tripathi, McEllistrem)

The role of E1 excitations in neutron inelastic scattering from ^{208}Pb has been explored. In essence, we find that the excitation of 1^- levels does not reflect their E1 strength, even when the transitions are to particularly collective levels. By "collective" 1^- levels, we mean those which have substantial E1 photon widths. We have made definite spin assignments to two J = 1 levels, at 5805.0 and 5946.4 keV and observed scattering intensities to six of them. This includes all known dipole levels below 6-MeV excitation. The neutron excitation strengths of these levels are compared with those from photon scattering, and with statistical model expectations. The neutron scattering cross sections to the 1^- levels are just those of the statistical model including the 5511.8-keV level, which has a photon width of ~20% of the single particle width, much larger than that of any other 1^- level. In contrast to this the lowest 2^+ and 4^+ levels, at 4085.4 keV and 4323.8 keV, have inelastic scattering cross sections 3 times as large as statistical model predictions.

The scattering cross sections were obtained from (n,n'γ) production cross sections using pulsed-beam time-of-flight techniques to reduce γ-ray backgrounds.

Table 1

COMPARISON OF NEUTRON INELASTIC SCATTERING CROSS SECTIONS FOR ^{150}Nd and ^{152}Sm

J^{π} and E_x denote the spin and parity and excitation energy of the level. $\sigma_{n'}$ denotes the scattering cross section to the level and σ_b denotes the sum of cross sections $\sigma_{n'}$ to all observed members of the identified band.

^{152}Sm				^{150}Nd			
J^{π}	E_x(keV)	$\sigma_{n'}$(mb)	σ_b(mb)	J^{π}	E_x(keV)	$\sigma_{n'}$ (mb)	σ_b(mb)
2^+	121.8	600	Ground State	2^+	130.1	617	Ground State
4^+	366.6	259		4^+	381.2	282	
6^+	707.0	64	929	6^+	720.2	55	954
8^+	1123.6	6		8^+	1129.2	--	
0^+_{β}	684.9	64	β	0^+_{β}	676.0	70	β
2^+_{β}	810.5	195		2^+_{β}	850.1	170	
4^+_{β}	1022.9	91	350	4^+_{β}	1137.2	67	307
1^-	963.3	224	Octupole	1^-	852.5	171	Octupole
3^-	1041.1	168	431	3^-	934.4	148	379
5^-	1221.4	39		5^-	1128.9	60	
2^+_{γ}	1085.8	133	γ	2^+_{γ}	1061.6	199	γ
3^+_{γ}	1233.8	100	288	3^+_{γ}	1200.0	151	398
4^+_{γ}	1371.5	55		4^+_{γ}	1350.9	48	
2^+	1292.6	85			1180.0	28	
1^-	1510.4	40		(1,2)	1283.6	53	
2^-	1529.8	65		(2,3)	1307.5	70	
3^-	1578.9	36			1426.7	37	
(2-4)	1650.3	43			1518.5	18	
(2-4)	1680.7	18			1544.4	28	
(5^-)	1730.0	27			1579.8	44	

B. THE (p,n) AND (α,n) REACTIONS

1. Reaction Rates for Nucleosynthesis (Flynn, Hershberger, Gabbard)

Cross sections for the (p,n) and (α,n) reactions are measured with a detection method with good sensitivity to very low energy neutrons, <30 keV. The neutrons are detected in a 60-cm-diameter polyethylene sphere detector with an efficiency which is independent of energy for neutrons having energies between 30 keV and 2.5 MeV. In some cases, cross sections for the inverse reactions have been obtained using the principle of detailed balance. Nucleosynthesis reaction rates $N_A(\sigma v)$ have been determined in most cases. The (p,n) reaction studies are of interest in establishing reaction systematics for p-process nuclei.

The important parameters in reaction rate calculations are:

$$E\,\bar{\sigma}^u_{jk}\,(J^\pi) \propto \frac{T^u_j\,T_k}{T} \qquad (1)$$

The Hauser-Feshbach theory gives this product as a function of the transmission coefficients for the incident and exit channels.

To first order, the strength function and the transmission coefficient for a given channel are related by,

$$T^u_{\ell,j} = 4\pi\,P_\ell \left\langle \frac{\gamma^2_{\ell,j}}{D} \right\rangle^u \qquad (2)$$

where $\left\langle \frac{\gamma^2_{\ell,j}}{D} \right\rangle^u$ is the strength function for channel $I^u + j$. We have chosen to present the data on (p,n) reactions in the form of strength functions. Accurate strength functions can provide an important data base for reaction rate calculations for applications in nucleosynthesis.

The proton strength functions for intermediate-mass nuclei are of interest, for example, in the reaction network of the p-process in supernovae. The so-called p-process nuclei range in mass number from 74 to 196 and range in solar mass fraction from one part per billion (10^{-9}) to one part per trillion (10^{-12}) in the solar system. Study of the systematics of (p,n), (p,γ), (n,γ), (n,p), etc. is important to the determination of stellar reaction rates.

The proton strength function measurements which have been made at Kentucky are for nuclei ranging in mass number from 88 to 124 and for the proton-energy range below 6.5 MeV.

The Kentucky-Polyethylene-sphere detector was used to measure the total number of neutrons produced in the (p,n) and (α,n) reactions. The most important feature of this detector is that the efficiency is nearly independent of energy for neutrons with energies less than about two MeV. The detector efficiency is known here to an accuracy of ±3%. The detector has been calibrated with the standard source, NBS II.

For the experiment, targets are placed at the center of the sphere and the beam is passed through them into a beam dump about two meters away. Backgrounds are determined by passing the beam through a target backing of an inert foil with a thickness about the same as that of the target material. This technique provides an estimate of background produced by particles scattered into the chamber walls.

Our most recent results include cross sections for the $^{56}Fe(\alpha,n)^{59}Ni$ reaction. Figure 4 shows results of an experiment to measure $^{56}Fe(\alpha,n)^{59}Ni$. This reaction is important in the radioactive waste storage problem as well as in the thermonuclear reactor design. For this measurement, the target was about 100 $\mu g/cm^2$ and no fine structure is seen.

The present results are cross sections more than a factor of 2 higher than those calculated by Woosley <u>et al</u>.[1] who used simple reaction model calculations to predict the cross sections in the absence of reliable measurements. The measured cross section rises smoothly from $\sigma \approx 1$ mb at 6 MeV to ≈ 5 mb near 6.7 MeV, with an extrapolated threshold of about 5.46 MeV α-particle energy. Reaction rates for several reactions of nucleosynthesis interest are shown for an assumed temperature of 2.5×10^9 °K in Table 1. The most recent measurements are the last three entries in the table, and all of them are compared to the model projections of Woosley <u>et al</u>.

---

[1] Woosley, Fowler, Holmes and Zimmerman, "Tables of Thermonuclear Reaction Rate Data for Intermediate Mass Nuclei", Report #OAP-422 California Institute of Technology.

Table 1. Reaction Rates for Selected Reactions at a Temperature of 2.5 x 10^9 K.

These rates, labelled "Exp." in Table 1 are compared to the calculations of Woosley *et al.*

Reaction	Exp.	Woosley *et al.*	Exponent
$^{27}Al(p,n)$	1.01	1.37	-03
$^{27}Al(\alpha,n)$	5.20	4.60	00
$^{29}Si(\alpha,n)$	2.64	2.55	01
$^{32}S\ (n,\alpha)$	2.06	1.99	05
$^{30}Si(\alpha,n)$	5.07	4.29	00
$^{33}S\ (n,\alpha)$	5.00	3.90	07
$^{56}Fe(\alpha,n)$	13.5	6.92	05
$^{59}Co(p,n)$	1.88	1.77	03
$^{59}Ni(n,p)$	1.05	--	07

2: Proton Strength Functions (Hershberger, Flynn, and Gabbard)

To study the systematics of many nuclear reactions important to nucleosynthesis, such as (p,γ), (p,α), (p,n), (γ,p), (γ,n), etc., it is useful and convenient to express average reaction strengths in terms of strength functions. Such strength functions or reduced cross sections are defined as:

$$S = R\left\langle\frac{\gamma^2}{D}\right\rangle_{Av} = \frac{R\langle\sigma(p,n)\rangle}{4\pi^2\ \lambda^2 \sum_{\ell} (2\ell+1)P^{\ell}} \qquad (3)$$

where P^{ℓ} is the penetrability function for the protons of orbital angular momentum ℓ.

Once the strength functions have been measured, their description in terms of the nucleon optical model or some other suitable model is desirable. In the mass region $88 \leq A \leq 115$ where most of our (p,n) measurements have been made, an optical-model potential was successfully used. The rotation of the potential is that of Pery and Perey.[2] The

[2] C. M. Perey and F. G. Perey, Atomic and Nuclear Data Tables 17, 1 - 101 (1976).

form factors are Saxon-Woods and Saxon-Woods derivative. The potential V was taken to be:

$$V = V_o - 0.32\ E + 24\ \frac{(N-Z)}{A} + 0.4\ \frac{Z}{A^{1/3}} \qquad (4)$$

The potential parameters are given in Table 2.

Table 2. Values of Fitting Parameters V_o, a_D, and W for the Optical Model Analysis of Data.

Isotope	V_o	a_D	W	a_DW
^{88}Sr	56.0	0.47	7.0	3.3
^{92}Zr	54.7	0.24	11.3	2.7
^{94}Zr	54.3	0.41	9.9	4.1
^{94}Mo	54.1	0.28	10.8	3.0
^{95}Mo	54.7	0.32	11.8	3.8
^{98}Mo	54.1	0.48	10.7	5.1
^{107}Ag	55.9	0.42	25.0	11.2
^{109}Ag	55.2	0.43	28.0	12.0
^{NAT}In	55.9	0.42	14.9	6.3
Sn	55.4	0.4	11.5	4.7

$R_o = 1.2\ A^{1/3}$; $V_{so} = 6.4$ MeV; $R_{so} = 1.03\ A^{1/3}$
$a_v = 0.73$; $a_{so} = 0.63$

C. PIXE AND OTHER TECHNIQUES: TRACE ELEMENT ANALYSIS IN COAL

1. Intercomparisons of Several Techniques (Pepper and Gabbard)

This program has three basic goals.

(1) to establish the reliability of the new particle-induced x-ray emission (PIXE) technique through continued comparisons with other techniques and with standard reference materials;

(2) to perform intercomparison studies for various

Institute of Mining and Minerals Research (IMMR) materials-analysis projects involving x-ray fluorescence, instrumental neutron activation, and other analysis techniques. We hope to contribute significantly to the characterization of Kentucky coals through the materials analysis program of IMMR.

(3) to continue incorporation of various automating features into our data acquisition and analysis systems in order to increase both the capacity and reliability of PIXE analysis.

General objectives are to be accomplished in four stages. In the first quarter, the principal objective has been to establish the reliability of new "clean" procedures in sample preparation. The specific work completed was as follows:

(1) Orientation of new senior chemist to the laboratory.

(2) Installation of clean room for sample preparation and storage.

(3) Preparation of "clean" Formvar backings using a pressurized filter system and other special procedures.

(4) Preparation of thin gravimetric standards on Formvar backings and investigation of the reproducibility of PIXE analyses with these standards.

In the second quarter, the principal objective was the intercomparison of PIXE analyses with standards previously calibrated using other analytical methods. The work completed then was as follows:

(1) Obtain standard reference materials previously analyzed by other techniques (primarily by IMMR staff) and compare with PIXE analyses.

(2) First studies of solid samples (coal) with immediate interest in providing preliminary data for matrix effects modeling.

(3) Final implementation of off-line computer code for automated analysis of PIXE spectra from thin samples.

Status:

(1) Preparation of "clean" Formvar backing for mounting thin targets has been completely successful and the preparation of gravimetric standards on Formvar backings and investigation of reproducibility continues.

(2) Implementation of off-line computer program for x-ray spectrum analysis has been completed.

Future Work:

(1) Comparison with other standard reference materials.

(2) Initial studies of matrix effects in coal.

(3) Development of <u>on-line</u> code for preliminary analyses.

(4) Studies of various methods of thick sample preparation.

(5) Preliminary work to incorporate matrix effects corrections into the off-line computer code.

Further plans are outlined in the Program Work Sheet.

LAWRENCE BERKELEY LABORATORY

UNIVERSITY OF CALIFORNIA

A. TABLE OF ISOTOPES PROJECT

E. Browne, J. M. H. Chong, J. M. Dairiki, D. P. Kreitz, C. M. Lederer, T. Prussin, M. E. Schwartz, M. A. Sharp, and V. S. Shirley

The publication of the seventh edition of the Table of Isotopes[1] in 1978 concluded a seven-year project involving a total effort of more than 50 man-years. Over 30,000 journal articles, reports, conference proceedings, private communications, and theses were used as source material for the present edition. In terms of both reference citations and data, the seventh edition is a factor of 4 times as large as the sixth; the complexity of the level schemes has increased even more--by almost an order of magnitude. The literature cutoff varies from about January 1977, for the lightest mass chains, to December 1977, for the heaviest.

The Table of Isotopes contains an extensive introduction which explains the scope, nomenclature, and evaluation policies used in the table. The authors' criteria for data selection are based on a determination to present the best measurements--clearly indicating conflicting results and avoiding redundancy.

The layout of the data in a single table (as opposed to the double-table format of the sixth edition) is described in Fig. 1, reproduced from the Introduction of the Table of Isotopes. Data categories included in the tabulated listings are more fully delineated in the Contents (Fig. 2). Several significant changes have been introduced in the present edition. Reported uncertainties are included for all quantities in tabular data listings. Smaller italic numbers following any value represent the uncertainty in the last place(s). A new reference-code format "journal volume page(year)" permits direct look-up of an article without the need to look up the code. A brief (12-page) list of the reference codes replaces a full bibliography, which otherwise would have increased the seventh edition by about 300 pages.

Figure 3 illustrates how a mass chain compilation is presented in the Table of Isotopes; a portion of the data for mass number A = 202 is shown. Sophisticated computer facilities and extensive programming (described in previous annual reports)[2,3] have made it possible to present the data in a variety of type sizes, styles, and intensities. The pages are thumb-tabbed by mass number for rapid data access.

This work was supported by the U.S. Department of Energy under contract No. W-7405-ENG-48.

Appendices include material of general interest to users of the Table of Isotopes (see Contents, Fig. 2). Three of the appendices deserve further comment. Appendix II contains tables of convenient standards for calibration of γ-ray, conversion-electron, and α-particle measurements. The γ-ray standard tables, prepared with the assistance

(Image size has been reduced to conform to NDC format)

II. General Features of the *Table of Isotopes*

II.A. *Layout:* An Isotope Index, ordered by atomic number (Z) and subordered by mass number (A), precedes the main table. It contains all stable nuclei, radioisotopes, and isomers that appear in the *Table of Isotopes*. (R-rated isotopes – those identified only in nuclear reactions – do not appear in the Isotope Index.) In addition to the isotope designation, the index includes the natural abundance, half-life, class (certainty of identification), and the number of the page on which the tabular data entry is found in the main table.

The main table is ordered by mass number and subordered by atomic number. For each mass number there is an abbreviated mass-chain decay scheme, showing the adopted half-lives, spin-parity assignments, and decay energies (Q-values) for the isobars, and the decay relationships between them. Noted near this scheme are the initials of the compiler(s) and, following a semicolon, those of the reviewer.

Following the mass-chain decay scheme, tabulated data and detailed nuclear level schemes are given for individual isotopes. Tabulated data entries are included for each ground state or isomer with half-life $\gtrsim 1$ s. A few shorter-lived isomeric species are also included – e.g., fission isomers and a few "historic" isomers, such as ^{24m}Na. The data include natural abundance, mass excess, nuclear spin, thermal neutron cross sections, all categories of data on radioactive decay, and excited-state half-lives. Data categories are shown to the left in **bold serif** type. The data are printed in sans-serif (plain) type. Each entry under a given data category concludes with the reference code or codes in braces {}. Longer data entries (radiation data in particular) begin on a new line, indented to the left of any continuation lines.

Detailed level schemes are given for each isotope (A,Z) for which there is information beyond that shown on the mass-chain decay scheme. The schemes are separated into a "decay-level" scheme, showing levels and transitions observed in the decay of all parent isotopes and isomeric states, and a "reaction" scheme, summarizing the information derived from nuclear reaction studies. Absence of a decay-level scheme, a reaction scheme, or both, means that excited levels have not been observed or that the scheme is not well established.

Decay-level schemes include all levels established in radioactive decay studies. Reaction schemes include most levels observed in nuclear reactions; when it is necessary to omit levels because of space limitations, the number of omitted levels, the energy cutoff above which they occur, and (usually) the reactions which populate them are noted in a comment. Not included are most neutron-capture resonances and other unbound states (e.g., giant resonances); these states are generally outside the scope of the present compilation, with a few exceptions in the light-element region. Some references to unbound levels other than neutron resonances are included under "other reactions" or "others".

Fig. 1. Description of data layout in the Table of Isotopes, from the Introduction. (XBL 786-9447)

(Image size has been reduced to conform to NDC format)

Contents

Fig. 2. Table of Contents from the seventh edition of the Table of Isotopes. (XBL 786-9448)

(Image size has been reduced to conform to NDC format)

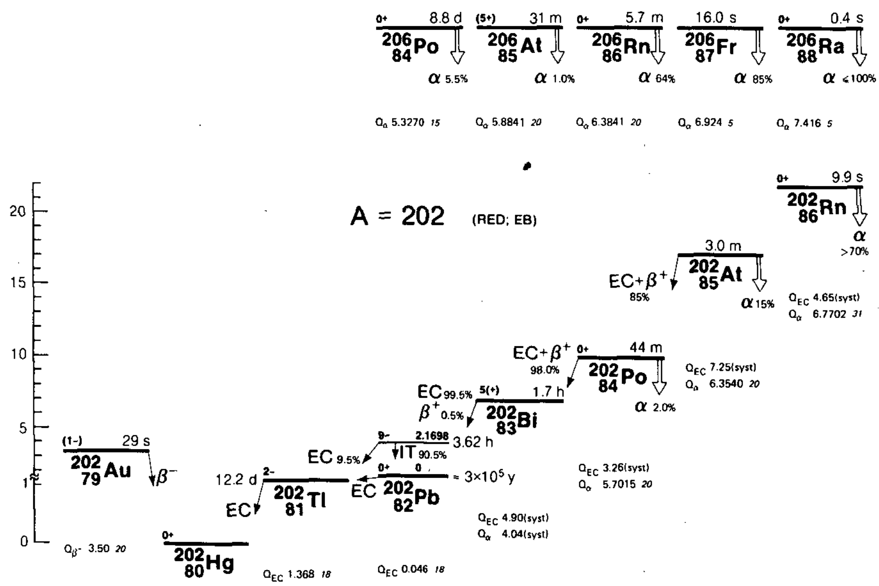

$^{202}_{79}$Au

Δ: −23.86*20* {ANDT 19 175(77)}
: β^- {PR 164 1545(67)}
$t_{1/2}$: 29*3*s {NP A184 157(72), SFen 42 267(72)}; 30*3*s {PR 164 1545(67)}; 27*2*s {JINC 34 1087(72)}; **others:** {PPSL 65A 945(52)}
Class: A; **Ident:** chem {PPSL 65A 945(52)}; cross bomb, genet energy levels {PR 164 1545(67), NP A184 157(72)}
Prod: ^{202}Hg(n,p) {PR 164 1545(67), PPSL 65A 945(52), NP A184 157(72)}; ^{205}Tl(n,α) {PR 164 1545(67), NP A184 157(72)}
β^-: (see also ^{204}Au)
3.5*2* (≈90%) *scint* {PR 164 1545(67)}
2.7*3* *abs* {JINC 34 1087(72)}
γ: (norm: $\gamma_{0.440}$ (γ ≈10%), from level scheme) $\gamma_{0.440}$ (I_γ100), **0.5203***4* (I_γ11*3*), **0.9086***4* (I_γ18*3*), $\gamma_{0.960}$ (I_γ<4), **1.1254***4* (I_γ25*5*), **1.2037***4* (I_γ21*5*), **1.3065***5* (I_γ23*5*) *Ge(Li)*, *Ge(Li)-scint γγ coinc*, *Ge(Li)-scint γβ coinc* {NP A184 157(72)}
others: {JINC 34 1087(72), PR 164 1545(67)}

$^{202}_{80}$Hg

%: 29.8 (^{198}Hg/^{202}Hg ratios vary from 0.336 to 0.341) {BNL-NCS-50605(77)}
Δ: −27.356*6* {ANDT 19 175(77)}
I: 0 *0* {ZP 72 423(31), PRSL 130A 558(31)}
σ_c: 5.0*4* {PC77 Holden}
$t_{1/2}$(0.440): 26*4*ps *Coulomb excit* {NP A147 161(70)}, 24*5*ps *nucl res fluor* {PR 98 200(55)}; **others:** {CR 242 1284(56), Phco 22 1129(56), PR 103 1801(56)}

$^{202}_{80}$Hg levels – References

Decay: NP A184 157(72), NP 75 81(66), IDO-17222(67), IIso 26 403(75)
^{201}Hg(n,γ): PR C11 546(75); **others:** NP A243 413(75), NP A135 241(69), PR 164 1548(67), NIM 36 29(65), IzF 27 1377(63), NP 21 66(60), NP 13 525(59)
Coul. ex.: NP A147 61(70); **others:** CR 242 1284(56), Phco 22 1129(56), PR 103 1801(56)
^{202}Hg(d,d'): PR C5 1678(72)
Other reactions:
^{202}Hg(n,n'): ZP 183 323(65)
^{202}Hg(n,n'γ): NP 80 198(66)
^{202}Hg(γ,γ'): NP A218 95(74)

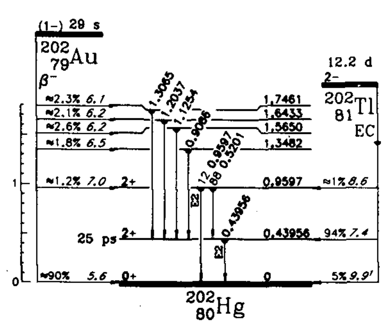

XBL 786-9445

Fig. 3a, b. A portion of the data for mass number A = 202 taken from the Table of Isotopes. Included is the mass-chain decay scheme which begins each A-chain compilation, tabulated data listings for several of the A = 202 isotopes, and "decay-level" schemes, "reaction" schemes, and their references for ^{202}Hg and ^{202}Tl. Note the stackplotting of all γ-ray transitions which proceed to the same final level in the ^{202}Hg reaction scheme. (a) XBL 786-9445; (b) XBL 786-9446

(Image size has been reduced to conform to NDC format)

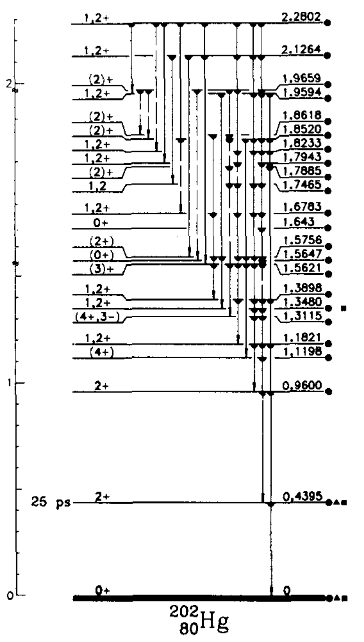

$^{202}_{81}$Tl levels – References

Decay: PR C5 2107(72), NP 3 513(57)

^{203}Tl(p,d): ND B5 581(71), PC70 Cleary; others: NP A170 187(71)

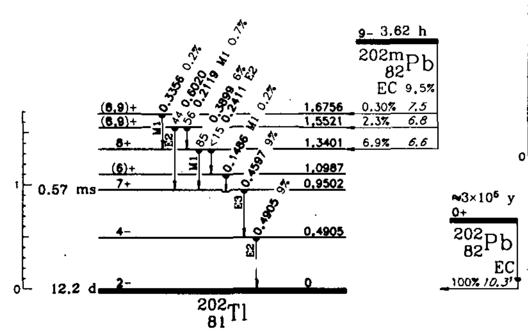

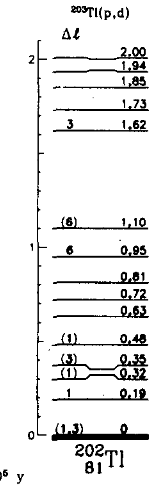

$^{202}_{81}$Tl

Δ: −25.988 *18* {ANDT 19 175(77)}
I: 2 *AB* {BAPS 3 319(58)}
ψ: EC {PCam 36 490(40), ZP 119 602(42)}; no β^+ {PR 79 1014(50)}
$t_{1/2}$: 12.23 *2* d {IIso 26 403(75)}; 12.4 *1* d {NP 75 81(66)}; 12.0 *1* d {Phca 23 1056(57)}; 12.50 *25* d {JINC 35 2139(73)}; **others:** {PR 86 565(52), PR 79 1014(50), PR 60 619(41)}
Class: A; **Ident:** chem, excit {PCam 36 490(40), PR 60 619(41)}
Prod: ^{202}Hg(d,2n) {PCam 36 490(40)}; ^{201}Hg(d,n) {Phca 25 326(59)}; ^{203}Tl(d,t) {Phca 25 326(59)}
γ: **0.43956** *1*, **0.52013** *7* *Ge(Li)* {IIso 26 403(75)}
0.4394 *2*, **0.5203** *3*, **0.9597** *4* *Ge(Li)* {IDO−17222(67)}
(norm: $\gamma_{0.440}$ (γ 91 *1*%), from level scheme, RED) $\gamma_{0.440}$ (I_γ100), $\gamma_{0.520}$ (I_γ1.0 *3*), $\gamma_{0.960}$ (I_γ0.13 *3*) *scint, scint−scint γγ coinc* {NP 75 81(66)}
0.4391 *4* (K/L_{1+2}/L_3 3.3/1/0.29) *mag conv* {PR 92 918(53)}
Hg LX (I_γ1.86 *6*), Hg KX (I_γ100 *2*), $\gamma_{0.440}$ (I_γ100 *3*, e_K/γ ≈0.034, K/L 2.7) *mag conv, scint, ion ch* {Phca 23 1056(57), Phca 22 208(56)}
$\gamma_{0.440}$ (I_γ100, I_K 100), $\gamma_{0.960}$ (I_γ0.074 *5*, I_K 0.0133 *13*) *mag conv, scint* {NP 62 337(65)}
$\gamma_{0.440}$ (I_γ100), $\gamma_{0.520}$ (I_γ≈0.1), $\gamma_{0.960}$ (I_γ0.10 *3*) *scint, scint−scint γγ coinc* {ArkF 17 337(60)}
$\gamma_{0.440}$ (I_γ100), $\gamma_{0.520}$ (I_γ0.410 *6*), $\gamma_{0.960}$ (I_γ0.053 *8*) *scint, scint−scint γγ coinc* {Phca 25 326(59)}
others: {NP A184 157(72), NuoC s10v14 509(59)}
γγ(θ): {PL 26B 374(68)}
$t_{1/2}$(0.950): 570 *10* μs {CEA−R−2900(66)}, 565 *10* μs *delay coinc* {NP 61 129(65)}, 585 *25* μs *delay coinc* {PR 112 1958(58)}, 600 *20* μs {NP A241 135(75)}, 608 *22* μs {NP A102 534(67), OesS 175p2 163(66)}, 536 *15* μs *delay coinc* {JINC 35 2139(73)}; **others:** {ZETF 45 1344(63), ArkF 12 237(57), PR 101 1067(56)}
EC(0): EC(L)/EC(K) 0.220^{+20}_{-15} {NP 75 81(66)}
EC(0.440): EC(L)/EC(K) 0.196 *2* {NP 75 81(66)}; **others:** {NuoC s10v14 509(59), Phca 25 333(59), Phca 23 1056(57), PPSL 69A 70(56), PR 96 548(54), PR 79 1014(50)}
EC(0.960): EC(L)/EC(K) 0.305 *20* {NP 75 81(66)}; **others:** {ArkF 17 337(60)}

$^{202}_{82}$Pb

Δ: −25.942 *11* {ANDT 19 175(77)}
ψ: EC {PR 96 548(54)}
$t_{1/2}$: ≈3×10^5 y *yield* {PR 96 548(54)}; **others:** {PR 78 191(50), PR 72 766(47)}
Class: A; **Ident:** chem, genet, mass spect {PR 96 548(54)}
Prod: ^{203}Tl(d,3n) {PR 96 548(54)}
$t_{1/2}$(levels): **1.383:** 1.97 *2* ns *delay coinc* {ZP A280 371(77)}, 2.00 *15* ns *delay coinc* {ArkF 14 439(59)}
2.208: 42 *4* ns *delay coinc* {NP A229 230(74)}

$^{202m}_{82}$Pb

Δ: −23.772 *11* {ANDT 19 175(77)}
ψ: IT 90.5%, EC 9.5% {PR C5 2107(72)}
$t_{1/2}$: 3.62 *3* h {ArkF 12 237(57)}; **others:** {Phca 20 521(54), PR 93 1433(54)}
Class: A; **Ident:** chem, excit {Phca 20 521(54), PR 93 1433(54)}; chem, mass spect {NP 3 513(57)}
Prod: ^{203}Tl(d,3n) {Phca 20 521(54), PR 93 1433(54)}; ^{203}Tl(p,2n) {PR C5 2107(72)}
γ with EC: (intensities relative to I_γ100 for $\gamma_{0.787}$ (with IT)) **0.14855** *15* (I_γ0.45 *15*, e_K/γ 2.9, K/L 6.1 *12*), **0.21192** *7* (I_γ1.5 *3*, e_{L1}/γ 0.14), **0.2411** *1* (I_K0.20 *2*, K/L_{1+2}/L_3 18 *3*/10/4.0 *5*), **0.33555** *10* (I_γ0.45 *10*, e_K/γ 0.23, K/L ≈5), **0.38994** *7* (I_γ12.4 *10*, e_K/γ 0.18, K/L 6 *3*), **0.45972** *7* (I_γ17.3 *10*, e_L/γ 0.041, K/L_{1+2}/L_3 18 *2*/10/2.0 *2*), **0.49047** *7* (I_γ18.4 *10*, e_L/γ 0.0073, K/L_{1+2}/L_3 39 *11*/10/1.2 *3*), **0.60195** *8* (I_γ1.2 *1*, e_K/γ 0.016) *Ge(Li), mag conv, Ge(Li)−Ge(Li) γγ coinc* {PR C5 2107(72), NP 3 513(57), Phil s7v46 61(55), Phil s7v46 65(55), RED}
γ with IT: **(norm:** $\gamma_{0.422}$ (γ 86 *1*%), from level scheme, RED) **0.12475** *9* (I_γ1.1 *3*), **0.1293** *1* (I_γ0.08 *3*, e_L/γ ≈700, K/L_1/L_2/L_3 <0.02/≈0/1.9/1.0), **0.2403** *1* (I_γ($\gamma_{0.240}$+$\gamma_{0.241}$(with EC)) 2.2 *3*, I_K0.31 *2*, K/L 5.0 *6*), **0.4173** *2* (I_γ0.8 *2*), **0.42212** *6* (I_γ172 *9*, e_K/γ assumed 0.030, K/L_{1+2}/L_3 31 *4*/10/1.8 *3*), **0.5476** *3* (I_γ0.25 *8*, e_K/γ 0.35, K/L_{1+2}/L_3 9^{+1}_{-4}/10/1.7 *4*), **0.65749** *6* (I_γ65 *3*, e_K/γ 0.0053, K/L 5.5 *7*), **0.78699** *6* (I_γ100, e_K/γ 0.079, K/L_{1+2}/L_3 13 *1*/10/≈1), **0.9545** *2* (I_γ2.0 *4*), **0.96070** *15* (I_γ184 *15*, e_K/γ 0.0056, K/L_{1+2}/L_3 54 *8*/10/≈0.7) *Ge(Li), mag conv, Ge(Li)−Ge(Li) γγ coinc, mag−mag ee coinc* {PR C5 2107(72), NP 3 513(57), RED}
$\gamma_{0.422}$ (e_K/γ 0.032 *2*), $\gamma_{0.787}$ (e_K/γ 0.088 *4*) *semicond−scint eγ coinc* {NP 56 689(64)}
(intensity relative to I_γ100 for $\gamma_{0.787}$) **1.3828** *5* (I_γ6.4 *1*×10^{-4}, K/L 3.4 *7*) *Ge(Li), Si(Li) conv* {PR C12 338(75), RED}
γ: **others:** {ArkF 11 105(56), Phca 20 521(54), PR 93 1433(54)}

Fig. 3b

XBL 786-9446

of R. A. Meyer, are the first such tables to present γ-ray energies based on the new "gold standard,"[4] the 411.80441 15 keV transition in ^{198}Au decay.

Appendix IV has been added to include information on half-thicknesses for γ-ray absorption and on the range and stopping power for absorption of electrons and various nuclei (protons through ^{136}Xe) in different stopping media.

Appendix VII is an updated version of the Table of Nuclear Moments[5] published in 1975. This table will continue to be updated (production is computerized), and future editions will appear at 2- or 3-year intervals. It is expected that the seventh edition of the Table of Isotopes will be the last in the series started in 1940. The project is now part of the U.S. Nuclear Data Network (NDN) and is compiling mass chains for inclusion in the Evaluated Nuclear Structure Data File (ENDSF) and for publication in the Nuclear Data Sheets. The compilation and evaluation of mass chains A = 146-152 and A = 163-194 has been assigned to LBL as a principal responsibility.

The project has just completed the Nuclear Wallet Cards[6] on behalf of the NDN. This 84-page "shirt-pocket" booklet contains tables of nuclear properties, elemental properties, fundamental constants, and energy conversion factors. The data presented in the nuclear properties table are adopted values from the seventh edition of the Table of Isotopes, and include spin and parity assignment, mass excess, half-life (level widths are given for particle-unstable nuclides), natural abundances, and decay mode. The NDN plans to update the wallet cards on a 4-year cycle.

References

1. C. M. Lederer and V. S. Shirley, eds.; E. Browne, J. M. Dairiki, and R. E. Doebler, principal authors; A. A. Shihab-Eldin, L. J. Jardine, J. K. Tuli, and A. B. Buyrn, authors; Table of Isotopes, Seventh Edition, John Wiley and Sons, Inc., New York (1978).

2. E. Browne, J. M. Dairiki, R. E. Doebler, J. M. Hollander, L. J. Jardine, C. M. Lederer, A. A. Shihab-Eldin, V. S. Shirley, and M. Whalley, LBL-2366 (1974), p. 3.

3. E. Browne, J. M. Dairiki, R. E. Doebler, L. J. Jardine, C. M. Lederer, E. Leon, M. Rinneberg, A. A. Shihab-Eldin, V. S. Shirley, and M. Whalley, LBL-4000 (1975), p. 3.

4. E. G. Kessler, Jr., R. D. Deslattes, A. Henins, and W. C. Sauder, Phys. Rev. Lett. 40, 171 (1978).

5. V. S. Shirley and C. M. Lederer, Table of Nuclear Moments, Proceedings of the Conference on Hyperfine Interactions Studied in Nuclear Reactions and Decay, Invited Papers with Table of Nuclear Moments, E. Karlsson and R. Wäppling, eds. (Almqvist and Wiksell Intern., Stockholm, 1975).

6. V. S. Shirley and C. M. Lederer, editors; E. Browne, J. M. Dairiki, R. E. Doebler, A. A. Shihab-Eldin, L. J. Jardine, J. K. Tuli, A. B. Buyrn, J. M. H. Chong, and D. P. Kreitz, Nuclear Wallet Cards, produced by the Isotopes Project on Behalf of the U.S. Nuclear Data Network (1979). Copies are available from the National Nuclear Data Center, Brookhaven National Laboratory, Upton, New York, 11973.

B. RADIOISOTOPE DATING WITH THE 88-INCH CYCLOTRON*

R. A. Muller, E. J. Stephenson,[†] and T. S. Mast

Since July 1976, we have been studying and developing the potential of the 88-inch cyclotron for radioisotope detection and dating.[1-4] This cyclotron is much larger and more powerful than required for dating, but its flexibility and ability to tune rapidly to accelerate almost any isotope has enabled us to study several different applications. We now have demonstrated the sensitivity of using the cyclotron for the detection at natural concentrations of tritium, beryllium-10, carbon-14, and chlorine-36.

The key feature that allows direct detection of low-level radionuclides is the high energy of the emerging beam, which allows particle-identification techniques to be used on an atom-by-atom basis. Without such particle identification, direct counting is impossible because unstripped background ions with the same charge-to-mass ratio always appear in the beam. For carbon-14 the main background is nitrogen-14. In order to apply the particle identification techniques the nitrogen beam intensity must be reduced to the level which will not damage or cause pile-up in the silicon detectors. When tandem accelerators are used for radiocarbon dating[5] this reduction occurs in the negative ion source. For the cyclotron we have developed a technique that achieves the required reduction after acceleration. We have built and used for this purpose a simple gas cell which completely stops the nitrogen beam while allowing the carbon-14 atoms to pass.

The separation technique makes use of the fact that the range of carbon-14 atoms is approximately 30% longer than that of nitrogen-14. Uniformity of the stopping material is essential to ensure the minimum range-straggling for the nitrogen ions. The best material we have found to meet this requirement is gas, separated from the cyclotron vacuum by a thin window. We found that 1/3μ of gold foil will support

1 atm of pressure difference if supported by a grid with gaps no larger than 1/3 mm (Fig. 1). Gold and platinum are convenient window materials because their high atomic number Z inhibit nuclear charge-exchange interactions which can generate spurious carbon-14 atoms. For the same reason, xenon was chosen for the gas.

With the xenon gas cell we were able to eliminate completely 10 nA of ^{14}N ions. A plot of the nitrogen penetration as a function of xenon pressure is shown in Fig. 2, measured using a single particle detector. The curve shows discrimination to a level of 10^{-9}; in several hours of coincident detection using both ΔE and total E detection, not a single nitrogen event perturbed the xenon cell, implying a discrimination factor for the coincident system better than 10^{-14}.

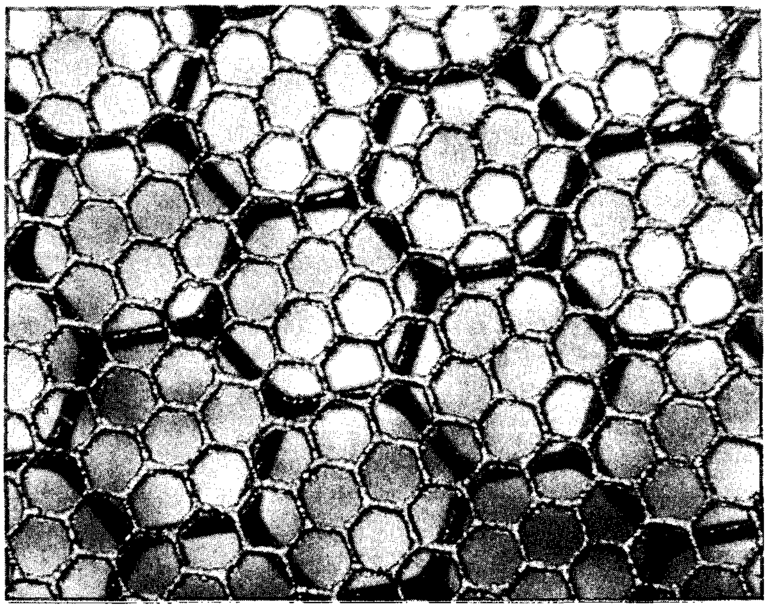

Fig. 1. The thin foil separating the xenon in the range cell from the vacuum of the cyclotron is supported on a tungsten grid, with hexagonal openings 0.33 mm in diameter. This grid is only 25 μ thick, and is supported in turn by a heavier 100 μ-thick tungsten grid with hexagonal openings 0.1 mm in diameter. The entire structure gives a clear aperture of 65%, over which 0.3 μ-thick gold foil can support a 1-atm pressure difference.

(XBL 781-163)

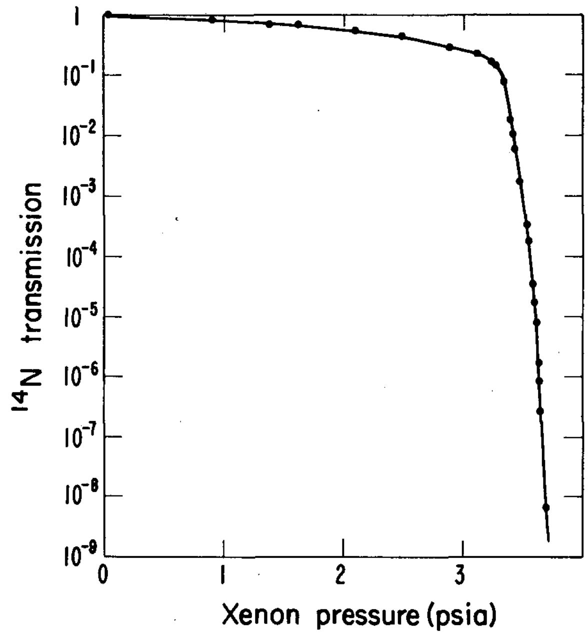

Fig. 2. Nitrogen-14 transmission through the xenon cell as a function of xenon pressure. The nitrogen-14 was detected with a single ionization chamber with a threshold energy loss of 0.8 MeV. When coincident detectors were used, the discrimination against nitrogen was found to be better than 10^{14}.

(XBL 783-2411)

For the range separation performed in the original tritium experiment[1] a single piece of aluminum foil was used. Because of the low level of background ^3He and its much shorter range than ^3H, non-uniformities in the foil were not critical. For beryllium-10 a solid foil is probably acceptable; for our measurements the xenon cell was used. For chlorine-36 the high uniformity of the xenon cell is essential. The "thickness" of the cell in milligrams per cm^2 can be adjusted remotely by changing the pressure of the xenon gas. The range-separation technique should prove to be valuable for those using tandems as well as cyclotrons.

Except for the case of carbon-14, the levels of background radioisotopes in real time from nuclear charge exchange reactions may, however, prove to be the ultimate limit to the cyclotron approach. For carbon-14 our sensitivity at present is limited by a high level of carbon-14 within the graphite-lined tank of the 88-inch cyclotron produced from years of scraping deuteron beams. The level of this carbon, which finds its way into the ion source during a run, has varied from 1/3 to several times the level of carbon-14 in the sample being measured. We have made dates in spite of this background by rapidly switching sample gases to allow the comparison of the unknown with a blank and a reference standard. The results of a blind measurement[2,3] of a sample are shown in Fig. 3. In this run the measured age (in radiocarbon years) was 5900 ±800, with the large error dominated by the statistics of the background subtraction. The Rochester tandem group has a similar background; their ability to measure dates as old as forty thousand years is a reflection of the fact that their background is about a factor of ten lower than ours.

In the carbon-14 measurements the carbon was conveniently introduced to the ion source in the form of CO_2 gas. The efficiency for acceleration of the $^{14}C^{3+}$ ions could be varied between 10^{-5} and 3×10^{-4}; in a typical run it was 3×10^{-5}.

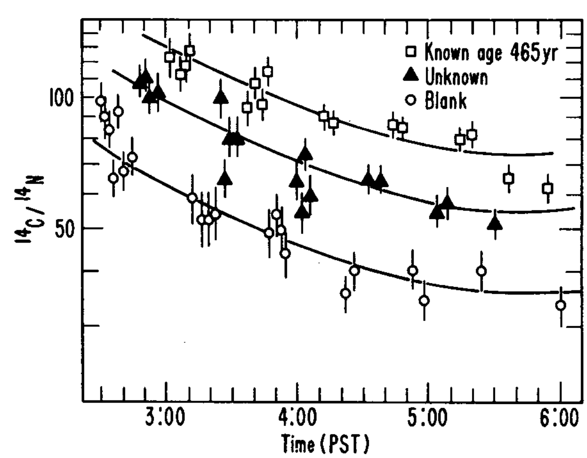

Fig. 3. The $^{14}C/^{14}N$ ratio as a function of time, for a blind sample.[2,3] The carbon-14 was measured with an ionization chamber, silicon-detector telescope. The nitrogen-14 was measured by integrating the current from slits which collimate the beam soon after it emerges from the cyclotron and well before it enters the xenon gas cell. Three samples were alternated: one of known age 465 years; a sample known to contain no carbon-14; and the unknown. The fit corresponds to an age of 5900 years, where the "standard" radiocarbon half-life of 5570 years has been assumed.

(XBL 7712-11088)

We have made nearly a dozen successful "nonblind" tests, and the successful "blind" test shown in the figure. More recently, however, we made a blind measurement in which our answer differed greatly from the answer achieved by decay-dating: we misestimated the age of an 8,000-year old sample dated by Rainer Berger to be 18,000 years old. This was the only collagen sample we have measured, and we suspect that impurities in the CO_2 affected the performance of the ion source, changing the level of background appropriate to subtract. The best hope for the elimination of such systematic errors lies in the elimination of the background. The easiest way to achieve this will be to use an external ion source which can pre-accelerate the ions to tens of keV before they enter the contaminated tank of the cyclotron. The design and construction of such a source is now under way, and we expect it to be operational later this year.

In our ^{10}Be measurements no comparable background has been detected. We have measured ^{10}Be/^{9}Be ratios in beryllium metal at the 10^{-9} level, comparable to that expected in sea floor sediments. We observed 800 ^{10}Be per second in our detectors, and the background was less than one count in five minutes. Our sensitivity for ^{10}Be is better than 10^{-14}, justifying all the optimism expressed in Ref. 1. A comparable sensitivity was achieved when BeO was substituted for beryllium metal in our Penning Ion Gauge (PIG) sputter source, but we have not yet achieved an accurate date with BeO.

Accurate ^{10}Be dating will require rapid cycling between samples of known and unknown concentrations. Since the samples are presently introduced in the back insert of the PIG source they cannot now be readily changed in the internal ion source. The new external ion source will allow this rapid cycling.

For ^{36}Cl our demonstrated sensitivity is 10^{-12} for the ratio ^{36}Cl/Cl. This sensitivity is sufficiently good to make ^{36}Cl an attractive tool for measuring the age of water in potential nuclear waste storage sites, useful in determining the geologic isolation of the deep site from the surface.

After only one and a half years of development, the accelerator approach has already proven its potential for several radioisotopes. Except for the case of carbon-14, there have been no unanticipated backgrounds, and we are optimistic that the full predicted[1] sensitivity of the accelerator approach will soon be utilized.

Footnotes and References

*Condensed from LBL-7585, and Proceedings, Rochester Conference on Radiocarbon Dating with Accelerators (April 1978).

†Present address: Argonne National Laboratory, Argonne, Illinois 60439.

1. R. A. Muller, LBL-5510 (Sept. 1976); Science 196, 489 (1977).

2. R. A. Muller, E. J. Stephenson, T. S. Mast, Radioisotope Dating with an Accelerator: A Blind Measurement, Lawrence Berkeley Laboratory Report, LBL-7249 (December 1977), submitted to Science.

3. E. J. Stephenson, T. S. Mast, and R. A. Muller, Radiocarbon Dating with a Cyclotron, LBL-7579 (April 1978), to be submitted to Nucl. Inst. Meth.

4. R. A. Muller, E. J. Stephenson, and T. S. Mast, Papers presented at the Conference on Radiocarbon Dating with Accelerators, LBL-7585.

5. D. E. Nelson, R. G. Korteling, W. R. Scott, Science 198, 509 (1977); C. L. Bennett et al. Science 198, 509 (1977); C. L. Bennet et al., preprint, Radiocarbon Dating Using Electrostatic Accelerators: Dating of Milligram Samples, to be published.

C. ISOMERIC STATES IN ^{212}Bi*

P. A. Baisden, R. E. Leber, M. Nurmia, J. M. Nitschke, M. Michel, and A. Ghiorso

During a search for superheavy elements via the reaction of ^{48}Ca with ^{248}Cm we discovered several alpha lines around 10 MeV with a half-life of 25 ± 1 min.[1] In addition, a line at 11.66 MeV was observed and found to contain a longer-lived component of 9 ± 1 min in addition to the expected 45-sec half-life of ^{212m}Po.[2] Both activities could be produced by the bombardment of ^{208}Pb with ^{40}Ar, and also from ^{238}U with a variety of projectiles such as ^{40}Ar, ^{48}Ca and ^{136}Xe.

A spectrum of a source obtained by irradiating ^{238}U with ^{40}Ar followed by electrolytic dissolution and extraction of the Bi-Po-At fraction into diphenylthiocarbazone-CCl_4 at pH 2.5 is shown in Fig. 1; the doublet at 6.3 MeV was found to decay with the same 25-min half-life as the group at 10 MeV.

The 25-min activity was found to follow the chemistry of Bi through the technique of residue adsorption or chemisorption[3] and its mass number was found to be 212 in three isotope separation runs made with chemically separated samples using the LBL Isotope Separator. Our studies indicate that this isomeric state, $^{212m1}Bi$, decays both by alpha emission to ^{208}Tl and by beta emission to excited levels in ^{212}Po, followed by the emission of "long-range" alpha particles to the ground state of ^{208}Pb.

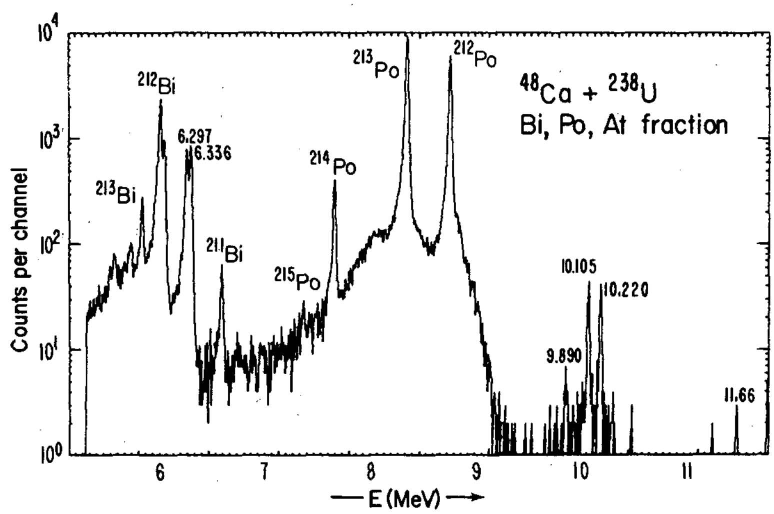

Fig. 1. Alpha spectrum of the Bi, Po and At fraction from ^{48}Ca + ^{238}U. Geometry 20%, resolution, FWHM = 25 keV. (XBL 783-332)

The fact that an isomeric state should exist in ^{212}Bi is suggested by analogy with the 9^- isomeric state in ^{210}Bi.[4-7] The configuration of ^{212}Bi, $(\pi h_{9/2})(\nu g_{9/2})^3$, differs from that of ^{210}Bi, $(\pi h_{9/2})(\nu g_{9/2})$, in that ^{212}Bi has two additional $g_{9/2}$ neutrons. Shell-model studies have been carried out on the ground state and low-lying states of the configuration $(\pi h_{9/2})(\nu g_{9/2})$ of ^{210}Bi by Kim and Rasmussen.[8] Their calculations, which are in excellent agreement with the experimental observations of Motz et al.,[9] indicate the level responsible for the isomeric state is a 9^- state located at 268 keV. Therefore, we suggest an analogous 9^- spin for the isomeric state in $^{212m1}Bi$.

Detailed shell-model calculations of the excited levels of ^{212}Po have been made by several authors. In one such calculation Glendenning and Harada, allowing for configuration mixing, predicted a state with $J\pi = 18^+$ to explain the 45-second ^{212m}Po.[10] Their results also indicate the possibility of another isomeric state J = 10-12 at an excitation energy of 1.2 MeV. On the other hand, calculations by Auerbach and Talmi, assuming no configuration mixing, indicate a spin of 16 for

^{212m}Po.[11] Likewise, their calculations also suggest a second isomeric state, however, of lower spin, around J = 8-10.

It is reasonable to assume that since the first excited state of ^{208}Pb is 2.6 MeV above the ground state, the 10-MeV group decays to the ground state of ^{208}Pb. This would place the levels in ^{212}Po responsible for the 10-MeV transitions at an excitation energy of 1.1 to 1.5 MeV. These levels are consistent with either of the shell-model calculations mentioned.

As a test for the assumption of a 9^- isomeric level in ^{212}Bi, one would expect a log ft value of 6-9 (first forbidden transition) for a beta decay from a 9^- to either an 8^+ or 10^+ state in ^{212}Po. In view of the possibility of gamma decay the ratio of alpha transitions from the 9^- state yields a lower limit of 7% for the beta branch to ^{212}Po. The resulting upper limit of 6.8 for the log ft value is then compatible with the spin assignment of 9^- for $^{212m1}Bi$.

We were unable to obtain a definite elemental or mass assignment of the 9-min activity in the chemisorption and isotope separation experiments but we did find out that it is coprecipitated with CuS from an acidic solution. Since our ^{48}Ca + ^{248}Cm work showed that it is genetically related to the 45-sec ^{212m}Po, it could, in principle, be an isomer in ^{212}At, ^{212}Po or ^{212}Bi. The first possibility was eliminated when we observed that we could volatilize the ^{211}At-^{211}Po activity away from our sources while the 9-min and 25-min activities remained.

In their discovery work on ^{212m}Po, Perlman et al.[2] irradiated a lead oxide target with 116-MeV ^{11}B ions and separated a Po fraction by a combination of volatilization and cation exchange. They found that ratio of the ^{211}Po and ^{212m}Po activities was not changed by the chemical procedure if the latter was assumed to have a half-life of 45 seconds; this apparently rules out the possibility that the 9-min activity is another isomer in ^{212}Po feeding the 45-second state. It is also difficult to postulate a second isomer in ^{212}Po that would decay into the known ^{212m}Po and yet have the required long half-life against alpha decay.

The remaining possibility, that the 9-min activity is another isomeric state in ^{212}Bi which beta decays into ^{212m}Po, appears quite plausible. If one breaks the pair of $g_{9/2}$ neutrons in ^{212}Bi and recouples the four particles outside the ^{208}Pb core to maximum spin, a 15^-state is obtained.[12] We consider this state in ^{212}Bi the most likely explanation of the 9-min activity; a consequence of this assignment would be that the spin of ^{212m}Po would be 16 as suggested by Auerbach and Talmi.[11] A decay scheme of the two isomers is shown in Fig. 2.

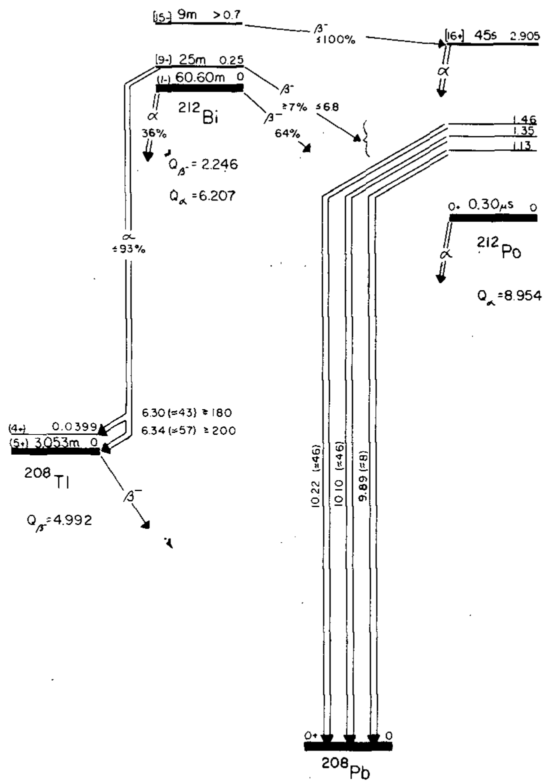

Fig. 2. Tentative decay scheme for isomeric states in ^{212}Bi. Relative alpha intensities are given in parentheses after the alpha energies. Other pertinent information shown, which was not explicitly determined in this work, was taken from Ref. 13. (XBL 783-330)

In conclusion we have shown evidence for the existence of two isomeric states in ^{212}Bi. Since these isomers are made in a variety of heavy reactions with heavy targets, the high energy alpha particles associated with their decay may be present in experiments aimed at the synthesis of superheavy elements. The possibility is accentuated by the fact that Bi is a homolog of element 115 and will follow the chemistry of the eka-Pb group of the superheavy elements.

Acknowledgments

The authors would like to thank Dr. R. Eggers for his help in the more recent phases of this work. We would also like to thank Mrs. Diana Lee and Miss Bonner Nishida for their help with the data acquisition.

Footnote and References

*Condensed from LBL-7708; also, published in Phys. Rev. Lett. 41, 738 (1978).

1. A. Ghiorso, 173rd American Chemical Society, National Meeting (New Orleans, Louisiana, March 1977).

2. I. Perlman, F. Asaro, A. Ghiorso, A. Larsh and R. Latimer, Phys. Rev. 217, 917 (1962).

3. H. W. Kirby, J. Inorg. Nucl. Chem. 35, 2043 (1973).

4. J. R. Erskine, W. W. Buechner and H. A. Enge, Phys. Rev. 128, 720 (1962).

5. E. H. Spejewski, Nucl. Phys. A 100, 236 (1967).

6. R. C. Lange, G. R. Hagee and A. R. Campbell, Nucl. Phys. A 133, 273 (1969).

7. D. G. Tuggle, Ph. D. Thesis, University of California, LBL-4460.

8. Y. E. Kim and J. O. Rasmussen, Nucl. Phys. 47, 184 (1963).

9. H. T. Motz, E. T. Jurney, E. B. Shera and R. K. Sheline, Phys. Rev. Lett. 26, 854 (1971).

10. N. K. Glendenning and K. Harada, Nucl. Phys. 72, 481 (1965).

11. A. Auerbach and J. Talmi, Phys. Lett. 10, 297 (1964).

12. This was also independently pointed out to us by C. M. Lederer, Lawrence Berkeley Laboratory.

13. C. M. Lederer, J. M. Hollander and I. Perlman, eds., Table of Isotopes, 7th Edition (John Wiley and Sons, Inc., New York, 1978).

D. NEW EXPERIMENTAL INSIGHTS INTO THE PRODUCTION OF SUPERHEAVY ELEMENTS USING HEAVY ION REACTIONS*

R. J. Otto, D. J. Morrissey, G. T. Seaborg, and W. D. Loveland†

Attempts at the Lawrence Berkeley Laboratory to produce superheavy elements (SHE) using the reactions of ^{48}Ca with ^{248}Cm and ^{136}Xe with ^{238}U have been unsuccessful. These negative results have led us to consider the possibility that these reactions (and their associated mechanisms) do not lead to the formation of superheavy nuclei with sufficiently low excitation energies. Consequently, the number of surviving atoms of superheavy elements is well below our detection thresholds even with using relatively low estimates for prompt fission losses. A summary of some new experimental evidence, supporting the above hypothesis, is presented and possible alternative heavy-ion heavy-target combinations are suggested for SHE synthesis.

We have considered several possible reasons for negative results in the synthesis and identification of superheavy elements obtained at heavy-ion accelerator laboratories around the world. Due to the limited choice of targets above uranium, projectiles heavier than ^{40}Ar have been used. However, for projectile ions near and above the mass and charge of ^{40}Ar, quasi-elastic transfer and deep-inelastic transfer comprise a significant fraction of the total reaction cross section. The deep-inelastic transfer reaction has many characteristics that tend to obscure the observation of the complete fusion and compound nucleus-fission reactions. As a result, previous measurements of the fraction of the total reaction cross section corresponding to complete fusion can only be taken as upper limits. Furthermore, mass and energy distributions associated with binary events from heavy-ion reactions for example, ^{40}Ar + ^{238}U (Ref. 1) or ^{40}Ar + ^{243}Am (Ref. 2) in which complete fusion was assumed to occur, cannot be safely interpreted as corresponding to the fission of a compound nucleus.

A recently developed differential recoil range method[3] can be employed to further test this broad role of the deep-inelastic transfer process in the production of a wide range of products from bombardments with ^{40}Ar and similar ions. This method has been used to deduce the general shapes of angular distributions of products ranging from approximately one-half the mass of the compound composite system to products near the target.[4] These recoil range distributions from the reaction of 250 MeV ^{40}Ar with ^{238}U were correlated with a trend in the angular distribution of the projectile-like fragment as a function of ΔZ similar to the trend observed in the ^{40}Ar + ^{197}Au reaction.[5-9] This is a trend that has been interpreted as evidence for viewing the deep inelastic reaction mechanism as a dynamical diffusion process.[6,7,9] Complete fusion is ruled out for products with backward- or forward-peaked angular distribution since the 1/sinθ -type angular distribution is expected for such a process.

These data indicated that non-complete fusion (and non-compound nuclear) processes accounted for an unexpectedly large portion of the mass distribution of the ^{48}Ca + ^{238}U reaction and, of the broad symmetric, previously labeled "fusion-fission," mass distribution of the ^{40}Ar + ^{238}U reaction.[1] Again, we can see that earlier work on the ^{40}Ar + ^{238}U system may have overestimated the cross section due to complete fusion processes. Thus we conclude that the use of ^{48}Ca as a projectile with heavy targets, considered a hopeful approach for the production of SHE's, must actually result in a much smaller production of compound nuclei than had been anticipated.

For ions heavier than argon, complete fusion-fission rapidly decreases, eliminating the possibility for production of SHE fission fragments in such reactions as krypton, xenon or uranium with uranium. In spite of the larger contribution from deep-inelastic transfer reactions, some complete fusion and compound nucleus formation is expected to occur in the ^{48}Ca + ^{248}Cm reaction. However, use of the proximity potential model[10] and the Bass model[11,12] predicts complete fusion thresholds 10 to 15 MeV higher than the interaction barrier, and the work of Saint-Simon et al.[13] using the similar reaction ^{40}Ar + ^{238}U provides experimental evidence for such an effect. As a result, the minimum attainable excitation energy for the compound nucleus (^{296}116) results in large prompt fission losses putting the SHE production level below the present experimental level of sensitivity.

For the ^{136}Xe + ^{238}U reaction, the probability of transferring the required number of protons and neutrons to reach the SHE region appears to be unacceptably low. This conclusion is supported by a study of the reaction of ^{136}Xe and ^{160}Gd.[14] The reaction ^{160}Gd(^{136}Xe;^{84}Kr,n's)^{212}Pb requires the transfer of 18 protons and 34 neutrons to ^{160}Gd from the ^{136}Xe projectile. This is the number of protons and neutrons required in a transfer from ^{136}Xe to ^{238}U to make (^{290}110) which is predicted to be in the "island of stability." Using a radiochemical separation procedure, an upper limit of 2×10^{-34} cm^2 was observed for production of ^{212}Pb in the reaction of 1150 MeV ^{136}Xe with a thick natural Gd target (21.9% ^{160}Gd).[14] The upper limit cross section for the reaction ^{160}Gd(^{136}Xe;^{84}Kr,n's)^{212}Pb is therefore 1×10^{-33} cm^2 or 1 nb. The 1 nb limit was applied to a similar or greater number of nucleons transferred from ^{136}Xe to ^{238}U by assuming that less than 10% of the Pb fragments fissioned and that the nucleon diffusion rates and the interaction times are nearly the same for the ^{136}Xe + ^{160}Gd and ^{136}Xe + ^{238}U reactions. It was pointed out that this limit is consistent with the theoretical prediction that the cross section for transfer of ~60 nucleons in the Xe + U reaction is about 1 nb.[15] Figure 1 summarizes the results of this work. The cross section for SHE production is estimated to be $\leqslant 4 \times 10^{-36}$ cm^2.

$$^{136}_{54}Xe + ^{160}_{64}Gd \rightarrow ^{212}_{82}Pb + ^{84}_{36}Kr + n's$$

$$\sigma_{DIT} \leqslant 1 \times 10^{-33}\ cm^2$$

Transfer to target ($\Delta p = 18$, $\Delta n = 34$)

Loss by Fission?

$$^{136}_{54}Xe + ^{238}_{92}U \rightarrow ^{290}(110)_{180} + ^{84}_{36}Kr + n's$$

$$\sigma_{SHE} \leqslant 1 \times 10^{-33} \left[\frac{\Gamma_n}{\Gamma_n + \Gamma_f}\right]^x \leqslant 1 \times 10^{-33} \times 4 \times 10^{-3}$$

$$\sigma_{SHE} \leqslant 4 \times 10^{-36}\ cm^2$$

Fig. 1. An upper limit cross section for the production of SHE's in the ^{136}Xe + ^{238}U reaction based on the experiments using the ^{136}Xe + ^{160}Gd reaction. Values of $x = 4$ and $[\Gamma_n/(\Gamma_n+\Gamma_f)]^4 = 4 \times 10^{-3}$ were used.[14] (XBL 789-11116)

The possibility remains that transfer reactions using very heavy-ion projectiles such as ^{197}Au, ^{208}Pb, ^{238}U, or ^{244}Pu with ^{254}Es or ^{257}Fm targets could lead to the production of SHE nuclei at relatively low excitation energies.

Recent studies of the ^{238}U + ^{238}U reaction at Gesellschaft für Schwerionenforschung[16,17] show that, for a given average width in the charge dispersion (mass dispersion), the energy damped into internal excitation energy is less than in Xe transfer reactions.[18,15] Such an observation can be interpreted as supporting the idea that there should be significantly larger cross sections for the production of heavy transuranium elements in the reaction of U + U[16] than in the Xe + U reactions.[19] Evidence for such an effect can be seen by making a comparison of the yields of Cf and Es isotopes ($\Delta Z = 6$ and 7, respectively) from these two reactions, where the cross sections for the production of the more neutron-excessive isotopes are 10 to 10^2 times larger from the U + U reaction.[17] Such an effect suggests the use of a very heavy target such as ^{248}Cm, ^{249}Cf, ^{252}Cf, ^{254}Es, or ^{257}Fm with a heavy-ion beam of ^{238}U (or possibly ^{197}Au, ^{208}Pb, or ^{244}Pu) as a way to produce SHE's. Figure 2 shows a number of interesting transfer reactions. The ^{165}Ho and ^{248}Cm reaction shown first could be driven by the closed shell at Z = 50. However, the diffusion process would probably favor symmetric division into two fragments near ^{208}Pb.

$$^{165}_{67}\mathrm{Ho} + ^{248}_{96}\mathrm{Cm} \rightarrow ^{289}(113)_{176} + ^{124}_{50}\mathrm{Sn}$$

$$^{165}_{67}\mathrm{Ho} + ^{248}_{96}\mathrm{Cm} \rightarrow ^{208}_{82}\mathrm{Pb} + ^{205}_{81}\mathrm{Tl}$$

$$^{238}_{92}\mathrm{U} + ^{238}_{92}\mathrm{U} \rightarrow ^{255}_{100}\mathrm{Fm} + ^{221}_{84}\mathrm{Po} \quad \sigma \approx 10^{-33}$$

Transfer ($\Delta p = 8$, $\Delta n = 9$)

$$^{254}_{99}\mathrm{Es} + ^{238}_{92}\mathrm{U} \rightarrow ^{271}(107)_{164} + ^{221}_{84}\mathrm{Po}$$

Transfer ($\Delta p = 8$, $\Delta n = 9$)

$$^{257}_{100}\mathrm{Fm} + ^{238}_{92}\mathrm{U} \rightarrow ^{283}(110)_{173} + ^{212}_{82}\mathrm{Pb}$$

Transfer ($\Delta p = 10$, $\Delta n = 16$)

Fig. 2. Hypothesized heavy-ion transfer reactions. Only the U+U reaction has been shown to occur experimentally.[17] No designation of emission of neutrons has been indicated. (XBL 789-11117)

Based on the results with the U + U reaction[17] studies at GSI to produce ^{255}Fm, an analogous reaction of ^{238}U with ^{254}Es is written to suggest the possibility of transfer reactions to produce elements near the SHE region with reasonable cross sections. However, the formation of SHE's requires a transfer with a larger neutron-to-proton ratio, as indicated in the reaction of ^{238}U with ^{257}Fm. It is important to note that the predicted stability of the products in the SHE region for these last two reactions varies from being unstable to having detectable half-lives.[20,21] Although such reactions would have many technical difficulties associated with them, these target- projectile combinations may provide a suitable reaction pathway to the formation of SHE's not available in the reactions that have been used up to now. The success of these experiments rely on the transfer reaction mechanisms and on an extrapolation of broad Gaussian distributions of primary products (before fission) around the target nucleus extending from the millibarn region into the nanobarn region. Also, the disadvantages of the extremely small amounts of ^{254}Es and ^{255}Fm available may more than offset these advantages for their use.

Footnotes and References

*Condensed from LBL-7710 and Proc. of the Intern. Symp. on Superheavy Elements, Lubbock, Texas, March (1978).

†Permanent Address: Department of Chemistry, Oregon State University, Corvallis, OR 97331.

1. J. V. Kratz, J. O. Liljenzen, A. E. Norris, and G. T. Seaborg, Phys. Rev. C 13, 1347 (1976).

2. R. Kalpakchieva, Yu. Ts. Oganessyan, Yu. E. Penionzhkevich, and H. Sodan, Z. Physik A 283, 253 (1977).

3. R. J. Otto, M. M. Fowler, and G. T. Seaborg, Phys. Rev. C 17, 1071 (1978).

4. R. J. Otto, D. J. Morrissey, G. T. Seaborg, and W. D. Loveland, Z. Physik A287 (1978) and Lawrence Berkeley Laboratory Report LBL-7188 (1978).

5. C. Ngo, J. Peter, B. Tamain, M. Berlanger, and F. Hanappe, Z. Physik A 283, 161 (1977).

6. L. G. Moretto, J. Galin, R. Babinet, Z. Fraenkel, R. Schmitt, R. Jared, and S. G. Thompson, Nucl. Phys. A 259, 173 (1976).

7. J. Galin, B. Gatty, D. Guerreau, M. Lefort, X. Tarrango, S. Agarwal, R. Babinet, B. Gauvin, J. Girard, and H. Nifenecker, Z. Physik A 283, 173 (1977).

8. A. G. Artukh, E. Gierlik, R. Gerstenberger, G. F. Gridnev, A. N. Mezentsev, V. L. Mikheev, T. S. Salamatina, V. V. Volkov, V. B. Zlokazov, Report, Joint Institute of Nuclear Reactions E7-10464.

9. R. Lucas, J. Poitou, H. Nifenecker, J. Peter, and B. Tamain, Z. Physik A 283, 257 (1977).

10. J. Blocki, J. Randrup, W. J. Swiatecki, and C. F. Tsang, Ann. Phys. 105, 427 (1977).

11. R. Bass, Nucl. Phys. A 231, 45 (1974).

12. R. Bass; Phys. Lett. B 47, 139 (1973).

13. M. de Saint Simon, R. J. Otto, G. T. Seaborg, Phys. Rev. C 18, 1651; and Lawrence Berkeley Laboratory Report LBL-7114 (1978).

14. R. J. Otto, A. Ghiorso, D. Lee, R. E. Leber, S. Yashita, and G. T. Seaborg, Radiochimica Acta 24(1) (1978).

15. J. R. Huizenga, Comments on Nucl. Part. Phys. 7, 17 (1976).

16. D. D. Hildenbrand, H. Freisleben, F. Puhlhofer, W. F. W. Schneider, R. Bock, D. V. Harrah, and H. J. Specht, Phys. Rev. Lett. 39, 1065 (1977).

17. J. V. Kratz, H. Ahren, W. Bruchle, G. Franz, H. Gaggeler, M. Schadel, I. Warnecke, G. Wirth, N. Tautman, M. Weis, and G. Herrmann, Report Gesellschaft für Schwerionenforschung-J-1-77 (1977); and M. Schadel et al., Phys. Rev. Lett. 41, 469 (1978).

18. U. Reus, A. M. H. Watzig, R. A. Esterlund, P. Patzelt, and I. S. Grant, Phys. Rev. Lett. 39, 171 (1977).

19. K. Wolf et al., American Physical Society Meeting, Chicago (1977), Abstract 25.7.

20. E. O. Fiset and J. R. Nix, Nucl. Phys. A 193, 647 (1972).

21. I. Reichstein and F. B. Malik, Ann. Phys. 98, 322 (1976); and F. B. Malik, private communication (1977).

LAWRENCE LIVERMORE LABORATORY

A. NUCLEAR DATA APPLICATIONS - MEASUREMENTS

1. Studies of (n,charged particle) Reactions with 14 - 15 MeV Neutrons. (R.C. Haight, S.M. Grimes, K.R. Alvar*, H.H. Barschall**, and R.R. Borchers***)

To assess candidate materials for fusion reactors, the Office of Fusion Energy requires cross sections for reactions that result in hydrogen or helium. These reactions are thought to be important sources of radiation damage induced by fusion neutrons. Under the sponsorship of the DOE Office of Basic Energy Sciences, we are continuing to measure these cross sections as well as the energy spectra and the angular distributions of the charged particles: protons, deuterons, and alpha particles and, for some light nuclei, tritons and ^{3}He as well. These detailed measurements allow stringent tests of nuclear reaction model calculations that are used to supply cross sections over a wide range of energies for fusion reactor studies and other applications.

In the past year we completed the measurements on ^{50}Cr, ^{52}Cr, and natural chromium.[1] Together with our past measurements on iron and nickel and their principal isotopes,[1] these new data permit assessments of many types of stainless steel for fusion reactors. In addition, we have made preliminary measurements on ^{12}C, ^{90}Zr, ^{92}Mo, and natural molybdenum at E_n = 15 MeV and on ^{12}C at E_n = 14 MeV. The 14-MeV measurements are now possible with a redesigned rotating target configuration. For light nuclei such as ^{12}C, the cross sections are not easily extrapolated with reaction models and so the 14-MeV values must be determined experimentally.

The new data for ^{50}Cr, ^{52}Cr, and Cr are given in Table A-1. The proton spectra for ^{50}Cr and ^{52}Cr are compared with nuclear model calculations in Figure A-1.

---

*Present address: IRT Corporation, San Diego, CA 92138.

**University of Wisconsin, Madison, WI 53706.

***University of Wisconsin, Madison, WI; presently on leave at the University of Colorado, Boulder, CO 80309

[1]Grimes, Haight, Alvar, Barschall, and Borchers, Phys. Rev. C (to be published); UCRL-81802 (preprint).

TABLE A-1

Proton, deuteron and alpha-particle emission cross sections and average charged-particle energy.

Target	Particle Emitted	Cross Section (mb)	Spectrum-Averaged Charged-Particle Energy (MeV)
^{50}Cr	p	830 ± 100	4.5 ± 0.2
	d	12 ± 4	5.6 ± 0.5
	α	94 ± 15	8.4 ± 0.3
^{52}Cr	p	180 ± 25	4.7 ± 0.2
	d	8 ± 3	4.9 ± 0.7
	α	36 ± 6	8.4 ± 0.4
Cr	p	180 ± 25	4.7 ± 0.2
	d	10 ± 3	5.7 ± 0.7
	α	38 ± 6	8.6 ± 0.4

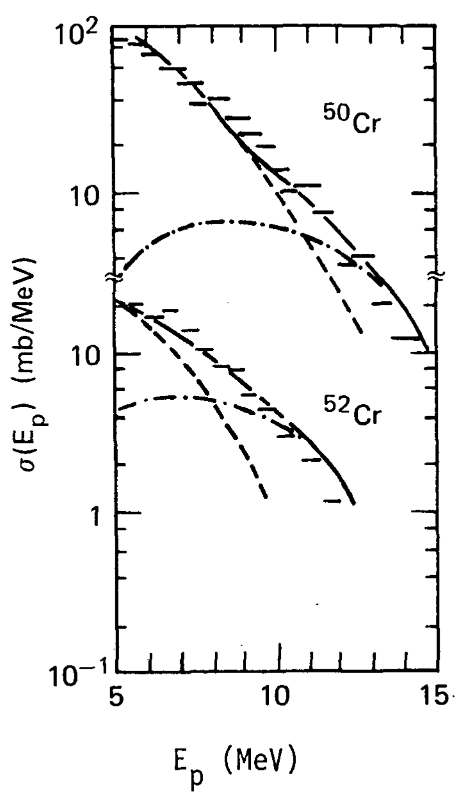

Fig. A-1. High-energy portions of the proton-emission cross sections are compared with hybrid-model calculations (dot-dashed line), multi-step Hauser-Feshbach calculations (dashed line), and the sum of these two contributions (solid line).

2. <u>Neutron Spectra From Materials Used in Fusion and Fusion-Fission Hybrid Reactors</u>. (L.F. Hansen, C. Wong, T. Komoto and B.A. Pohl)

The neutron leakage spectra from pulsed spheres of Cu (1.0, 3.0 and 5.0 mean-free-path, mfp), Nb (1.0 and 3.0 mfp), ^{232}Th (1.0 mfp) and ^{238}U (0.8 and 2.8 mfp) have been measured using time-of-flight techniques. The neutron spectra from the above materials used in fusion and hybrid reactors have been measured between 0.8 and 14 MeV using a stilbene scintillator, pulse shape discrimination and flight paths of around 10 meters. The measured spectra were compared with calculations carried out with TARTNP, a coupled neutron-photon Monte-Carlo transport code. The Lawrence Livermore Laboratory neutron and photon cross sections library (ENDL) and the ENDF/B-IV library were used in these calculations. Figures A-2(a) and A-2(b) show the measurements and calculations for 1-mfp of Cu and Nb, respectively. The measured and calculated integrals for the energy intervals 0.8-5, 5-10 and 10-15 MeV are tabulated in Table A-2.

TABLE A-2

Mat	ΔE	Exp ± 7%	ENDl ± 2%	B-IV ± 2%	Exp ± 7%	ENDL ± 2%	B-IV ± 2%	Exp ± 7%	ENDL ± 2%	B-IV ± 2%
			1 mfp			3 mfp			5 mfp	
Cu	0.8-5	0.313	0.343	0.281	0.465	0.430	0.379	0.285	0.238	0.210
	5.0-10	0.041	0.040	0.025	0.037	0.042	0.019	0.017	0.021	0.010
	10.0-15	0.642	0.627	0.634	0.236	0.221	0.224	0.082	0.078	0.075
Nb	0.8-5	0.308	0.333	0.235	0.422	0.402	0.265			
	5.0-10	0.031	0.025	0.018	0.033	0.029	0.021			
	10.0-15	0.707	0.686	0.698	0.265	0.233	0.238			
^{232}Th	0.8-5	0.442	0.438	0.467						
	5.0-10	0.039	0.038	0.020						
	10.0-15	0.645	0.636	0.628						
^{238}U†	0.8-5	0.670	0.644	0.595	0.803	0.905	0.846†			
	5.0-10	0.059	0.055	0.046	0.063	0.060	0.052			
	10.0-15	0.669	0.639	0.645	0.232	0.225	0.237			

†The ^{238}U spheres are 0.8 and 2.8 mfp instead of 1 and 3 mfp.

The calculated neutron spectra using the ENDL library were in fair agreement with the measurements (5 to 10% discrepancies for the 1-mfp spheres and less than 25% for the larger spheres). Calculations for Cu, Nb and Th carried out with the ENDF/B-IV library, badly underestimates the neutron emission between 5 and 10 MeV. The discrepancies with the

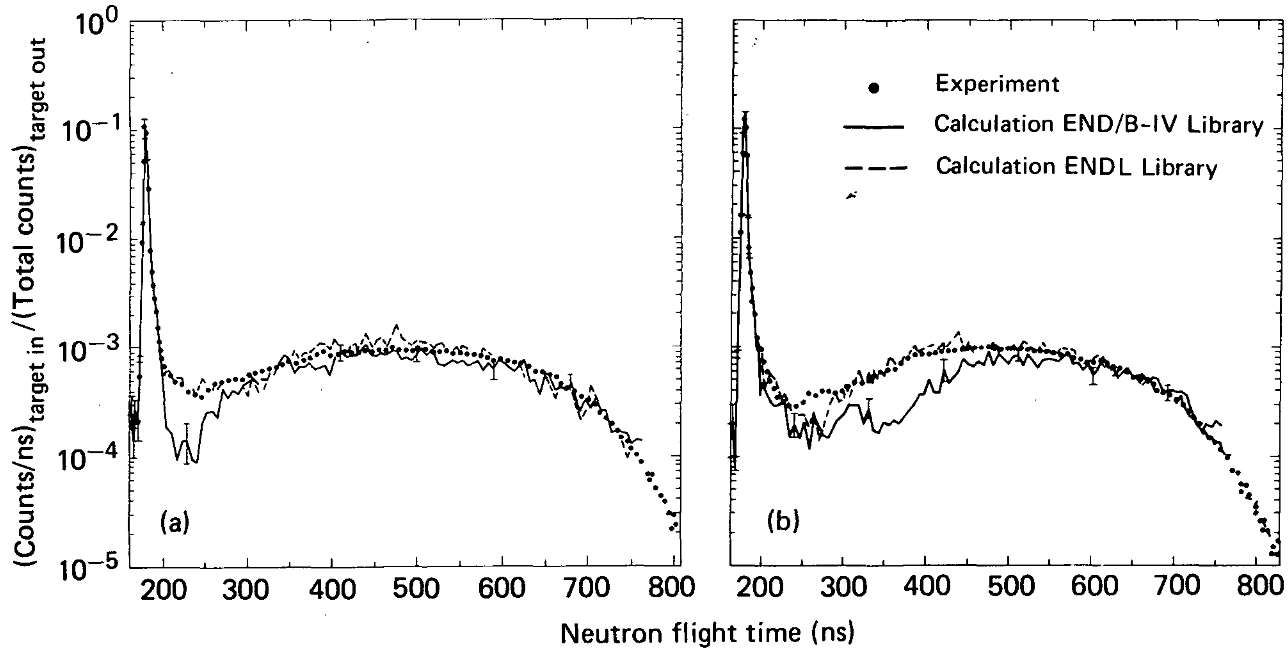

Figure A-2. Measured and Calculated Neutron Spectra for 1 mfp of Cu (a) and Nb (b).

measurements in this energy region are as large as a factor of two. For ^{238}U, the two libraries reproduce very well the integral in the 10-15 MeV inerval while in the region of 5 to 10 MeV the ENDF/B-IV underestimates the magnitude of the integral by ∿25%. These results were presented at the International Conference on Neutron Physics and Nuclear Data for Reactors and Other Applied Purposes, Harwell, U.K., September 25-29, 1978.

3. Mo(n,α) and (n,p) Cross-Section Measurements. (R.J. Nagle)

We have measured the ^{92}Mo(n,p) ^{92m}Nb, the ^{92}Mo(n,α) ^{89}Zr, and the ^{98}Mo(n,α) ^{95}Zr cross sections at average neutron energies of 15.0 and 13.7 MeV. Neutrons were generated by the ^{3}H(d,n) ^{4}He reaction with the 10-mA beam of 400 keV deuterons impinging on a thick target of titanium tritide at the Livermore ICT. The two 1.27 cm diameter packets of Mo target foils and Al neutron flux monitor foils were placed at 0° and at 117° (with respect to d^+ beam), and subtended angles of ±11° and 2°, respectively. The neutron energy distributions for the target packets at these two angles are approximately those given in LAMS-2162.[2]

Radiochemically-purified Zr and Nb fractions (of known chemical yield) from the irradiated Mo target foils were counted with Ge(Li) gamma-spectroscopy systems to determine the (n,α) and (n,p) products. The cross sections in Table A-3 are based on the known cross section for the ^{27}Al (n,α)^{24}Na reaction.[3]

TABLE A-3

Preliminary Cross-Section Results*

θ	$\langle E_n \rangle$	$\bar{\sigma}_{Al(n,\alpha)}$ (Assumed)	^{92}Mo(n,p)^{92m}Nb	^{92}Mo(n,α)^{89}Zr	^{98}Mo(n,α)^{95}Zr
0°	15.0	109 mb	58 mb	25 mb	6.6 mb
117°	13.7	123 mb	84 mb	19 mb	5.0 mb

[2]Seagrave, Graves, Hipwod, and McDole, Los Alamos Scientific Laboratory Rept. No. LAMS-2162, 1957-1958 (unpublished). At 0° the neutron energy range is from ∿14.4 to 15.6 MeV, while at 117° it is from ∿13.5 to ∿13.9 MeV.

[3]Nethaway, Nucl. Phys. A190, 635 (1972), and private communication (1972).

*The statistical precision is less than ±3%, while the systematic errors could be as much as 5% or more. Assumed isotopic abundance (atom %): ^{92}Mo (15.86%), ^{98}Mo (23.75%).

4. $\bar{\nu}$ for the ^{232}Th (n,f) Reaction. (R.E. Howe)

Fission neutron multiplicities for the ^{232}Th nucleus may provide an indicator of fission channel effects near the (n,f) and (n,n′f) thresholds. Measurements of this quantity relative to ^{235}U recently have been completed from the (n,f) threshold to 30 MeV.

Representative uncertainties were $\pm$ 3% at 1.5 MeV and $\pm$ 4% at 15 MeV. Some indication of nonlinear behavior was noted near the (n,f) threshold. No unusual effects were observed at the onset of "second-chance," (n,n′f), fission.

5. Fission Cross Section for ^{242m}Am. (J.C. Browne, R.E. Howe, E.J. Dupsyk, J.H. Landrum and R.J. Dougan)

The analysis of the ^{242m}Am (n,f) cross section data has been completed for the energy range 0.01 eV to 20 MeV. Resonance parameters were extracted for resonances below 20 eV. A preliminary discussion of this experiment was presented at the International Conference on Nuclear Physics and Nuclear Data for Reactor Applications and Other Applied Purposes held at Harwell in September, 1978. A complete paper on these data is in preparation.

6. A New Isotope of Curium and its Decay Properties: ^{251}Cm. (R.W. Lougheed, J.F. Wild, E.K. Hulet, R.W. Hoff, and J.H. Landrum)

The nuclide ^{251}Cm ($t_{1/2}$ = 16.8 $\pm$ 0.2 min) was produced by neutron capture from ^{250}Cm with an approximate cross section of 80 barns. In the decay of ^{251}Cm, we measured the energies and intensities of 12 γ-rays from which we constructed a level scheme for ^{251}Bk and for the configurations for six single-particle states in ^{251}Bk and for the ground state of ^{251}Cm $(1/2)^+$. The levels of ^{251}Bk fed by ^{251}Cm β-decay are compared with those of ^{249}Bk fed by ^{249}Cm β-decay. We also compare our measured Q_β-value of 1.42 MeV for ^{251}Cm with previous closed-cycle estimates. Details are published in Ref. 4.

7. Excited levels in ^{249}Cm from Neutron Capture γ-Ray Measurements. (R.W. Hoff, W.F. Davidson*, D.D. Warner*, K. Schreckenbach*, H. Borner*, A.F. Diggory*, and T. von Egidy*)

Excited levels in ^{249}Cm have been studied at Institut Laue-Langevin, Grenoble by measuring gamma rays and conversion electrons from

---

*Institut Max von Laue-Paul Langevin, Grenoble, France.

[4] Lougheed, Wild, Hulet, Hoff, and Landrum, A New Isotope of Curium and Its Decay Properties: ^{251}Cm, J. Inorg. Nucl. Chem. 40, 1865 (1978).

neutron capture in ^{248}Cm targets. A level scheme for ^{249}Cm has been constructed that includes new configuration assignments for the following Nilsson model single-particle states: 1/2[501], 1/2 [761], 3/2 [752], 1/2 [750]; the latter two configurations have not been identified before in actinide nuclei. This paper was presented at the Third International Symposium on Neutron Capture Gamma-Ray Spectroscopy and Related Topics, Brookhaven National Lab., September 18-22, 1978.

8. Excited Levels of ^{238}Np from Alpha Decay of ^{242m}Am. (R.W. Hoff, W.D. Ruhter, L.G. Mann, J.H. Landrum, and R.J. Dupzyk)

The level structure of ^{238}Np nucleus has been examined by measuring alpha particles, gamma-ray singles, and gamma-gamma coincidences arising from the alpha decay of 152-year ^{242m}Am. We produced 2 mg of enriched ^{242m}Am (99.3 atom-percent) for these experiments by use of the LLL electromagnetic isotope separator. The lower-lying levels of ^{238}Np are interpreted as four rotational bands based upon single-particle excitations involving both parallel and anti-parallel couplings of two proton configurations, 5/2[642] and 5/2 [523], and one neutron configuration, 1/2 [631]. We observe all levels in these bands up to and including I = 5. In the band populated by favored alpha decay of ^{242m}Am, a π 5/2 [523] + ν 5/2 [622] configuration, we observe the following level energies with indicated spin assignments: 342.6 keV (5^-), 407.9 keV (6^-) and 477.8 keV (7^-). We also observe alpha decay to four other levels, the first pair at 275.5 keV (5^+) and 389.2 keV (7^+) having been assigned a π 5/2 [642] + ν 5/2 [622] configuration and indicated spins and the second pair at 459.8 keV (6^+) and 517.8 keV (7^+) having been assigned a π 5/2 [523] + ν 7/2 [743] configuration. Our level scheme information complements and is in agreement with data reported by Kern et al.[5] who have measured (n,γ) and (d,p) population of ^{238}Np levels and by Asaro et al.[6] who have studied ^{242m}Am alpha decay. A paper will be presented at the ACS/CSJ Chemical Congress, Honolulu, Hawaii, April 1-6, 1979.

9. Information on Gamma Strength Functions in the Mass-90 Region From Proton-Induced Reactions. (F.S. Dietrich, D.W. Heikkinen, and D.G. Gardner)

In order to understand the systematics of gamma production in the mass-90 region, we have recorded the excitation function and spectral distributions of gammas produced by proton bombardment of ^{88}Sr, ^{89}Y, and ^{90}Zr from 3 MeV to energies well above the (p,n)

[5]Kern et al., submitted to Nucl. Phys. (1978).

[6]Asaro, Michel, Thompson, and Perlman, proceedings of the International Congress of Nuclear Physics, Paris, p. 564 (July 1964).

thresholds. The gammas were detected with Ge(Li) and with anticoincidence-shielded NaI spectrometers.[7] The results were compared with statistical-model calculations using the STAPRE code.[8] The excitation functions of individual gamma lines measured in the Ge(Li) detector and the total energy released in gamma radiation are in reasonable qualitative agreement with the calculations. However, the measured gamma spectra show a significantly lower yield of gammas in the 2 to 6 MeV range than predicted by the calculations, as shown in Fig. A-3 for the ^{89}Y and ^{90}Zr targets. The more likely cause of the discrepancy appears to be the energy dependence of the E1 gamma-ray strength function, which was parametrized in the Brink-Axel (Lorentzian) form in the calculations. Attempts are under way to determine a more appropriate parametrization from these experiments.

10. Inelastic Proton Scattering at 12 MeV on the Transitional Nuclei ^{151,152,153,154}Eu. (R.G. Lanier, L.G. Mann, G.L. Struble, I.D. Proctor, and D.W. Heikkinen)

Scattered protons from isotopically-enriched targets of ^{151,152,153,154}Eu were measured with an Enge split-pole spectrograph at a bombarding energy of 12 MeV.[9-11] The odd-odd nuclei ^{152}Eu and ^{154}Eu are radioactive and special procedures were employed to fabricate targets of these isotopes.[12] Absolute differential cross sections were measured at 10° intervals between 30° and 40° for the first four excited rotational states in the deformed nuclei ^{152,153,154}Eu. The experimental angular distributions were compared with an adiabatic coupled-channels calculation and values of the quadrupole (β_2) and hexadecapole (β_4) deformations were extracted from the data. The measured deformations are ^{152}Eu (0.28, 0.06), ^{153}Eu (0.28, 0.06), and ^{154}Eu (0.30, 0.04). Inelastic scattering from the spherical nucleu ^{151}Eu was measured at selected angles between 30°-140° and the results compared with a distorted-wave Born approximation calculation. The measurements suggest β_2 = 0.13 for this nucleus. These results will be used for statistical model calculations for neutron-induced reactions on the Eu isotopes.

---

[7] F. S. Dietrich and D. W. Heikkinen, Nucl. Inst. and Meth. 155, 103 (1978).

[8] M. Uhl, Acta Physica Austriaca, 31, 245 (1970).

[9] Lanier, Struble, Mann, Proctor, and Heikkinen, Phys. Lett. 78B, 217 (1978).

[10] Lanier, Mann, Struble, Proctor, and Heikkinen, Phys. Rev. 18C, 1609 (1978).

[11] Lanier, Mann, Struble, Proctor, and Heikkinen, (submitted to Phys. Rev. 1979).

[12] Dupzyk, Henderson, Buckley, Struble, Lanier, and Mann, Nucl. Instr. Methods 153, 53 (1978).

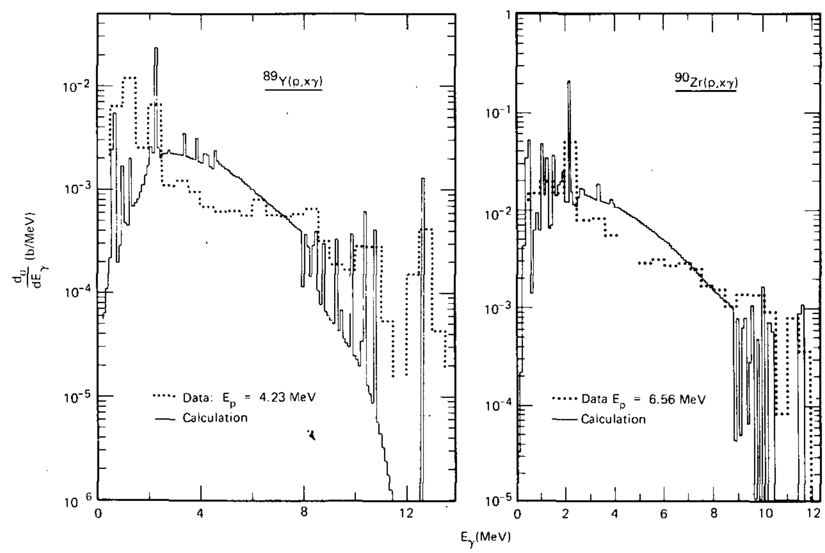

Figure A-3. Gamma spectral distributions inferred from NaI data by unfolding, compared with STAPRE statistical-model calculations. The data are binned in 0.5-MeV intervals, whereas those for the calculations are 0.1 MeV. The break in the data above 4 MeV for ^{90}Zr is due to a ^{12}C impurity.

B. NUCLEAR DATA APPLICATIONS - CALCULATIONS

1. An Improved Model for Radioactive Capture of Fast Nucleons with Application to ^{208}Pb (n,γ). (F.S. Dietrich and A. K. Kerman*)

Simple descriptions of fast-nucleon radiative capture have most often been made using the direct-semidirect (DSD) model.[13] This model is qualitatively successful in many cases, but has poor predictive capability. This is largely due to lack of knowledge about the origin and nature of an imaginary form factor[14] for excitation of the giant-dipole resonance by the incident nucleon. By using projection-operator techniques, we have derived the DSD model, together with an alternative calculational method based on identical physical assumptions. In the new method, this giant-dipole resonance is explicitly projected out of this combined (target-plus-nucleon) system. This results in the absence of a nonresonant term in the new model, which we term the pure-resonance model (PRM).

Calculations of ^{208}Pb (n,γ) (Ref. 15) in both models with identical input parameters are shown in Fig. B-1. DSD calculations are shown for both real and complex form factors); the shape and magnitude may be varied rather arbitrarily by changing the strength of the imaginary form factor. Introduction of an imaginary form factor has very little ($\lesssim$15%) effect on the PRM calculations, which are shown with a real form factor only.

Since the two models are formally the same, the differing results must be due to the approximations (such as a parametrization of the optical model) necessary for calculation. In the DSD model, both the direct and semidirect amplitudes contain effects of single-particle resonances which must cancel when the two terms are added; it is possible that the imaginary form factor achieves this cancellation, and does not represent a true physical mechanism. In the PRM, these single-particle resonances are removed *a priori* by the projection technique.

---

*Massachusetts Institute of Technology, Cambridge, Massachusetts.

[13] F. Cvelbar and S. L. Whetstone, Charge-Particle-Induced Radiative Capture, International Atomic Energy Agency, Vienna, 1974, p. 271, and references therein.

[14] M. Potokar, Phys. Lett. 46B, 346 (1973).

[15] Bergqvist, Drake and McDaniels, Nucl. Phys. A191, 641 (1972).

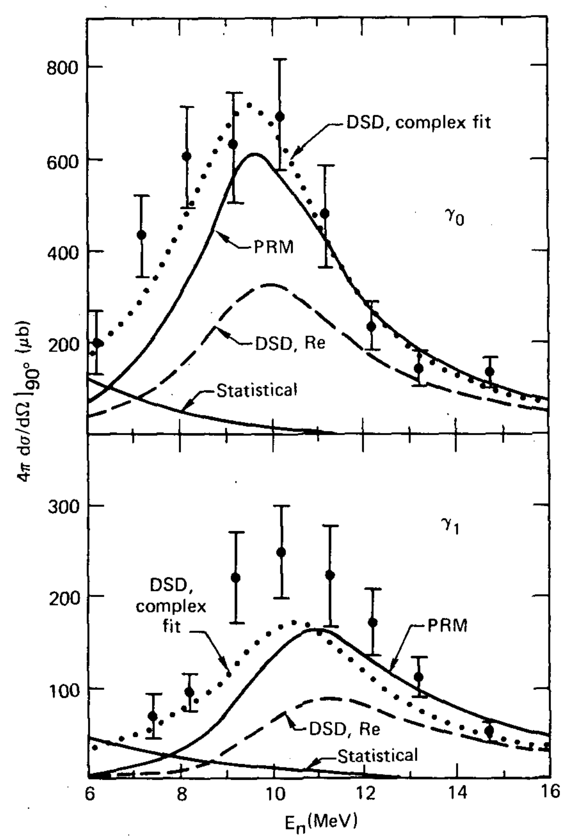

Figure B-1. Model calculations compared with the ^{208}Pb (n,γ) data of Ref. 15. The strength of the imaginary form factor was varied to yield a fit to the data for (n,γ_0) in the DSD model. The PRM calculations are insensitive to this parameter.

2. Calculated Neutron Capture Cross Sections for the Ground States and Isomers of ^{93,94,95}Nb. (M.A. Gardner and D.G. Gardner)

Neutron-induced capture cross sections on the ground states of ^{93}Nb, ^{94}Nb, and ^{95}Nb have been studied from the resolved resonance region to 4 MeV via statistical model calculations. Capture cross sections for inelastic processes leading to the production and depletion of all of the isomers and unstable ground states were calculated also. Gamma-ray production spectra were obtained for each target state over the full incident neutron energy range.

The latest versions of the statistical model nuclear reaction codes, STARPRE[8] and COMMUC,[16] were used for these calculations. The $\bar{\Gamma}_\gamma/D$ ratios were derived from gamma-ray strength function systematics.[17]

Total capture cross sections on the ground states are found to be within a factor of two of each other. Capture cross sections on the isomeric targets are found to be too large to be ignored, particularly since the inelastic scattering from the ground state to the levels that decay to the isomer in each nucleus was observed to reach values of 0.3 to 0.6 b in the MeV region. The depopulation of the isomers by inelastic scattering must also be considered since these cross sections exceed those of the ground state to isomer inelastic scattering for all three nuclei, particularly at low neutron energies.

Comparison of the ^{93}Nb calculated gamma-ray spectra with experimentally-determined spectra[18,19] indicated that a unique E1 strength function could not be extracted from these data alone. We plan to obtain more strength function information for other Nb isotopes by continuing the analysis of gamma-ray production spectra for incident neutrons up to 20 MeV in energy on ^{93}Nb.

---

[16] C. Dunford, AI-AEC-12931 (July, 1970).

[17] D. G. Gardner and M. A. Gardner, UCID-17566 (July, 1977).

[18] V. J. Orphan, et al., AD-717, 639 (July, 1970).

[19] J. K. Dickens, et al., ORNL-TM-4972 (1975).

3. <u>Beta-Delayed Neutron Spectra from Short-Lived Fission Products.</u> (S.F. Prussin*, Z.M. Oliveira** and K.-L. Kratz†

Delayed neutron spectra and branching ratios to excited states in final nuclei have been calculated with the statistical model and compared to experimental data for the decay of ^{87}Br, ^{137}I, ^{85}As and ^{135}Sb.[20] For the first two precursors, the calculations support the experimental β-strength functions reported previously. For the latter two, it has been shown that the statistical model cannot simultaneously reproduce both spectra and branching ratios for any choice of β-strength function when all levels populated by neutron emission are included in the calculations. The comparisons demonstrate that partial widths for neutron emission are not compatible with optical model transmission coefficients. This has led to the conclusion that structure effects in the energy range probed by delayed-neutron emission are not averaged out to the extent required by the statistical assumptions.

C. NUCLEAR DATA FOR REACTOR SAFETY

1. <u>Determination of Properties of Short-Lived Fission Products.</u> (R.A. Meyer, E.A. Henry, H.G. Hicks, O.G. Lien and T.N. Massey)

Decay data on short-lived fission products are required to resolve a number of problems associated with the design and operation of both thermal and fast reactors. Existing reactors cannot exceed power levels which are determined by the amount of heat generated in the core following a loss of coolant accident. This decay heat is produced by fission products. Existing plants must also carefully monitor effluents and the production of poisons (neutron absorbers) in the reactor core. Both these procedures depend on an accurate fission product data-base. Finally the properties of the short-lived fission products which are beta-delayed neutron emitters impact on predictions of the kinetic behavior of thermal and fast reactors. Our program is directed toward the measurement of the total decay energies, the γ-ray spectra, beta, delayed neutron spectra, and the average γ- and β-energy releases from these isotopes. Isolation of individual nuclides are performed with

---

*Consultant to LLL, Univ of California, Berkeley, CA.

**Department of Nuclear Engineering, Univ. of California, Berkeley, CA.

†Institut fur Kernchemie, Mainz, Germany.

[20]Prussin, Oliveira, and Kratz, Nucl. Phys. (in press) 1979.

rapid automated radiochemical separation procedures because these techniques yield isotopes of elements not available with the purely physical separation systems currently being used.

In the past year we have developed our system to be able to study half lives as short as 5 s via batchwise separation procedures.[21] This has allowed us to study the short-lived arsenic isotopes ^{80}As (16 s), $^{82}As^{g}$(13 s), $^{82}As^{m}$ (19 s), ^{83}As(5 s), and to a limited extent ^{85}As(2s). We have identified transitions in 5 s ^{84}As up to 8 MeV and demonstrated they populate levels up to 9.5 MeV in ^{84}Se via 3-parameter ($\gamma\gamma t$) spectrscopy.[22] Average decay energies will be reported upon completion of the calibration of our spectroscopy system for 9-MeV γ rays.

2. Determination of Multi-γ-Ray Source Calibration Set for Use in the Study of Short-Lived Fission Products. (R.A. Meyer and E.A. Henry)

The determination of γ-ray decay properties is dependent upon well-calibrated systems. As in a number of research applications, the study of short-lived fission products by γ-ray spectroscopy often requires detector calibration for each experimental configuration. To facilitate the rapid and accurate calibration of such spectrometer systems we have developed a unified set of multigamma-ray calibration sources. The values are published in manual form[23] and include the isotopes given in Table C-1.

---

[21] R. A. Meyer, Rapid Nuclear Chemistry for Determining the Properties of Short-Lived Fission Products, Energy and Technology Review, p. 19, September 1978.

[22] Meyer, Henry, Lien, Hicks, and Stevenson, Automated Rapid Nuclear Chemistry Facility for the Study of Short-Lived Fission Products, Proc. IEEE (in press, April 1979).

[23] R. A. Meyer, Multigamma-Ray Calibration Sources, LLL Manual 100, Dec. 1978.

TABLE C-1

Multi-gamma-ray calibration sources included in Ref. 23.

1. ^{152}Eu(13.4y)	12. ^{183}Re(70d)	23. ^{83}Rb(83d)	34. ^{131}Ba(11.7d)
2. ^{110}Ag^{m}(252d)	13. ^{185}Os(94d)	24. ^{90}Nb(14.6h)	35. ^{132}Cs(6.47d)
3. ^{182}Ta(115d)	14. ^{28}Mg^{28}Al(21.0h)	25. ^{95}Zr(64.0d)	36. ^{143}Ce(33.0h)
4. ^{56}Co(78.5d)	15. ^{44}Sc^{m+g}(58.6h)	26. ^{96}Mo(23.35h)	37. ^{150}Eu(35y)
5. ^{108}Ag^{m}(130y)	16. ^{48}V(16.21d)	27. ^{99}Mo(66.2h)	38. ^{155}Eu(4.9y)
6. ^{124}Sb(60.20d)	17. ^{48}Sc(43.8h)	28. ^{103}Ru(39.35d)	39. ^{187}W(23.9h)
7. ^{133}Ba(10.7y)	18. ^{52}Fe(8.28b)	29. ^{105}Ag(41.0d)	
8. ^{134}Cs(2.062y)	19. ^{52}Mn(5.59d)	30. ^{121}Te^{m}(150d)	
9. ^{75}Se(120d)	20. ^{67}Ga(78.3h)	31. ^{125}Sb(2.73y)	
10. ^{113}Sn(115d)	21. ^{67}Cu(61.7h)	32. ^{126}I(13.0d)	
11. ^{154}Eu(8.2y)	22. ^{82}Br(35.30h)	33. ^{131}I(8.041d)	

D. NUCLEAR DATA FOR SAFEGUARDS

1. Photofission Neutron Multiplicities and Cross Sections. (B.L. Berman, P. Meyer, and R.A. Alvarez, J.T. Caldwell* and E.J. Dowdy*)

Photofission data have been obtained with monoenergetic photons from the LLL Electron-Positron Linear Accelerator facility in an LLL-LASL collaborative project. Analysis of the data has been completed for ^{235}U, ^{236}U, ^{238}U, and ^{232}Th, and papers on the neutron multiplicities and the cross sections are being submitted to Nuclear Science and Engineering and Physical Review C, respectively. The prompt neutron multiplicity $\bar{\nu}_p$ for these four nuclei are shown as functions of photon (excitation) energy in Fig. D-1, and the parameters of straight-line fits to the $\bar{\nu}(E_\gamma)$ data are given in Table D-1. The unusual behavior of $\bar{\nu}(E_\gamma)$ for ^{232}Th can be seen readily in part (d) of Fig. D-1. The total photofission cross section for ^{236}U is shown in Fig. D-2, and the ratio of first-chance photofission $\sigma(\gamma,f)$ to total photofission $\sigma(\gamma,f) = \sigma[(\gamma,f) + (\gamma,nf)]$ is shown in Fig. D-3. The significant change in the slope of $\sigma(\gamma,f)$ at the (γ,nf) threshold can be seen in Fig. D-2, and the asymptotic approach to roughly equal components of first-chance and second-chance photofission can be seen in Fig. D-3. It should be noted that except for the spin difference resulting from the dipole selection rule, the results for ^{236}U [including part (b) of Fig. D-1] can be compared to ^{235}U+n fission data.

---

*Los Alamos Scientific Laboratory, Los Alamos, NM 87545

TABLE D-1. Photofission $\bar{\nu}_p(E)$ Results

Isotope	Least-Squares Fit
^{235}U	$\bar{\nu}_p = 1.610 + 0.133\ E$
^{236}U	$\bar{\nu}_p = 1.881 + 0.116\ E$
^{238}U	$\bar{\nu}_p = 1.862 + 0.123\ E$
^{232}Th	$\bar{\nu}_p = 2.823 - 0.143\ E$ $(6.0 < E < 8.2\ \text{MeV})$
	$\bar{\nu}_p = 0.453 + 0.175\ E$ $(E > 8.5\ \text{MeV})$

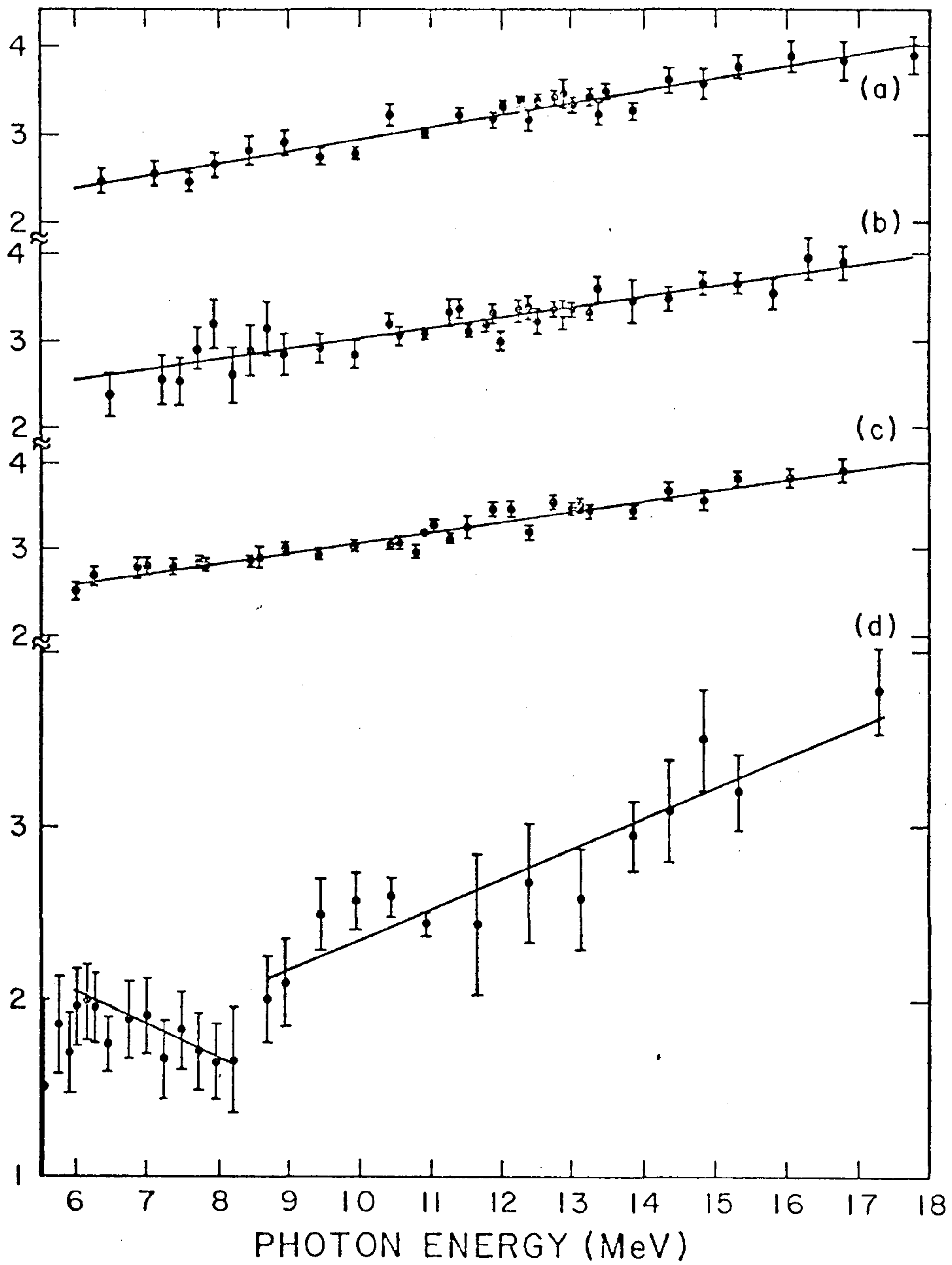

Figure D-1. Prompt Neutron Multiplicity for Photofission of (a) ^{235}U; (b) ^{236}U; (c) ^{238}U and ^{232}Th (d).

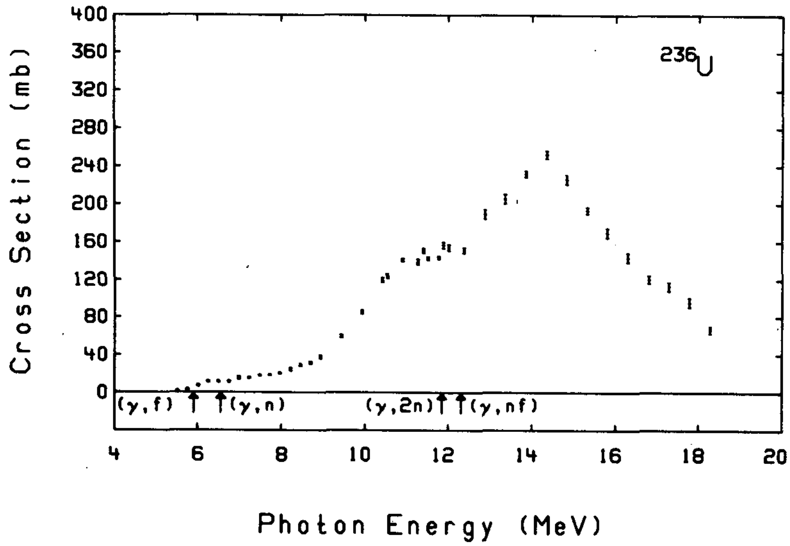

Figure D-2. The total photofission cross section for ^{236}U.

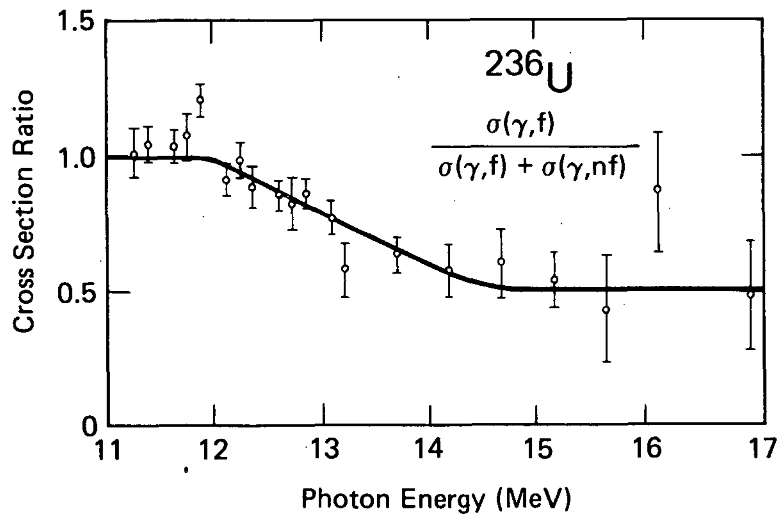

Figure D-3. Ratio of first-chance photofission to total photofission for ^{236}U.

E. FISSION PHYSICS

1. Spontaneous-Fission Decay Properties of ^{259}Md. (J.F. Wild, E.K. Hulet, R.W. Lougheed, P.A. Baisden, J.H. Landrum, R.J. Dougan, J.M. Nitschke, and A. Ghiorso*)

We are presently studying the mass and kinetic-energy distributions of fragments from the spontaneous-fission (SF) decay of 95-min ^{259}Md.[24] The ^{259}Md was prepared as the E.C.-decay daughter of 62-min ^{259}No, produced by the ^{248}Cm (^{18}O,α3n) reaction. The No after chemical separation from all interfering actinides, was evaporated onto a thin plastic film which was placed between two facing surface-barrier detectors. The energies of coincident SF fragments were measured and stored along with the time of each event. After eighteen 2-h bombardments we have succeeded in accumulating $\gtrsim$ 400 coincident SF events. We have corrected the fragment energies for the average energy lost in transmission through the plastic foils supporting the samples and for the pulse-height defect. In addition to using ^{252}Cf as the primary calibration source, we have also calibrated with ^{256}Fm and ^{257}Fm.

Our results from the SF of ^{259}Md (Fig. E-1) show a highly symmetric mass distribution, very much like those obtained for ^{258}Fm[25] and ^{259}Fm.[26] However, the average total kinetic energy ($\overline{TKE}$) release in the SF of ^{259}Md is very different from the $\sim$240 MeV found for the heavy Fm isotopes, being about 50 MeV lower. Such a low $\overline{TKE}$ associate with symmetric mass division is unique and is entirely inconsistent with current fission theory in which fragment shells appear to govern the fission process. Symmetrical division of the heavier Fm isotopes leads to fragments approaching the magic nucleon numbers Z=50, N=132, and due to their spherical rigidity, they possess low internal excitation energy. Therefore, SF events with near-symmetric mass division exhibit correspondingly higher TKE than those with asymmetric division,

---

*Lawrence Berkeley Laboratory.

[24] Wild, Hulet, Lougheed, Landrum, Nitschke, and Ghiorso, 175th National Meeting of the American Chemical Society, Anaheim, California, March 21-25, 1978, UCRL-80293A.

[25] Hoffman, Wilhelmy, Weber, Daniels, Hulet, Landrum, Lougheed, and Wild, to be submitted to Phys. Rev. C.

[26] Hoffman, Weber, Wilhelmy, Hulet, Lougheed, Landrum, and Wild, Proceedings of the 3rd International Conference on Nuclei Far from Stability, Cargese, Corsica (CERN, Geneva, 1976), p. 558.

which yields fragments that are soft toward deformation. Thus, our ^{259}Md results are seemingly unexplainable by theories based on fragment shell effects in two-body fission.

These SF properties, together with the fact that a 95-min half life in this region of nuclide charge and mass is considerably longer than might be expected make ^{259}Md an interesting isotope for further experimental and theoretical consideration

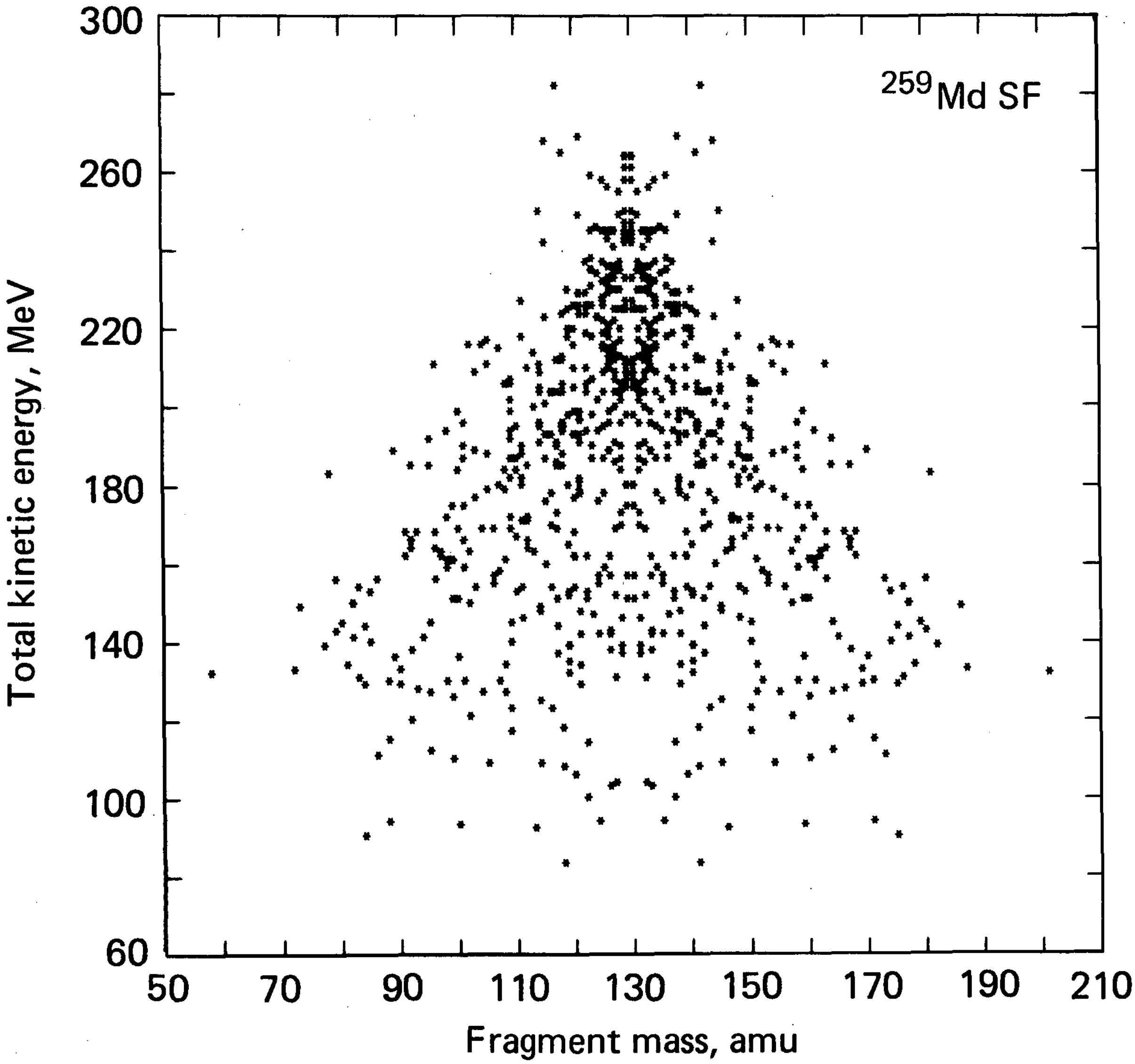

Figure E-1. Mass-TKE distribution of events from the S.F. of ^{259}Md.

LOS ALAMOS SCIENTIFIC LABORATORY

A. NUCLEAR CROSS SECTIONS

1. Magnesium (n,α) Cross Sections (Reedy)

Mass spectrometric analyses of neutron-irradiated targets of natural magnesium yield cross sections of 59 $\pm$ 14, 160 $\pm$ 8 and 11.0 $\pm$ 3.3 mb for ^{20}Ne, ^{21}Ne and ^{22}Ne, respectively, at 14.1 MeV and of 94 $\pm$ 8, 152 $\pm$ 12 and 13.0 $\pm$ 2.0 mb at 14.7 MeV. Incorporation of these cross sections in a calculation modeling cosmic-ray interactions with meteorites satisfactorily reproduces the increase in ^{21}Ne production and decrease of ^{22}Ne/^{21}Ne ratio with depth observed in the Keyes chondrite. The reaction ^{24}Mg(n,α)^{21}Ne predominantly controls these trends.

2. Cross Section Measurements for the Radioactive Nuclei ^{88}Y and ^{88}Zr (Prestwood; Nethaway, Smith, Nego (LLL))

We have measured the cross sections at 14.8 MeV for the (n,2n) reaction on ^{88}Y and the (n,2n) and (n,np) reactions on ^{88}Zr. The yields of reactions on short-lived target materials such as these are difficult to measure because the target radioactivity interferes with the measurement of the products. In this case the measurements are possible only because we were able to chemically separate and measure the ^{87m}Sr daughter of ^{87}Y. The targets for the neutron irradiations consisted of dried mixtures of ^{88}Y (10 mCi) and thulium hydroxide, and ^{88}Zr (50 mCi) and thulium hydroxide. The (n,2n) reaction on thulium was used as an internal neutron-fluence monitor. The ^{88}Zr target material was prepared by irradiation of molybdenum with high-energy protons at the Los Alamos LAMPF accelerator. The ^{88}Y was separated from the purified ^{88}Zr material.

3. ^{242}Pu(n,γ)^{243}Pu (Bendt, Jurney)

We have measured the gamma ray production spectrum from thermal neutron capture by ^{242}Pu. The detector was a 6.3 cm diam by 15 cm long NaI scintillator surrounded by a NaI anticoincidence annulus for reduction of pulses caused by escape events. Figure A-1 shows the unfolded gamma spectrum. Summing over the spectrum gives a value of 18.5 $\pm$ 1 b for σ(n,γ), in agreement with earlier values of 18.7 $\pm$ 0.7

b obtained by α-counting the ^{243}Am produced in a long reactor irradiation,[1] and a fast chopper measurement[2] of 18.5 ± 1 b. These values all refer to the 2200 m/s cross section.

The gamma multiplicity derived from the spectrum of Fig. A-1 is 4.5 ± 0.2 photons per captured neutron.

4. Neutron Elastic and Inelastic Scattering Cross Sections for ^{242}Pu (Drake, Drosg, Lisowski)

We have measured neutron scattering cross sections for ^{242}Pu at 10 angles for incident neutron energies of 0.57, 1.0, and 1.5 MeV. Although the low-lying states in ^{242}Pu are closely spaced and weakly excited at these energies, we were able to measure the inelastic cross section for the 0.044 MeV state for incident 0.57 MeV neutrons, and for the 0.044 and 0.147 MeV states at an incident neutron energy of 1.0 MeV. Figures A-2 and A-3 show the results, uncorrected for multiple scattering.

5. Simulated (n,f) Cross Sections for Exotic Actinides (Britt, Wilhelmy)

The fission cross sections of 34 actinide nuclei have been inferred from direct-reaction fission correlation experiments. In this technique, an actinide nucleus is excited by a direct reaction and its excitation energy determined from a measurement of the energy of the outgoing direct particle. The probability that the nucleus will then decay by fission is determined from the relative number of events that include coincident fission fragments. We have found that ^{3}He reactions can be used to measure fission probabilities in the excitation energy range from threshold up to 11-12 MeV, and the data can be then used to estimate pseudo (n,f) cross sections for the neutron energy region of 0.5 to ~ 5-6 MeV.

The use of (^{3}He,df) and (^{3}He,tf) reactions are particularly useful, since they lead from relatively stable even-z targets to odd-z fissioning systems, many of which cannot be studied directly. Table I lists the fissioning nuclei we have studied. Of particular interest are many of the inaccessable isotopes of Np, Am, Cm, Bk, and Cf which may be of practical concern in detailed calculations of nuclear breeding, heavy element production, and nuclear waste burnup.

---

[1] R. W. Durham and F. Molson, "Capture Cross Section of ^{242}Pu," Can. J. Phys. 48, 716 (1970).
[2] T. E. Young, F. B. Simpson, and R. E. Tate, "The Low Energy Total Neutron Cross Section of ^{242}Pu," Nuc. Sci. Eng. 43, 341 (1971).

A paper giving detailed results has been submitted to Nuclear Science and Engineering.

Table 1

Equivalent Neutron Targets and Half Lives of Those Targets for Fissioning Nuclei That Have Been Studied Via (^{3}He,xf) Reactions Where x = d (Deuteron) or t (Triton)

"Neutron Target"	$T_{1/2}$	x	"Neutron Target"	$T_{1/2}$	x
^{229}Pa	1.4 d	t	^{238}Am	1.63 h	t
^{230}Pa	17.4 d	d	^{239}Am	11.9 h	d
^{231}Pa	3.25 x 10^{4} y	t	^{240}Am	51 h	d
^{232}Pa	1.32 d	d	^{241}Am	433 h	t
			^{242}Am	152 y	d
^{230}U	20.8 d	t	^{243}Am	7380 y	t
^{231}U	4.2 d	d	^{244}Am	10.1 h	d
^{232}Np	14.7 m	t	^{240}Cm	26.8 d	t
^{233}Np	35 m	d	^{241}Cm	36 d	d
^{234}Np	4.4 d	d	^{242}Cm	163 d	t
^{235}Np	396 d	d	^{243}Cm	28 y	d
^{236}Np	1.3 x 10^{6} y	d			
^{237}Np	2.1 x 10^{6} y	d	^{244}Bk	4.4 h	t
^{238}Np	2.12 d	d	^{245}Bk	4.9 d	d
			^{246}Bk	1.8 d	d
^{236}Pu	2.85 y	t	^{247}Bk	18 h	d
			^{248}Es	27 m	t
			^{249}Es	1.7 h	d
			^{250}Es	8.6 h	d

6. Low Energy Cross Section Project (Jarmie, Ohlsen, Hardekopf, Brown)

Construction of the apparatus for measurement of the important fusion cross sections ^{2}H(t,α)n, ^{2}H(d,p)^{3}H, ^{2}H(d,^{3}He)n, and ^{3}H(t,α)2n in the bombarding energy range 5-120 keV continues. The ion source and acceleration system is undergoing acceptance tests at the vendor's laboratory, and the windowless gas target and a double-compensated calorimeter for measuring the beam flux are being tested here. We expect to have the complete system assembled for initial testing during late summer 1979.

7. Neutron Emission Spectra and Angular Distributions (Drake, Drosg, Lisowski)

Our data on neutron emission spectra include ^{6}Li, ^{7}Li, ^{10}B and ^{11}B each taken at 10 angles and each with incident neutron energies of 6, 10, and 14 MeV. In addition we have spectra from ^{12}C at 10 angles and with an incident neutron energy of 14 MeV. These data await final refinement of the detector efficiency curve before release.

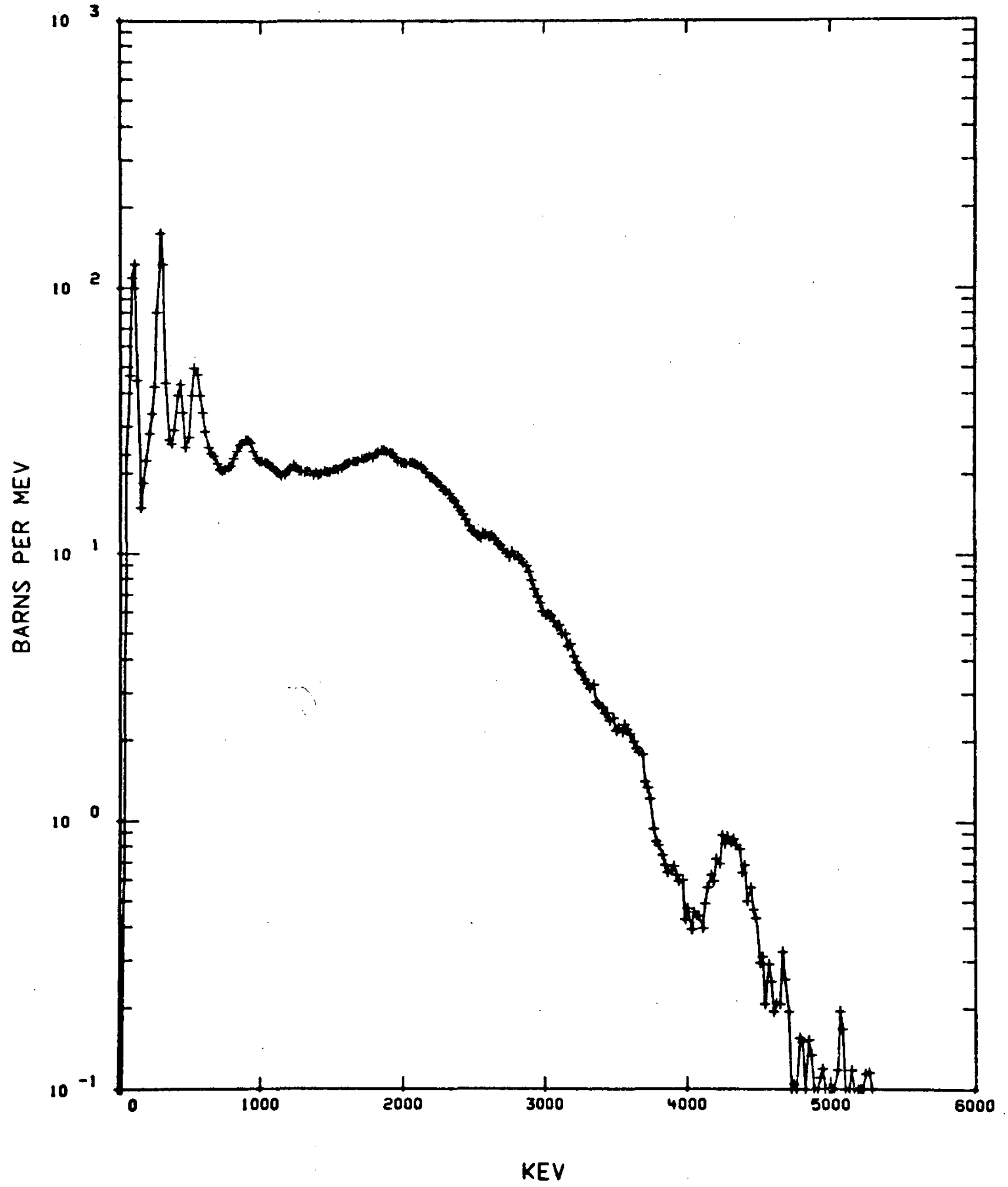

Fig. A-1. Photon production spectrum from thermal neutron capture by ^{242}Pu. The gamma energy bin widths are 20 keV.

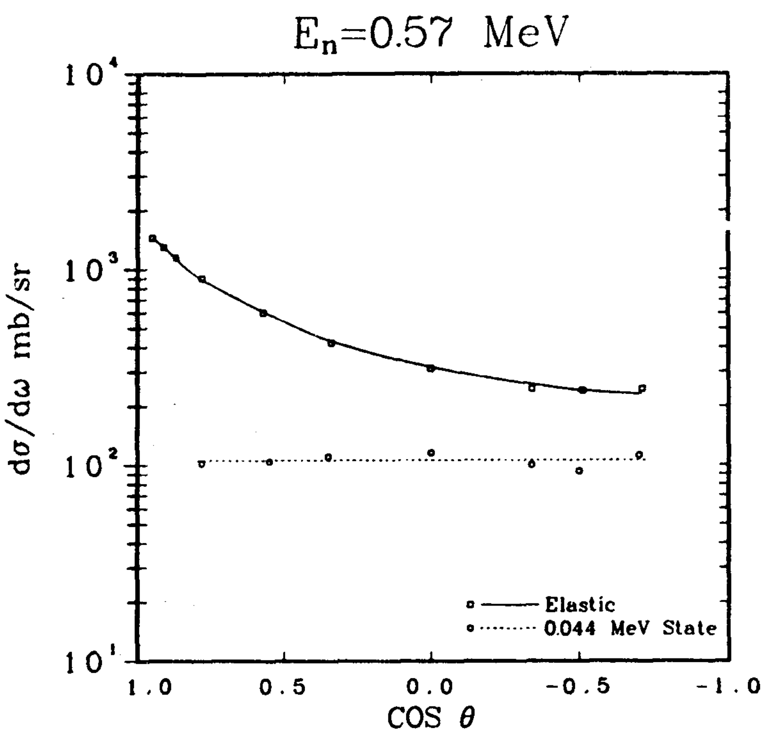

Fig. A-2. Elastic and inelastic differential cross sections for ^{242}Pu for incident 0.57 MeV neutrons.

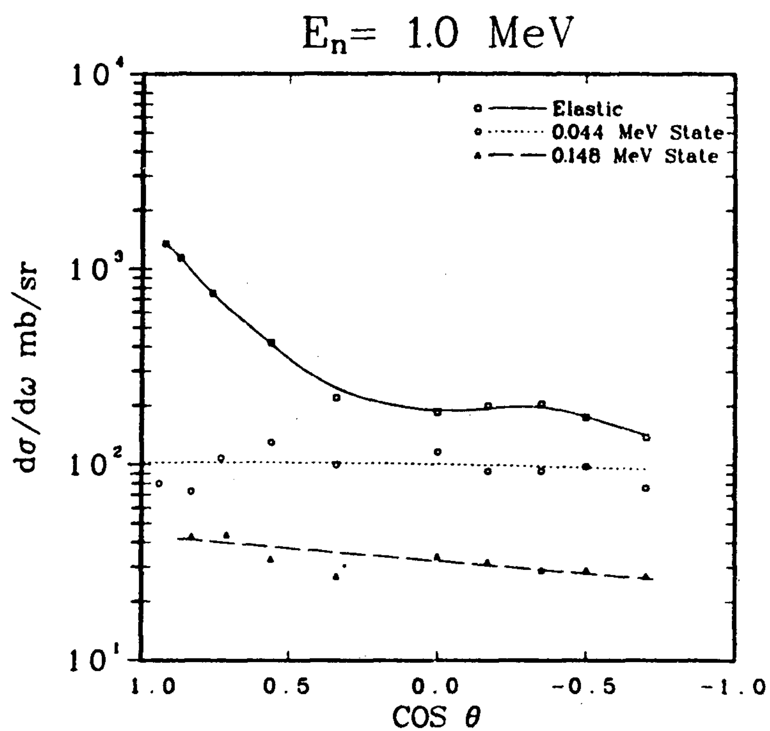

Fig. A-3. Elastic and inelastic differential cross sections for ^{242}Pu for incident 1.0 MeV neutrons.

B. OTHER NUCLEAR DATA

1. Polarization Effects in Three-Nucleon Breakup (Ohlsen, Correll, Brown, Hardekopf, Jarmie)

Very little data exist on polarization effects in the three-nucleon breakup reaction p + d → p + p + n. We have initiated a series of such measurements using a 16-MeV polarized deuteron beam. So far all possible analyzing powers have been measured for the kinematically incomplete experiment $^1H(d,p)pn$, and several analyzing powers have been measured for the kinematically complete experiment $^1H(d,pp)n$ in geometries characterized by equal relative energies of the three nucleons in the final state.

2. ^3He + ^3He Reactions from 17.9 to 24.0 MeV (Brown, Correll, Ohlsen)

The yields have been measured of most of the charged particles produced in the ^3He + ^3He interaction at bombarding energies of 17.9, 21.7 and 24.0 MeV. These data can be combined to give total reaction cross sections needed in the theoretical study of the ^3He + ^3He system with resonating-group calculations.[1] Furthermore, the cross section for the α + 2p channel should be useful in evaluating certain "clean" fusion systems, such as the migmatron.[2,3]

3. d + α Scattering from 12 to 17 MeV (Brown, Hardekopf, Correll, Jarmie, Ohlsen)

Differential cross sections and vector and tensor analyzing-power angular distributions have been measured for d + α scattering from 12 to 17 MeV bombarding energy. The data are tabulated in the Los Alamos report LA-7378-MS.

---

[1]D. R. Thompson et al., "Odd-Even Absorption in ^3He + ^3He Scattering and Level Structure of ^6Be," Nucl. Phys. A201, 301 (1973).
[2]J. R. Teglio, "A Study of the Feasibility of Fusion Power with Negligible Neutron Production," Nucl. Instrum. Methods 141, 353 (1977).
[3]B. C. Maglic et al., "Fusion Reactions in Self-Colliding Orbits," Phys. Rev. Lett. 27, 909 (1971).

c. Fission-Product Gamma Decay Spectra (Jurney, Bendt, and England)

The fission-product gamma spectra of ^{233}U, ^{235}U, and ^{239}Pu have been measured at 12 cooling times following 20 000-s irradations in the thermal column of the Omega West Reactor. The mean-cooling times ranged from 29 to 146 500 s. The total gamma energies were obtained by integrating over the energy spectra, and both the spectra and the total energies are compared with calculations using the CINDER-10 code and ENDF/B-IV data base.

The measured and calculated gamma spectra are compared in a series of figures. The measured total gamma energies are ~14% larger than the calculated energies during the earliest counting period (~4 to 53 s cooling time). For ^{235}U, the measured and calculated total gamma energies are nearly the same after 1200 s cooling time, and the measurements are 2 to 6% lower at longer cooling times. For ^{239}Pu, the measured and calculated total gamma energies are nearly the same at cooling times longer than 4000 s, and for ^{233}U this condition prevails at cooling times longer than 10 000 s. All results are available in Ref. 4.

---

[4]E. T. Jurney, P. J. Bendt, and T. R. England, "Fission Product Gamma Spectra," Los Alamos Scientific Laboratory report LA-7620-MS (Jan. 1979).

C. NUCLEAR DATA EVALUATION

1. Light Element Studies

a. Charge-Independent R-Matrix Analysis for the Four-Nucleon System (Hale and Dodder)

Our on-going study of the four-nucleon reactions has been extended to higher energies and expanded to include a number of new measurements. The analysis presently includes ^{4}He system data at energies up to 11 MeV in the proton channels (10 MeV neutron energy) and up to 10 MeV in the deuteron channels. Recent and, in many cases, preliminary data have been added for the T(p,p), T(p,n), D(d,p), and D(d,n) reactions. The fit to all the data in this expanded analysis remains quite satisfactory overall, indicating that our information about the levels in ^{4}He and ^{4}Li at excitation energies below 30 MeV is stabilizing. We continue to seek an explanation of the differences in the two branches of the d + d reaction in terms of an isospin-1 enhancement mechanism.

b. R-Matrix Analysis of the t + t Reactions (Hale, Young, and Jarmie)

We have done an R-matrix analysis of reactions in the ^{6}He system, including T(t,t)T elastic scattering and the fusion reaction T(t,2n)^{4}He, at triton energies below 2 MeV. Although the R-matrix parameterization is fairly simple, with only s-waves considered in the t + t channel, and the 2n-^{4}He channel represented as a pseudo two-body n-^{5}He channel, we are able to obtain an excellent fit to the T(t,t)T angular distributions and to most of the T(t,2n)^{4}He cross sections measured at triton energies below 2 MeV.

Figure C-1 shows measurements[1-4] of the T(t,2n) cross section compared with the R-matrix calculation. The calculation clearly

---

[1]H. M. Agnew, W. T. Leland, H. V. Argo, R. W. Crews, A. H. Hemmendinger, W. E. Scott, and R. F. Taschek, "Measurement of the Cross Sections for the Reaction T + T → ^{4}He + 2n + 11.4 MeV," Phys. Rev. 84, 862 (1951).

[2]R. C. Allen and N. Jarmie, "Triton Reaction Cross Sections," Phys. Rev. 111, 1129 (1958).

[3]A. M. Govorov, L. Ka-Yend, G. M. Osetinskii, V. I. Satatskii, and I. V. Sizov, "Total Cross Section of the T+T Reaction in the 60-1140 keV Energy Range," J. Exptl. Theor. Phys. (USSR(42, 383 (1962) (English Trans. Sov. Phys. JETP 15, 266 (1962)).

[4]V. I. Serov, S. N. Abramovich, and L. A. Morkin, "Total Cross Section Measurement for the Reaction T(t,2n)^{4}He," At. Eng. 42, 59 (1977) (English Translation Sov. At. En. 42, 66 (1977)).

prefers recent low-energy values of Serov et al.[4] to those of earlier measurements.[1-3] The suggestion of a bump in the data at 2 MeV indicates a resonance in the ^{6}He system that has been seen in other reactions at 13.4 MeV excitation energy. Our analysis gives a tenta- tive assignment and resonance parameters for this level.

Maxwellian-averaged reaction rates for T(t,2n) at temperatures below kT = 100 keV have been calculated using the reaction cross sections obtained from this analysis. We have also evaluated neutron spectra for low incident triton energies, based on measurements made by Wong et al.[5]

c. Reaction Rates for ^{6}Li(p,α)^{3}He (Hale and Dodder)

One result of our combined charge-independent R-matrix analysis of reactions in the ^{7}Li and ^{7}Be systems, discussed in the previous report and described in a recent conference contribution,[6] has been a determination of the ^{6}Li(p,α)^{3}He cross section at energies below 2.5 MeV. This cross section has had astrophysical significance for many years, and more recently is receiving attention in "exotic fuel" fusion studies.

We have used the cross section obtained from our R-matrix analysis to calculate Maxwellian-averaged reaction rates for ^{6}Li(p,α) at temperatures below kT = 1 MeV. The results are shown in Fig. C-2 and are compared with those of Hirshfield[7] and those from the compilation of McNally and Sharp.[8] Our calculations indicate generally higher ^{6}Li(p,α) reaction rates than those obtained previously.[7,8]

---

[5]C. Wong, J. D. Anderson, and J. W. McClure, "Neutron Spectrum for the T+T Reaction," Nucl. Phys. 71, 106 (1965).

[6]D. C. Dodder and G. M. Hale, "Applications of Approximate Isospin Conservation in R-Matrix Analyses," Proc. Intnl. Conf. on Neutron Physics and Neutron Data for Reactors and Other Applied Purposes, Harwell (1978).

[7]J. L. Hirschfield, "Fusion Reactors Based on ^{6}Li(p,α)^{3}He," Proc. of the Review Meeting on Advanced-Fuel Fusion (EPRI ER-536-SR), p. 261 (1977).

[8]J. Rand McNally and R. D. Sharp (unpublished), reported in Ref. 7 above.

2. Calculations for Medium and Heavy Mass Nuclei

a. Self-Consistent Analysis of Neutron Reactions on Yttrium and Zirconium Isotopes (Arthur)

Complete and consistent calculations of neutron-induced reactions on yttrium and zirconium isotopes were performed in which both stable and unstable isotope data provided important tests of nuclear-model techniques and input parameters in this closed neutron shell (N=50) mass region. In addition, new experimental information[9] relating to total proton-production cross sections obtained through charged-particle simulation of neutron-induced reactions on ^{89}Y provided unique opportunities to test optical model parameter values for low-energy proton emission. Our proton optical model parameters, determined from fits to the ^{89}Y(p,n) and ^{87}Sr(p,n) data are in general agreement with recent results of Johnson et al.[10] for sub-Coulomb-barrier protons. In both our work and that of Ref. 10, it was necessary to decrease the imaginary well depth to approximately one-third of its value as determined from fits[11] to proton angular distribution data at higher energies.

b. Calculation of (n,xn) and (n,xnf) Reactions for ^{235}U and ^{238}U (Arthur)

Using the GNASH preequilibrium-statistical nuclear model code, we have calculated (n,xn) and (n,xnf) reaction cross sections for ^{235}U and ^{238}U in the neutron-energy range from 6 to 22 MeV. We also calculated individual spectra of the two (n,2n) and the three (n,3n) neutrons to provide information needed to correct the scintillation tank measurements of Veeser.[12] Figure C-3 compares the calculated fission cross sections to recent results of Leugers et

---

[9]H. C. Britt et al., ERDA-NDC-9, p. 108 (1977).

[10]C. H. Johnson, A. Galonsky, and R. L. Kernell, "Anamolous Optical Model Potential for Sub-Coulomb Protons for 89 < A < 130," Phys. Rev. Lett. 39, 1604 (1977).

[11]F. G. Perey, "Optical Model Analysis of Proton Elastic Scattering in the Range of 9 to 22 MeV," Phys. Rev. 131, 745 (1962).

[12]L. R. Veeser and E. D. Arthur, "Measurements of (n,3n) Cross Sections for ^{235}U and ^{238}U," Proc. of Internl. Conf. on Neutron Physics and Neutron Data for Reactors and Other Applied Purposes, Sept. 1978, Harwell, England.

al.[13] Fission barrier parameters were determined to be similar to those of Back et al.[14]

c. Neutron-Nucleus Optical Potential for the Actinide Region (Madland and Young)

A new neutron-nucleus optical potential has been determined for coupled-channel calculations in the actinide region.[15,16] Since the actinides display strong nuclear deformation effects, use of a spherical optical model is inadequate. A method has been developed to determine a deformed global potential by use of additional experimental data, i.e., resolved inelastic differential cross sections for low-lying collective rotational states. The method consists of a series of constrained iterations between best fits using a spherical global search code and best fits using a coupled-channels search code. The present potential reproduces measured total cross sections to within a few percent for the neutron-energy range 10 keV $\leqslant E_n \leqslant$ 10 MeV and the target mass range 232 $\leqslant A \leqslant$ 239.

d. Calculation of Prompt Fission Neutron Spectra (Madland and Nix)

A new calculation of the prompt fission neutron spectrum has been made.[17] Standard nuclear-evaporation theory has been used to

---

[13]B. Leugers et al., "The ^{235}U and ^{238}U Neutron-Induced Fission Cross Sections Relative to the H(n,p) Cross Sections," Proc. of the NEANDC/NEACRP Specialists Meeting on Fast Neutron Cross Sections of ^{233}U, ^{235}U, ^{238}U, and ^{239}Pu, Argonne National Laboratory report ANL-76-90, p. 246-157 (1976).

[14]B. B. Back et al., "Fission of Doubly Even Actinide Nuclei Induced by Direct Reactions," Phys. Rev. C9, 1924 (1974); B. B. Back et al., "Fission of Odd-A and Doubly Odd Actinide Nuclei Induced by Direct Reactions," Phys. Rev. C10, 1948 (1974).

[15]D. G. Madland and P. G. Young, "Neutron-Nucleus Optical Potential for the Actinide Region," Proc. of Internl. Conf. on Neutron Physics and Neutron Data for Reactors and Other Applied Purposes, Harwell, (Sept. 1978).

[16]D. G. Madland and P. G. Young, "Neutron Nucleus Optical Potential for the Actinide Region," to be presented at the American Physical Society, Spring Meeting in Washington, D.C. (April 23-26, 1979).

[17]D. G. Madland and J. R. Nix, "Calculation of Prompt Fission Neutron Spectra," to be presented at the 1979 Annual Meeting of the American Nuclear Society (June 3-8, 1979) and LA-UR-79-147.

calculate the neutron energy spectrum in the fission-fragment center-of-mass system, followed by a transformation to the laboratory system. The resulting prompt fission neutron spectrum, expressed in terms of the exponential integral and incomplete gamma function, reproduces the experimental results better than do either the Maxwellian or Watt distributions, especially at high neutron energy, as shown in Fig. C-4. The improved agreement with the experimental data is achieved without the use of any adjustable parameters, i.e., all constants used in the calculation are determined a priori from other physical considerations.

3. ENDF/B-V Evaluations

a. ENDF/B-V Dosimetry File (Stewart, Hale, Foster, and Young)

The LASL revisions for ENDF/B-V consist of the total helium (^{4}He) production cross sections for neutron-induced reactions with ^{6}Li and ^{10}B. Since revisions to Version IV were made to both evaluations, new helium production cross sections were generated, placed in the ENDF format, and new File 1 comments provided for each evaluation. The data have been forwarded to the NNDC in preparation for the forthcoming review process.

For the Al(n,p) and Al(n,α) cross sections, the Version IV cross sections are carried over to Version V unchanged.

b. n + ^{233}U Evaluation (Stewart, Madland, and Young)

New ENDF/B-V cross section files have been provided from thermal to 20 MeV. Both ν_p and ν_d were reevaluated and an energy-dependent fission spectrum was added to the data set. The resolved resonance parameters were changed to an Adler-Adler representation and unresolved parameters were added at energies up to 10 keV. This work was performed with contributions from several other laboratories.

---

[18] P. I. Johansson and B. Holmquist, "An Experimental Study of the Prompt Fission Neutron Spectrum Induced by 0.5 MeV Neutrons Incident on Uranium-235," Nucl. Sci. Eng. 62, 695 (1977).

c. n + ^{242}Pu Evaluation (Madland and Young)

An evaluation of the n + ^{242}Pu cross sections has been completed for the neutron-energy range of 10 keV to 20 MeV.[19-21] The total fission and radiative capture cross sections are based upon experimental measurements on ^{242}Pu. The remaining cross sections, together with the elastic and inelastic angular distributions to low-lying states, have been calculated using various reaction models. An expression is presented for the energy dependence of the average number of neutrons produced per fission. The results have been placed in ENDF/B-V format and combined with a recent evaluation of data below 10 keV by the Hanford Engineering Development Laboratory so that a complete data set covering the energy range of 10^{-5} eV to 20 MeV is available.

d. Fission-Product Yields for ENDF/B-V (England and Liaw (U. of Oklahoma))

The final sets of fission-product yields for ENDF/B-V (set V-E) has been sent to the National Nuclear Data Center at Brookhaven National Laboratory. Independent and cumulative yields and corresponding uncertainties are included. Twenty evaluated yield sets of each type for eleven fissionable nuclides are included, each set containing ~1100 yields (~88 000 data entries).

4. <u>Fission-Product Studies</u>

a. Evaluated Photon and Neutron Spectra from Decay of Uranium Isotopes (Foster)

An evaluation of the photon and neutron spectra emitted by isotopes of uranium and their immediate decay products has been completed. Decay chains were followed only as far as the first descendant with a half-life greater than 10^4 years.

---

[19] D. G. Madland and P. G. Young, "Evaluation of n + ^{242}Pu Reactions from 10 keV to 20 MeV," Los Alamos Scientific Laboratory report LA-7533-MS (Oct. 1978).

[20] D. G. Madland and P. G. Young, "Evaluation of n + ^{242}Pu Reactions from 10 keV to 20 MeV," presented at the Specialist Meeting on the Nuclear Data of Higher Plutonium and Americium Isotopes for Reactor Applications, Brookhaven National Laboratory, Nov. 20-22, 1978, proceedings to be published.

[21] P. G. Young and D. G. Madland, "ENDF/B-V Cross Sections for ^{242}Pu from 10 keV to 20 MeV," to be presented at the 1979 Annual Meeting of the American Nuclear Society, Atlanta, GA (June 3-9, 1979).

The evaluation makes extensive use of new compilations for all of the nuclides and attempts to trace all gamma decays through their internal conversion to the resulting x-ray spectra. The neutron spectra are generated from one-parameter evaporation theory, using nuclear systematics to derive nu-bar from the mass number and the temperature from nu-bar.

b. Decay Heat (England, Schenter (HEDL), and Schmittroth (HEDL))

The new ANS 5.1 Standard for Fission Product Decay Heat has been completed and approved by ANS 5 and the Nuclear Power Plant Standards Committee. The standard data, based on recent experiments at ORNL, LASL, IRT, UC (Berkeley), and France combined with calculations, was a cooperative effort between LASL and HEDL. The basis and methodology of the final standard and comparisons of calculations with related experiments are given in Ref. 22.

d. Fission-Product Absorption in Thermal Reactors (Wilson, England, and LaBauve)

Extensive sensitivity calculations and comparisons of calculated aggregate absorption buildup with measurements using ENDF/B-IV data were completed and reported in Ref. 23. Multigroup cross section data and a collapsing code have been supplied to RSIC and are described in Ref. 24.

---

[22] T. R. England, R. E. Schenter, and F. Schmittroth, "Integral Decay Heat Measurements and Comparisons to ENDF/B-IV and V," Los Alamos Scientific Laboratory report NUREG/CR-0305 (LA-7422-MS) (July 1978).

[23] W. B. Wilson and T. R. England, "Status of Fission-Product Data for Absorption Calculations, presented at the seminar on "Nuclear Data Problems for Thermal Reactor Applications," EPRI sponsored conference at BNL on May 22-24, 1978.

[24] W. B. Wilson, T. R. England, and R. J. LaBauve, "Multigroup and Few-Group Cross Sections for ENDF/B-IV Fission Products; the TWOAFEW Collapsing Code and Data File of 154-Group Fission Product Cross Sections," Los Alamos Scientific Laboratory report LA-7174-MS (March 1978).

e. Absorption Effects on Decay Heat and Spectral Pulse Kernels (LaBauve, England, and Wilson)

All of the extensive ENDF/B-IV aggregate fission-product decay spectra, supplemented by estimates of the missing spectra, have now been fitted to simple fission pulse kernels of the form[25,26]

$$f_g(t) = \sum_{i=1}^{N} \alpha_{ig} \, \mathrm{EXP}(-\lambda_{ig} t) \quad \mathrm{MeV/FISS\text{-}s} \quad , \qquad (1)$$

where g denotes 1 of 11 energy groups; N depends on g, accuracy of the fit, and the cooling time range, t_{max}, over which Eq. (1) is valid. Currently, for $0.1 \leq t \leq 10^9$ s, N is typically 15 for accuracies 2%. The functions $f_g(t)$ are available for $^{233,235,238}U$, ^{239}Pu, and ^{232}Th for beta and gamma spectra, their sum being the total decay heating. The expression $f_g(t)$ can be folded into any fission history, S(T'), to produce the energy release rate per group subsequent to T, the fission period.

Because pulse kernels apply in the absence of neutron absorption, high-fluence power reactors require an absorption correction. We have identified all (n,γ) reactions significantly affecting the group spectra. The time-dependent changes can be accurately represented for any contemporary reactor by a single general equation for a simple two-nuclide chain using the actual cross sections, decay parameters, and yields for approximately 10 such chains. In one case (coupling leading to ^{156}Eu) a significant effect due to multiple (n,γ) reactions has also been accurately treated.

---

[25] R. J. LaBauve and T. R. England, Trans. Am. Nucl. Soc. 28, 749 (June 1978).

[26] R. J. LaBauve et al., "The Application of a Library of Processed ENDF/B-IV Fission-Product Aggregate Decay Data in the Calculation of Decay-Energy Spectra," Los Alamos Scientific Laboratory report LA-7483-MS (Sept. 1978).

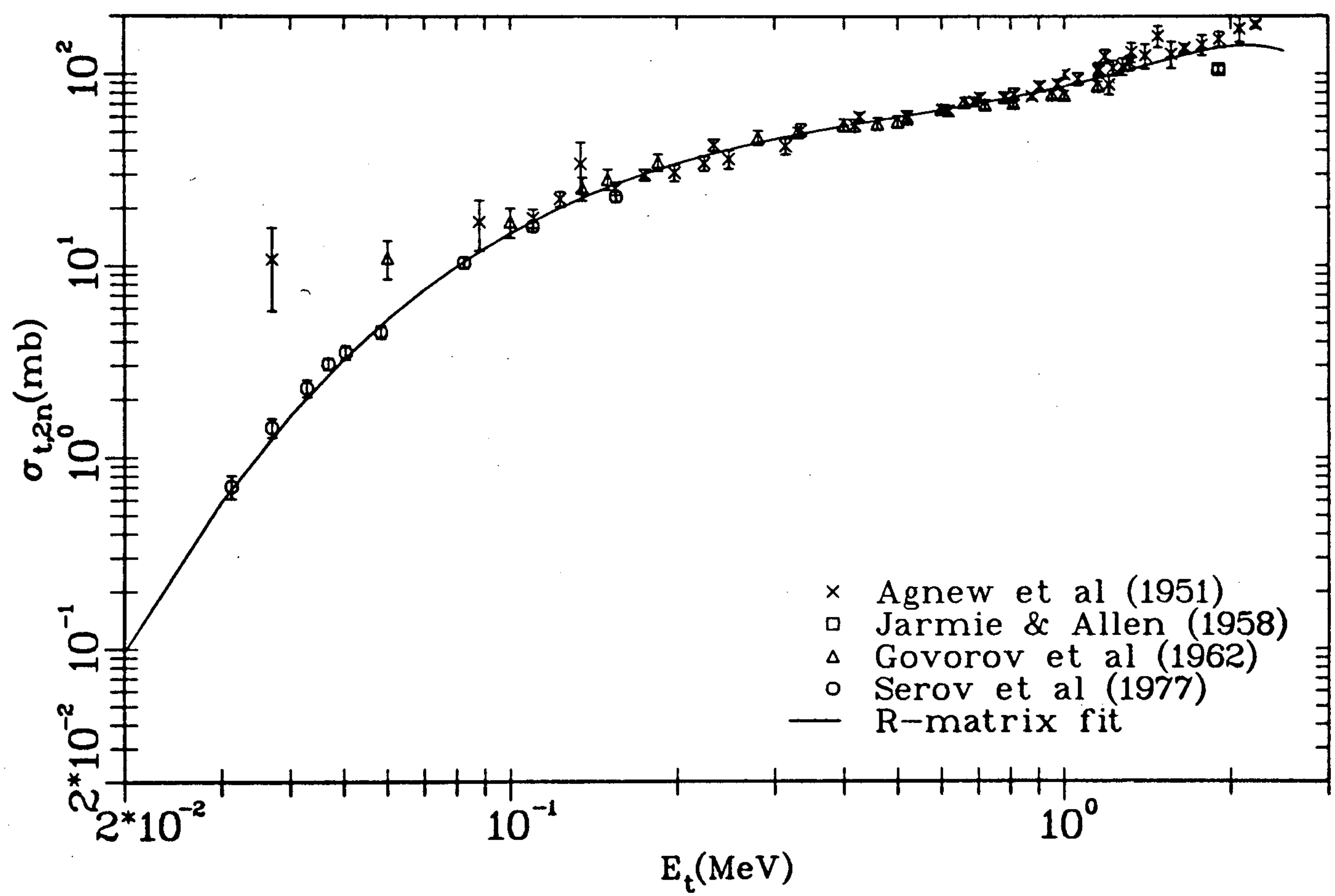

Fig. C-1. Measurements of the T(t,2n)^{4}He cross section compared with calculations from the present ^{6}He R-matrix analysis.

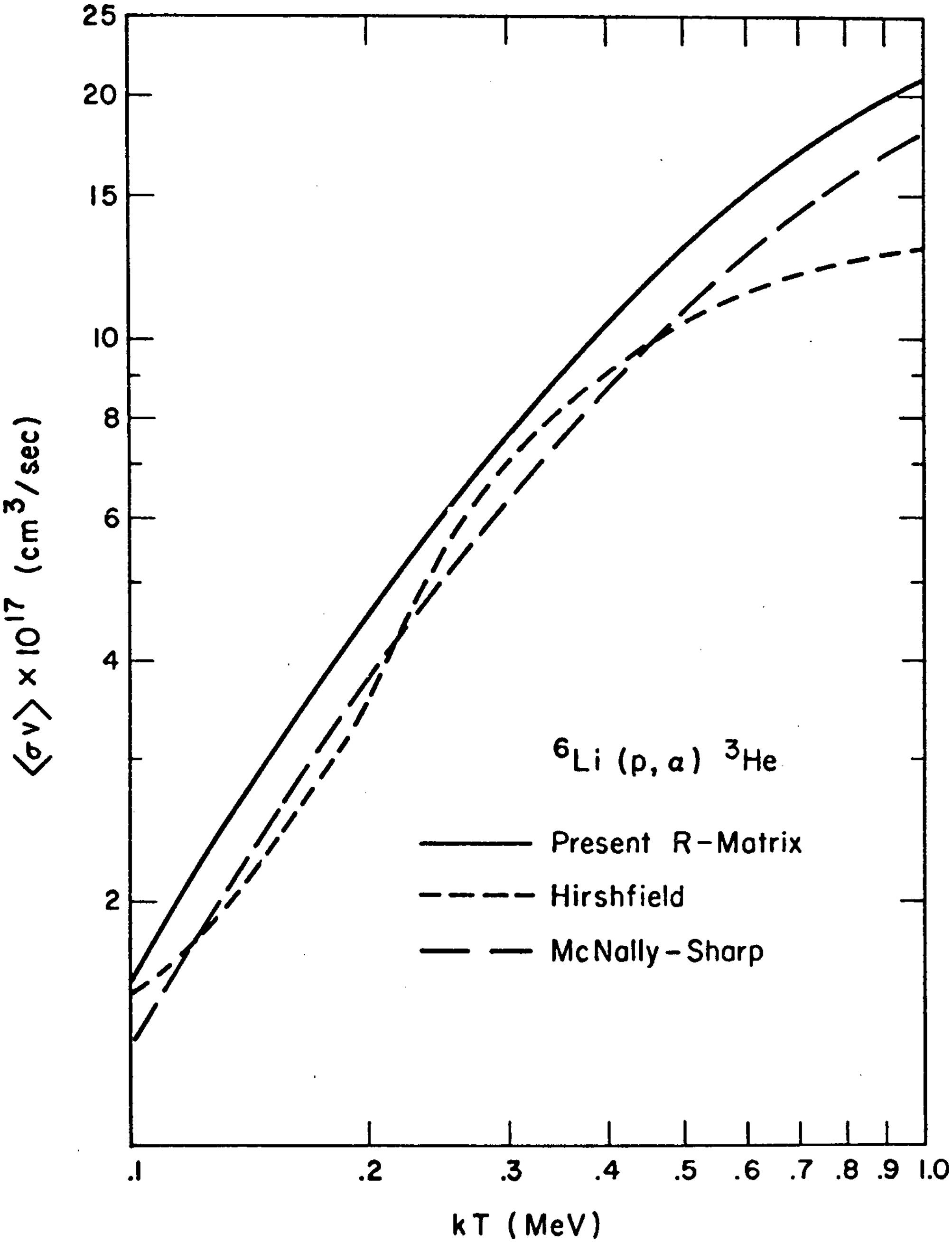

Fig. C-2. $^6Li(p,\alpha)^3He$ reaction rates. The two broken-line curves are from Refs. 7 and 8.

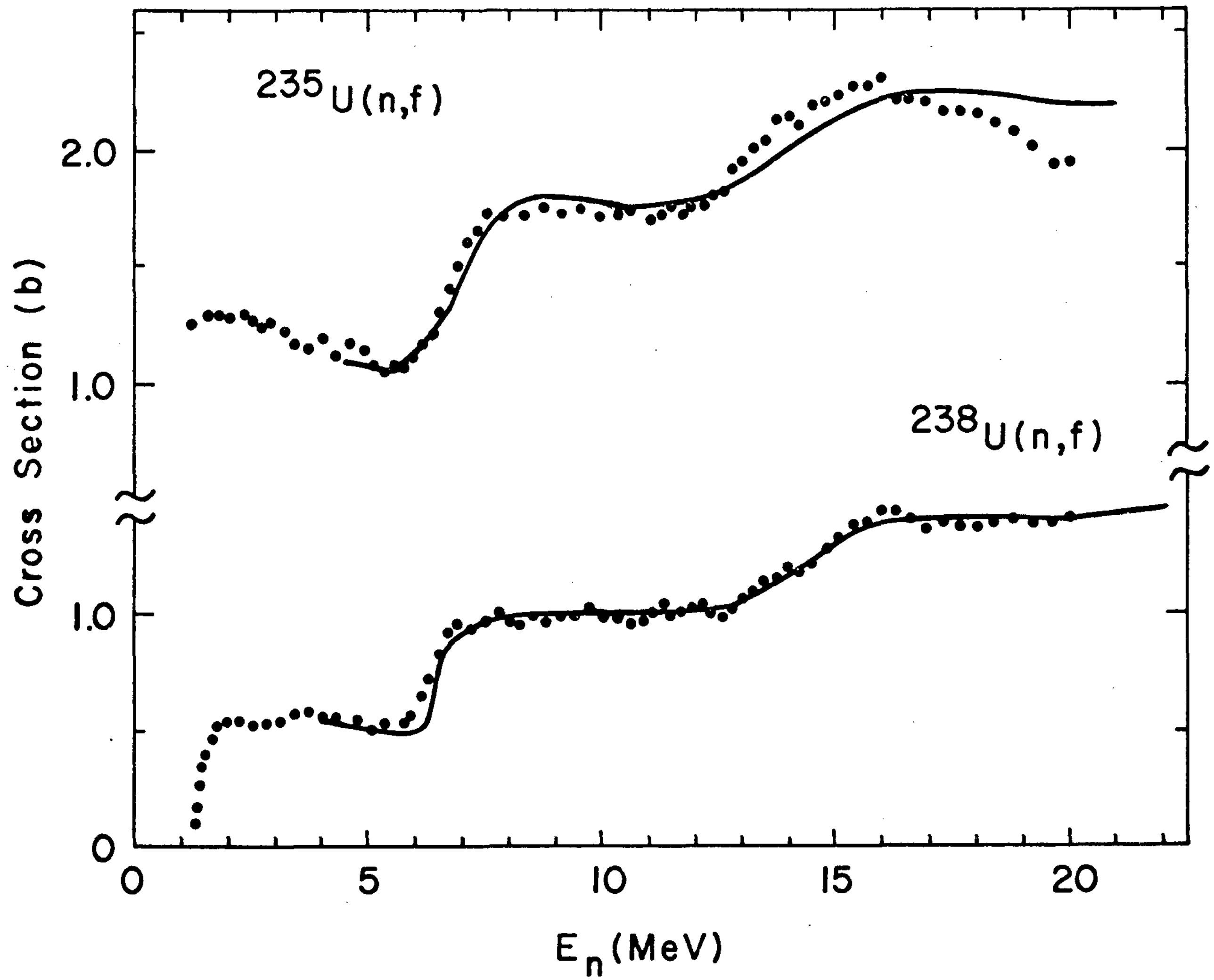

Fig. C-3. The calculated ^{235}U and $^{238}U(n,f)$ cross sections compared with the data of Leugers, et al. in the neutron energy range from 6 to 22 MeV.

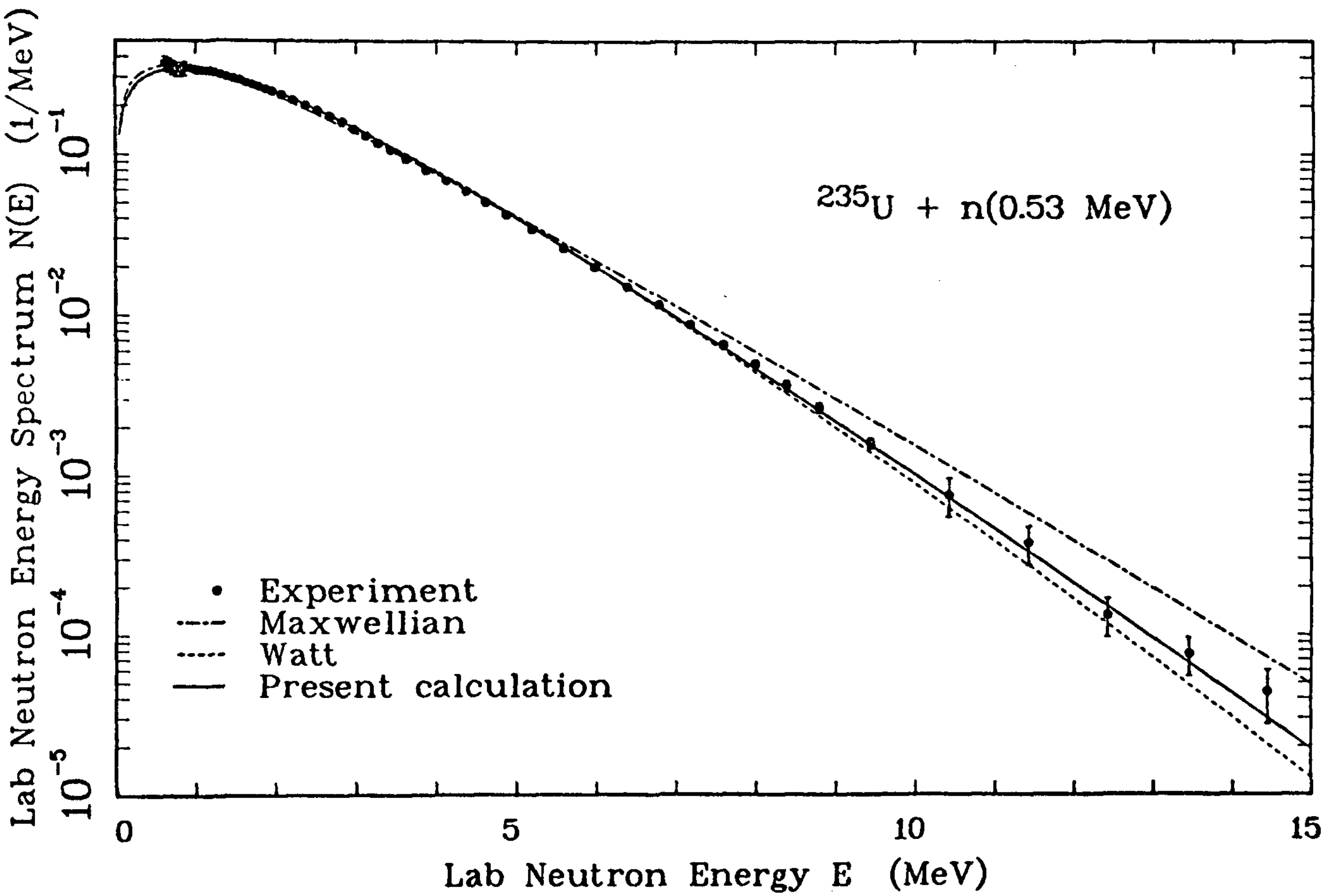

Fig. C-4. Comparison of experimental (Ref. 18) and calculated prompt fission neutron spectra. The values of the two constants in our present calculation are E_f = 0.716 MeV and T_m = 1.008 MeV, whereas those in the Watt distribution are E_f = 0.716 MeV and T_W = 0.896 MeV. The value of the single constant in the Maxwellian distribution is T_M = 1.373 MeV.

UNIVERSITY OF LOWELL

A. NEUTRON PHYSICS

1. Neutron Scattering on ^{232}Th and ^{238}U

(G.H.R. Kegel, L.E. Beghian, G.P. Couchell, J.J. Egan, A. Mittler, D.J. Pullen, W.A. Schier and E. Sheldon)

Gamma-ray production cross sections in the ^{232}Th (n,n'γ) reactions have been measured at 125° in 50 keV bombarding energy intervals over the range 0.85 MeV to 2.10 MeV. The level and decay schemes have been studied up to 2 MeV excitation with the observation of many previously unreported transitions. The final corrections for finite sample effects are being applied to the data.

A study of the same region of excitation in ^{232}Th and ^{238}U will be undertaken this year using the (n,n') technique in order to obtain directly the neutron cross sections at certain favorable energies. These cross sections can be compared with those obtained from the analysis of the gamma-ray production data in order to determine the significance of effects such as internal conversion, electric monopole transitions, weak branching and extrapolation of the 125° data to integrated angular distributions.

The two sets of data will then be used to determine nuclear level cross sections in this energy region where earlier measurements have indicated discrepancies between data obtained via the two techniques.

2. Iron (n,n'γ) (Couchell, Nardini, Barnes, Egan, Harihar, Kegel, Mittler, Pullen and Schier)

Analysis of this study has now been completed and will shortly be submitted for publication. Differential gamma-ray production cross sections were measured at 125° over the energy range E_n = 0.9 - 3.9 MeV. With the exception of the 847-keV transition in ^{56}Fe, statistical model calculations were used to predict angular distribution shapes, from which angle-integrated production cross sections were extracted. These have enabled neutron inelastic cross sections to be deduced for 12 levels in ^{56}Fe (91.7% natural abundance) and 4 in ^{54}Fe (6%).

Angle-integrated cross sections for the 847-keV gamma-ray transition were determined below E_n = 2 MeV with the aid of the ANL[1] angular dis-

[1] D.L. Smith, ANL/NDM-20 (May, 1976)

tribution measurements between threshold and 2.03 MeV. Above 2 MeV, statistical model distributions were again used. In Fig. 1(a) are shown the neutron scattering cross sections for the E_n = 847 keV level in ^{56}Fe. The solid curve represents the ENDF/B-IV data which is based primarily on the high resolution measurements of Voss et al[2] below E_n = 2.0 MeV. This curve has been energy averaged in this region to allow for the ≃100 keV beam-energy spread in our measurements. Above 2.2 MeV, ENDF cross sections for that level are listed in energy increments of several hundred keV. Our results indicate that below 2 MeV the ENDF data consistently over estimate the level cross sections, the discrepancy being particularly large near threshold.

In Figure 1(b) the total neutron inelastic cross sections for iron deduced from the present study are shown in comparison with those of ENDF-IV. The discrepancy below 2 MeV is due primarily to the 847-keV cross section, which amounts to over 90% of the total cross section in this region.

---

[2] E. Voss, S. Cierjacks and C. Kropp, Proceedings 3rd Conf. on Neutron Cross Sections and Technology. USAEC Report CONF-710301, I, 218 (1971).

(a)

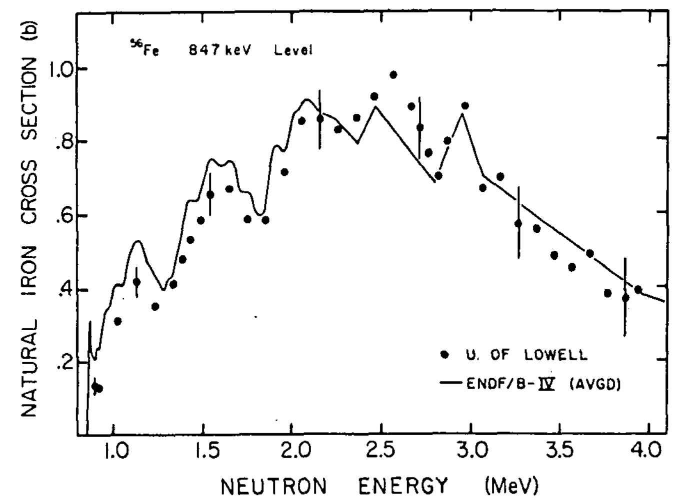

(b)

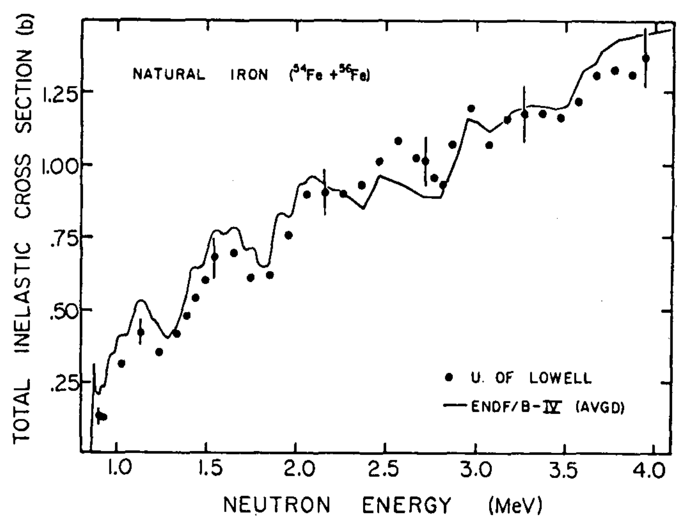

Figure 1. (a) Natural iron cross section for the 847 keV level

(b) Total inelastic cross section for natural iron.

The solid lines are averaged ENDF/B-IV

3. Silicon (n,n'γ)

The absolute 125° differential gamma-ray production cross section for the 1780-keV transition in the $^{28}Si(n,n'\gamma)^{28}Si$ reaction has been measured from 0.96 to 4.15 MeV bombarding energy.[3] This transition represents the decay of the 2^+ first excited state to the 0^+ ground state of ^{28}Si. The data were corrected for neutron multiple scattering as well as neutron and gamma-ray attenuation in the sample. The angle-integrated neutron scattering cross section was inferred from the gamma-ray production data using the shape of the gamma-ray angular distributions obtained from compound nucleus statistical model calculations. Incident neutrons were produced via the $^3H(p,n)^3He$ reaction using a target which was approximately 100-keV thick for 3.5 MeV protons and this energy spread is reflected in the structure observed in the cross section.

4. Chromium (n,n'γ)

Absolute 125-deg differential gamma-ray production cross sections have been measured for 21 gamma rays produced in natural chromium by the (n,n'γ) reaction in the incident neutron energy range from 0.84 to 3.97 MeV.[4] The pulsed beam time-of-flight technique was employed for background reduction. The data were corrected for neutron multiple scattering and neutron and gamma-ray attenuations in the scattering sample. Angle-integrated gamma-ray production cross sections were inferred from the differential measurements using gamma-ray angular distributions obtained from compound nucleus statistical model calculations. On the basis of the angle-integrated cross sections and measured branching ratios, neutron inelastic scattering cross sections were deduced for 22 energy levels in the four naturally occurring isotopes of chromium. These results were compared to previous measurements and the Evaluated Nuclear Data File (ENDF/B-IV, MAT 1191). The present measurements suggest that in the threshold energy region for inelastic neutron scattering to each of the first excited 2^+ - states in $^{50,52,54}Cr$, the cross sections are significantly overestimated in ENDF/B-IV.

---

[3] N.B. Sullivan, J.J. Egan, G.H.R. Kegel and P. Harihar, accepted for publication in Nuclear Science and Engineering.

[4] P.T. Karatzas, G.P. Couchell, B.K. Barnes, L.E. Beghian, P. Harihar, A. Mittler, D.J. Pullen, E. Sheldon and N.B. Sullivan, Nucl. Sci. & Eng. 67, 34(1978).

5. Nickel (n,n'γ)

A total of twenty-two gamma-ray transitions were measured from (n,n'γ) reactions on the four even-even nickel isotopes $^{58,60,62,64}Ni$.[5] Absolute gamma-ray production excitation functions at 125° were extracted for these transitions from their thresholds up to neutron energies of 4 MeV. Inelastic neutron scattering cross sections for nineteen levels were inferred from the gamma production data and compared to ENDF/B-IV, MAT 1190. Cross section agreement for the first excited 2^+ states in these four isotopes is generally good but excitation functions associated with many of the higher excited states in nickel are in strong disagreement with the file.

6. Cobalt (n,n'γ)

The $^{59}Co(n,n'\gamma)^{59}Co$ reaction was employed to obtain neutron inelastic scattering cross sections for nineteen levels in ^{59}Co in the incident neutron energy range 1.11 to 3.32 MeV.[6] These cross sections were deduced from measure γ-ray production cross sections for thirty-six γ rays observed in the decay of ^{59}Co using a 40 cm^3 Ge(Li) detector. Branching ratios have been determined for forty transitions from levels up to 3016 keV. The pulsed-beam time-of-flight technique was employed for background reduction. The data were corrected for neutron multiple scattering and neutron and γ-ray attentuation effects. The neutron inelastic scattering cross section data for the nineteen levels were compared to compound nucleus statistical model calculations. On the basis of these calculations and the branching ratios previously assigned spins for states up to 2062 keV have been confirmed. Spin assignments were made for 12 states.

---

[5] S. Traiforos, A. Mittler, W.A. Schier, B.K. Barnes, L.E. Beghian and P. Harihar, accepted for publication in Nucl. Sci. & Eng.

[6] R.V. LeClaire, J.J. Egan, L.E. Beghian, G.P. Couchell, G.H.R. Kegel, S.C. Mathur, A. Mittler and W.A. Schier, Phys. Rev. C, 18, No. 3, 1185, (1978).

7. Uranium (n,n')

The University of Lowell high-resolution time-of-flight spectrometer has been used to measure angular distributions and 90-deg excitation functions for neutrons scattered from ^{238}U in the energy range from 0.9 to 3.1 MeV.[7] This study was limited to the elastic and the first two inelastic groups, corresponding to states of ^{238}U at 45 keV (2^+) and 148 keV (4^+). Angular distributions were measured at primary neutron energies of 1.1, 1.9, 2.5 and 3.1 MeV for the same three neutron groups. Whereas, our elastic data are in fair agreement with the evaluation in the ENDF/B-IV file, there is substantial disagreement between our inelastic measurements and the evaluated cross sections.

---

[7] L.E. Beghian, G.H.R. Kegel, B.K. Barnes, G.P. Couchell J.J. Egan, T.V. Marcella, A. Mittler, D.J. Pullen and W.A. Schier, Nucl. Sci. & Eng. 69, 191 (1979).

The University of Michigan

A. INTRODUCTION

As in the past years, our efforts have continued to stress the application of photoneutron sources to the measurement of absolute neutron cross sections. These small spherical sources are activated prior to each experimental measurement, and are calibrated against the National Neutron Standard NBS-2 using the University of Michigan maganese bath facility. When used in our low-albedo irradiation laboratory, they provide absolutely calibrated and nearly monoenergetic neutron fluxes ranging from 23 to 964 keV. The experimental details have been outlined in past progress reports and will not be repeated here. As a significant extension of our past efforts, we are beginning a major effort to extend our measurements to the 14 MeV energy region.

The work reported below has involved the joint efforts of J. C. Engdahl, D. J. Grady, G. T. Baldwin, and G. F. Knoll.

B. ABSOLUTE FISSION CROSS SECTIONS

Having completed our work on ^{235}U and ^{239}Pu, we are currently carrying out similar measurements using targets of ^{233}U and ^{237}Np. These are similar to the uranium and plutonium foils used in our past measurements, and consist of vapor deposited samples of the oxide on platinum backings, with the deposit being approximately 1 milligram per square centimeter in thickness. In both cases, dual foils were obtained with nearly identical masses to enable us to continue use of the dual geometry for irradiation.

Mass data has been supplied by the fabricator of the foils, Oak Ridge National Laboratory, based on weighings before and after the evaporations. In all cases, the foils were fired at 800° C for several hours to ensure complete conversion of all the deposited material to the most highly oxidized form. Our intent is to check these mass determinations by comparative alpha counting of our foils against standard foils maintained at the National Bureau of Standards at a later time.

Because of the threshold nature of the ^{237}Np cross section, it is possible for us to use only the two highest energy sources available, at 770 and 964 keV. We have now completed all fission rate measurements on this nuclide, including measurements at variable source-target spacing in order to independently determine the contribution of room-return neutrons. These data are now undergoing analysis.

Experimental work is just beginning on the ^{233}U series of measurements. Here we expect to be able to carry out determinations at five energies: 23, 140, 265, 770, and 964 keV.

C. THE ANGULAR DISTRIBUTION OF ^{239}Pu FISSION FRAGMENTS

Because our fission measurements involve limited solid angle detection, we need to use angular distribution data in deriving a cross section value. We have in the past reported on measurements made at the Argonne National Laboratory Tandem Dynamitron in which we determined the ^{235}U fission fragment anisotropy by direct measurement using track-etch films. We have carried out similar measurements for ^{239}Pu at neutron energies of 265, 770, and 964 keV.

The data from this experiment is being processed in two stages. An initial count has been completed in which the the tracks within a $\pm$ 3° spread about each of the angles 0°, 30°, 60°, and 90° were recorded. These data have been analyzed using the same methods described previously with the following results:

ENERGY	ANISOTROPY
265 keV	.037 $\pm$ .018
770	.072 $\pm$ .040
964	.161 $\pm$ .029

The anistropy value shown are the value of A in the expression

$$W(\theta) = 1 + A\cos^2\theta$$

where W (θ) is the fragment yield corrected for various experimental factors.

The same track-etch films are now being recounted at a greater variety of angles to provide a more complete set of data for analysis.

D. ABSOLUTE MEASUREMENT OF $^{6}Li(n,alpha)^{3}H$ CROSS SECTION AT 23 keV

An absolute determination of the $^{6}Li(n,alpha)^{3}H$ cross section was performed utilizing our newly-constructed Sb-Be photoneutron source. Independent measurements of the reaction rate, neutron source strength, and the number of target nuclei were performed. A unique rotation scheme was developed for the detection geometry to minimize dependence on the knowledge of the angular distribution. The shape of the angular distribution was roughly determined from the measurement and compared to a relative angular distribution measurement at 25 keV using the iron filtered beam at the National Bureau of Standards. As an absolute measurement, the value reported does not depend on any other cross section data except for correction factors totalling about 8 percent.

The reaction rate was determined by counting alpha particles in limited sold angle geometry using five independent source-target orientations. The cellulose nitrate track recording detector, Kodak LR115, was employed to register the alpha particles while remaining insensitive to the tritons. The alpha particle registration efficiency was measured and determined to be 100 percent to within 1 percent.

A weighting scheme was developed to combine the results of five detector orientations into an approximation of a 4π detector. The weighting coefficients were derived by computing the fractions of polar angles subtended by each of the rotated geometries and summing these results for the five cases. Use of this weighting scheme made the result nearly independent of the assumed anisotropy from the reaction.

Targets of ^{6}LiF were fabricated by vapor deposition onto thin aluminum backings. The number of target nuclei for a thick (3 mg/cm^2) reference target was calibrated by a series of microbalance weighings before and after target deposition.[1] The targets used in the reaction rate determination were comparatively thin (0.1 mg/cm^2) and direct weighing techniques yielded insufficient accuracy. The number of target nuclei in the thin targets was therefore determined

[1] Y. leGuigou and K. F. Lauer, Nucl. Instr. and Met., 97 (1971) 199-200).

from a ratio of the reaction rates of the thick-to-thin targets performed in thermal neutron beam. Flux normalization was accomplished by measuring the reaction rates relative to a ^{235}U traget in a fixed geometry.

The Sb-Be source is comprised of a solid antimony sphere surrounded by a beryllium shell. The neutron source strength was determined by comparison to NBS-2 in our manganese bath. The source spectrum was calculated using a Monte Carlo computer program. The spectrum was calculated to be a primary energy peak of about 3 keV FWHM containing 67 percent of the neutrons.[2] A correction factor was applied for the source spectrum to normalize to 23 keV.

A measurement to determine the relative angular distribution of emitted alpha particles was performed at 25 keV using the iron filtered beam at the National Bureau of Standards. Cellulose nitrate track recording film recorded alpha particles emitted into a 110° arc from a ^{6}LiF target in the neutron beam. Two runs were required to include all polar angles and were normalized at 90°.

The absolute $^{6}Li(n,alpha)^{3}H$ cross section at 22.8 keV was measured to be 0.945 ± 0.023 barns (one standard deviation). The angular distribution of the emitted alpha particles in the laboratory frame was found to be well represented by the expression,

$$\frac{d\sigma(\theta)}{d\Omega} = 0.075 - 0.019\cos\theta \text{ (mb/st)},$$

where θ is the polar angle of the alpha particle with respect to the incident neutron direction.

E. RECALIBRATION OF NBS-2

Most of the results reported in the past by our project are dependent on the assumed emission rate of the NBS-2 source standard. These include all the absolute cross section measurements and the determination of nu-bar for ^{252}Cf.

Within the past year, NBS-2 has been returned to the National Bureau of Standards for recalibration. It is our

[2] J. S. Robertson, M. C. Davis and J. C. Engdahl, NBS 425 (1975).

understanding that the NBS-2/NBS-1 ratio has been reconfirmed to high precision, thereby reinforcing the accuracy of the emission rate assumed for NBS-2 based on older calibrations. Results will be reported by V. Spiegel of NBS.

F. NEUTRON CAPTURE CROSS SECTIONS

Preliminary measurements have been completed which demonstrate the feasibility of measuring the ^{115}In capture cross section at each of our photoneutron source energies. These measurements have included a close determination of the contribution of room-return neutrons for a source-foil spacing of 5 centimeters. Results range from 16.5% at the lowest energy of 23 keV to 5.2% at 964 keV. The induced activity in the indium foils is determined using 4π β-γ absolute counting techniques. The beta detection channel of this system is composed of a dual chamber flow gas proportional counter, tailored after a design by Campion.[3]

Feasibility studies are currently underway regarding a possible measurement of the capture cross section in ^{232}Th. We are interested in using the activation technique recently reported for a filtered neutron beam by Chrien, et. al.[4] Factors being weighed are required counting efficiencies, source strengths, potential counting interferences, and the advisability of radiochemical separation processes to enhance signal -to-background ratios.

G. MEASUREMENTS AT 14 MeV NEUTRON ENERGY

In a cooperative program with Professor Craig Robertson at the University of New Mexico, we are beginning to develop facilities necessary to extend many of our cross section measurements to the 14 MeV neutron energy range. Neutrons will be provided from a tritiated target using a small 150 keV deuteron accelerator. The measurements will be carried out under extremely low scattering conditions using a large-

---

[3] P. J. Campion, The Standardization of Radioisotopes by the Beta-Gamma Coincidence Method Using High Efficiency Detectors", Internat'l. J. of Appl. Rad. & Isotopes, Vol. 4, 1959, pp. 232-248.

[4] Chrien, Liou, Kenney, and Stelts, BNL-25407 (1978).

volume open experimental bay. Neutron fluxes will be determined both by the associated particle method and through the use of a proton recoil flux monitor.

The first measurement to be carried out will be fission cross section measurements of ^{235}U, ^{233}U, ^{239}Pu, and ^{237}Np. The same target foils will be used as in our low energy fission measurements to take advantage of their excellent mass documentation. We will continue to use our method of track etch fission fragment counting because of the excellent precision attainable. This detection method also allows minimum mass in the vicinity of the target to reduce inscatter corrections.

In order to avoid uncertainties connected with past measurements, special attention will be given to a number of experimental factors. These include the effects of deuteron energy loss on the exact neutron energy, effects of neutron scattering in the target backing, and possible contamination of the associated alpha particles by competing reactions.

NATIONAL BUREAU OF STANDARDS

A. NEUTRONS

1. Measurement of the ^{6}Li, ^{7}Li, and C Total Cross Sections From 3 to 45 MeV (J. D. Kellie,[1] G. P. Lamaze, R. B. Schwartz)

In order to provide data in the energy range appropriate for the neutrons generated by the FMIT Facility, a total cross section program covering the energy range up to 45 MeV was started using the 200 m flight path on the NBS Linac Neutron Time-of-Flight Facility. Measurements were made on ^{6}Li, ^{7}Li, and C, with hydrogen also being measured as a check. Comparison of our hydrogen data with the accepted values (Breit-Hopkins for $E \lesssim 30$ MeV; the Binstock parametrization for $E \gtrsim 20$ MeV) shows agreement within $\lesssim 1\frac{1}{2}\%$ for energies between 3 and 35 MeV, and agreement within $\sim 3\%$ at 45 MeV. Comparison of our carbon data with ENDF/B-V shows agreement at the 2%-3% level over the range 2.5-20 MeV. Our lithium data are not yet completely analyzed, but show generally good agreement with the existing data, which go up to ~ 30 MeV. These data are now being analyzed and prepared for publication.

2. Measurement of the Absolute $^{235}U(n,f)$ Cross Section (O. A. Wasson, M. M. Meier, K. C. Duvall)

The Standard Neutron Beam facility at the 3 MV Van de Graaff was used to measure the absolute ^{235}U fission cross section from 200 to 1200 keV. This measurement used the spatially uniform neutron fluence incident on a large volume fission chamber of known ^{235}U mass. This fission chamber was located approximately 1.2 m from the neutron source while the incident flux was determined by means of a large plastic scintillator of known absolute efficiency which was placed approximately 6 m from the neutron source. The cross section results submitted to the Nuclear Data Center in Sept. 1978 along with more recent measurements are shown in figure A-1. These results, which are approximately 3% lower than the ENDF/B-V evaluation, are in agreement with the relative measurements performed on the NBS linac which used the same fission chamber but different flux monitors.

---

[1] Kelvin Laboratory, Glasgow, Scotland

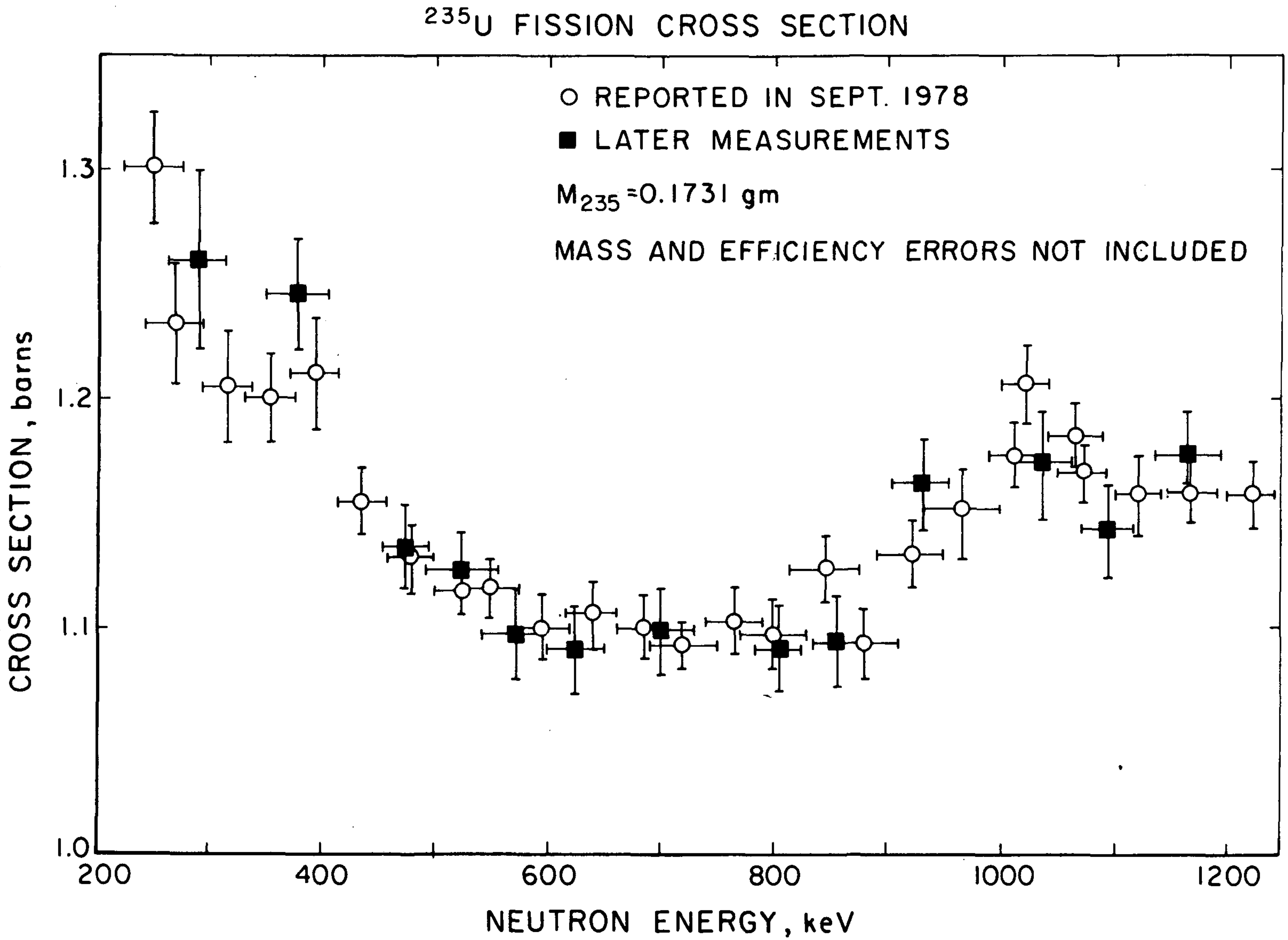

Figure A-1. Present measurements of the ^{235}U fission cross section.

3 . ^{235}U(n,f) and ^{237}Np(n,f) Cross Section Measurements in the MeV Energy Region (A. D. Carlson, B. H. Patrick[1])

Measurements of the energy dependence of the ^{235}U and ^{237}Np neutron fission cross sections have been made from 1 to 20 MeV at the 60 m flight path of the NBS neutron time-of-flight facility. Separate thin film uranium and neptunium fission chambers were used to detect the fission events. The neutron flux was determined with a special annular proton telescope. Data from the fission chambers and the proton telescope were obtained simultaneously with a multiexperiment 2-parameter data acquisition system.

The ^{235}U measurements were reported on at the International Conference on Neutron Physics and Nuclear Data for Reactors and Other Applied Purposes at Harwell. This work is now essentially complete and is being prepared for journal publication.

The ^{237}Np data have been analyzed from 3 - 20 MeV. Further analysis in the region from 1 - 3 MeV is now in progress.

The preliminary results of the measurements on ^{235}U and ^{237}Np are shown in Fig. A-2 and Fig. A-3 respectively. The error for these data is 2-3% throughout the entire energy region.

---

[1] A.E.R.E., Harwell, England

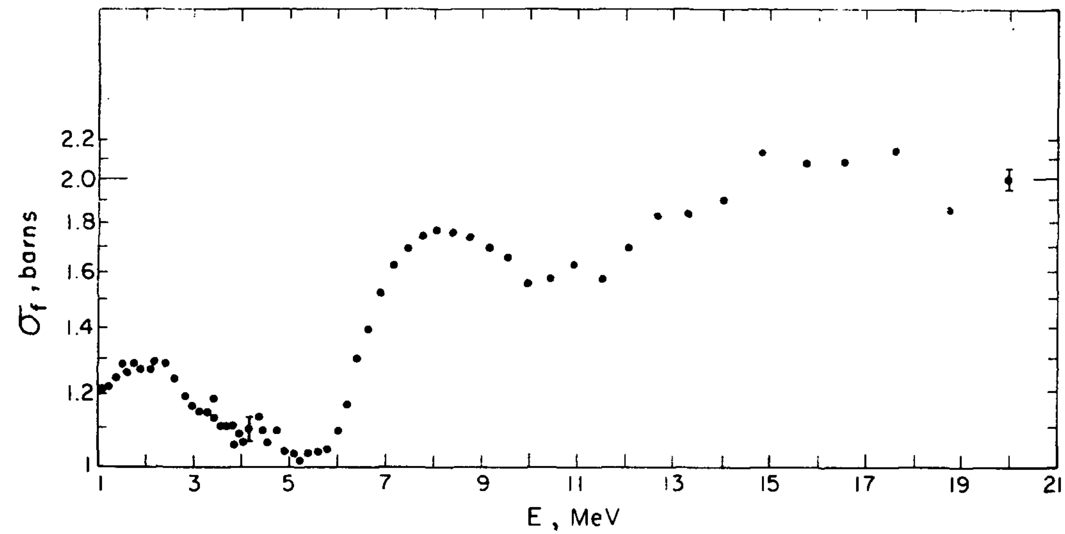

Figure A-2. Present measurements of the ^{235}U fission cross section.

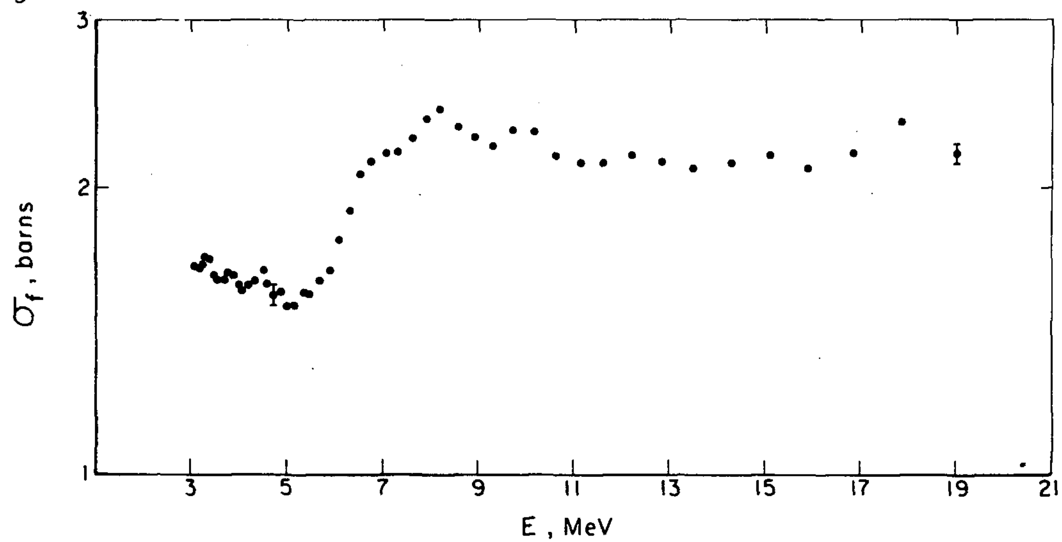

Figure A-3. Present measurements of the ^{237}Np fission cross section.

4. Molecular Effects on $^{10}BF_3(n,\alpha)$ Cross Section (C. D. Bowman, J. W. Behrens, A. D. Carlson (NBS), J. Todd, R. Gwin (ORNL))

The NBS is conducting a general study of the effects of atomic and molecular properties on neutron- and γ-ray-induced reaction cross sections.[1-3] These studies have led us to expect a difference between the (n,α) cross section for solid boron compared with a free molecule of $^{10}BF_3$. The effect should arise from the momentum transfer of the neutron which can induce molecular dissociation or transitions of the molecule to high vibrational states.

Experiments conducted at ORNL and at NBS indicated that the onset of these effects would lie above 1 eV. For the higher energy region two detectors of essentially identical design were compared at NBS. One detector was a parallel plate ionization chamber containing two foils with evaporated boron at a total thickness of 57.9 $\mu g/cm^2$ with the deposits facing a center collecting plate. The other was a counter of the same geometry filled with one atmosphere of $^{10}BF_3$ gas. Counting rates were measured using a flight path of 20 meters with a Cd filter. The two detectors were placed against each other and the ratio measured. The ratio was remeasured with the detector package reversed. The geometric mean of these results cancels any effects of background, flight path differences, etc. The results are given in Fig. A-4, which shows the ratio of BF_3 to solid boron normalized to 1.0 in the energy region above 100 eV. We assume that above 100 eV the boron is driven out of the BF_3 molecule whereas in the region below, the molecule in the initial absorption process is excited to high lying but bound vibrational states. The effect of 2% is less than predicted from a simple model but is in the expected direction.

---

1 C. D. Bowman and R. A. Schrack, Phys. Rev. C17, 654 (1978).

2 R. A. Schrack and C. D. Bowman "The Influence of Vibrations of Gas Molecules on Neutron Reaction Cross Sections," International Conf. on Physics and Nuclear Data for Reactors and Other Applied Purposes, Harwell, October 1978.

3 R. A. Schrack and C. D. Bowman "Chemical and Temperature Effects on Thermal ^{235}U Fission" Ibid.

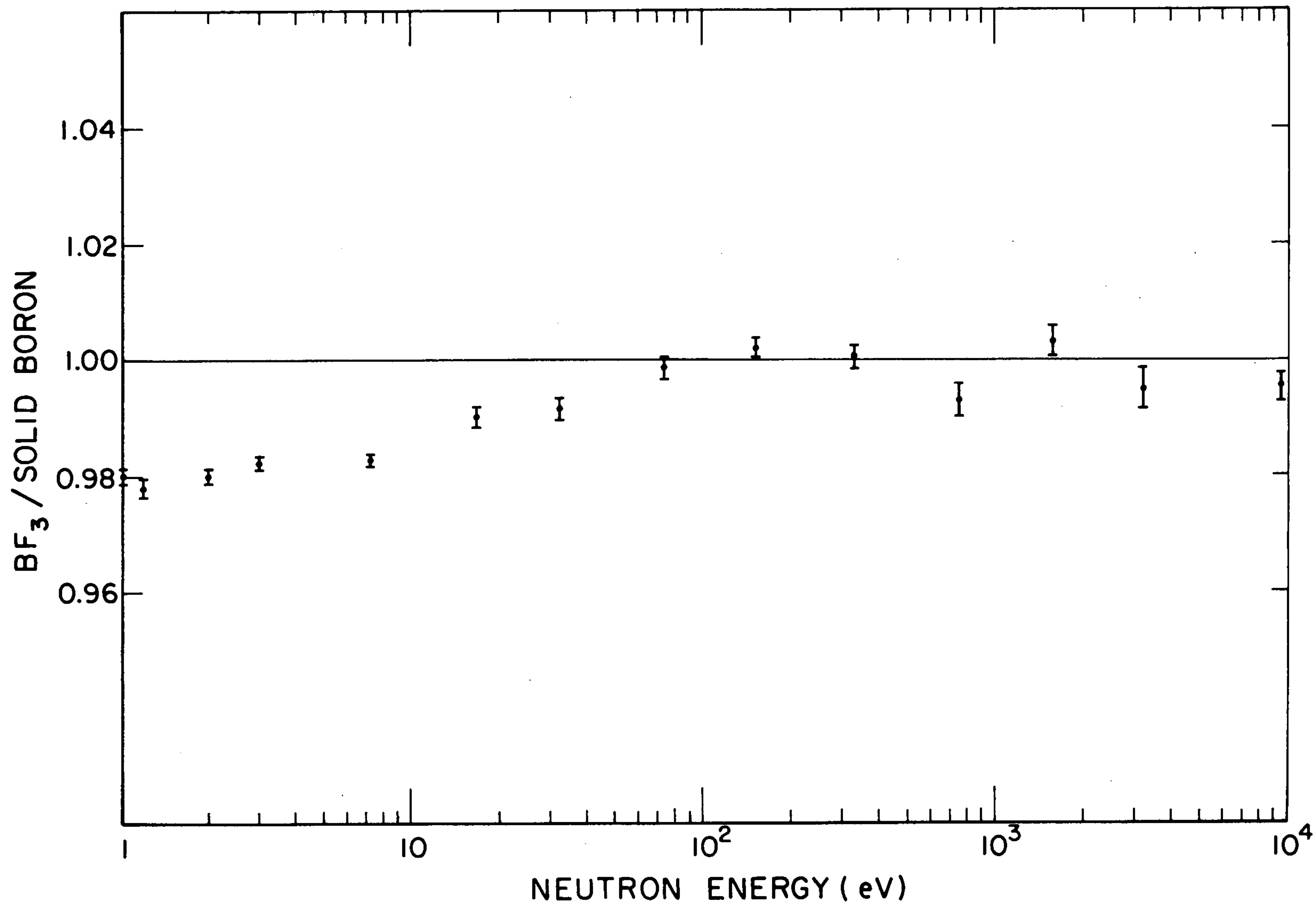

Figure A-4. Measurements of the (n,α) cross section for $^{10}BF_3$ compared with solid boron as a function of neutron energy.

5. Comparison of ^3He and $^{10}BF_3$ Cross Section Energy Dependence (C. D. Bowman, J. W. Behrens, R. B. Schwartz)

The ratio of cross sections for the $^3He(n,p)$ and $^{10}BF_3(n,\alpha)$ reactions has been measured using the thermal and 2 keV neutron beams at the NBS reactor. Two identical proportional counters were filled with these gases and the ratio of the cross sections compared for the two neutron energies. The detectors were placed together in the beam so that the beam could irradiate both simultaneously. Their positions were then reversed and the geometric mean taken of the ratio of the counting rates. The same process was repeated for the 2 keV beam. The ratio BF_3/He was found to be $4 \pm \frac{1}{2}$% higher at 2 keV than at thermal. Two percent of this effect apparently is the molecular effect mentioned above. The remaining 2% is due to non 1/v nuclear effects in either $^{10}BF_3$, ^3He or both.

6. NBS Intermediate-Energy Standard Neutron Field (ISNF) (C. M. Eisenhauer)

The last report gave a comparison of integral responses calculated by the discrete ordinates method using 240 energy groups and ENDF/B4 cross sections (LASL) and 40 groups and ENDF/B3 cross sections (NBS). A further test of the sensitivity of calculated spectra and integral responses to calculational techniques can be made by including 171-group discrete ordinates calculations by ORNL and Monte Carlo calculations by LASL.

Calculations of the spectra have been collapsed to a 22-group structure which combines the 15-group structure currently used in the ENDF error file and the 7-group structure used by NBS to study error propagation of evaluated fission spectra. When the LASL 240-group calculation is used as a reference, the average departure of the three other calculations does not exceed 2% in any of the 15 energy groups between 1 keV and 3 MeV. Departures of individual calculations in this energy range does not exceed 4%. Thus, for the same input data, various calculations produce consistent estimates of the ISNF spectrum.

A comparison of integral detector responses for the four calculations is shown in Table A-1. It can be seen that the calculations are generally consistent to within about 1% except for the NBS calculations of the $^{58}Ni(n,p)$ reaction, where only four energy groups contribute to the response.

Table A-1

Comparison of Calculated Spectrum-Averaged Cross Sections in ISNF

Reaction	Cross Section LASL 240-group ENDF/B4	Ratio to LASL 240-group NBS 40-group ENDF/B3	ORNL 171-group ENDF/B4	LASL Monte Carlo ENDF/B4
Pu-239(n,f)	1.818	1.002	0.999	1.004
U-235(n,f)	1.631	1.003	0.998	1.011
Np-237(n,f)	0.783	1.003	1.005	0.988
U-238(n,f)	0.1363	1.012	1.007	0.993
Ni-58(n,p)	0.0368	1.024	1.005	0.992

7. Intermediate Energy Standard Neutron Field Measurements (D. M. Gilliam, J. A. Grundl, V. Spiegel)

A preliminary measurement of the Np-237 fission cross section (relative to the U-235 fission cross section) has been carried out in the Intermediate Energy Standard Neutron Field (ISNF). After correction for slight changes in the neutron energy spectrum due to scattering in the fission chamber and fissionable deposit backings, the observed fission cross section ratio was

$$\sigma_f(\text{Np-237})/\sigma_f(\text{U-235}) = 0.510$$

No correction has been made for epithermal neutron streaming through the fission chamber penetration in the boron shell. Activation foil measurements have been made with and without the penetration present to assess the magnitude of this effect. This correction could be as much as 3%, but further work is still required before a final value can be given. All other uncertainties combined in the cross section ratio quoted above amount to less than 2.5% (1σ).

8. A Remeasurement of the ^{235}U Mass Contained in the Large Volume Multiplated Fission Chamber (O. A. Wasson, M. M. Meier, D. M. Gilliam)

In order to verify that the ^{235}U content of the large fission chamber was constant during the two-year period of cross section measurements, the ^{235}U mass was remeasured in October 1978 and found to agree within 1% with the value obtained in the original measurement of October 1976. We thus conclude that the ^{235}U content of the fission chamber was constant during this time interval. The mass of the large chamber ($\sim$ 0.173 g) was measured relative to smaller ($\sim$ 200 μg) reference deposits by means of fission fragment counting of the fission events produced by a large area spatially uniform thermal neutron beam at the NBS reactor. One of the larger errors in the measurement is the uncertainty in the scattering of the reference deposits. New measurements of the neutron scattering from platinum foils in the thermal energy region would be of value for the standards program since most standard reference deposits utilize platinum backings.

9. Neutron Radiography (J. Behrens, A. Carlson, R. Schrack, C. Bowman)

A program to develop a resonance neutron radiography system has been initiated at NBS with the support of the Nuclear Regulatory Commission. Utilizing resonances in the neutron total cross section at neutron energies below 1000 eV, the technique offers the possibility of a technique that will provide both an image of the distribution of an isotope in a complex matrix as well as an assay of the isotope. The NBS Linac is used to provide a pulsed neutron source which is then collimated into a vertical beam. The sample to be examined is then stepped by the beam so that a succession of slit images formed by the position sensitive detector can be processed to form an image. Fig. A-5 shows the experimental arrangement and the results of a measurement made to determine the distribution of silver solder in a brazed part. A defect was deliberately introduced and is clearly evident in the reconstructed image. The resolution of the image shown is about 4 mm using a commercially available position sensitive neutron detector.

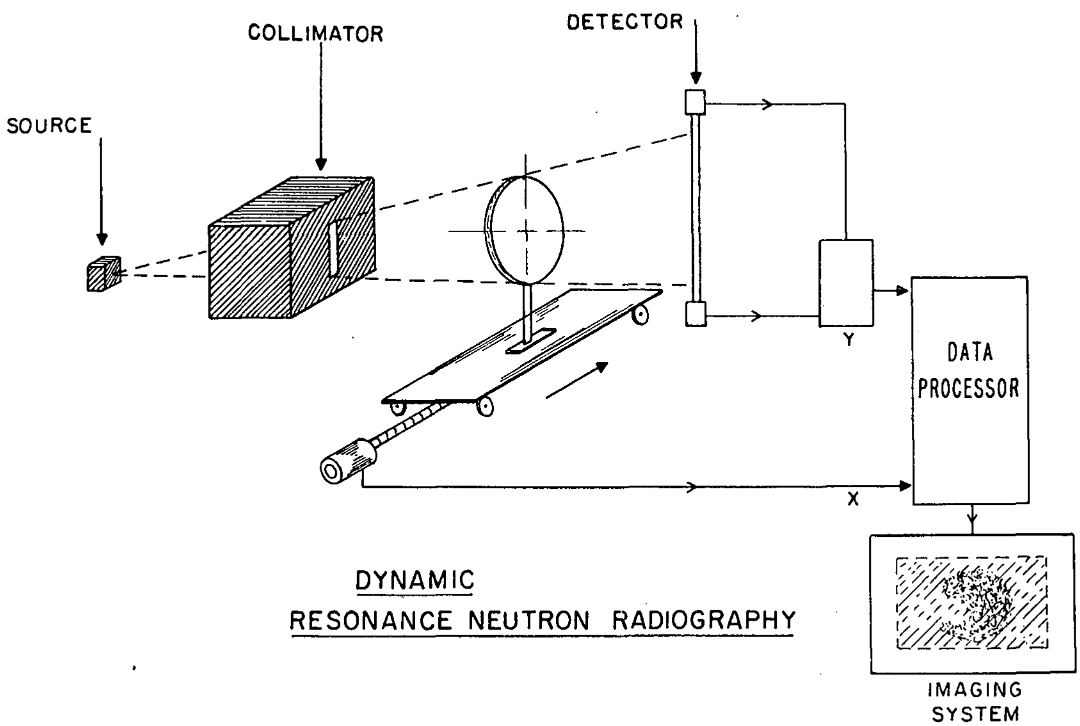

DYNAMIC
RESONANCE NEUTRON RADIOGRAPHY

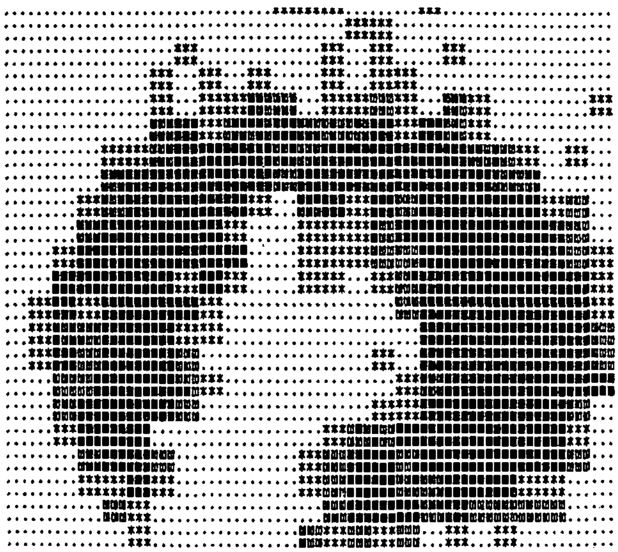

NEUTRON RADIOGRAPH
IMAGE OF SILVER DISTRIBUTION

Figure A-5. Schematic diagram of resonance neutron radiography system and sample radiograph.

10. Development of High Spatial Resolution Position-Sensitive Proportional Counters (J. W. Behrens, M. K. Kopp,* J. A. Williams*)

Experimental gas-filled position-sensitive proportional counters (PSPC) are being built for use in development of resonance neutron radiography as a laboratory reference method for measurements for safeguarding nuclear fuel. For this application linear PSPCs having sub-millimeter spatial resolution are needed; however, commercially available PSPCs have spatial resolutions of 4 to 5 mm. For this reason the NBS together with Oak Ridge National Laboratory are presently developing suitable high spatial resolution PSPCs. Fig. A-6 shows our first PSPC. It contains 3 atm ^3He, 7.5 atm Xe, and 0.5 atm CO_2. The sensitive length is 50 mm and the spatial resolution is 1.2 mm. Position sensing is determined using resistance-capacitance position encoding as described in Ref. 1.

11. Neutron Dosimetry and Instrument Calibrations (R. B. Schwartz, O. A. Wasson, K. C. Duvall)

We are continuing our calibration program, using the thermal, 2 keV, 24 keV, and 144 keV reactor neutron beams, and using the standard neutron beam facility at the 3 MV Van de Graaff for higher energy neutrons up to 1.2 MeV. We have, by now, provided calibration services to the scientific and industrial community of conventional remmeters as well as thermoluminescent personnel dosimeters. The variable characteristics of these instruments are starting to become well-understood.

---

*Oak Ridge National Laboratory, Oak Ridge, Tennessee.

1 C. J. Borkowski and M. K. Kopp, Rev. Sci. Instrum. 46, 951 (1975).

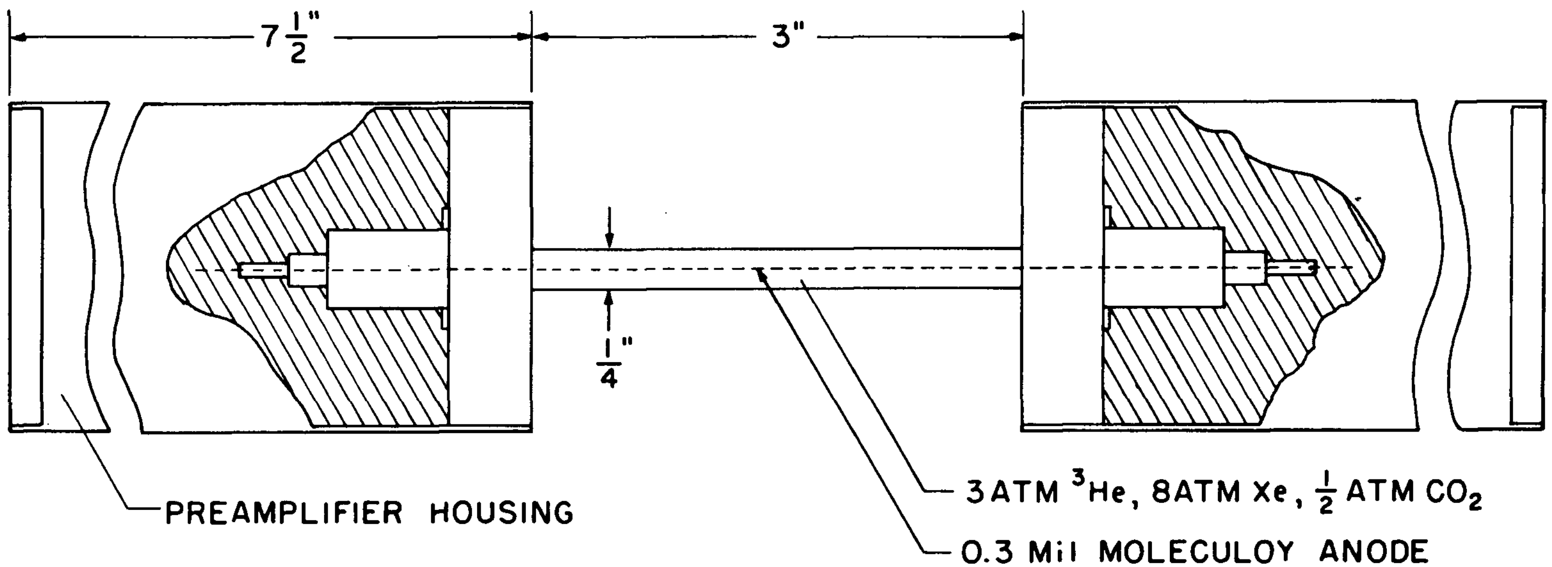

Figure A-6. High spatial resolution position sensitive proportional counter assembly.

B. FACILITIES

1. 3 MV Positive Ion Van de Graaff (M. M. Meier, K. C. Duvall, O. A. Wasson)

The machine has continued to be heavily utilized for standard neutron cross section measurements, detector calibration services, and nuclear physics studies. The vacuum system is in the process of upgrading. The main system oil diffusion pump was replaced with a 1000 ℓ/s (for hydrogen) turbomolecular pump in April 1978 which has maintained reliable operation. The remaining oil diffusion pumps on the beam lines are in the process of being replaced with turbomolecular pumps in order to reduce target contamination.

A new scattering chamber was constructed to utilize the $^{3}H(d,n)^{4}He$ reaction for 14 MeV neutron studies. Beam line modification for this facility is in progress.

The data acquisition hardware was improved by the construction of a second two-parameter multiplexor, tagging unit, and interrupt interface. The system, which now includes two multiplexors, five ADC's, and CAMAC MCA, provides the experimenter with increased flexibility in acquiring data at selectable levels of priority.

C. DATA COMPILATION

1. X-Ray and Ionizing Radiation Data Center (J. H. Hubbell)

In addition to publication of a new pair and triplet production cross section analysis with H. Gimm (MPI, Mainz, Germany)[1] and completion of a relativistic atomic form factor and coherent photon scattering data compilation with I. Øverbø (TH Trondheim, Norway),[2] both described in the previous report, this Data Center responded to a total of 206 requests for data or information in 1978.

---

[1] H. A. Gimm and J. H. Hubbell, "Total Photon Absorption Cross Section Measurements, Theoretical Analysis and Evaluations for Energies above 10 MeV," NBS Tech. Note 968 (1978).

[2] J. H. Hubbell and I. Øverbø, J. Phys. Chem. Ref. Data 8, 69-105 (1979).

OAK RIDGE NATIONAL LABORATORY

A. CROSS SECTION MEASUREMENTS

1. Gamma-Ray Production Data

a. The $O(n,x\gamma)$ Reaction Cross Section for Incident Neutron Energies Between 6.5 and 20.0 MeV* (G. L. Morgan and G. T. Chapman)

Differential cross sections for the neutron-induced gamma-ray production from oxygen have been measured for incident neutron energies between 6.5 and 20.0 MeV. The Oak Ridge Electron Linear Accelerator (ORELA) was used to provide the neutrons and a NaI spectrometer to detect the gamma rays at 125°. The data presented are the double differential cross section, $d^2\sigma/d\Omega dE$, for gamma-ray energies between 1.6 and 10.6 MeV for coarse intervals in incident neutron energy. The integrated yield of gamma rays of energies greater than 1.6 MeV with higher resolution in the neutron energy is also presented. The experimental results are compared with the Evaluated Nuclear Data File (ENDF).

b. The $^{23}Na(n,x\gamma)$ Reaction Cross Section** (D. C. Larson and G. L. Morgan)

Differential cross sections for neutron-induced gamma-ray production from sodium have been measured for incident neutron energies between 0.2 and 20.0 MeV. Gamma rays with energies $0.35 \leq E_\gamma \leq 10.6$ MeV were detected with a sodium iodide spectrometer at 125°. The data presented are the double-differential cross section $d^2\sigma/d\Omega dE$, for coarse intervals in incident neutron energy, the measured results are compared with calculations based on multistep Hauser-Feshbach theory, and with a benchmark gamma-ray production measurement performed at the Oak Ridge Tower Shielding Facility.

c. The $Th(n,x\gamma)$ Reaction Cross Section for Incident Neutron Energies Between 0.3 and 20.0 MeV† (G. L. Morgan)

Differential cross sections for the neutron-induced gamma-ray production from thorium have been measured for incident neutron energies between 0.3 and 20.0 MeV. ORELA was used to provide the neutrons and a NaI spectrometer to detect the gamma rays at 125°. The data presented are the double differential cross section, $d^2\sigma/d\Omega dE$, for gamma-ray energies between 0.3 and 10.6 MeV for coarse intervals in incident neutron energy. The integrated yield of gamma rays of energies greater than 300 keV with higher resolution in the neutron energy is also presented.

* Abstract of ORNL-5545 (to be published).
** Abstract of note to be submitted for publication in Nucl. Sci. Eng.
† Abstract of ORNL/TM-6758 (to be published).

d. Measurement of $^{238}U(n,n'\gamma)$ and $^{7}Li(n,n'\gamma)$ Gamma-Ray Production Cross Sections* (D. K. Olsen, G. L. Morgan, and J. W. McConnell)

Employing a 95-cm^3 Ge(Li) detector, positioned 20 m from the ORELA white neutron source, 125° cross sections for gamma-ray production from 0.48 to 5.0 MeV incident neutrons on ^{238}U and ^{7}Li samples were measured by time-of-flight techniques. The incident neutron flux was determined with a proton-recoil telescope which used a solid-state, recoil-proton detector. Altogether, 28 cross sections for ^{238}U transitions from levels with 680 to 1224 keV of excitation were measured. In addition, seven branching ratios for weak ^{238}U transitions and the $^{7}Li(n,n'\gamma)^{7}Li^*$ (478-keV) cross section were measured. From these data and other level-decay information, neutron inelastic scattering cross sections from the 680-, 732-, and 827-keV levels and the 965-, 1045-, and 1170-keV pseudo-levels of ^{238}U were constructed and compared with those of the proposed ENDF/B-V evaluation.

2. Capture Cross Sections

a. Neutron Cross Sections of the Os Isotopes and Nucleosynthesis (R. R. Winters, J. Halperin, J. A. Harvey, N. W. Hill, and R. L. Macklin)

The neutron capture cross sections of the osmium isotopes 186, 187, and 188 were measured in the keV energy because of their interest to nucleosynthesis. The total cross sections of these three isotopes have also been measured from ∿200 eV to 300 keV. The duration of nucleosynthesis prior to the formation of the solar system is calculated from the natural abundance of ^{187}Os, produced from the decay of the long-lived ^{187}Re, and the capture cross sections of ^{186}Os and ^{187}Os. A preliminary estimate of $\sim 12 \times 10^9$ years agrees well with that of Browne and Berman,[1] but is significantly larger than estimates from uranium-thorium dating. However, the neutron inelastic scattering of ∿30-keV neutrons to the 10-keV level in ^{187}Os is an important input in the calculation. An experimental measurement of this cross section using 24-keV Fe window neutrons combined with the time-of-flight technique is planned.

b. Capture Cross Section Measurements of Fission Product Poisons (R. L. Macklin, J. Halperin, and R. R. Winters)

Isotopes of Pd and Ru, produced from fission, account for a considerable fraction of the poisoning in a fast reactor. Capture cross section measurements have been made in the keV energy region on five isotopes of Pd (including the important fission product 105) and four isotopes of Ru (including the important isotope 101). Parameters for individual Pd resonances (∿100 in each isotope) were obtained up to ∿10

* Abstract of ORNL/TM-6832 (to be published).

[1] Nature 262, 197 (1976).

keV and the average cross sections were analyzed at the higher energies to obtain strength functions Γ_γ/D_0, S^1, S^2, and S^0 (the last only for ^{105}Pd). A similar analysis on the data for the isotopes of Ru is in progress.

3. Total Cross Sections

a. Neutron Total Cross Sections for H, C, O, and Fe from 0.5 to 50 MeV (D. C. Larson, J. A. Harvey, and N. W. Hill)

We have measured the transmission of neutrons through samples of CH_2(n_H=0.822 at/b), C(n=0.412 at/b), O(n=0.548 at/b), and Fe(n=0.430 at/b). The Be block target of ORELA provided the neutrons, which were detected by a NE110 proton recoil detector located 80 m from the source. The data were corrected for deadtime losses and background effects, and converted to cross sections. Our measured hydrogen cross section is in good agreement over the complete energy range with the results from the various extensive phase shift analyses of this cross section. Data for C, O, and Fe are needed for shield design of the Fusion Material Irradiation Test Facility (FMIT).

b. Measurement of the Neutron Total Cross Section of Natural Magnesium from 9 keV to 39 MeV* (D. C. Larson, J. A. Harvey, N. W. Hill, and H. Weigmann**)

The neutron transmission through a 5.09-cm sample of natural magnesium has been measured for neutron energies between 9 keV and 39 MeV. The Oak Ridge Electron Linear Accelerator (ORELA) was used to provide the neutrons, which were detected at the 200-m flight path by a NE-110 proton recoil detector. The experimental results are tabulated and compared with the total cross section in the ENDF/B-IV file for magnesium.

c. Neutron Transmission Measurements of the Thick Neutron Filters (J. A. Harvey, N. W. Hill, and J. R. Harvey†)

Transmission measurements have been made upon thick samples of ^{58}Ni (99.93%), ^{60}Ni (99.68%), ^{64}Zn (97.87%) to assess their usefulness as neutron filters to produce neutron beams of ∿14, ∿4, and ∿2 keV energy, respectively. This window neutron technique is presently used at several reactors to produce beams of 2, 24, and 120 keV using thick filters of Sc, Fe, and Si. Windows at 160 eV in ^{184}W (94.51%) and 7.5 keV in natural copper are also being investigated. These "monoenergetic" neutron beams can be used for basic nuclear physics, instrument calibrations, fundamental radiobiology, and for radiotherapy of brain tumors.

---

* Abstract of ORNL/TM-6420 (to be published).

** Visiting scientist from the Central Bureau of Nuclear Measurement, Geel, Belgium.

† Berkeley Nuclear Laboratories, UK.

d. Recent Results for ^{58}Ni and ^{56}Fe at ORELA* (F. G. Perey, G. T. Chapman, W. E. Kinney, and C. M. Perey)

Transmission and capture data from ^{58}Ni have been analyzed up to 120 keV and are reported. High resolution scattering measurements for Fe are discussed and the determination of the J^{π} value for most resonances seen in transmission data up to 400 keV is given including an attempt at evaluation of the resonances of ^{56}Fe on the basis of recently published data.

e. ^{6}Li(n,α)T Cross Section from 70 to 3000 keV via ^{235}U(n,f) Calibration of a Thin Glass Scintillator (R. L. Macklin, R. W. Ingle, and J. Halperin)

The efficiency of a 0.5 mm ^{6}Li glass scintillation monitor was determined above the "1/v" region by comparison with the counting rate of a 10 plate ^{235}U fission ionization chamber in a neutron beam from the Oak Ridge Electron Linear Accelerator (ORELA). The chief difference in derived ^{6}Li(n,α) cross sections from the ENDF/B-V evaluation is a slightly greater width ($\sim$8%) of the prominent resonance peaking near 240 keV and a higher cross section in the wings. The peak value, 3.37 barns, is slightly higher than ENDF/B-V, 3.3087 barns, but is in good agreement with the value of 3.36 ± 0.06 barns obtained from an R-matrix fit to the absolute measurements by Renner *et al.*[1] The steep rise in efficiency from 3500 to 5000 keV is attributed primarily to the ^{16}O(n,α) reaction.

f. Measurement of the 2.35-MeV Window in ^{16}O + n (J. L. Fowler, C. H. Johnson, N. W. Hill, and J. M. Ortolf)

Stelson and Barnett have suggested[2] that the transmission of a thick oxygen scatterer can be used to measure the temperature of a d-d plasma. For a thick oxygen scatterer, neutrons are transmitted only near the 2.35-MeV minimum in the total cross section. The relative number of plasma neutrons near this minimum depends on the ion temperature. Accurate transmission measurements have been made on a 1.5-m liquid oxygen sample using the 200-meter flight path at ORELA. After correcting for the 0.17% impurities of N_2 and A, a value of 114.0 ± 1.7 mb at the minimum was obtained. The cross sections on the sides of the minimum were also measured using thinner matched samples of BeO and Be. Calculations show that the transmission of d-d neutrons will increase up to an ion temperature of about 6 keV.

---

* Proc. Specialists' Meeting on Neutron Data of Structural Materials for Fast Reactors, ed. K. H. Böckhoff, Pergamon Press Ltd. (1978).

1 INDC(USA)-79/U, p. 233.

2 Bull. Am. Phys. Soc. 23, 882 (1978).

4. Scattering and Reactions

a. Cross Sections for the $^{14}N(n,p_0)$, (n,α_0), and (n,α_1) Reactions from 0.5 to 15 MeV* (G. L. Morgan)

Cross sections have been measured for the $^{14}N(n,p_0)$ reaction from 0.5 to 7.0 MeV and for the (n,α_0) and (n,α_1) reactions from 1 to 15 MeV and 4 to 15 MeV, respectively. The data were obtained using a gaseous scintillator containing N_2 and Xe mixtures. A linac was used as a pulsed, white neutron source with a 29-m flight path. The results of the measurement are compared to the current evaluated file for nitrogen; agreement is good for neutron energies below 8 MeV, but the measurement is substantially higher than the evaluation for neutron energies near 10 MeV.

b. Cross Sections for the Ti(n,xn) and Ti(n,xγ) Reactions between 1 and 20 MeV** (G. L. Morgan)

Differential cross sections for the production of secondary neutrons and gamma rays from neutron interactions in natural titanium have been measured at 130 deg. (lab) for incident neutron energies in the range 1 to 20 MeV. An electron linac was used as a pulsed, white neutron source. Incident neutron energies were determined using time-of-flight techniques for a source-to-sample distance of 48 m. Secondary spectra were determined by unfolding the pulse-height distributions observed in a NE-213 scintillation counter. The results are compared to the current evaluated nuclear data file (ENDF/B-IV, MAT 1286).

c. Cross Sections for the Cu(n,xn) and Cu(n,xγ) Reactions between 1 and 20 MeV† (G. L. Morgan)

Differential cross sections for the production of secondary neutrons and gamma rays from neutron interactions in natural copper have been measured at 130 deg. (lab) for incident neutron energies in the range 1 to 20 MeV. An electron linac was used as a pulsed, white neutron source. Incident neutron energies were determined using time-of-flight techniques for a source-to sample distance of 48 m. Secondary spectra were determined by unfolding the pulse-height distributions observed in a NE-213 scintillation counter. The results are compared to the current evaluated nuclear data file (ENDF/B-IV, MAT 1295).

---

* Abstract of ORNL/TM-6528 (November 1978).
** Abstract of ORNL-5544 (to be published).
† Abstract of ORNL-5499, ENDF-273 (February 1979).

d. High Resolution Neutron Transmission and Scattering Measurements on ^{206}Pb (D. J. Horen, J. A. Harvey, and N. W. Hill)

High resolution neutron transmission and differential measurements have been made with ^{206}Pb samples. The data have been analyzed to obtain the E_0, J, ℓ, and neutron widths of $\sim$200 resonances up to $\sim$600 keV. Doorway states are observed in the s-, p-, and d-wave neutron channels. Resonances in both the $p_{1/2}$ and $p_{3/2}$ channels are evident and are consistent with observations in the ^{207}Pb + n system. These doorways probably arise from a $d_{5/2}$ particle, 3^- core excitation. A major fraction of the resonances assigned from photonuclear work as p-wave are found to be s- or d-wave. In the interval from 3 to 600 keV we can deduce a value of <24 eV for the M1 ground-state radiation $\Sigma g_\gamma \Gamma_{\gamma 0} \Gamma_n / \Gamma$. The average level density of the s-wave resonance shows an increase of about 12% per 100 keV up to 800 keV. The s-wave data (up to 800 keV) can be fitted by a constant temperature model with T = 0.9 MeV. The d-wave level density is consistent with a (2J+1) dependence, but the number of p-wave resonances is greater than expected. The data also indicate that the level density for J = 1/2 is not parity independent.

5. Actinides

a. Actinide Neutron Cross Sections Program (J. W. T. Dabbs, L. W. Weston, J. A. Harvey, S. Raman, C. E. Bemis, R. L. Macklin, J. Halperin, K. Rush, N. W. Hill, J. H. Todd, C. H. Johnson, and M. L. Williams)

Fission - Development of a new type (honeycomb) fission chamber for $>10^8$ α/sec samples was completed. Together with specially developed ultrafast amplifiers and a new Xe gas scintillator $^6Li(n,\alpha)$ neutron beam monitor of large area, this chamber permitted the measurement of the fission cross section of ^{241}Am over the energy range thermal to 20 MeV at ORELA. The ^{241}Am fission cross section in the 1 to 100 keV energy region is much lower than was obtained with earlier underground explosion measurements. Other laboratories have also confirmed the strikingly lower fission cross section in this energy range. Papers on fission of ^{234}U and ^{235}U were completed and published. In the latter paper, a collaboration between LASL and ORNL, the spins of some 375 resonances and structures below 300 eV were definitively established.

Capture - Results of capture cross section measurements on ^{240}Pu were published. Measurements of the capture cross section of ^{241}Pu with a simultaneous fission cross section determination were completed and published. Multilevel resonance parameters for this nuclide (Adler formalism) were derived and published. The $^{232}Th(n,\gamma)$ cross section from 2.6 to 800 keV has been revised and updated. Additional data have been taken on ^{237}Np capture to extend the neturon energy range from 0.01 eV to 400 keV. Data reduction and analysis are in progress. Below 8 eV the data are in only fair agreement with ENDF/B-IV and resonance parameters will be derived for the new data. Agreement of the average capture cross section with optical model calculations within about 15% above 200 eV is found; these calculations have been used for ENDF/B-IV in the absense of differential data.

Total - Analysis of transmission data on 98% ^{249}Bk was completed and reported. The sample was permitted to decay to ^{249}Cf (330 day half-life) and remeasured twice. A preliminary analysis of data from the 70% ^{249}Cf was made and data have been taken on 86% ^{249}Cf and converted to cross section. A resonance analysis is in progress.

Integral Cross Section Determinations - Several separated actinide samples ranging from ^{232}Th to ^{241}Pu were irradiated for four years in EBR-II at Idaho Falls. A new program of measuring the present composition of these samples has been initiated in conjunction with the Analytical Chemistry Division of ORNL. First results, for a ^{239}Pu sample, have been published recently.

Actinide Newsletter - The second actinide newsletter detailing worldwide developments in actinide research (edited by S. Raman) was published by ORNL in February 1979.

b. Measurement and Analysis of the Fission Cross Section and the Fission Fragment Anisotropy in the MeV-Neutron Induced Fission of ^{232}Th* (S. Plattard,** G. F. Auchampaugh,† N. W. Hill, R. B. Perez, and G. de Saussure)

The $^{232}Th(n,f)$ to $^{235}U(n,f)$ fission ratio and the fission fragment anisotropy in the $^{232}Th(n,f)$-reaction have been measured at ORELA with a nominal resolution of 0.10 ns/m and for incident neutron energies from 0.6 to 10 MeV.

As far as the gross structures of the fission cross section are concerned, our data are in very good agreement with ENDF/B-V and with the results of the recent measurements of Blons *et al.*,[1] but our data do not reproduce the fine structure reported by Blons *et al.*

K-quantum numbers have been assigned to all major broad resonances from 0.9 to 2.5 MeV. None of these resonances can be described by a single K-quantum number. The two resonances at 920 and 1015 keV have predominantly K=1/2, with weaker contribution with K=5/2.

---

* IAEA Symposium on Physics and Chemistry of Fission, Jülich, Germany, May 14-18, 1979.

** Centre d'Etudes de Bruyères-le-Châtel, France.

† Los Alamos Scientific Laboratory, Los Alamos, New Mexico.

[1] J. Blons, C. Mazur, and D. Paya, Phys. Rev. Lett. 35, 1749 (1975).

Using a code[1] based on the statistical model, calculations of the fission cross section and of the fission fragment angular distribution have been performed in the range 1.4 to 1.7 MeV, within the framework of the double humped fission barrier.

c. Delayed Beta- and Gamma-Ray Production Due to Thermal-Neutron Fission of ^{235}U, Spectral Distributions for Times After Fission Between 2 and 14000 sec: Tabular and Graphical Data* (J. K. Dickens, T. A. Love, J. W. McConnell, J. F. Emery, K. J. Northcutt, R. W. Peelle, and H. Weaver)

Fission-product decay energy-release rates have been measured for thermal-neutron fission of ^{235}U. Samples of mass 1 to 10 μg were irradiated for 1 to 100 sec using the fast pneumatic-tube facility at the Oak Ridge Research Reactor. The resulting beta- and gamma-ray emissions were counted for times-after-fission between 2 and 14,000 secs. The data were obtained for beta and gamma rays separately as spectral distributions, $N(E_\gamma)$ vs E_γ and $N(E_\beta)$ vs E_β. For the gamma-ray data the spectra were obtained using a NaI detector, while for the beta-ray data the spectra were obtained using an NE-110 detector with an anticoincidence mantle. The raw data were unfolded to provide spectral distributions of moderate resolution. These distributions are given in graphical and tabular form as differential cross-section values of dσ/dE/fission for gamma-ray energy intervals ranging from 10 keV for $E_\gamma < 0.18$ MeV to 100 keV for $E_\gamma > 6.8$ MeV, and beta-ray energy intervals ranging from 20 keV for $E_\beta < 0.25$ MeV to 160 keV for $E_\beta > 6.4$ MeV. Counting-time intervals range from 1 sec for times-after-fission (t_w) < 6 sec to 4000 sec for $t_w = 10^4$ sec. The graphical representations also include calculated spectra using summation methods and the ENDF/B-IV fission yield and decay scheme data base.

d. Measurement of the ^{238}U to ^{235}U Fission Cross Section Ratio for Neutron Energies Between 0.1 and 25 MeV** (F. C. Difilippo,† R. B. Perez, G. de Saussure, D. K. Olsen, and R. W. Ingle)

The ^{238}U to ^{235}U fission cross-section ratio has been measured for incident neutrons from 0.1 to 25.0 MeV. A ratio shape measurement was normalized by the threshold cross-section method. A fission cross-section ratio .436 ± .004 was found averaged over neutron energies from 2.35 to 2.95 MeV.

---

[1] J. Trochon, H. Abou Yehia, J. Jary, and Y. Pranal, "Propriétés dynamiques de la fission de ^{233}Th," to be presented at IAEA Symposium on Physics and Chemistry of Fission, Jülich, Germany, May 14-18, 1979.

* Abstract of ORNL/NUREG-39 (June 1978).

** Nucl. Sci. Eng. 68, 43 (1978).

† IAEA Fellow from the Comisión Nacional de Energia Atomica, Argentina.

e. The Neutron Induced ^{238}U Subthreshold Fission Cross Section for Neutron Energies Between 5 eV and 3.5 meV* (R. B. Perez, F. C. Difilippo, G. de Saussure, and R. W. Ingle)

A measurement of the ^{238}U neutron-induced fission cross section has been performed at the ORELA Linac facility in the neutron energy range between 5 eV and 3.5 MeV. The favorable signal-to-background ratio and high resolution of this experiment resulted in the identification of 85 subthreshold fission resonances or clusters of resonances in the neutron energy region between 5 eV and 200 keV. The fission data below 100 keV are characteristic of a weak coupling situation between Class I and Class II levels. The structure of the fission levels at the 720 eV and 1210 eV fission clusters is discussed. There is an apparent enhancement of the fission cross section at the opening of the 2^+ neutron inelastic channel in U-238 at 45 keV. An enhancement of the subthreshold fission cross section between 100 keV and 200 keV has been tentatively interpreted in terms of the presence of a Class II, partially damped vibrational level. There is a marked structure in the fission cross section above 200 keV up to and including the plateau between 2 and 3.5 MeV.

f. Statistical Tests for the Detection of Intermediate Structure: Application to the Structure of the ^{238}U Neutron Capture Cross Section Between 5 keV and .1 MeV** (R. B. Perez, G. de Saussure, R. L. Macklin, and J. Halperin)

Recent measurements of the ^{238}U neutron capture cross section show a considerable amount of fluctuation between 5 and 100 keV.

Statistical tests performed on the measured cross section suggest that the fluctuations are not compatible with the statistical model of nuclear reactions and imply the existence of intermediate structure, which is interpreted in terms of doorway states. The validity of the statistical tests used here is confirmed by numerical experiments with simulated cross sections generated by the Monte Carlo method, in accordance with the statistical method.

The behavior of the capture cross section is compared to those of the subthreshold fission cross section and of the inelastic scattering cross section. The threshold anomaly at the opening of the inelastic channel at 45 keV is seen in the form of a rounded step.

g. Fission-Product Yields for Thermal-Neutron Fission of ^{239}Pu† (J. K. Dickens and J. W. McConnell)

Absolute yields have been determined for 49 fission products representing 36 mass chains created during thermal-neutron fission of

* Abstract of ORNL/TM-6788 (March 1979).

** Submitted for publication in Physical Review.

† To be submitted for publication in Nuclear Science and Engineering.

^{239}Pu, including three mass chains for which no prior data exist. Using Ge(Li) spectroscopy spectra were obtained of gamma rays due to decay of fission products between 1550 sec and 31 days after a 100-sec irradiation. Data were obtained for all fission products simultaneously. Gamma rays were assigned to the responsible fission products by matching gamma-ray energies and half lives. The resulting fission-product yields are compared with previous measurements and with recommended yields given in two recent (and independent) evaluations. The present results are significantly larger for mass chains between 101 and 107, somewhat smaller for mass chains 87 and 151, and in reasonable agreement with the remaining mass chains. Uncertainties assigned to the present results range between 2.5 and 25%, and are smaller than or comparable to uncertainties assigned to other experimental or evaluated yields for 14 mass chains.

h. Fission-Product Energy Release for Times Following Thermal-Neutron Fission of ^{241}Pu Between 2 and 14000 Seconds* (Dickens, Emery, Love, McConnell, Northcutt, Peelle, and Weaver)

Fission-product decay energy-release rates have been measured for thermal-neutron fission of ^{241}Pu. Samples of mass 1 and 5 μg were irradiated for 1 to 50 sec using the fast pneumatic-tube facility at the Oak Ridge Research Reactor. The resulting beta- and gamma-ray emission spectra were recorded for times-after fission between 2 and 14000 secs. The data were obtained for beta and gamma rays separately as spectral distributions, $N(E_\gamma)$ vs E_γ and $N(E_\beta)$ vs E_β. For the gamma-ray data the spectra were obtained using a NaI detector, while for the beta-ray data the spectra were obtained using an NE-110 detector with an anticoincidence mantle. The raw data were unfolded to provide spectra distributions of modest resolution. Total yield and energy integrals as a function of time after fission were obtained from integration over E_γ and E_β. The final differential spectral and integral data are given in tabular and graphical form.

The total integral energy-release data are compared with similar data previously obtained for ^{235}U and ^{239}Pu. Following a pulse of fissions the total decay-heat power for ^{241}Pu fission is greater by ∿5% than that for ^{235}U for times after a fission pulse <2500 sec, and greater by up to 40% than that for ^{239}Pu. For times after a fission pulse greater than 5000 sec the decay-heat power for ^{241}Pu asymptotically approaches that for ^{239}Pu, and is less than that for ^{235}U by ∿25% at 14000 sec.

On an infinite irradiation basis, the decay-heat power for ^{241}Pu is equal to that for ^{235}U for times after shutdown less than 100 sec, less than that for ^{235}U for times after shutdown greater than 300 sec. The decay-heat power for ^{241}Pu is greater than that for ^{239}Pu for times after shutdown less than 50 sec, asymptotically approaching and becoming equal to the ^{239}Pu decay-heat power for longer times after fission.

* Abstract of NUREG/CR-0171, ORNL/NUREG-47 (August 1978).

i. Fission Yields for Thermal-Neutron Fission of ^{241}Pu* (J. K. Dickens)

Cumulative fission yields for seventeen fission products (sixteen mass chains) created by thermal-neutron fission of ^{241}Pu were determined from analysis of gross fission-product gamma-ray spectra obtained using a large volume Ge(Li) detector. Uncertainties assigned to nine of the measured yields are smaller than existing evaluated uncertainties.

j. Interim Report on the ORNL Absolute Measurements of $\bar{\nu}_p$ for ^{252}Cf** (R. R. Spencer, R. Gwin, R. Ingle, and H. Weaver)

An initial effort has been made to measure absolutely the average number of neutrons, $\bar{\nu}$, emitted in spontaneous fission of ^{252}Cf to an unprecedented accuracy of ±0.25%. Fission neutrons were counted with a large, gadolinium poisoned, liquid scintillator. A "white source" of neutrons from the ORELA was used to calibrate the detector efficiency as a function of neutron energy. Source neutrons were scattered into the large scintillator by a thin NE-213 proton-recoil detector which employed pulse shape discrimination to eliminate unwanted γ-ray background. The resulting neutron energy- and scattering angle-dependent efficiencies were used to normalize a Monte Carlo calculation of the scintillator efficiency for fission neutrons. Under the assumptions that the effects of parasitic charged particle reactions and multiple neutron scattering in the proton-recoil counter have negligible influence on the energy calibration, the value of the average number of prompt neutrons emitted per ^{252}Cf fission was found to be 3.783 ± 0.010. This report is intended as a documentary and guide for future measurements incorporating improvements suggested by the analysis of this first determination.

6. Experimental Techniques

a. Scintillation Detectors for Neutron Physics Research† (J. A. Harvey and N. W. Hill)

The characteristics of scintillation detectors for neutron physics such as efficiency, timing, resolution, size, pulse height resolution, backgrounds, are reviewed. Solid and liquid organic scintillation detectors are now widely used for neutrons from 10 keV to 200 MeV. Detailed calculations and measurements of the pulse height distributions and efficiencies for several organic scintillation detectors are presented. ^{6}Li glass scintillation detectors are valuable as neutron flux monitors and as efficient neutron detectors below 10 keV. Problems associated with these ^{6}Li glass scintillation detectors are discussed. Examples of many scintillation detectors in use today are described.

* Submitted for publication in Nuclear Science and Engineering.
** Abstract of ORNL/TM-6805.
† Abstract of a Review Article for a Special Volume on Detectors in Nuclear Science, Nucl. Instr. Methods.

B. DATA ANALYSES

1. Theoretical Calculations

a. Contributions to Few-Channel Spectrum Unfolding* (F. G. Perey)

In this report are two papers dealing with the subject of spectrum unfolding. These papers are closely related and will appear in the proceedings of two different conferences. Although they deal with analysis of dosimetry data, the method presented in these two papers is very general and applicable to any few-channel unfolding problem.

b. A Consistent Nuclear Model for Compound and Precompound Reactions with Conservation of Angular Momentum** (C. Y. Fu)

An attempt is made to develop a multi-step Hauser-Feshbach model capable of calculating the compound and precompound cross sections consistently and conserving angular momentum in both compound and precompound reactions.

The model is coded into a computer program, TNG. Results calculated with pre-fixed parameters are compared with experimental data for 14-MeV (n,xn), (n,xp), and (n,xα) cross sections and spectra for 13 isotopes ranging from Al to Nb. Agreements between the calculations and experiments are reasonably good for 90% of the (n,xn) and (n,xp) spectra, but are good for only 50% of the (n,xα) spectra. Calculations with another set of optical-model parameters did not improve the agreement.

c. Comparison of One- and Two-Dimensional Cross-Section Sensitivity Calculations for a Fusion Reactor Shielding Experiment† (Y. Seki,‡ R. T. Santoro, E. M. Oblow, and J. L. Lucius)

Cross-section sensitivities calculated with one- and two-dimensional models of a fusion reactor shielding experiment are compared. The effectiveness of the 2-D calculation in accurately modeling the experiment and detector configurations is demonstrated. At the same time the validity of a 1-D sensitivity study is also demonstrated.

d. Cross Section Sensitivity Analysis of a Proposed Neutron Streaming Experiment with a Two-Dimensional Model¶ (Y. Seki,‡ R. T. Santoro, E. M. Oblow, J. M. Barnes, and J. L. Lucius)

Cross section sensitivity analysis of a proposed streaming experiment for a typical penetration in a fusion reactor shield has been

* Abstract of ORNL/TM-6267 (February 1978).
** To be submitted for publication in Physical Review.
† Abstract of ORNL/TM-6667 (January 1979).
‡ Visiting scientist from Tokai Research Establishment, Japan.
¶ Abstract of ORNL/TM-6588 (February 1979).

performed using a two-dimensional sensitivity method. The neutron streaming was shown to be determined mostly by the 4.5-cm-thick duct liner made of iron and the concrete structure immediately surrounding the liner. The neutrons scattered near the surface of the liner were found to be very important. A recommendation is made to move the proposed detector position to improve spatial resolution in the measurements without changing the sensitivity of the measurement to the nuclear characteristics of the duct materials.

2. ENDF/B Related Evaluations

a. Evaluations Performed for ENDF/B-V (C. Y. Fu, D. C. Larson, and L. W. Weston)

Evaluations of neutron-induced reactions and gamma-ray production were performed for carbon, fluorine, sodium, magnesium, silicon, calcium, iron, copper, lead, and $^{240-241}$plutonium. Updates were based on recent experimental data combined with results of advanced model calculations. Uncertainty files were given for all materials except magnesium and copper. Evaluations of special purpose activation, dosimetry, and gas production cross sections are underway for the requested reactions and materials.

b. Status of ENDF/B-V Neutron Emission Spectra Induced by 14-MeV Neutrons* (D. M. Hetrick, D. C. Larson, and C. Y. Fu)

ENDF/B-V neutron emission spectra induced by 14.6-MeV incident neutrons are graphically compared with experimental data. The elements selected for the comparisons include Na, Mg, Al, Si, Ca, Ti, V, Cr, Fe, Ni, Cu, Nb, W, and Pb. Partial as well as total spectra from the ENDF/B-V evaluations are shown in each graph, while experimental data were available only for the total. Energy distribution laws utilized for the reaction types in each element are explained. Agreement between evaluated and experimental data is discussed, and recommendations for improvements are made. In general, evaluations which utilized advanced nuclear model codes, including precompound effects, agree well with measured spectra.

c. Expectations for ENDF/B-V Covariance Files: Coverage, Strength and Limitations** (F. G. Perey)

The concept of the estimated data covariance files of ENDF/B is explored in detail. The relationship between uncertainties and "possible mistakes" is discussed in order to avoid likely misunderstanding concerning the use of the data covariance files. Some perceived strengths and weaknesses of the ENDF/B-V data covariance files are mentioned.

* Abstract of ORNL/TM-6637 (to be published).

** Abstract of paper presented at Workshop on Theory and Application of Sensitivity and Uncertainty Analysis, Oak Ridge, August 22-24, 1978.

d. Covariance Matrices of Experimental Data* (F. G. Perey)

A complete statement of the uncertainties in data is given by its covariance matrix. It is shown how the covariance matrix of data can be generated using the information available to obtain their standard deviations. Determination of resonance energies by the time-of-flight method is used as an example. The procedure for combining data when the covariance matrix is non-diagonal is given. The method is illustrated by means of examples taken from the recent literature to obtain an estimate of the energy of the first resonance in carbon and for five resonances of ^{238}U.

e. Evaluation of Resonance Parameters for Iron** (C. M. Perey and F. G. Perey)

A new evaluation of the resonance parameters of the iron isotopes is necessary for ENDF/B-V, and is justified by new high resolution measurements made at ORELA. For the first time this version of ENDF gives an estimate of the errors of the resonance parameters.

Since the publication of ENDF/B-IV, Ribon and Le Coq[1] have made an evaluation of the iron resonance parameters which was based on data up to the end of 1973 to which they added many resonances obtained from plots of ORELA raw data. Since 1973 ORELA data were reduced and published. These new data gave information on many resonances previously unresolved for ^{54}Fe and ^{56}Fe.

f. Review of Cross Section Data Important to the Uranium Plutonium Fuel Cycle in Thermal Reactors† (L. W. Weston)

Since there are hundreds of cross sections involved in the design of a thermal reactor, this paper will be limited to the important fissile and fertile nuclide cross sections with emphasis on the problems and discrepancies in these cross sections. Before considering such problems it should be noted that the overall data base and the evaluations of this data base have improved markedly in recent years — even with a dramatic reduction in experimental measurements. The fact that discrepancies still exist should not overshadow the fact that experimenters and evaluators have made progress in providing an increasingly reliable differential cross section data base for reactors.

---

* Abstract of paper presented at Int. Conf. on Neutron Physics Data for Reactors and other Applied Purposes, Harwell, England, 25-29 Sept. 1978.

** Abstract of ORNL/TM-6405 (to be published).

[1] "Notes sur l'évaluation des paramètres de résonance et de la section efficace de capture du fer," unpublished (1975).

† Abstract of paper presented at Seminar on "Nuclear Data Problems for Thermal Reactor Applications," BNL, New York, 22-24 May 1978.

g. Review of Microscopic Neutron Cross Section Data for the Higher Plutonium Isotopes in the Resonance Region* (L. W. Weston)

The microscopic neutron cross section data for plutonium-240, -241, and -242 in the resonance region are reviewed. In the context of importance to reactors the data on plutonium-240 are acceptable except for the resonance parameters of the 1-eV resonance. Plutonium-241 has discrepancies in the cross sections from thermal to 3 eV and to a lesser extent in the fission and capture cross section in the unresolved resonance region. The plutonium-242 cross sections appear to be known with sufficient accuracy as compared with the other plutonium isotopes.

3. Validation of ENDF/B Evaluations Through Integral Measurements

a. Sensitivity Coefficient Compilation for CSEWG Data Testing Benchmarks** (C. R. Weisbin, J. H. Marable, J. Hardy, Jr.,† and R. D. McKnight‡)

This report compiles and documents sensitivity coefficients generated by member laboratories of the Cross Section Evaluation Working Group (CSEWG) in the course of ENDF/B data testing. The work will be continuously updated as new benchmarks and new types of data are developed. The scope of this effort is sensitivities to many cross section data types for fast reactors, thermal reactors, shielding, etc. Detailed tabulations of the energy-integrated sensitivity coefficient (i.e., the change in response due to a uniform one percent change in cross section over the entire energy domain), sensitivities to changes in individual resonance parameters, and illustrative examples of energy dependent sensitivity profiles are given. The entire compilation of energy dependent coefficients is available in a computer-retrievable format along with programs for editing, mode changing, folding with projected changes to the reference data file, and performance parameter uncertainty estimation.

---

* Abstract of paper presented at the Specialist Meeting on the Nuclear Data of Higher Plutonium and Americium Isotopes for Reactor Applications, BNL, New York, 20-22 November 1978.

** Abstract of BNL-NCS-24853 (ENDF-265) (August 1978).

† Bettis Atomic Power Laboratory, Pittsburgh, Pennsylvania.

‡ Argonne National Laboratory, Argonne, Illinois.

C. NUCLEAR DATA PROJECT ACTIVITIES — 1978

(R. L. Auble,* S. J. Ball,** J. R. Beene,* F. E. Bertrand,* S. H. Dockery,** Y. A. Ellis, W. B. Ewbank, R. L. Haese, M. L. Halbert,* J. Halperin,* B. Harmatz, F. W. Hurley,** M. J. Martin, M. R. McGinnis,** J. T. Miller,** S. Ramavataram,* M. R. Schmorak, K. S. Toth,* and M. P. Webb*)

The Nuclear Data Project (NDP) is a comprehensive information analysis center which provides the basic research community with indexed references and collections of critically evaluated nuclear structure data. The systematic publication in *Nuclear Data Sheets* of new evaluations provides nuclear structure physics with an information service far in advance of what is available to most areas of science. The computer files of evaluated data developed by the NDP also present the basic research scientist with a valuable tool for looking at extensive nuclear level information in order to make comparison with new measurements or new theoretical calculations.

These computer files of nuclear data also are being used as a means of making the results of basic research quickly and easily available to a broader audience. Radioactivity information, in particular, has wide application in fields such as nuclear medicine, reactor engineering, environmental impact assessment, and nuclear waste management. Often the specialists in these areas have neither the time nor the training to make effective use of the data generated by basic nuclear research. The NDP has made important progress during the last few years toward providing a channel through which the results of new nuclear measurements can be transferred to any engineer or scientist who needs evaluated data to factor into his or her own work.

1. Data Evaluation

As part of the international network for nuclear structure data evaluation, the Nuclear Data Project has continuing responsibility for approximately 100 mass chains in three regions: A=45-69, 101-118, and 195-up. A total of 20 new mass chains was prepared and published during 1978, and six more from temporary or former NDP evaluators are nearly complete as of the beginning of 1979. Figure 1 gives the publication status of the mass chains for which NDP is responsible. For comparison, the status of all published mass chains is shown in Fig. 2.

In addition to its evaluation responsibility, NDP is committed to maintaining uniform, high standards for ENSDF (and consequently for *Nuclear Data Sheets*) by providing training for new evaluators, followed by a thorough review of the first few mass chains prepared by each new evaluator. The NDP staff members have organized training seminars for 28 new data evaluators in order to introduce them to NDP evaluation techniques, analysis programs, and conventions used in ENSDF and *Nuclear Data Sheets*.

* Part-time assignment to Nuclear Data Project.

** Technical support staff.

During 1977-1978, NDP staff have reviewed 14 mass chains prepared by new evaluators from six other data evaluation centers. About half of these have already been published in *Nuclear Data Sheets* or accepted for publication. Others are undergoing final revisions before acceptance.

2. Evaluated Nuclear Structure Data File

The Evaluated Nuclear Structure Data File (ENSDF), developed and implemented by the NDP, contains a documented summary of the current status of nuclear measurements. The ENSDF now contains 6600 distinct sets of evaluated nuclear information. This includes:

1950	sets of adopted level properties	
1850	decay schemes	
3020	nuclear reaction data collections, including	
	230	(n,γ) reactions
	225	(d,p) reactions
	500	(charged-particle,xnγ) reactions.

All decay scheme information in ENSDF is now at least as complete as the most recent *Nuclear Data Sheets* warrant. Normalization information is included wherever available, and details of electron capture and internal conversion have been added systematically, so that complete tables of atomic and nuclear radiations can be assembled for more than 1200 decay schemes. This information is being assembled for distribution in microfiche form.

The ENSDF computer format has been adopted as an international standard for the systematic storage and exchange of nuclear structure data. At six-month intervals, beginning in 1977, NDP has prepared complete copies of ENSDF on magnetic tape for distribution through an international network of data centers.

3. Nuclear Structure References

Nuclear Data Project's Nuclear Structure References (NSR) file contains ≈65,000 entries. Approximately 5000 indexed new research works are added each year. About half of the additions are journal publications; the other half consists of reports, conference abstracts, preprints, etc. The keyword indexing system used in the NSR file since 1964 has been shown[1] to allow more complete retrievals from the nuclear structure literature than the much larger INIS system (extended from the former *Nuclear Science Abstracts*).

The NSR file is used routinely to direct interested users to the nuclear structure literature. Special reference collections are assembled in partial response to most of the 100 information requests processed each year. A shorter version of the NSR file (1969 to present) is available for interactive search through the remote terminals of the DOE/RECON network. This file is queried an average of two times every working day.

[1] H. Behrens and J. W. Tepel, *Comparison of the International Nuclear Information System (INIS) and Recent References (RR) (Mass Chains A=27 and A=86)*, ZAED-M-13, Zentralstelle für Atomkernenergie-Kodumentation, Karlsruhe, West Germany (October 1977).

Each month an SDI (selective dissemination of information) service is provided from new entries to the NSR file. The service is used by data evaluators from the international network and by other extensive users of new nuclear structure data.

An index to the new literature is published three times per year as "Recent References" includes both isotope and reaction indexes for both journal and non-journal literature. A second indexed cumulation of journal literature was published in 1978.[1]

The NSR file is used as an international standard for the systematic computer storage and exchange of indexed reference information. Two copies of the complete indexed file have been distributed to the international network of data evaluation centers. The regular distribution of computer-readable copies of the new literature summarized in "Recent References" will begin in 1979.

4. Publications

The Nuclear Data Project is the editorial and publications office for the journal *Nuclear Data Sheets*. The NDP prepares camera-ready copy which is sent to Academic Press for publication and distribution. Implementation of the ENSDF system, with computer programs to select information from the data file, organize it into tables or drawings, and assemble the tables or drawings onto pages, has revolutionized the preparation of copy for *Nuclear Data Sheets*. The principal advantage of the computer system is the elimination of much redundant data copying and most proofreading. Although the same data item may appear in several places in the data sheets and drawings, it is usually contained only once in ENSDF, and must therefore be correctly entered only one time. Tables or drawings are also prepared in a precisely reproducible way. The computer programs have helped to establish and maintain greater uniformity among manuscripts from different evaluators, so that the user needs to adjust to fewer style variations.

Manuscripts are now being received from several data evaluation centers other than NDP. Twenty percent of the new evaluations published during 1978 were prepared by non-NDP evaluators. The distribution of mass-chain responsibility requires that this fraction increase to more than fifty percent. Maintaining tolerant limits on the style variations used by many different evaluators has added to the editorial work for *Nuclear Data Sheets*. The ENSDF system has avoided a much more substantial problem in the production of manuscripts.

---

[1] W. B. Ewbank, R. L. Haese, F. W. Hurley, and M. R. McGinnis, *Nucl. Data Sheets* 24, 445 (1978).

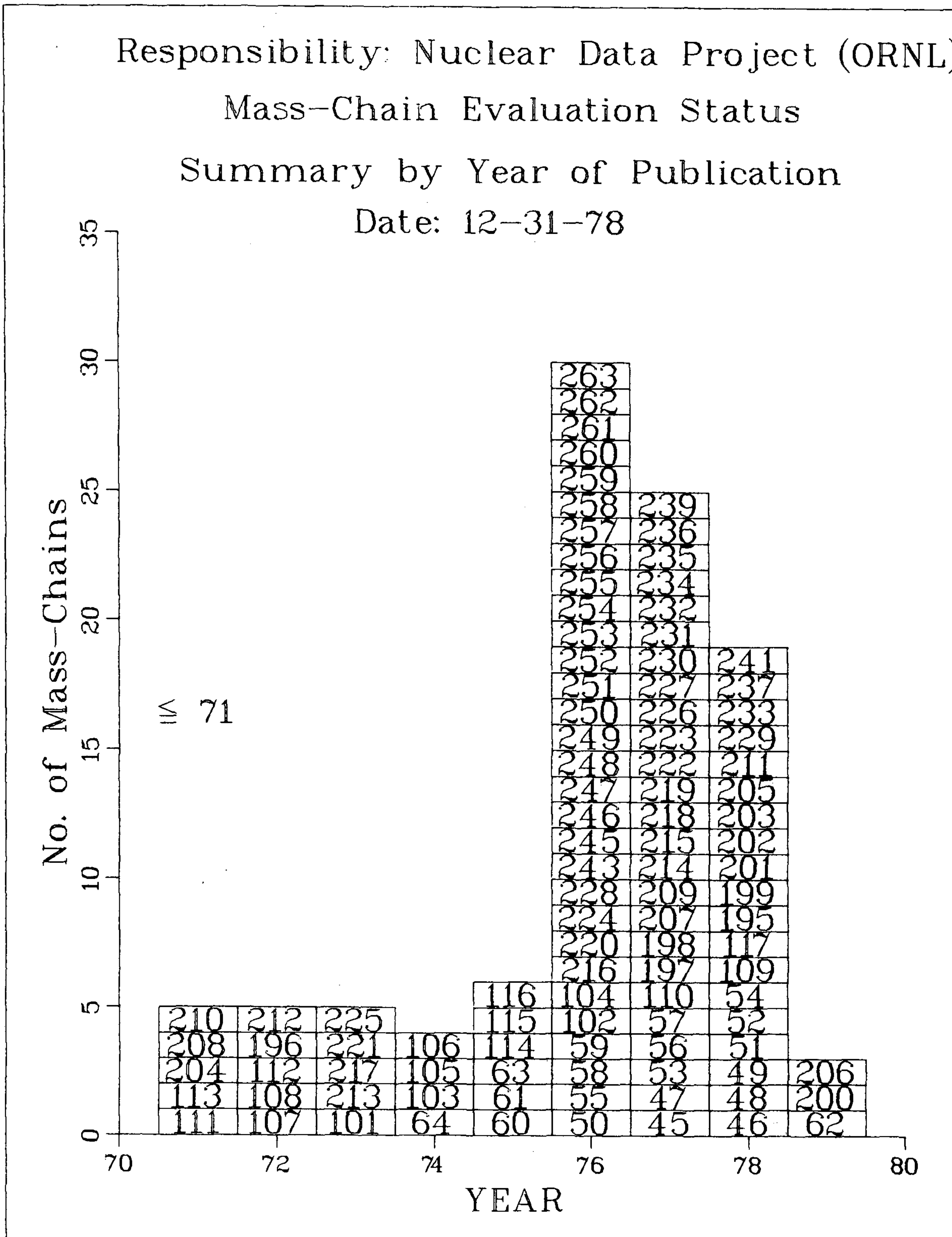

Fig. 1. Status of mass-chain evaluations in NDP's regions of responsibility.

ORNL-DWG 79-8772

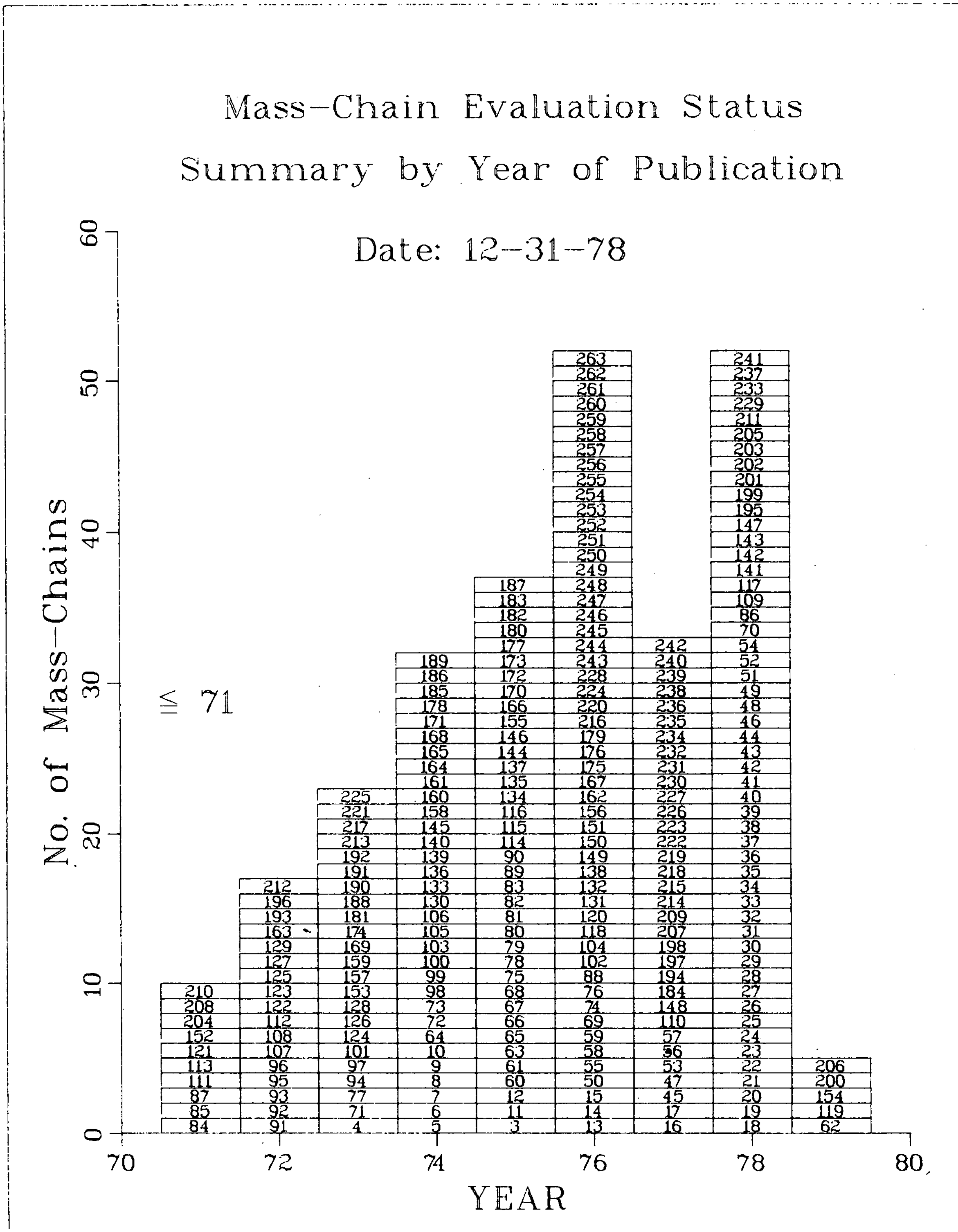

Fig. 2. Status of all mass-chain evaluations, A ≥ 5.

OHIO UNIVERSITY

A. NEUTRON MEASUREMENTS

1. ^{6}Li and ^{7}Li (4 MeV to 7.5 MeV) (H. Knox, R. White, R. Lane)

Our earlier differential elastic measurements on ^{6}Li and differential ($n_o + n_1$) measurements on ^{7}Li for $4 \leq E_n \leq 7.5$ MeV have been completed and a paper describing these results has been accepted for publication by Nuclear Science and Engineering. These data have also been sent to the National Neutron Data Center for placement in data file.

2. ^{6}Li and ^{7}Li (2.3 MeV to 4.1 MeV) (H. Knox, R. White, D. Resler, P. Koehler, R. Lane)

Using new highly enriched scattering samples, elastic and inelastic (0.478 MeV level) differential cross sections for neutrons scattered from ^{7}Li have been obtained at five incident neutron energies between 2.2 and 4.1 MeV. These data were obtained with a 6.5 m flight path which was necessary to resolve the two groups. Along with the ^{7}Li data, elastic differential cross sections for neutrons scattered from ^{6}Li were also obtained at the same five incident energies. Analysis of the present inelastic data is currently underway and preliminary results show the inelastic cross sections to be nearly isotopic in this energy region.

3. ^{11}B and ^{13}C (D. Resler, P. Koehler, R. White, R. Lane, H. Knox)

Elastic and inelastic differential cross sections of neutrons scattered from enriched samples of ^{11}B and ^{13}C have recently been completed. Angular distributions of elastic and inelastic (2.12 MeV level) neutrons scattered from ^{11}B were obtained at energies of 5.46, 5.62 and 6.00 MeV where considerable resonance structure exists in ^{11}B. Distributions for ^{13}C were obtained at 5.34 and 6.00 MeV in a region of a broad resonance in the total cross section. Inelastic groups for the 3.09, 3.68 and 3.85 MeV levels, together with the elastic group were obtained at 6.00 MeV, while the 3.09 MeV group and elastic group were obtained at 5.34 MeV. No previous inelastic measurements on ^{13}C have been reported. Analysis of these data is presently underway.

B. R-MATRIX ANALYSIS

1. ORMAP Modifications (R. White, D. Carter, J. O'Donnell)

The Ohio University R-matrix analysis program, ORMAP, has been reprogrammed to operate on the IBM 370 computer, and our Tektronix 4025/4631 graphics terminal has been brought on line. This combination of the faster computer and new graphics terminal with faster turn-around time and visual display of both experimental data and calculated fits, provide a very efficient means for studying nuclear structure. The program is currently being updated for faster running time by changing the method used for transforming parameters from j-j to channel coupling. It is hoped that this change may decrease the present running time substantially.

2. Analysis of ^{11}B + n Data Using ORMAP (R. White, P. Koehler, D. Resler, R. Lane)

The analysis of elastic neutron scattering data for ^{11}B should be completed within the next two months. In addition to our elastic data from 4 to 8 MeV, this analysis includes newer data obtained at this laboratory in the 2 to 4 MeV region.

3. Analysis of Inelastic Cross Sections (H. Knox, R. White)

With our increasing interest in inelastic scattering a new R-matrix analysis program is being developed. With this program analysis of elastic scattering and inelastic scattering to two levels in the target nucleus will be possible. Angular momentum values up to $\ell = 3$ will be included. This program, as ORMAP, allows the the use of either j-j or channel coupling schemes. This program should be operational within the next month.

C. MAGNETIC QUADRUPOLE TRIPLET SPECTROMETER (R.W. Finlay, S.M. Grimes, V. Kulkarni, J. Rapaport, J. Weber)

During the last year, design and construction of a large-angle magnetic quadrupole triplet spectrometer have been completed. This spectrometer is similar in concept to the one at Lawrence Livermore Laboratory and will also be used for the study of neutron-induced charged-particle producing reactions.

Because the neutron flux available at Ohio is much reduced from that available at LLL, a major design aim was a large solid angle, $\Omega \sim 10$ msr. This goal has been met, with the major change relative to the LLL spectrometer being an increase in aperture from 10 cm to 20 cm. Other changes relative to the LLL spectrometer are the use of time-of-flight for mass identification and the use of an intrinsic germanium detector rather than sliicon surface barrier detectors.

Studies of the shielding requirements are now underway. It is anticipated that measurements can begin in about a month. These measurements will be made for neutrons with energies both above and below 14 MeV and should complement the LLL data.

PACIFIC NORTHWEST LABORATORY

A. DELAYED NEUTRON STUDIES WITH AN ON-LINE MASS SPECTROMETER

1. Delayed Neutron Emission Probabilities (P_n) (P. L. Reeder and R. A. Warner)

The delayed neutron emission probabilities of Rb and Cs precursors have been remeasured by two techniques in order to resolve the discrepancies between our previous measurements[1] and other literature values. In the first technique the total number of precursors atoms present in a given sample was determined by counting the ions deposited on the first dynode of an electron multiplier detector - as was done previously. In the second technique, P_n values were measured by simultaneously following the decay of beta particles and neutrons after short periods of sample deposition. Beta particles were detected by a thin Si solid state detector. Analysis of both the beta and neutron decay curves by the computer program CLSQ gave the initial beta and neutron activities of the precursor. The ratio of these initial activities after correction for beta and neutron counter efficiencies gave the value for P_n. The P_n values recently measured by the ion counting and beta counting techniques are given in Table 1 along with our previously published values. The uncertainties given in Table 1 for the recent data include only the random errors. The ion counting and beta counting data have systematic uncertainties of 7% and 10.1% respectively. The new Cs P_n values are in good agreement with literature values but the disagreement still exists on the Rb data.

2. Average Energy of Delayed Neutrons ($\bar{E}$) (P. L. Reeder and R. A. Warner)

In conjunction with the P_n measurements described above, the average energies of the delayed neutrons were measured by a technique utilizing the ratio of counts in three concentric rings of counter tubes in the neutron detector. This ring ratio technique was also used in our previous measurements.[2] Several refinements have improved the internal consistency of the ring ratio technique. Our recent results are presented in Table 2 along with our previous values for comparison.

---

[1] P. L. Reeder, J. F. Wright and L. J. Alquist, Phys. Rev. C 15, 2108 (1977).

[2] P. L. Reeder, J. F. Wright and L. J. Alquist, Phys. Rev. C 15, 2098 (1977).

TABLE I. DELAYED NEUTRON EMISSION PROBABILITIES FOR Rb AND Cs PRECURSORS

Mass	1976 Ion	1978 Ion	1978 Beta
92	.012± .002	.0118± .0004	±
93	1.86 ± .13	1.66 ± .06	1.87 ± .02
94	13.7 ±1.0	12.4 ± .2	12.3 ± .2
95	11.0 ±0.8	10.8 ± .1	10.3 ± .1
96	17.0 ±1.2	17.7 ± .4	17.2 ±1.0
97	35.9 ±2.6	32.5 ±1.4	
98		16.5 ±1.9	
141	.043± .007	.034 ± .001	
142	.096± .008	.094 ± .004	.097± .006
143	1.95 ±0.14	1.79 ± .04	1.70 ± .02
144	4.3 ± .3	2.89 ± .21	2.92 ± .13
145	21.8 ±1.5	13.0 ± .3	
146		11.3 ±2.5	

TABLE 2. AVERAGE NEUTRON ENERGIES (keV) of Rb AND Cs PRECURSORS

Mass	1976	1978
92	180±40	200±85
93	560±10	482±11
94	570±10	486±7
95	530±10	454±15
96	560±10	500±59
97	>720	650±46
98		>303
141	240±50	216±76
142	240±60	182±24
143	350±10	267±10
144	290±20	245±16
145	460±30	356±27
146	530±70	500±183
147		>69

B. INDEPENDENT ISOMERIC YIELD RATIOS OF ^{90}Rb AND ^{138}Cs IN THERMAL NEUTRON FISSION OF ^{235}U (P. L. Reeder and R. A. Warner)

Experiments are currently underway to measure independent isomeric yield ratios for thermal neutron induced fission of ^{235}U. Fission products are produced and mass analyzed in the SOLAR on-line mass spectrometer facility. With the spectrometer tuned for a particular nuclide having isomeric states, a short burst of neutrons is obtained from the TRIGA reactor. The nuclide of interest is collected for a short time interval during and after the TRIGA pulse on a thin foil in front of a beta detector. The ion beam is then switched off and the decay of the beta activity is followed. The resulting decay curve is analyzed by the computer program CLSQ to give the initial activities of the isomeric components. After possible corrections for the particular decay scheme the ratio of initial activities leads to the isomeric yield ratio. Initial experiments are being done on ^{90}Rb and ^{138}Cs. Future experiments will include measurements on In, Br and I isomers.

UNIVERSITY OF PENNSYLVANIA

A. COMPILATION OF INFORMATION ON THE ENERGY LEVELS OF THE LIGHT NUCLEI

1. "Energy Levels of A = 18-20" was published in Nuclear Physics A300 (1978) 1-224.

2. "Energy Levels of 5-10" will be published by Nuclear Physics shortly. The page proofs for the article have been corrected.

3. We are well under way on the manuscript for "Energy Levels of 11-12." A preprint of A = 11 is being mailed in March 1979. We expect to complete A = 12 in 1979. At that point we will move on to A = 13-15 which we expect to complete in the fall of 1980.

F. Ajzenberg-Selove
C. L. Busch

B. EXPERIMENTAL RESEARCH

1. In the past year we have published the following three papers:

a. "States of ^{122}In and ^{124}In" by F. Ajzenberg-Selove, E. R. Flynn, J. W. Sunier and D. L. Hanson, Physical Review C17 (1978) 960-963.

b. "(t,p) reactions on ^{4}He, ^{6}Li, ^{7}Li, ^{9}Be, ^{10}B, ^{11}B and ^{12}C" by F. Ajzenberg-Selove, E. R. Flynn and Ole Hansen, Physical Review C17 (1978) 1283-1293.

2. We have submitted for publication two papers:

a. "Levels in ^{78,80,82}As from the ^{78,80,82}Se(t,^{3}He) reactions" by F. Ajzenberg-Selove, E. R. Flynn, D. L. Hanson and S. Orbesen. This paper has been accepted by Physical Review C and should be published shortly.

b. "Mass and excited states of ^{100}Nb" by F. Ajzenberg-Selove, E. R. Flynn and S. Orbesen. This paper has just been submitted to Physical Review and we do not yet have a report on it.

F. Ajzenberg-Selove

RENSSELAER POLYTECHNIC INSTITUTE

A. NEUTRON CROSS SECTION MEASUREMENTS

1. Neutron Capture and Transmission Measurements of Krypton Samples (Maguire, Jr., Fisher and Block)

Neutron capture and transmission time-of-flight (tof) measurements were carried out upon gaseous samples of elemental and enriched krypton. The measurements were carried out with the 1.25-m-dia. large liquid scintillator capture detector at the 25.68-m flight path and the ^{10}B-NaI transmission detector at the 28.32-m flight path. The Kr samples were contained in 1.2-liter aluminum cylindrical gas cells which were 30.48-cm long and had 0.79-mm-thick end windows. The sample compositions and thicknesses are listed in Table A-1.

The transmission data were analyzed for resonance parameters using the Harvey-Atta area analysis.[1] The capture data were analyzed in terms of the capture yield which, for each tof channel, is defined as $Y_i=(C-B)/k\eta_i\phi_{rel}$; where, Y_i is the number of captures per incident neutron in isotope i, C is the deadtime-corrected capture detector counts, B is the background counts, η_i is the capture detector efficiency for isotope i, ϕ_{rel} is the relative number of incident neutrons, and k is a normalization constant relating the relative number of incident neutrons to the absolute number. The background B was determined with resonance absorbers placed in the beam and ϕ_{rel} was measured with the transmission detector. The product $k\eta_i$ was determined by the method of Hockenbury et al.[2] for isolated resonances which are observed in both transmission and capture and for which the neutron width Γ_n is small compared to the radiation with Γ_γ. Unfortunately, only the 28.05-eV resonance in ^{83}Kr and the 39.63-eV resonance in ^{82}Kr satisfied the Hockenbury et al.[2] criteria. However, according to Hockenbury et al.[3] the capture detector efficiency of intermediate mass nuclei vary approximately linearly with binding energy and therefore the efficiencies of the other Kr isotopes were assumed to be linearly related to the measured ^{82}Kr and ^{83}Kr efficiencies. We have normalized the data to the ^{83}Kr efficiency by defining e_i as the ratio of capture efficiency for isotope i to that of ^{83}Kr. These e_i are listed in column 6 of Table A-1. The e_i errors include the estimated uncertainty introduced by this linear assumption.

The results of the transmission and capture measurements are listed in Table A-2. Included are the neutron and radiation widths which were determined from the transmission data. From the 28.05-eV and 39.63-eV resonances we deduced a value of $\Gamma_\gamma \approx 0.23$ eV which was then assumed constant for analysis of some of the smaller resonances seen in transmission. The errors in Γ_n were determined from the Harvey-Atta analysis. An example of the transmission data and Harvey-Atta fit is shown in Figure A-1.

The capture data are shown in Figure A-2 as $e_i Y/N$ vs tof channel number. We observed ≈70 peaks up to 9 keV, many of which are partially resolved multiplets. The resonance energies and isotopic assignments for these resonances were deduced from both the transmission and capture data and are listed in Table A-2. The 30.48-cm length of the samples introduced a large uncertainty in the flight path, thus producing complex capture line shapes; thus, resonance energies based on the capture data have larger uncertainties than those based on the transmission data. Where the isotopic assignment is uncertain, or is composed of more than one isotope, all possible isotopes are listed. The capture areas $e_i A_\gamma/N = \int e_i Y_i/N dE$, integrated over the resonance, are also listed in Table A-2. The errors for these last quantities are essentially equal to the quadrature sum of the normalization error of ≈10% and the errors in e_i; the counting statistical errors are negligible in comparison.

Included in Table A-2 are the resonance parameters reported by Mann et al.[4] Their resonance at 106 eV has been resolved into two resonances: one in ^{80}Kr and the other in ^{78}Kr. Their resonance at 640 eV with uncertain assignment we find to be actually three resonances: a doublet in ^{82}Kr and one in ^{78}Kr (possibly ^{80}Kr). Their resonance at 233 eV for ^{83}Kr has been found to consist of three resonances: one ^{83}Kr, and two in ^{83}Kr, ^{84}Kr, or ^{86}Kr. Their reported resonance at 580 eV in ^{84}Kr was not seen in this experiment and we conclude that it does not exist, for if it did and had their assigned parameters, it would have been strongly visible. Many other resonances were seen for the first time in this experiment.

A measure of neutron absorption in a reactor is the capture resonance integral, which, for single level Breit-Wigner contributions, is given (in barns) by:

$$I_\gamma = \int(\sigma_\gamma/E)dE = 4.1\ (10^6)\ [(A+1)/A]^2 \sum[(\Gamma_n\Gamma_\gamma)/\Gamma E_o^2)]$$

summed over the resolved resonances. The capture resonance integral for the energy region from 20 eV to 1200 eV is determined in this experiment to be 20 ± 1 barns for ^{78}Kr and 56 ± 7 barns for ^{80}Kr. This is compared with the I_γ's of 5.3 ± 2.3 barns and 56.1 ± 5.6 barns listed in BNL-325[5] respectively for ^{78}Kr and ^{80}Kr. It is the 108.4 eV resonance in ^{78}Kr, seen for the first time in this experiment, that produces the large value of I_γ for ^{78}Kr, this resonance providing over 70% of the capture resonance integral.

Table A-1

Sample Compositions and Relative Capture Detector Efficiencies

Isotope (i)	Sample Composition (a/o)		Sample Thickness (10^{-3} a/barns)		e_i
	ENRICHED	ELEMENTAL	ENRICHED	ELEMENTAL	
78	50.99	0.35	0.4341	0.00738	0.81±0.12
80	40.98	2.27	0.3489	0.0478	0.75±0.11
82	6.19	11.56	0.0527	0.2436	0.69±0.05
83	1.00	11.55	0.00849	0.2434	1
84	0.841	56.90	0.00716	1.199	0.64±0.12
86	<0.01	17.37	<0.00009	0.3660	0.32±0.13
		N =	0.851	2.11	

Table A-2

Krypton Resonance Parameters

E_o (eV)	Isotope (i)	Γ_n (eV)	Γ_γ (eV)	e_iA_γ/N (barns-eV)	
				ENRICHED	ELEMENTAL
28.05±.02	83	*045±.001	.21±.05	39	300
**27.9 ±.3	83	*067±.01	.22±.06		
39.63±.06	82	.124±.002	+.23±.05	270	320
**39.8 ±.5	82	.091±.012			
89.2 ±.5	80			14	
106.0±.1	80	.44±.01	+.23		100
**106. ±2.	80	.336±.030	.29±.03		
108.4±.1	78	.049±.003	+.23		
171.9±.5	78,80			19	
229.2±.5	83				
232.2±.5	83,84,86				
235.1±.5	83,84,86				
**233. ±6.	83	*.29±.04	+.20		
314. ±1.	83				70
450.9±.2	78	.23±.03	+.23	500	
478. ±2.	#Kr			9	
515. ±2.	83				70
**519. ±2.	84	.345±.070	+.20		
580. ±20.	NOT OBSERVED IN THIS EXPERIMENT				
**580. ±20.	84	.087±.020			
640. ±2.	++(78)	1.5±.5	+.23		30
**640. ±25.	78	1.5±.3			

Table A-2
(continued)

E_o (eV)	Isotope (i)	Γ_n (eV)	Γ_γ (eV)	$e_i A_\gamma / N$ (barns-eV) ENRICHED	ELEMENTAL
**640. ±25.	80	1.0±.2	+.20		
646. ±2.	82				
657. ±1.	82				
716. ±3.	#Kr			15	
810. ±2.	83,84,86				31
927. ±1.	80	2.3±.2	+.23	464	48
983. ±7.	#83,84,86				
1042. ±7.	++(78)			433	

E_o (eV)	Isotope (i)	E_o (eV)	Isotope (i)	E_o (eV)	Isotope (i)
1100.±2.	++(83)	2120.±20.	#82,83,84,86	3580.±50.	#78,80
1136.±5.	#78,80	2160.±10.	#78,80	3946.±50.	#78,80
1164.±8.	#83,84,86	2224.±15.	#82,83,84,86	4110.±50.	#78,80
1240.±15.	#78,80	2263.±15.	#78,80	4260.±50.	#78,80
1407.±2.	#84,86	2323.±15.	#82,83,84,86	4430.±50.	#78,80
1466.±2.	80	2357.±15.	#78,80	4640.±50.	#78,80
1481.±3.	83,84,86	2416.±15.	#Kr	4830.±50.	#78,80
1500.±2.	80	2440.±15.	#Kr	5330.±50.	#Kr
1550.±20.	#82,83	2593.±18	#78,80	5382.±50.	#78,80
1605.±10.	#82	2700.±20.	#78,80	5660.±50.	#83,84,86
1659.±3.	++(82)	2800.±20.	#82,83,84,86	6410.±50.	#Kr
1668.±3.	83,84,86	2850.±20.	#78,80	6470.±50.	#Kr
1675.±3.	80	2945.±20.	#78,80	6870.±50.	#Kr
1878.±6.	++(80)	3090.±50.	#78,80	7110.±50.	#78,80
1923.±15.	#83,84,86	3322.±50.	++(82)	8060.±50.	#78,80
2045.±10.	80	3455.±50.	#78,80	8360.±50.	#82,83,84,86

* $2g\Gamma_n$ for ^{83}Kr

** Mann et al.[4]

\+ Assumed value

++ Most probable assignment

\# More than one resonance

1. S. E. Atta and J. A. Harvey, "Numerical Analysis of Resonances," ORNL-3205, Oak Ridge National Laboratory (1964).

2. R. W. Hockenbury, W. R. Moyer, and R. C. Block, Nucl. Sci. Eng. 49, 153 (1972).

3. R. W. Hockenbury, Z. M. Bartolome, J. R. Tatarczuk, W. R. Moyer and R. C. Block, Phys. Rev. 178, 1746 (1969).

4. D. P. Mann, W. W. Watson, R. E. Chrien, R. L. Zimmerman and R. B. Schwartz, Phys. Rev. 116, 1516 (1959).

5. S. F. Mughabghab and D. I. Garber, BNL-325, 3rd ed., Brookhaven National Laboratory (1973).

2. The Neutron Total Cross Section of ^{232}Th from 0.1 eV to 18 eV (Little, Block, Harris and O. N. Carlson (Ames Laboratory))

The neutron total cross section of ^{232}Th was investigated from approximately 0.006 eV to 18 eV at the RPI Gaerttner Laboratory. Transmission measurements were made using the 100-MeV electron linear accelerator and the time-of-flight method.[1] The total cross section was found to differ significantly from ENDF/B-IV[2].

Neutron extinction effects are observed in the transmission results at energies below ≈0.05 eV. Extinction[3,4] is a microcrystalline effect which causes a reduction in the coherent Bragg scattering and causes structure in the observed cross section due to separate peaked contributions from each set of lattice planes. The reduction in coherent scattering leads to an increase in transmission, and hence a decrease in the deduced cross section. It is felt that the useful range of these data is limited to energies greater than ≈0.1 eV where extinction effects are expected to be negligible.

The total cross section results above 0.1 eV are plotted in Figure A-3, along with the evaluated data of ENDF/B-IV and a multilevel fit to the measured cross section. The statistical uncertainty of each measured datum point is $\lesssim$1%. It can be seen that ENDF/B-IV underpredicts the measured results by 5 to 10% in the energy range from 0.1 eV to 10 eV. (The discontinuity at 10 eV in ENDF/B-IV occurs at the change from point cross section representation to resonance parameter representation.)

The program MLEVL[5] was used to calculate the fit to the experimental results. All positive energy resonance parameters were taken from ENDF/B-IV. A picket fence distribution of negative energy levels was also included, starting two average level spacings from the first positive energy s-wave level at 21.78 eV. The ENDF/B-IV average values of $\bar{D}$ = 17 eV, Γ_γ = 24 meV and $\Gamma_n{}^o$ = 1.2417 meV were used for these picket fence levels. The scattering radius was increased from the 8.9874 f value of ENDF/B-IV to a more recent value of 9.65 f[6]. The energy and reduced neutron width of the first negative energy level were allowed to vary in order to fit the experimental results as well as provide consistent values of the thermal capture and scattering cross sections; MLEVL results are plotted in Figure A-3 for first negative energy level parameters of E_o = -2.5 eV, Γ_γ = 25.9 meV and $\Gamma_n{}^o$ = 0.3638 meV. This selection of parameters leads to a total cross section which passes through the experimental points from about 0.2 to 10 eV and which exceeds the experimental data by $\leq$1.5% below 0.2 eV and $\leq$2.0% above 10 eV. The thermal capture and scattering cross sections determined from these parameters are 7.39 b and 12.89 b, as compared respectively to the BNL-325[7] values of 7.40 $\pm$ .08 b and 12.67 $\pm$ .08 b.

In summary, the measured ^{232}Th total cross section is 5 to 10% greater than ENDF/B-IV from 0.1 to 10 eV and 35 to 40% greater than ENDF/B-IV from 10 to 18 eV. The measured cross section can be fit over this energy range with multilevel resonance parameters which also fit the thermal capture and scattering cross sections.

---

1. R. W. Hockenbury, Z. M. Bartolome, J. R. Tatarczuk, W. R. Moyer, and R. C. Block, Phys. Rev., 178, 1746 (1969).

2. ENDF/B-IV, National Nuclear Data Center, Brookhaven National Laboratory.

3. D. J. Hughes, Pile Neutron Research, Addison-Wesley, 1953, pp. 249-254, 270-272.

4. R. S. Carter, H. Palevsky, V. W. Myers, and D. J. Hughes, Phys. Rev., 92, 716 (1953).

5. S. H. Kim, D. R. Harris, and R. C. Block, "Practical Multilevel Cross Sections in the Envelope of R-Matrix Prediction," Proc. of Int'l Conf. on Neut. Phys. and Nucl. Data for Reactors and Other Applications, Sept. 25-29, 1978, Harwell.

6. K. Kobayashi, Y. Fujita, T. Oosaki, and R. C. Block, NSE, 65, 347 (1978).

7. S. F. Mughabghab and D. I. Garber, "Neutron Cross Sections, Volume 1, Resonance Parameters," BNL-325, 3rd ed., Brookhaven National Laboratory (1973).

3. ^{238}U Resonance Self-Indication Capture Measurements and Analysis (Block, Harris, Kim and Kobayshi*)

This experiment has been completed and a report bearing this title has been issued by the Electric Power Research Institute as EPRI NP-996, February, 1979.

4. A Hemispherical Fission Ion Chamber Developed for ≤1 μg Samples (Bicknell**, Block and Nakagome*)

A hemispherical fission ion chamber and associated electronics system has been designed to measure the fission cross section from 1 eV to 100 keV of fissile samples weighing 1 μg or less.[1] The chamber was developed for use with Rensselaer Polytechnic Institute Gaerttner Laboratory 75 ton lead Rensselaer Intense Neutron Spectrometer (RINS), and was tested with 1 μg of both ^{252}Cf and ^{235}U.

The hemispherical chamber was designed to be utilized with the heavy actinides, which exist only in small quantities. The chamber is effective in these conditions because of small sample size, high neutron flux, and α-pile up suppressing geometry. In the measurement of fission cross sections, the problem of α-pile up has been shown[2] to be partially remedied by using a spherical plate ion chamber, and making use of pulse height discrimination. This is accomplished by maximizing the ratio of fission fragment pulse height to alpha pulse height, by adopting a spherical geometry, and should lead to a high degree of α-rejection.

The present chamber is made of machined aluminum, stainless steel, ceramic, and teflon. The inner hemisphere is formed from a stainless steel rod 0.64 cm in diameter. The outer hemisphere has a 1.10-cm inside dia., and is made of aluminum. The chamber is filled with pure CH_4 gas at 1 atm pressure, and biased at 200V. The chamber was tested with 1 μg of ^{252}Cf, and was shown that, under operating conditions the electronic gain shift due to the "gamma" flash (associated with the linac electrons hitting the target) corresponded to a shift of ≤5% of the mean fission fragment pulse height at 1 μs after the gamma flash.[3]

---

* Kyoto University Research Reactor Institute, Kumatori, Japan

** Now at Combustion Engineering, Windsor, Conn.

The chamber was subsequently used in an attempt to determine the fission cross section of ^{235}U from 1 eV to 100 eV. The inner hemisphere was coated with 1 μg of 93% enriched U. The measurement was performed with 950 watts average power on the Ta photo neutron target, and the total data collection time was less than 5 hours.

The data were reduced to relative fission cross section vs. neutron energy, and then the cross section was normalized to the resolution-broadened ENDF/B-IV cross section over the energy range 10 eV to 10^4 eV. These two results are plotted together in Figure A-4. Upon examination of Figure A-4 it is apparent that, except for the high and low energy extremes, there is good agreement between the data obtained in RINS and the resolution-broadened ENDF/B-IV cross section. All the major resonances structure is accurately represented by the histograms.

The first area of disagreement occurs between energies of 2.4 eV where, although the RINS data has the same peak value as the ENDF/B-IV data, the RINS data do not fall to as deep minima on either side of the peak as the ENDF/B-IV data. This implies that the resolution of the RINS spectrometer may not be as narrow as expected[4] at neutron energies below 10 eV.

The other region of disagreement between the experiment and the ENDF/B-IV results occurs above 10 keV. In this energy region there is little if any structure in the ^{235}U fission cross section and the cross section just falls off with energy at a more or less uniform rate. The difference between the RINS and ENDF/B-IV data is in two small dips which occur at ≈30 eV and ≈80 keV. The aluminum that makes up the bulk of the chamber is suspected to be the cause of these dips above 10 keV, where aluminum has two broad scattering resonances, one at 35 keV and the other at 88 keV. Since there is so much aluminum in the chamber (i.e., the chamber has 0.64-cm-thick aluminum walls) these scattering resonances could have a profound effect upon the neutron flux by scattering the neutrons at these energies away from the chamber. This in turn would lead to a flux depression at these energies which would result in a lower apparent fission cross section.

The hemispherical fission chamber produced results in generally good agreement with the ENDF/B-IV cross section. It is thought that this chamber could give acceptable results with extremely α-active samples weighing fractions of a microgram, just by increasing the electron linac power and lengthening the data collection time.

---

1. P. A. Bicknell, "A Hemispherical Fission Ion Chamber Designed for <1 Microgram Samples", Master's Thesis, RPI, 1977.

2. J. W. T. Dabbs, N. W. Hill, E. E. Bemis, B. Raman, "Fission Cross Section Measurements on Short Lived Alpha Emitter", NBS Spec. Publ., 425, 1975.

3. P. A. Bicknell, R. C. Block, Y. Nakagome, G. Krycuk, "A Fission Chamber for Cross Section Measurements with ≤ 1 μg Samples", Bull. Amer. Phys. Soc., 22, 646, 1977.

4. R. E. Slovacek, D. S. Cramer, E. B. Dean, J. R. Valentine, R. W. Hockenbury, R. C. Block, "^{238}U (n,f) Measurements Below 100 keV", Nucl. Sci. and Eng., 62, 445, (1977).

1 eV ～ 100 keV での ^{245}Cm(n,f) 断面積測定

Measurement of the ^{245}Cm(n,f) Cross Section from 1 eV to 100 keV

京大炉，RPI* 　○中込良広，Robert C. BLOCK*
KUR 　Yoshihiro Nakagome,

原子炉燃料要素内の重アクチノイド核種の蓄積量を予想する上で，超プルトニウム核種の中性子反応断面積を知る事は不可欠である。ここでは ^{252}Cf 生成過程のうちで重要な核種の1つである ^{245}Cm の(n,f)反応に注目し，データの非常に少ない 1eV～100 keV 領域での核分裂断面積(σ_f)を測定したので報告する。実験は RPI－Linac と鉛減速スペクトロメータ(RINS)[1] を組合わせた強中性子源を用い，中性子減速時間測定法により微量の ^{245}Cm 試料で行なった。
The experiment was carried out by using RPI 100 MeV Linac and a lead slowing-down spectrometer (RINS).

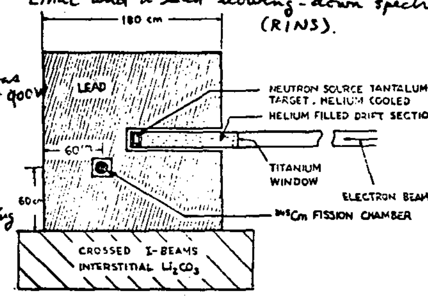

第1図　実験配置
Fig. 1. Experimental Set up

実験配置を第1図に示す。Ta ターゲットでのビーム出力は約 900 W であった。検出器は LLL で使用したものを譲り受けたイオンチェンバで，^{245}Cm 試料は約 3.25 μg，チェンバ内は1気圧のメタンガス充てんで用いた。検出器位置での中性子束(n/cm²/sec/eV)は，1～20 eV で $\phi(E) \propto E^{-0.638}$，20 eV 以上で $\phi(E) \propto E^{-0.775}$ で表わされる。[2] データは PDP-7 に蓄積された。σ_f の値は，1.4 eV～17.8 eV の間で Browne ら(LLL)の値[3] に規格した。
Experimental set up is shown in Fig. 1. beam power was about 900 W. Cm sample was about 3.25 μg. Inside of the chamber was filled with 1 atm. methane gas. neutron flux. σ_f-value was normalized to Browne's data between 1.4 eV and 17.8 eV.

測定結果　実験結果を次の2つのデータと比較した。① 1～20 eV 領域：Browne ら，20 eV～100 keV 領域：Moore ら(LASL)の実験値[4]，及び ② JENDL－2。比較は，これらのデータに関し RINS のエネルギ分解能($\Delta E/E$)＝0.39 を考慮して計算した値を用いて行ない，その結果を第2図に示す。20 eV 以下での Browne らの結果との不一致は，単なるエネルギ分解能だけの問題では説明できず，現段階では不明である。100 eV 付近における σ_f は，そのエネルギ依存性から見て，JENDL－2 より Moore らの結果に近い。又 50 keV 以上では Moore らの結果と大きな相違が見られた。
results. Below 20 eV, we can not explain the difference between Browne's data and our results by energy resolution of RINS.

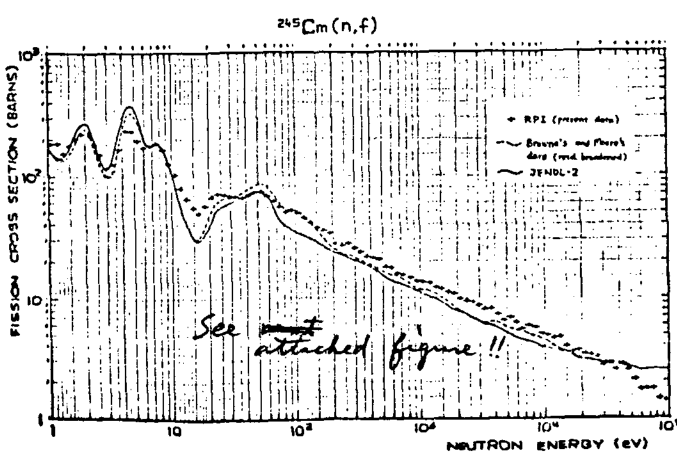

第2図　^{245}Cm 核分裂断面積　neutron-induced fission cross section for ^{245}Cm

JENDL－2 の使用に際し原研 五十嵐，中川 両氏の御好意に依る所大にて，感謝致します。

1) Rensselaer Intense Neutron Spectrometer
2) R.E. Slovacek et al., NSE 62 455 (1977)
3) J.C. Browne et al., NSE 65 166 (1978)
4) M.S. Moore & G.A. Keyworth, P.R. C3 1656 (1971)

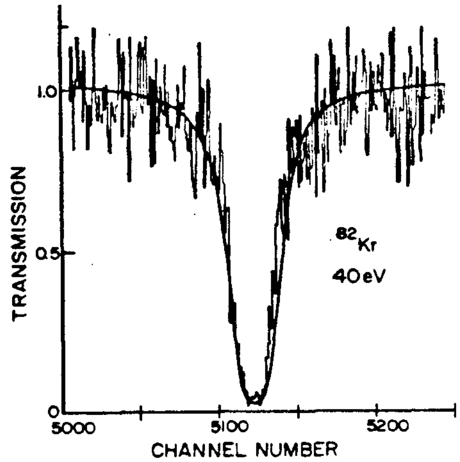

Fig. A-1 Transmission Data and Harvey-Atta Fit for Elemental Kr Sample

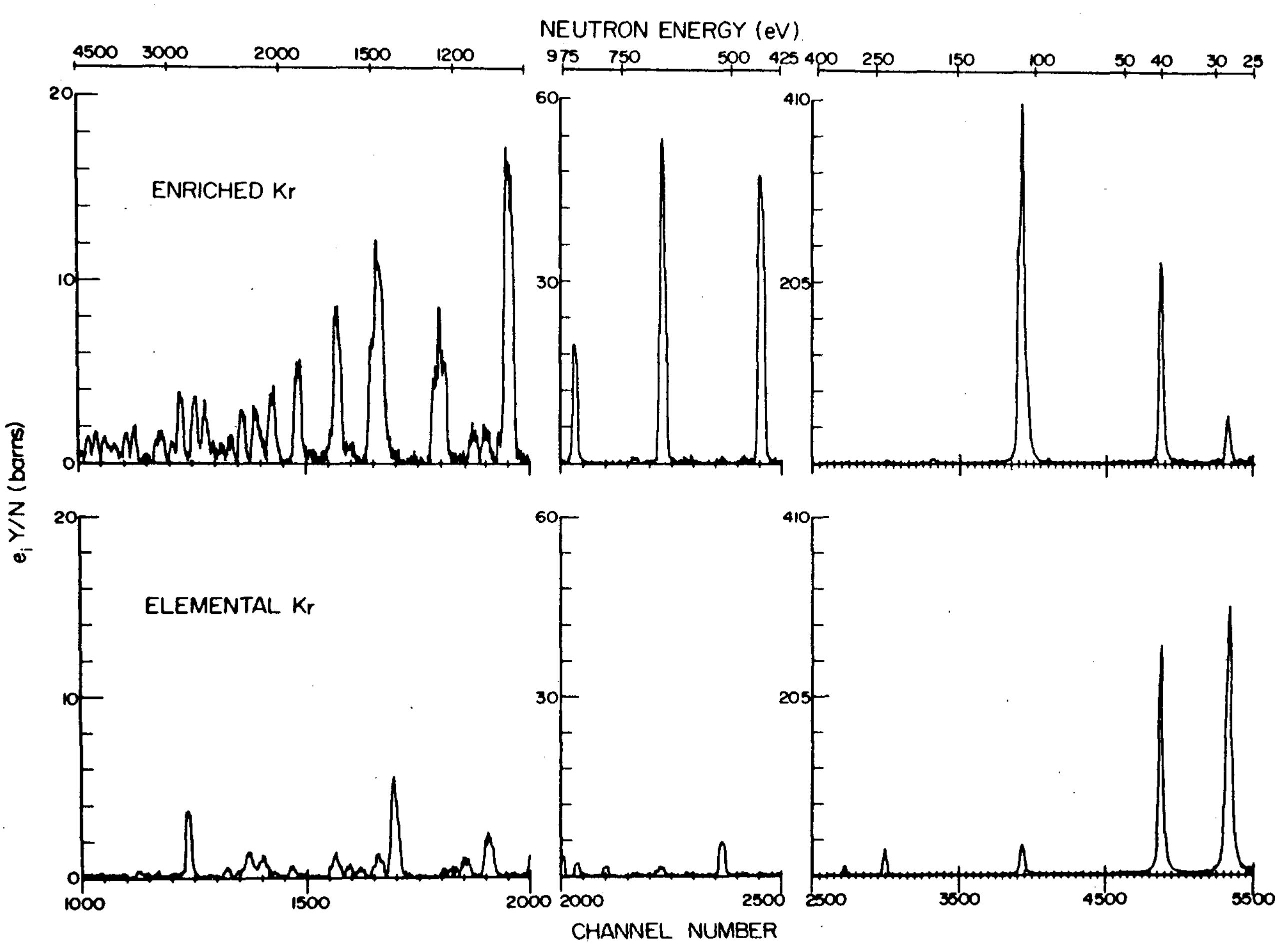

Fig. A-2 Neutron capture yield Y times e_i divided by sample thickness N vs. tof channel number for enriched and elemental samples of krypton

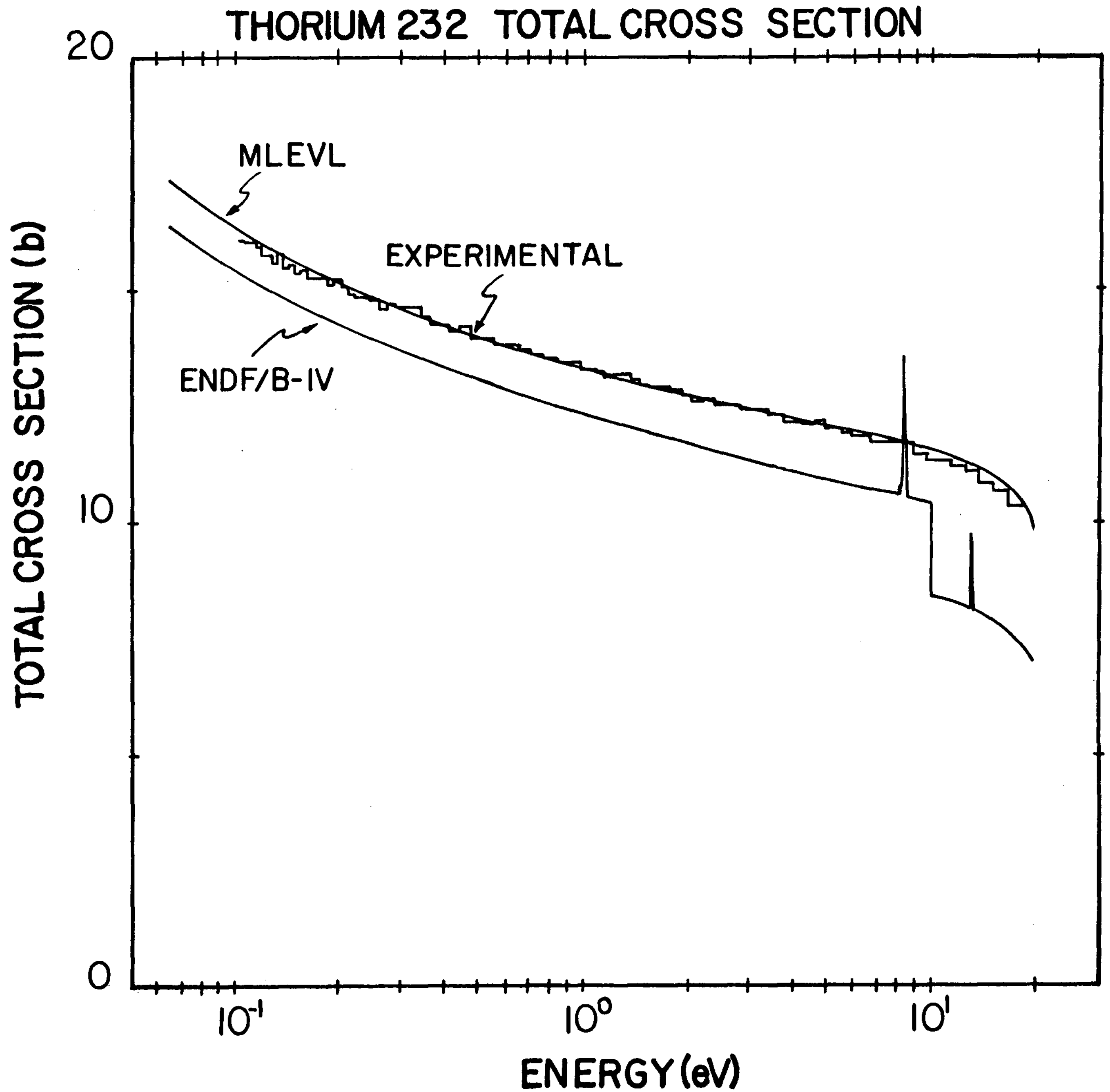

Fig. A-3 The neutron total cross section of ^{232}Th from 0.1 to 18 eV

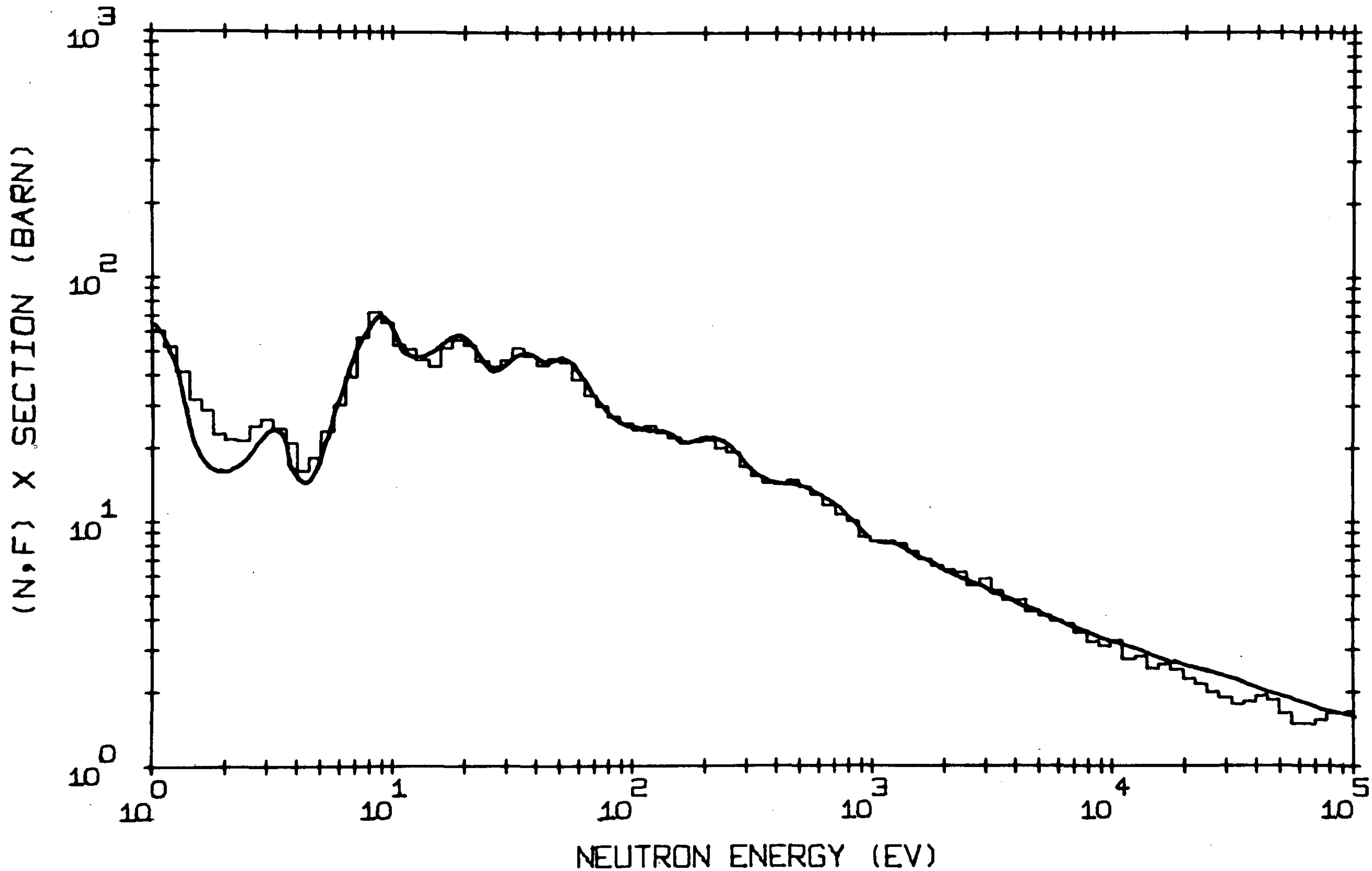

Fig. A-4 The $^{235}U(n,f)$ cross section from 1 eV to 100 keV. The RINS data are represented by the uniform-lethargy histograms and the resolution-broadened ENDF/B-IV data by the smooth curve

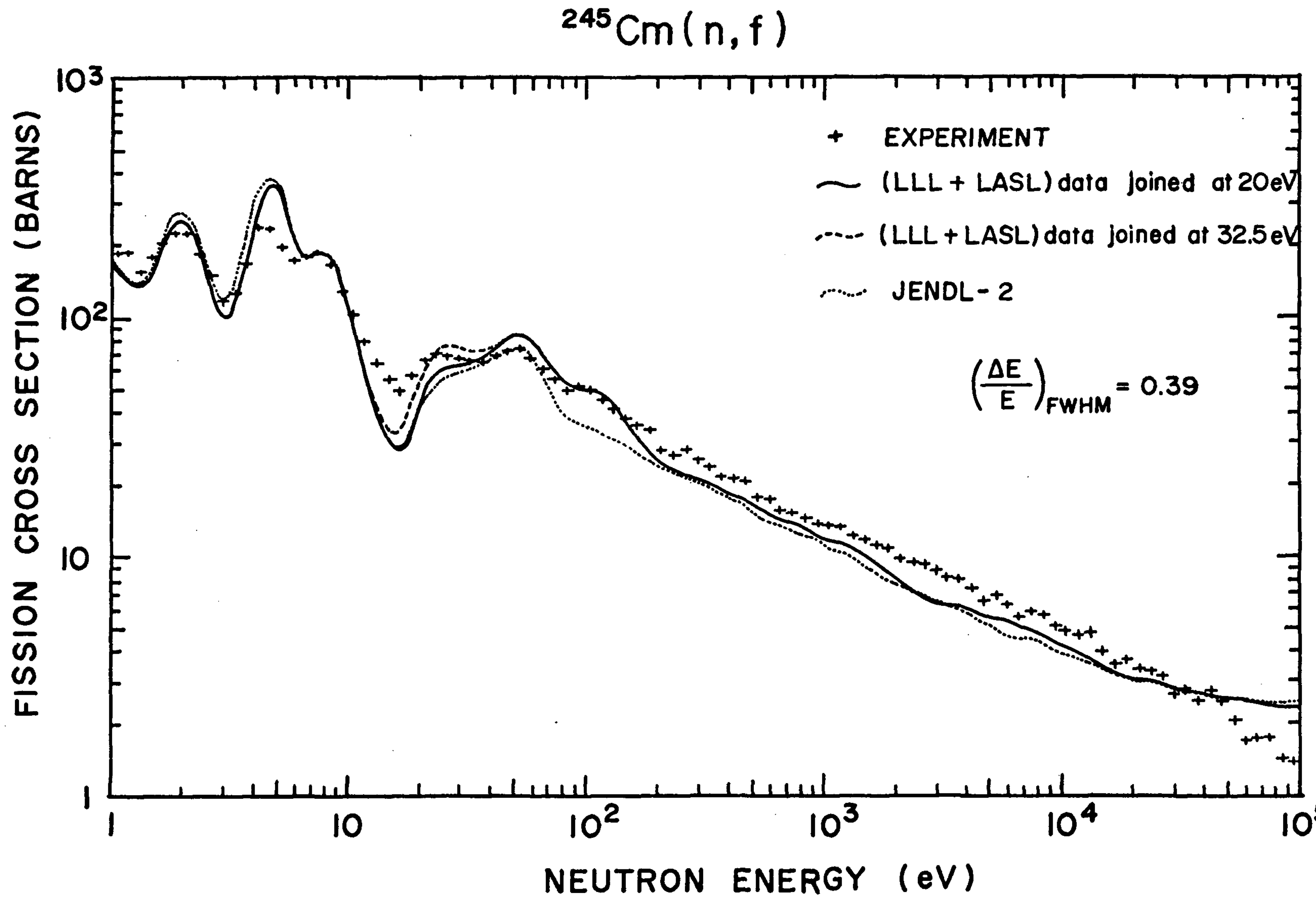

Fig. A-5 The $^{245}Cm(n,f)$ cross section from 1 eV to 100 keV

B. INTEGRAL CROSS SECTIONS

1. Neutron Spectra Measurements Upon Thoria (Block, Becker, (Harris, Malaviya, Bokharee, Hayashi* and Yamamoto*)

A cooperative program between Kyoto University and RPI is underway to measure the neutron spectra in a ThO_2 assembly. The 0.6-m-dia. spherical assembly containing 300 kg of ThO_2 that was constructed at the Kyoto University Research Reactor Institute (KUR)[1] was shipped to RPI along with a borated-graphite prism assembly, a ^6Li glass detector, a proton-recoil detector and a cylindrical lead photoneutron target of the same design used at KUR.

Neutron angular distribution measurements have been carried out with the KUR 5-cm-dia. by 5-cm-high cylindrical lead target at electron energies of 32 and 63 MeV using the $^{27}Al(n,\alpha)^{24}Na$ and $^{58}Ni(n,p)^{58}Co$ threshold reactions. At 32 MeV, an energy approximately equal to the electron energy used for spectra measurements at KUR, the corners of the lead cylindrical target introduced a depression in the angular distribution near 45^o and 135^o, and the departure from isotropy was ≈30% and ≈25% respectively for the $^{27}Al(n,\alpha)^{24}Na$ and $^{58}Ni(n,p)^{58}Co$ reactions. At 63 MeV the angular distribution was also depressed near 45^o and 135^o, with departures from isotropy of ≈50% and ≈16% respectively for the $^{27}Al(n,\alpha)^{24}Na$ and $^{58}Ni(n,p)^{58}Co$ reactions. As a result of this observed anisotropy in the high-energy neutron angular distribution, a Ta spheroidal target was designed and constructed for the ThO_2 spectra measurements (as described in the following report B.2).

Neutron spectrum measurements have been carried out upon the bare Ta target, the ThO_2 assembly and the boron-graphite assembly. For the high energy measurements the 100-m flight station was used with both the RPI 51-cm-dia. by 13-cm-thick and the KUR 13-cm-dia. by 13-cm-thick liquid scintillator proton-recoil detectors. For the low energy measurements the RPI 30-cm-dia. by 5-cm-thick ^{10}B-Vaseline and the KUR 13-cm-dia. by 1.3-cm-thick ^6Li glass detectors were used at the 30-m flight station. The data are being reduced to neutron spectra.

1. H. Nishihara, I. Kimura, K. Kobayashi, S. A. Hayashi, S. Yamamoto and M. Nakagawa, "Measurement and Analysis of Neutron Spectrum in Spherical Pile of Thoria", J. of Nucl. Sci. and Tech. 14, 426 (1977).

* Kyoto University Research Reactor Institute, Kumatori, Japan

2. Photoneutron Target Design for Fast Neutron Spectrum Measurements (Bokharee, Emmett, Block, Harris, Hayashi* and Yamamoto*)

A new photoneutron target has been designed and tested for use in fast neutron spectrum measurements on a large homogeneous assembly of thoria (ThO_2). The analysis and interpretation of such measurements for extracting improved thorium data requires a target which yields a uniform angular distribution of emergent photoneutrons. A cross section of the new target is shown in Figure B-1. The design of this air-cooled spheroidal tantalum target involves a compromise in maintaining an isotropic emergent neutron yield while at the same time reducing forward-directed bremsstrahlung from leaving the target and entering the thoria under bombardment by electron beams of 30 and 64 MeV. It is found that the new design yields both greater permissible input power and a nearly isotropic neutron angular distribution as compared with a 5-cm-high lead cylindrical target. Integral measurements on the thoria pile using this target are currently under way.

3. Sensitivity Analysis (M. Becker and D. R. Harris)

Sensitivity analysis has been developed and applied for relating uncertainties in nuclear data to uncertainties in fuel cycle cost and in other parameters related to the fuel cycle. A report, "Sensitivity of Nuclear Fuel Cycle Cost to Uncertainties in Nuclear Data," EPRI NP-985, was issued in February 1979. Extensions of this work have been made to other fuel cycle parameters, such as resource requirements, and to a variety of fuel cycle options - eighteen month cycles, alternate fractional core loading, alternate recycle options, thorium-related cycles, and heavy water reactors. In addition, analogous work has been done for fast breeder reactor uncertainties.

4. Measurement of $^{245}Cf(n,f)$ from 1 eV to 100 keV---Y (Y. Nakagome* and R. C. Block)

The fission cross section of ^{245}Cf has been measured with the RINS system from approximately 1 eV to 100 keV. The data were taken with the fission chamber containing 3.2-μg of ^{245}Cm that was used in the measurement of LLL by Browne et al.[1] The data are shown in Figure A-4 along with the experimental LLL data[1] and LASL data of Moore and Keyworth[2] and the evaluated data JENDL-2[3]. The RINS gaussian resolution function of $\Delta E/E \approx 0.39$ FWHM was used to broaden the LLL, LASL and JENDL-2 data. The RPI data have been normalized to the LLL results.

---

* Kyoto University Research Reactor Institute, Kumatori, Japan

The RINS data exhibit the structure seen in the resolution-broadened LLL data, although below ≈15 eV the RINS peaks and valleys are not as pronounced. This is probably caused by an underestimate of the RINS resolution width in this low-energy region. Between ≈20 eV and ≈40 keV the RINS data are similar to the LASL data, but above ≈40 keV the RINS data continue to decrease compared to the leveling off of the LASL data. At 100 keV the RINS cross section is about one half of the LASL cross section.

---

1. J. C. Browne, R. W. Benjamin and D. G. Karraker, Nucl. Sci. Eng. 65, 166 (1978).

2. M. S. Moore and G. A. Keyworth, Phys. Rev. C3, 1656 (1971).

3. S. Igarashi and T. Nakagawa, Japan Evaluated Nuclear Data Library-Version 2.

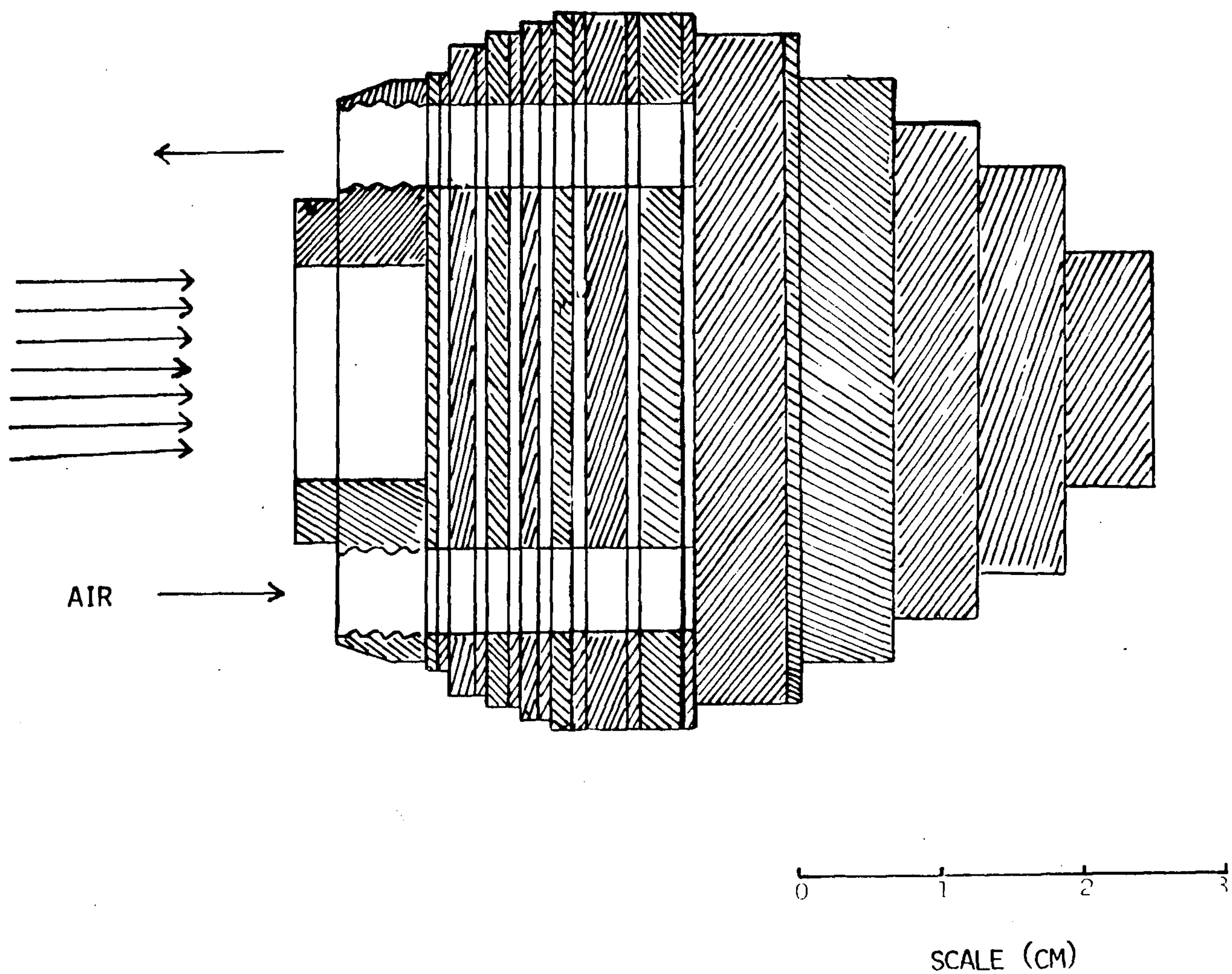

Fig. B-2 The spheroidal air-cooled tantalum target designed for the ThO_2 assembly measurements

TRIANGLE UNIVERSITIES NUCLEAR LABORATORY

A. NEUTRON PHYSICS (A. Beyerle, S.G. Glendinning, C.R. Gould, Sadiq El-Kadi, C.E. Nelson, F.O. Purser, L.W. Seagondollar, R.L. Walter)

The TUNL neutron scattering program emphasizes measurements of elastic and inelastic scattering of neutrons in the energy range 6 to 15 MeV from a variety of target nuclei. The early work concentrated on elastic and discrete inelastic neutron scattering from p-shell nuclei (Li, Be, B, C, O) with the $D(d,n)^3He$ source reaction. This work is essentially completed and is summarized in Section I. The main thrust of the present program is towards measurements of continuum neutron emission from heavier elements such as Fe, Ni, Cu. This work necessitated 1) the installation of a tritium gas target assembly, 2) construction of a second neutron shield and collimator, 3) design of a new beam leg, 4) a new electronics arrangement for the neutron detector system, and 5) a careful calibration of the efficiencies of the two detectors at low bias. These developments and our present experimental capabilities are described in Section II. The present status of our continuum measurements is summarized in Section III.

1. Discrete Elastic and Inelastic Scattering Angular Distribution Measurements.

a. Lithium-6 and Lithium-7

These results have been published in Nucl. Sci. and Eng. 69, 22 (1979).

Differential cross sections were reported for the elastic and discrete inelastic scattering of neutrons from ^6Li and ^7Li. Source neutrons were provided by the $^2H(d,n)^3He$ reaction in the energy range from 7 to 14 MeV. Scattered neutrons were detected at a distance of 3.9 m at angles from 25° to 160° in 5° intervals. Total cross sections for elastic scattering from ^7Li were obtained by integrating the differential cross sections. Inelastic scattering cross sections were obtained for the 2.18-MeV state in ^6Li and the 4.63-MeV state in ^7Li. The results were compared to ENDF/B-IV predictions and to previous measurements. Inelastic scattering to the 4.63-MeV state in ^7Li accounts for less than half of the total tritium production cross section for neutron interactions with ^7Li.

b. Beryllium-9

These results have been published in Nucl. Sci. and

Eng. 68, 38 (1978). Elastic scattering cross sections were obtained along with inelastic scattering cross sections for the sum of the 1.69-, 2,43-, 2.8- and 3.06-MeV states. Bombarding neutron energies were in the range 7 to 14 MeV and measurements were made in 1 MeV steps.

c. Boron-10 and Boron-11

These results are currently being readied for publication. Eight angular distributions were measured for incident neutron energies from 8 to 14 MeV. For ^{10}B, inelastic scattering to the 0.717-MeV state was only partially resolved from the elastic group. For ^{11}B, inelastic scattering to levels at 2.14, 4.46, and 5.04 MeV was observed.

The total elastic scattering cross sections for ^{10}B and ^{11}B are shown in figures A1 and A2 respectively. The crosses in fig. A1 are the sums of the elastic and the 0.717-MeV state inelastic scattering cross sections for ^{10}B. The crosses in fig. A2 are the sums of the elastic and 2.14-, 4.46 and 5.04 MeV state inelastic scattering cross sections for ^{11}B.

d. Carbon-12

These results were published in Nucl. Sci. and Eng. 61, 521 (1976) and consisted of 28 point angular distributions at 15 energies from 9 to 15 MeV for elastic and 4.43-MeV-state inelastic scattering.

e. Oxygen-16

These results are currently being corrected for multiple scattering. The measurement consists of 12 elastic scattering angular distributions from 9.25 to 15 MeV along with partial angular distributions for inelastic scattering for levels around 6 MeV in excitation in ^{16}O. Fig. A3 shows the total elastic scattering cross sections obtained for ^{16}O.

f. Iron-54 and Iron-56

In support of the continuum neutron emission studies, elastic and first excited states inelastic scattering angular distributions have been measured at 10 and 12 MeV neutron bombarding energy with isotopically enriched iron targets. Additional data at nearby energies will be obtained to complete this data set.

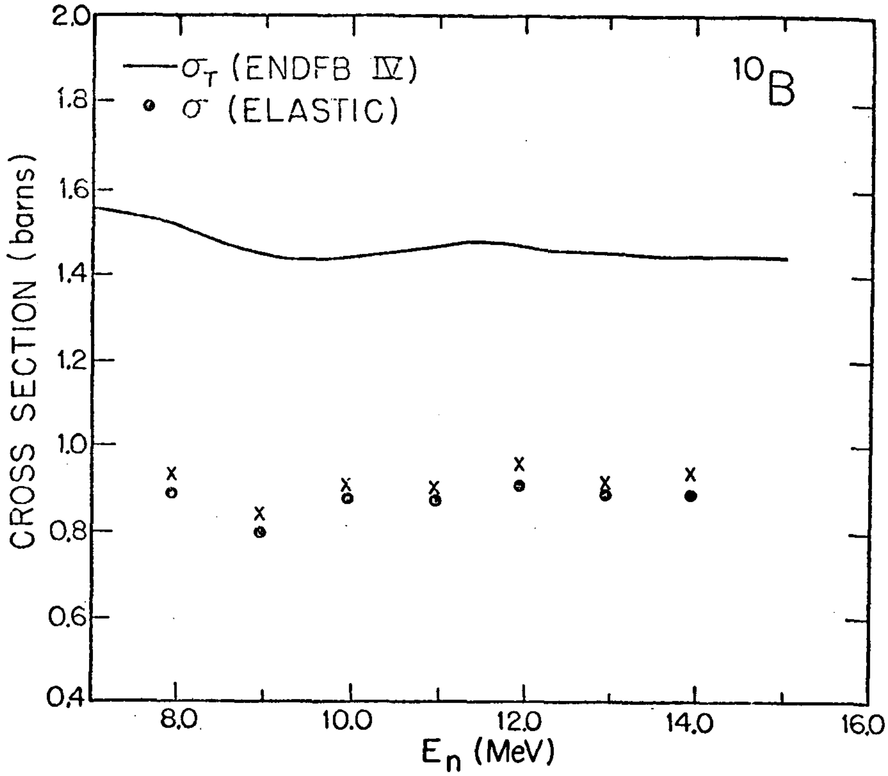

σ_T (ENDFB IV)
σ (ELASTIC)
^{10}B
CROSS SECTION (barns)
2.0
1.8
1.6
1.4
1.2
1.0
0.8
0.6
0.4
8.0
10.0
12.0
14.0
16.0
E_n (MeV)

Fig. A1

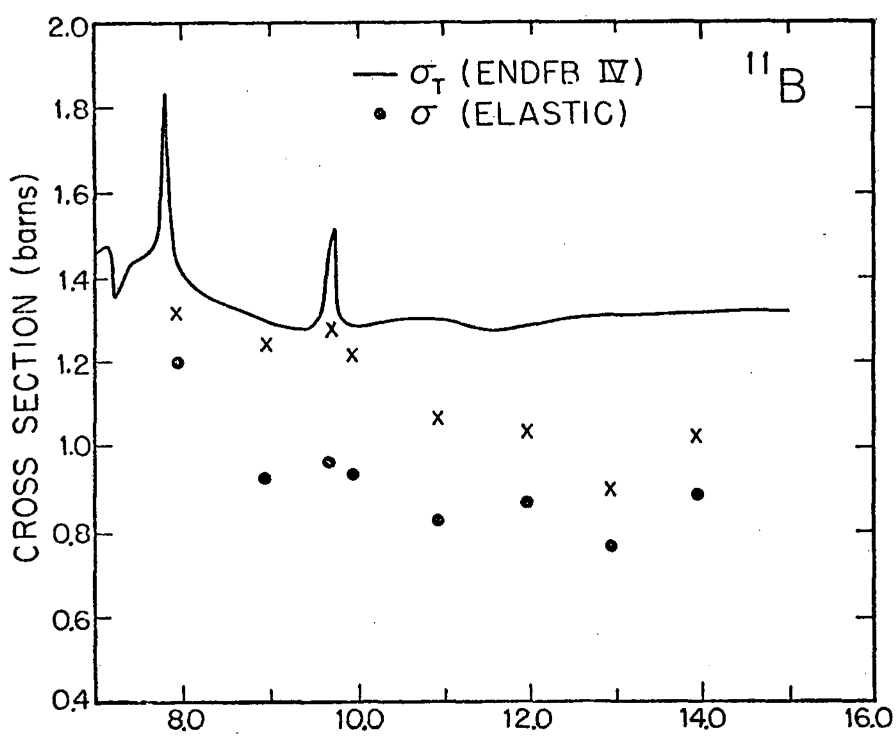

σ_T (ENDFB IV)
σ (ELASTIC)
^{11}B
CROSS SECTION (barns)
2.0
1.8
1.6
1.4
1.2
1.0
0.8
0.6
0.4
8.0
10.0
12.0
14.0
16.0

Fig. A2

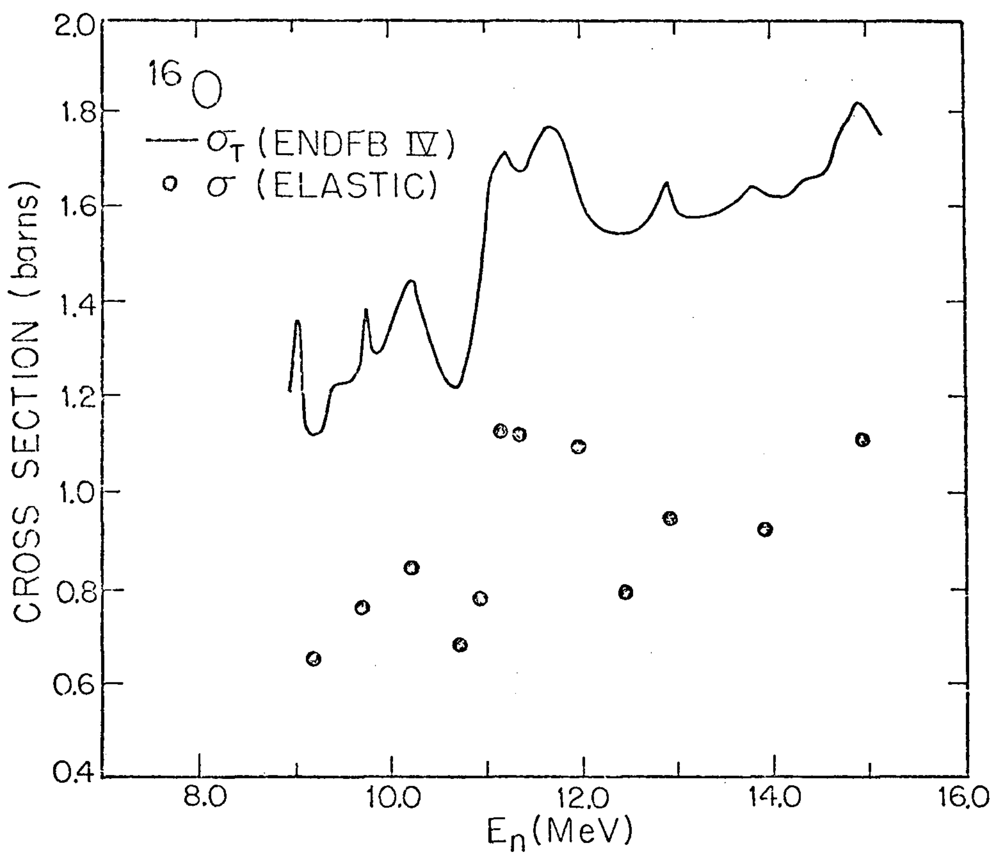
2.0
1.8
1.6
1.4
1.2
1.0
0.8
0.6
0.4
16O
σT (ENDFB IV)
σ (ELASTIC)
CROSS SECTION (barns)
8.0
10.0
12.0
14.0
16.0
En(MeV)

Fig. A3

2. Experimental Developments and Facility Improvements

a. Neutron Detector

The original TUNL detector was a 3" diameter NE-218 encased in a 5 ton shield which could be positioned a maximum of 4m from the scattering sample. An additional neutron shield and collimator now has been installed in the same target room. The new shield weighs approximately 6 tons and was constructed similar to the original shield acquired from Wright Patterson Air Force Base. Principal differences are that the detector is positioned to obtain additional shielding from the rear, additional lead has been added for increased γ-ray attenuation, and the collimation system is designed for a 5" diameter NE-218 scintillator. The angular and radial carriages for the shield allow measurements at angles between 0^{o} and 160^{o} and flight paths from 2.5m to 6m.

In addition to doubling our data acquisition rate, the additional flight path increases our energy resolution capability which allows better separation of closely spaced discrete groups. The additional shielding of the new detector is also beneficial in low bias measurements of continuum neutron emission.

b. New Time of Flight Beam Leg

In order to obtain maximum use of our two neutron detectors and also to allow optimum incorporation of tritium safeguards, a new beam leg has been constructed serving the neutron target area. This leg utilizes on existing 38.6^{o} part on the steering magnet immediately downstream from the tandem, and eliminated the former use of the two 90^{o} magnets and 70^{o} switching magnet. Beam optics for the new leg are much simpler than that of the former setup.

The new beam leg is again of all metal and ceramic construction, except for O-rings for vacuum gate valve seals. The system utilizes two 4" oil diffusion pumps plus a titanium sputtering pump to attain high vacuum. All pumping stations are vented to an outside stack located above the laboratory. A fast acting gate valve (5-9 milliseconds) actuated by a passive trigger device has been installed at the gas target cell. This short closure time will be sufficient to isolate all tritium within the neutron beam leg in the case of a target foil rupture.

c. Tritium Target Capability

In order to safely utilize gaseous tritium targets for neutron production in a university environment, extensive modifications of the neutron target room and associated vacuum equipment have been accomplished. Air handling equipment has been installed capable of cycling the air in the target room within a five minute period. Air is exhausted through a stack approximately 30' above the laboratory roof. All forepump exhausts are vented into the air exhaust system. Tritium levels in the air system are monitored and tritium readings above a preset level automatically activate room exhaust procedures. The tritium gas handling system and gas target cell are installed under a separately powered exhaust hood whose output is to the stack. The target room tritium monitor samples the air from this hood.

During tritium target operation, the forelines of all diffusion pumps are trapped with LN_2 activated charcoal traps which have the capacity to trap tritium released to the vacuum system. In addition to the diffusion pumps, a Ti sublimation pump is installed within 1 meter of the target cell. This pump has a pumping speed of 450 ℓ/sec for hydrogen which should reduce beam line contamination if pin holes develop in the target foil. All vacuum readings and tritium monitor readings are remoted to the tandem control room and manual overrides are provided to allow the experimenter to activate room exhaust and fast acting valve closure.

Fume hood storage facilities and a glove box for handling tritium contaminated components have been provided and are also exhausted to the monitored air system.

d. New Electronics Arrangement

The electronics for the neutron time of flight (TOF) detectors have been upgraded to take advantage of the superior pulse shape discrimination (PSD) capabilities of the Canberra Model 2160 NIM modules. The wide dynamic range of these units also permit operation at low bias settings without saturating the electronics for high energy recoil events.

A block diagram of the electronic setup for one of the four TOF scintillators is shown in Fig. A4. The anode signal from the photomultiplier is used for both PSD information and linear information. The single channel analyzer (SCA) in the ORTEC 490B is used for setting the bias level for the experiment. The constant fraction discriminator (CFD) strobes the PSD unit and also provides the start signal for a Canberra 1443 time-to-amplitude converter (TAC). The stop signal comes from the PSD unit which is operated in the $n + \gamma$ mode, and the SCA output of the TAC is used to select neutron and/or gamma ray events. A separate ORTEC 437A TAC is used for the neutron TOF measurement with the stop signal coming from a capacitive beam pick off. Any of the three signals--neutron TOF, neutron PSD, or the linear neutron energy signal can be gated through to an ADC subject to the logic requirements established in the ORTEC 418A universal coincidence unit.

Presently four neutron detectors are operational. The two main detectors are in the heavily shielded collimators, usually at flight paths of 4m and 6m respectively for measurements of elastic and discrete inelastic scattering. For low bias continuum measurements these detectors are moved in to flight paths of $\sim$ 3m. Two small scintillators are used to monitor the source reaction. One is at zero degrees at about 7m and is used to monitor timing variations in the pulsed beam. The other detector is mounted above the reaction plane at about 90^{o} and at a flight path of 2.0m. It is used for normalizing angular distribution measurements from angle to angle.

e. Detector Efficiency Studies

As a result of the new electronics setup and in preparation for low bias ($\sim$ 500 keV) measurements of continuum neutrons, new detector efficiency curves have been determined for the two main neutron detectors. Efficiencies for two bias settings were obtained by measuring the response functions of the detectors to monoenergetic neutrons produced by the D(d,n) and T(p,n) reactions. Angular distributions were measured for incident particle energies of 6.0 MeV and 10 MeV for the D(d,n) reaction and at 2.5 MeV, 5.0 MeV and 10 MeV for the T(p,n) reaction. The overlapping data sets spanned the neutron energy range from 300 keV to 13 MeV. The energy range was extended to 16.8 MeV by measuring 0^{o} excitation functions for the D(d,n)^{3}He reaction. All cross section data used to convert yields to efficiencies were obtained from the compilation by Drosg[1)] except for the 2.5 MeV T(p,n)^{3}He data which were taken from Liskien and Paulsen.[2)] Efficiency curves for the two bias conditions are shown in Fig. A5.

f. Computer Program Development for Neutron Data Correction

Considerable work has been invested in Monte Carlo data corrections programming for the neutron time-of-flight group. This activity proceeded toward three main objectives: (1) A general capability for correcting data for multi-element samples; (2) An extension of the methods in use for correcting elastic and discrete inelastic scattering data to the problem of correcting continuum scattering; (3) Reorganize the iterative correction procedure to make it more straightforward. Two codes, dubbed EFFIGY and EFFIGYC, came about as a result of the work.

---

1) M. Drosg, Nuclear Science and Engineering <u>67</u>, 190 (1978)

2) H. Liskien and A. Paulsen, Nuclear Data Tables, Vol. II, no. 7, 1973

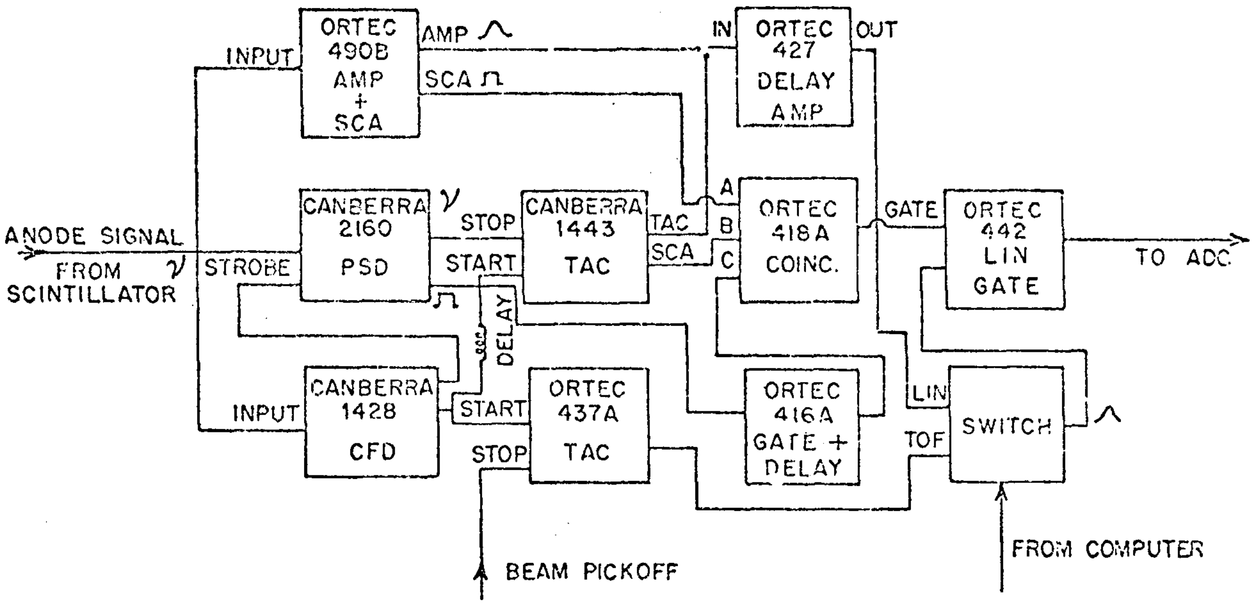

Fig. A4. Block diagram of the time-of-flight scintillator.

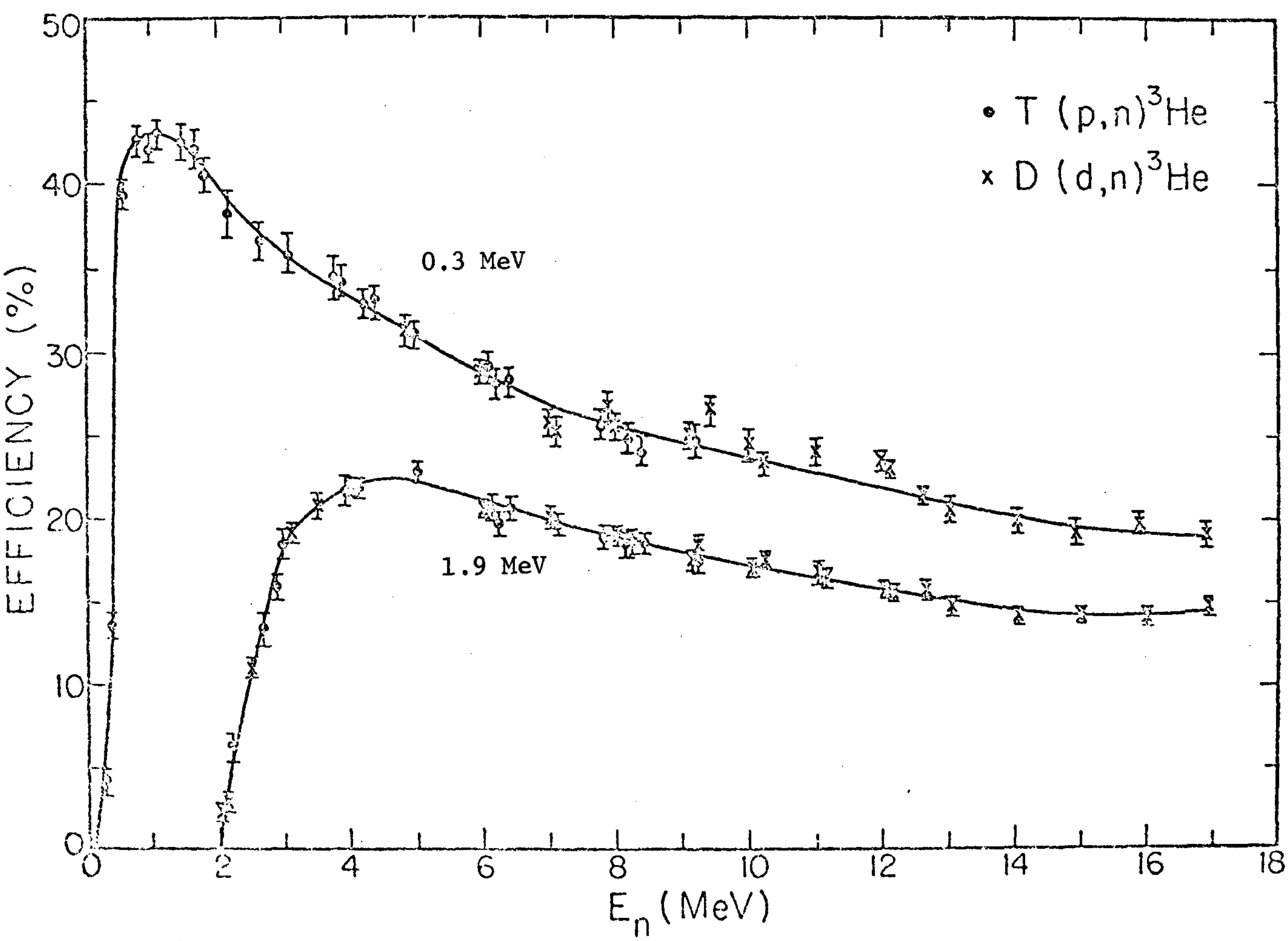

Fig. A5 Measured efficiency of NE-218 scintillator system.

Program EFFIGY is a reorganized version of the earlier program MC. Its purpose is to calculate attenuation, finite geometry, and multiple scattering effects for cylindrical samples of one or more elements. In the process of obtaining these corrections, differential cross-section libraries are input and time-of-flight spectra, analogous to the experimental spectra, are calculated and summed over the time windows used in the experiment. A facility for subtracting previously calculated "out-count" spectra from the calculated spectra before window summation has been included. Thus, secondary effects of truncation of the timing tails in summing experimental spectra and over- or under-subtraction of the "out-count" spectra are corrected.

Program EFFIGYC is a companion program for EFFIGY, using most of the same subroutines but designed to correct "continuum" scattering data. The program takes as input differential cross section libraries for scattering to states at excitations low enough to give distinct groups in the time-of-flight spectra. It then determines the energy distribution resulting from all other scattering processes, which (after correction for attenuation, finite geometry, and multiple scattering effects), gives the observed time-of-flight spectra. The removal from the scattering spectra of scattered gas breakup neutrons from the target cell has also been included in EFFIGYC. This code is still in the programming stages and has to be carefully checked out.

3. Neutron Continuum Measurements

For continuum neutron studies we are primarily concentrating on the low energy neutrons. The detectors are biased at 300 keV equivalent neutron energy. Flight paths of 2.7 m and 3.7 m are employed and the T(p,n) source reaction is used because of the reduced background of neutrons from three-body breakup in the gas compared to the D(d,n) reactions. Low bias measurements have been made at 5.9 MeV bombarding energy for ^{54}Fe, ^{56}Fe, Cu and Ni targets and at 9.1 and 10.1 MeV for the iron isotopes. Preliminary measurements have been made at 12 MeV for natural irons and copper samples. We have also taken some test data at 14 MeV using the T(d,n) reaction where the incoming deuteron beam is slowed down in a stopping foil prior to entering the tritium gas cell. This method permits one to take advantage of the large cross section for neutron production at the 100 keV resonance. For all measurements, except those at 14 MeV, we obtain four scattering spectra corresponding to tritium gas in with sample in and out, and tritium gas out (helium in) with sample in and out. An example of a time-of-flight spectra obtained by normalizing and subtracting these four scattering spectra is shown in Fig. A6. An energy spectrum, corrected for detector efficiency, is shown in Fig. A7. No correction for multiple scattering effects and the contribution of elastic scattering of gas breakup neutrons have been made.

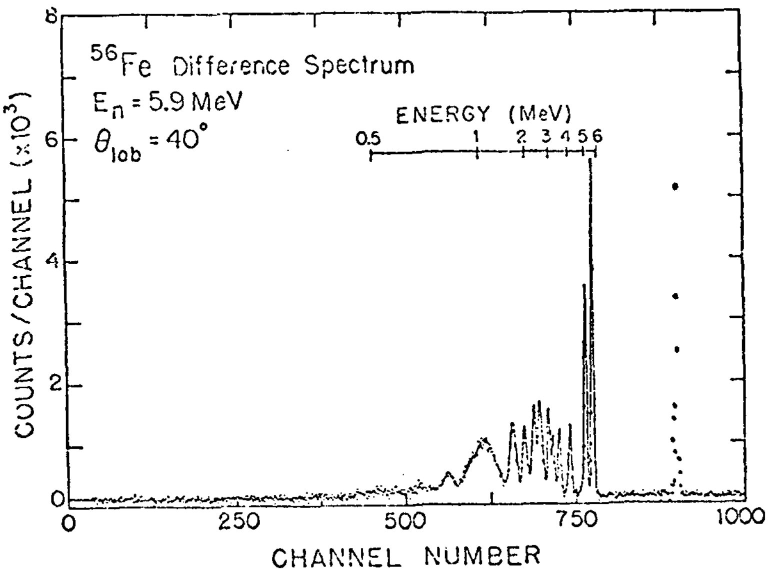

Difference TOF spectrum for ^{56}Fe(n,n') at E_n=5.9 MeV. This spectrum was obtained with the T(p,n) source reaction and a gas cell with a ^{58}Ni beam dump. The isotopically enriched ^{56}Fe sample was of mass 63 gms.

Fig. A6

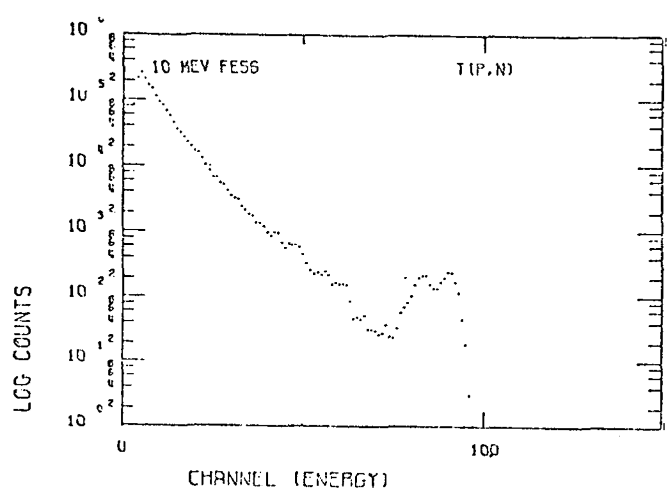

Neutron energy spectrum, corrected for detector efficiency, obtained at 80° in the ^{56}Fe(n,n') reaction at 10 MeV. Gas breakup neutrons and multiple scattering effects have not been corrected for.

Fig. A7

We are still in the process of optimizing our experimental procedures for these continuum measurements and testing the multiple scattering codes. Final cross-section data are not yet available from these spectra. On the basis of our present experience we can make the following comments:

i) At 6 MeV bombarding energy there is still pronounced structure in the scattering spectra obtained with even mass nuclei, and measurements with isotopic samples appear appropriate and feasible.

ii) At higher neutron bombarding energies (9-12 MeV) there are substantial backgrounds due to scattering of the low energy neutrons coming from the beam dump and gas cell walls. (This was not unexpected.) There is little or no structure in the (n,n') continuum spectra and it appears more appropriate to use natural samples for the scattering measurements since one can use samples that are several times larger than the isotopic samples presently available to us.

iii) At 14 MeV the background in our detectors is substantial at low bias. Again the larger natural samples appear to us to be more appropriate for studying continuum neutron emission here.

iv) The scattering of neutrons produced in breakup reactions in the gas will distort our measured continuum spectra for bombarding energies above $\sim$9 MeV when the T(p,n) source reaction is used. (This is true to a greater extent for the D(d,n) source.) We will subtract out this contribution using the known 0^{o} gas breakup cross sections and the ENDF/B library of elastic and inelastic scattering cross sections for the sample involved. The presence of pronounced structure in the scattering cross sections for elements such as iron at low energies may eventually limit the accuracy of this procedure.

B. FISSION PHYSICS

1. Single Nucleon Induced Fission (R.Y. Cusson, H.W. Meldner, ((L.L.L.)), D. Epperson, F.O. Purser, C. Kalbach, H.W. Newson)

The Ph.D. thesis of D. Epperson has been completed on the analysis of multiple chance proton induced fission. The occurrence of a low mass shoulder in the fission fragment mass distribution could signify that a weak branch for heavy element decay is the emission of p-f shell nuclei. The abstract follows.

"The Cyclo-Graaff facility of the Triangle Universities Nuclear Laboratory, located at Duke University, was used to make fission fragment energy correlation measurements for three isotopes of uranium. From these measurements, fission fragment mass yield distributions have been determined. The proton induced fission of the ^{236}U and ^{235}U targets used incident proton energies ranging in energy from 6.25 MeV to 30.0 MeV in energy steps of 0.25 MeV to 1.0 MeV. Protons ranging in energy from 6.5 MeV to 14.5 MeV were used on the ^{234}U target. A total of ninety-nine fragment energy correlation measurements were made with the three targets. Commercially available heavy ion silicon surface barrier detectors were used to detect the fission fragments. The uranium targets were supplied by Oak Ridge National Laboratory and were of isotopic purity greater than ninety-nine percent.

For incident proton energies greater than approximately 7 MeV, neutron emission competes favorably with fission for all of the uranium isotopes. Therefore, to obtain mass distributions due solely to the first chance fission of ^{237}Np, ^{236}Np, ^{235}Np, and ^{234}Np from sharp excitation energy states ranging from below the fission barrier to 20 MeV, a method for separating experimental multichance fission mass yields was developed. This method utilizes a statistical formalism to describe the decay of the excited compound nucleus through fission, neutron emission, or gamma emission. Neighboring isotopes provide self-consistency checks. A comparison is also made with published neutron induced fission mass yield data.

First chance mass yields from sharp states of excitation energy are presented for ^{237}Np, ^{236}Np, ^{235}Np, and ^{234}Np for excitation energies ranging from approximately 4 MeV to 20 MeV. Preliminary evidence for an enhanced fragment yield in the region of the doubly magic nucleus A = 78 (Z = 28, N = 50) is also shown. The effects of preequilibrium neutron emission for excitation energies between 12 MeV and 33 MeV are also discussed."

In addition, the code NIFTE7D is being used in systematic studies of n-induced fission parameters. An invited paper for the IAEA Symposium on Physics and Chemistry of fission in Julich, May 79 is being prepared. The abstract follows.

"A progress report on current results of neutron fission cross section calculations is given. This is part of a more general program which combines various semi-empirical nuclear theories for the calculation of all significant cross sections for heavy elements exposed to typical thermonuclear neutron spectra. The computer code development was motivated by many interests, e.g., in both laser fusion and in thermonuclear macro-explosions neutron fluences can be high enough to result in significant nuclear transmutations, especially in high-Z targets. A theoretical analysis of these processes requires cross sections for fission, capture, (n,p), (n,n'), (n,2n), etc., reactions for a large number of isotopes for most of which no data are available. Other applications are found in the calculation of neutron reactions, the actinide waste problem of the nuclear power industry, astrophysical r-process calculations, the neutron capture synthesis of very heavy, possibly super-heavy nuclei, etc.

Since neutron-rich isotopes have a decreasing neutron-emission threshold (Fermi energy) as more neutrons are added the number of evaporated neutrons for incident energies of order 15 MeV can be as high as 3 to 4 before fission takes place. Earlier attempts at a calculation of multiple-chance fission were limited to two neutron evaporations because of the claimed necessity of performing a very time-consuming multi-dimensional energy integral to obtain the multiple chance fission probability. A major new feature of our code is the use of a recursive algorithm for computing the (n-1st)-chance fission given the results of the nth-chance case. Thus, the size of the calculation is linear in the number of chances and it becomes possible to take into account as many neutron evaporations as required before fission of γ-emission.

A statistical model is used for the calculation and the recursive algorithm for including the effects of higher-chance fission on the lower-chance fission and neutron-emission probabilities. The correct inclusion and/or prediction of shell structure shifted threshold positions (fission barrier heights) is clearly most important in achieving any accuracy. Empirical rules are used for the evaluation of the compound nucleus level density at the fission saddle point. Pre-equilibrium processes are taken into account via the Griffin model. The complete code is designed to predict multiple-chance neutron-induced fission, neutron capture, multiple neutron emission, (n,p) and (n,α) reactions. Our goal is the extension of the ENDL-type cross section libraries used in thermonuclear Monte-Carlo calculations to include uranium and several transuranium isotopes of interest, up to A 260. Some sample results are presented for the fission of the various isotopes of U, from A = 233 to A = 253. The calculated energy-dependence of the neutron-induced fission of $^{235-239}U$ is compared with experimental data."

C. MODEL DEVELOPMENT (C. Kalbach)

1. Angular Distributions for Preequilibrium Emitted Particles*

A phenomenological approach for the calculation of angular distributions of particles emitted in the preequilibrium phase of nuclear reactions is being studied. Experimental angular distributions of preequilibrium particles from a variety of reactions are being analyzed in terms of Legendre polynomials, and the systematics of the resulting coefficients are quite striking. These coefficients will be used in conjunction with a new version of the Griffin model preequilibrium code PRECO which keeps track of how much of the reaction cross section has passed only through a series of unbound states. Kerman and Feshbach[1] have suggested that this part of the cross section should have forward peaked angular distributions, while the remainder should exhibit symmetry about 90° in the center of mass.

2. Shell Effects in Preequilibrium Reactions*

Work is in progress to implement the shell-shifted equi-spacing model for the calculation of particle-hole state densities in the Griffin preequilibrium model. All pertinent equations have been derived and are being programmed. This work requires a complete reworking of the computer code since, for the calculation of shell effects, it is necessary to keep track of the proton and neutron degrees of freedom separately. When this work is completed the validity of the Griffin model should be extended to include both light $(A < 40)$ and also heavier nuclei in the vicinity of nuclear shell closures.

3. Exciton Number Dependence of The Griffin Model Two-Body Matrix Element

The exciton number dependence of the residual two-body matrix element has been determined using published particle-hole pair creation

---

* This work is being performed on a consulting basis for Westinghouse Hanford Co.

[1] C. Kalbach, Nuov. Cim. 29A (1975) 283

rates obtained from semi-phenomenological calculations. The previous energy dependence of the mean squared matrix element has been replaced by a dependence on the average excitation energy per degree of freedom, E/n. For E/n less than 7 MeV or greater than 15 MeV, the form of the energy dependence has been slightly modified. These changes result in a factor of three reduction in the predicted Griffin model composite nucleus equilibration times but in only minor changes in the calculated energy spectra for emitted particles. This work has been published in Z. Phys. A 287 (1978) 319.

4. Non-Equilibrium Reaction Mechanisms for Loosely Bound Projectiles

A study has been made of the dominant non-equilibrium reaction mechanisms for charged particle emission in d and τ induced reactions. The results of simple statistical calculations are compared with experimental angle-integrated energy spectra appearing in the literature. A consistent picture of the reactions involved can be obtained by including the following spectral components: (1) Griffin model pre-equilibrium, (2) nucleon transfer in the form of stripping, pickup and exchange, (3) inelastic scattering and knockout involving nucleon clusters, and (4) projectile breakup. Simple methods for calculating these components are presented. This work has been submitted for publication. Preprints are available on request.

UNIVERSITY OF WASHINGTON

A. DELAYED NEUTRON SPECTRA

1. ^{240}Pu Equilibrium Spectrum (Patrick J. Grant and G. L. Woodruff)

The near-equilibrium energy spectrum of the delayed neutrons associated with the fast neutron-induced fission of ^{240}Pu have been measured at the University of Washington Nuclear Physics Laboratory. The apparatus and procedure used were those described in Ref. 1 except that the delay time between sample irradiation and counting was reduced from 0.08 seconds to 0.04 seconds.

The measured spectrum is generally similar to that previously measured from ^{235}U.[1] In particular the peaks that were observed in the ^{240}Pu results have the same energies as those measured earlier within the accuracy of the experiment. The overall quality of the ^{240}Pu data is lower than most of the earlier results. The most important complicating factor is the spontaneous fission of the sample. This produced a background of both neutrons and gamma rays which contributed additional uncertainty and increased the minimum energy below which neutrons and gamma rays could not be separated.

B. ALPHA N YIELDS (Patrick J. Grant and G. L. Woodruff)

Apparatus for the measurement of (α,n) yields from low Z targets is now being constructed. Alpha energies will range up to 9 MeV and initial measurements will use O isotopes as targets. The major improvement over previously reported experiments of this type is expected to be in the flatter response of the neutron detection assembly at higher neutron energies. This improvement should result from the use of a Be liner as the innermost region of a large graphite stack containing ^{3}He neutron detectors.

---

[1] G. W. Eccleston and G. L. Woodruff, Nucl. Sci. Eng., 62, 636 (1977)

YALE UNIVERSITY

A. FAST NEUTRON PHYSICS

1. A Global Analysis of the n-^{6}Li Interaction at Energies up to 4 MeV (Y. -H. Chiu and F. W. K. Firk)

Our measurements of the asymmetries of polarized neutrons elastically scattered from ^{6}Li, and of the differential cross sections at energies been 1.8 and 4 MeV have been included in an analysis of recent data from thermal energy to 4 MeV. We have incorporated the n-α channel using the Thomas R-function method. Clear evidence has emerged from the analysis for a p-wave triplet; the locations of these states are found to be in excellent agreement with the shell model predictions of Barker. The parameters obtained from the global analysis are listed in Table A-1:

J	ℓ	S	E_λ (MeV)	E_x (MeV)	γ^2 (MeV)	Γ_α (MeV)
1/2	0	1/2	-0.93 ±0.13	6.33 ±0.13	0.23±0.01	8.57 ±0.53
3/2	0	3/2	2.19 ±0.03	9.45 ±0.03	1.22±0.02	0.49 ±0.01
1/2	1	1/2				
3/2	1	1/2				
1/2	1	3/2	2.49 ±0.06	9.75 ±0.06	1.87±0.19	
3/2	1	3/2	1.76 ±0.14	9.01 ±0.14	0.19±0.05	2.16 ±0.21
5/2	1	3/2	0.212±0.001	7.462±0.001	1.01±0.01	0.036±0.0005

Table A-1

All quantities are given in the center-of-mass system. Distant level effects were required for the states at -0.93 MeV(R_o ∿ 0.18) and 1.76 MeV (R_o ∿ 0.94). Small changes in the above parameters may occur when we include new data sets in our analysis that were not available previously.

2. An Analysis of the n-^{9}Be Interaction at Energies up to 4 MeV (P. McGuire and F. W. K. Firk)

Our measurements of the asymmetries of polarized neutrons elastically scattered from ^{9}Be, and of the differential cross sections at energies between 2 and 4 MeV have been included in an analysis of all data currently available from the NNCSC from thermal energy to about 4 MeV. The analysis is greatly complicated by the large number of possible channels, and this has meant the development of a new and general fitting procedure based upon the Davidon-Fletcher-Powell method of non-linear least-squares analysis. Our general program is now complete, and the analysis is underway.

3. Polarization Effects in the Elastic Scattering of Neutrons from Bismuth in the MeV Region (M. Ahmed and F. W. K. Firk)

We are studying the Mott-Schwinger scattering of neutrons from Bismuth between 2 and 4.5 MeV as a continuous function of energy. The asymmetry of polarized neutrons elastically scattered from Bismuth has been measured in the angular range 5° to 15°. We have also measured the asymmetry between 20° and 160° in order to determine the optimum optical model parameters in this energy region, which is well below that covered in previous work. High precision polarization measurements are required at backward angles if we are to pin down the appropriate optical model, and hence shed light on the spin-dependent terms.